

PATTERNING TECHNIQUES FOR  
POLYMER LIGHT-EMITTING DEVICES

FLORIAN PSCHENITZKA

A DISSERTATION  
PRESENTED TO THE FACULTY  
OF PRINCETON UNIVERSITY  
IN CANDIDACY FOR THE DEGREE  
OF DOCTOR OF PHILOSOPHY

RECOMMENDED FOR ACCEPTANCE  
BY THE DEPARTMENT OF  
ELECTRICAL ENGINEERING

June 2002

© Copyright by Florian Pschenitzka, 2002. All rights reserved.

# Abstract

Organic light-emitting devices (OLED) based on emissive polymeric materials have gained tremendous attention from industry and academia because of the potential to replace current display technologies. In addition to low fabrication costs, this technology holds the prospect of flexible and light-weight displays.

However, the sensitivity of the organic thin film (polymer as well small molecules) to oxygen, water and solvent vapor poses a serious problem for product design because it severely limits available patterning techniques. Once the organic film is deposited, conventional processing (such as photolithography or wet etching) is not possible without damaging the organic film.

Two patterning approaches will be introduced in this thesis which have been developed to avoid any device degradation due to the fabrication process: The first method (large-area dye transfer) discusses the fabrication of three-color devices where the emissive color is defined by the dye introduced into the polymer matrix of the device after the polymer layer has been deposited. The second method focuses on dry etching using a chlorine plasma to pattern the metal cathode layer.

The method of large-area dye transfer for patterning the emissive color of OLEDs using transferred photoresist is introduced. Using a large-area dye diffusion source, the dye is diffused into the emissive layer of the OLED. To locally pattern the emissive color, either a shadow mask or a patterned dye source has to be used. The implementation of both approaches using photolithographic patterning and transferred photoresist is outlined in this thesis.

To pattern the cathode layer, a shadow mask is mostly employed which patterns the cathode metal film during the evaporation process. But it is problematic to obtain very small feature sizes over a large area using this technology. In this thesis we demonstrate that dry processing of OLED to pattern a blanket cathode metal film can be used to obtain very small features despite the incompatibility of the photoresist materials with organic LED materials.

# Table of Content

---

## 1. Introduction ..... 1

- 1.1 Organic Light-Emitting Devices ..... 1
- 1.2 Human Perception of Color and Brightness ..... 2
- 1.3 Full-Color Organic Displays ..... 3
- 1.4 Thesis Outline ..... 4
- 1.5 References ..... 5

---

## 2. Light-Emitting Devices based on Polymers ..... 6

- 2.1 Electrical Conduction in Polymers ..... 6
- 2.2 Absorption and Emission ..... 9
  - 2.2.1 Photoluminescence and Franck-Condon-Shift ..... 10
- 2.3 Energy Transfer ..... 12
  - 2.3.1 Förster Transfer ..... 12
  - 2.3.2 Dexter Transfer ..... 13
- 2.4 Charge Transfer ..... 13
- 2.5 Electroluminescence and Charge Injection ..... 14
- 2.6 Single Layer OLED ..... 15
  - 2.6.1 Indium-Tin-Oxide ..... 16
  - 2.6.2 Cathode Materials ..... 16
  - 2.6.3 Device Structure ..... 17
- 2.7 Organic Materials ..... 17
  - 2.7.1 Electron and Hole Transport Materials ..... 17
  - 2.7.2 Emissive Materials ..... 19
- 2.8 Device Fabrication and Characterization ..... 20
  - 2.8.1 Device Fabrication ..... 21
    - Patterning of ITO substrate ..... 21
    - Substrate Cleaning ..... 21
    - Oxygen Plasma Treatment ..... 21
    - Polymer Deposition ..... 21
    - Cathode Metal Deposition ..... 22
  - 2.8.2 Device Characterization ..... 22
- 2.9 Electroluminescence versus Photoluminescence ..... 24
- 2.10 Efficiency versus Dye Concentration ..... 30
- 2.11 Surface Morphology of the Polymer Film ..... 33
- 2.12 Summary ..... 38
- 2.13 References ..... 39

---

## 3. Patterning Techniques of the Emissive Layer for Full-Color Organic Displays ... 46

- 3.1 Patterning Techniques using Materials Emitting Different Colors ..... 47
  - 3.1.1 Direct Deposition of Red, Green, and Blue Emitters ..... 47
    - Shadow mask ..... 47
    - Ink-Jet Printing of Polymers ..... 48

Screen Printing .....	49
Dry Etching .....	49
3.1.2 Direct Emission of RGB by Local Dye Doping .....	50
Ink-Jet Printing of Dye Solution .....	50
Dye Transfer Method .....	50
3.1.3 Photobleaching .....	51
3.2 Patterning Techniques using a Uniform Emissive Material .....	52
3.2.1 RBG emission by white emission and color filtering .....	52
3.2.2 Emission of RGB with color converting materials .....	52
3.2.3 Microcavity .....	53
3.2.4 Stacked OLED .....	53
3.3 References .....	54
<hr/>	
<b>4. Dye Transfer by Thermal Processing .....</b>	<b>58</b>
4.1 Concept of Large-Area Dye Transfer .....	58
4.2 EL Performance of Devices with Transferred Dye and Post-Dye-Transfer Annealing	61
4.2.1 Performance of the Device with Transferred Dye .....	61
4.2.2 Photoluminescence and Post-Dye-Transfer Annealing .....	62
4.2.3 Electroluminescence and Post-Dye-Transfer Annealing .....	63
4.3 Secondary Ion Mass Spectroscopy .....	66
4.3.1 Method for Probing the Dye Profile by SIMS .....	66
4.3.2 Sulfur as Marker for C6 and Oxygen Interference .....	66
4.3.3 Resolution Limit of SIMS .....	67
4.3.4 Dye Profiles Before Annealing .....	68
4.3.5 Dye Profiles after High-Temperature Annealing .....	68
4.4 Diffusion-Depth-Sensitive Photoluminescence .....	70
4.4.1 Introduction to Diffusion-Depth-Sensitive Photoluminescence .....	70
4.4.2 Quantitative Analysis .....	71
4.4.3 Limitations .....	74
4.4.4 Experimental Results .....	76
4.5 Modelling of Dye Transport in Polymers .....	77
4.5.1 Fick's Laws of Diffusion .....	78
4.5.2 Solutions of Diffusion Equations .....	78
Diffusion with Constant Amount of Dopant .....	78
Unlimited Source .....	79
4.5.3 Diffusion in Polymers - Free Volume Theory .....	79
4.6 Glass Transition in Mixed Systems .....	83
4.6.1 Fox Equation .....	83
4.6.2 Prediction for PVK/PBD .....	85
4.7 Diffusivity of C6 in PVK/PBD Films .....	85
4.8 Summary .....	85
4.9 References .....	86
<hr/>	
<b>5. Solvent-Vapor-Assisted Dye Diffusion .....</b>	<b>89</b>
5.1 Basic Concept of Dye Diffusion Enhancement in Solvent Vapor .....	90

5.2 Annealing in Saturated Solvent-Vapor .....	91
5.2.1 Experimental Apparatus .....	91
5.2.2 Dye Diffusion Characterization by Photoluminescence and SIMS .....	92
5.2.3 Volume Expansion Measurements of Polymer Films .....	95
5.2.4 Device Performance after Anneal in Saturated Acetone Vapor .....	98
5.2.5 Discussion .....	99
5.3 Controlled Partial Pressure Annealing .....	100
5.3.1 Experimental Apparatus .....	100
5.3.2 Volume Expansion Measurements of Polymer Films .....	100
Time Dependence .....	100
Effects of Partial Pressure of the Solvent Vapor .....	103
5.3.3 Dye Profile after Anneal at Low Partial Pressure of Solvent Vapor .....	105
Partial Pressure of Acetone of 87.4 torr .....	105
5.3.4 Device Performance after Anneal at Low Partial Pressure of Acetone .....	110
Partial Pressure of Acetone of 87 torr .....	110
Dependence of the Device Performance on Partial Pressure of Acetone ..	114
5.4 Dye Concentration Control .....	115
5.5 Model for Diffusivity of C6 in PVK:PBD .....	117
5.6 Summary .....	121
5.7 References .....	121

---

## **6. Patterning Approaches using Local Dye Transfer ..... 124**

6.1 Patterning Approaches using a Diffusion Mask .....	124
6.1.1 “Scotch Tape” Method .....	124
6.1.2 Stainless Steel Mask .....	125
6.1.3 Silicone and Polyurethane Mask .....	126
6.1.4 Transferred Photoresist (“RISTON”) .....	127
Riston Photoresist .....	127
Patterned Riston-Mask and Laminated Technology .....	128
Dye Transfer Experiments .....	129
6.2 Patterned Dye Source .....	131
6.2.1 Photoresist Patterning of Dye Source Layer .....	131
6.2.2 Doped Photoresist .....	131
6.2.3 Dry-Etched Dye Source using a Laminated Photoresist Mask .....	133
6.3 Stability of Transferred Dye Pattern .....	135
6.3.1 Thermal Stability of the Dye Pattern .....	136
6.3.2 Stability of Dye Pattern during Solvent Vapor Anneal .....	137
6.4 Summary .....	141
6.5 References .....	142

---

## **7. Cathode Patterning ..... 143**

7.1 Dry Etching of the Cathode Metal Layer .....	145
7.1.1 Device Fabrication .....	146
7.1.2 Device Characterization .....	148
7.2 Cathode Patterning by Transferred Photoresist .....	153

7.2.1 Device Fabrication .....	153
Lamination of Pre-Patterned Photoresist .....	153
Adhesion Promotion using conventional Adhesive .....	154
Adhesion Promotion using a Thin Metal Layer .....	157
Cathode Metal Lift-off .....	159
7.2.2 Lateral Conduction due to Transferred Photoresist .....	160
7.3 Summary .....	162
7.4 References .....	165

---

## **8. Summary and Future Work .....**

8.1 Realization of Integrated RGB Device using the Dye Transfer Technique .....	167
8.2 Future Work .....	169
8.3 References .....	171

---

## **9. Appendix .....**

9.1 MATLAB code for Diffusion Depth Sensitive Photoluminescence .....	172
9.2 Publication and Conference Presentations .....	175

# List of Figures

- Figure 1-1:** Spectral response of cones in the human eye. .... 3
- Figure 1-2:** Spectral sensitivity of the human eye. Photopic vision refers to the response of the cones when sufficient illumination is present (day vision). Scotopic vision is the response of the rods which are more sensitive but are unable to distinguish color (night vision). .... 4
- Figure 2-1:** Chemical structure of polyethylene. .... 7
- Figure 2-2:** Energy levels of interacting molecular orbitals. .... 7
- Figure 2-3:** Chemical structure of PPV (a). The HOMO level of the benzene ring is the symmetric configuration of the  $\pi$ -orbitals [4](b). The energy diagram (c) shows the relative energy levels of the  $\sigma$  and  $\pi$  orbitals. .... 8
- Figure 2-4:** Relationship between HOMO, LUMO, ionization potential and electron affinity. .... 9
- Figure 2-5:** Franck-Condon-Shift in a diatomic molecule,  $r$  represents the interatomic distance. .... 11
- Figure 2-6:** Absorption and emission spectra of 2-Methoxy-5-(2'-ethylhexyloxy)-1,4-phenylenevinylene copolymer. .... 12
- Figure 2-7:** Förster transfer. .... 13
- Figure 2-8:** Dexter transfer. .... 13
- Figure 2-9:** Excitation by charge transfer. .... 15
- Figure 2-10:** Band diagram of an OLED. .... 16
- Figure 2-11:** Structure of a single layer polymer light-emitting device. .... 17
- Figure 2-12:** Chemical structure of (a) poly-(9-vinyl-carbazole) (PVK) and (b) 2-(4-Biphenyl)-5-(4-tert-butyl-phenyl)-1,3,4-oxadiazole (PBD) .... 18
- Figure 2-13:** Absorption spectra of a solid PVK film (dotted line) and of a solution of N-isopropylcarbazole in hexane (solid line). .... 18

- Figure 2-14:** Chemical structure of (a) Coumarin 47, (b) Coumarin 6, (c) Nile red, and (d) bimane ..... 20
- Figure 2-15:** Electroluminescence spectra of standard PVK/PBD devices doped with either C47, C6 or Nile red. .... 24
- Figure 2-16:** Current-voltage characteristics of a standard PVK:PBD:C6 device. The detected photocurrent is also shown. The device area was  $2 \text{ mm}^2$  and the thickness of the polymer film was  $800 \text{ \AA}$ . .... 25
- Figure 2-17:** EL spectra of PVK/PBD devices containing the dyes C47 and Nile red at  $50 \text{ mA/cm}^2$  (closed symbols) and  $100 \text{ mA/cm}^2$  (open symbols). The inset shows the normalized spectra of these devices. No spectral change could be detected. .... 26
- Figure 2-18:** Photoluminescence (solid line) and electroluminescence (dashed line,  $50 \text{ mA/mm}^2$ ) of a PVK/PBD film containing the dyes C47 and Nile red. .... 26
- Figure 2-19:** Process of excitonic transfer to both dyes in PL. .... 27
- Figure 2-20:** Absorption and emission spectra of C47 and Nile Red in solid film. .... 28
- Figure 2-21:** Schematic energy level diagram showing electron capture (process A and C) and thermal re-emission (process B) in a PVK/PBD device containing C47 and Nile red. .... 29
- Figure 2-22:** Normalized electroluminescence ( $50 \text{ mA/cm}^2$ ) spectrum at room temperature (dashed line), and at  $77 \text{ K}$  (solid line) of a PVK/PBD device containing the dyes C47 and Nile red. .... 29
- Figure 2-23:** Photoluminescence intensity (dotted line) and electroluminescence (at  $50 \text{ mA/cm}^2$ ) intensity (solid line) for a PVK/PBD device as a function of dye concentration (C6). .... 31
- Figure 2-24:** Normalized EL spectra (at  $50 \text{ mA/cm}^2$ ) of PVK/PBD devices with different C6 concentration. .... 31
- Figure 2-25:** Luminance as a function of current density of a PVK:BPBD:C6 device with different dye concentrations. No superlinear increase in luminance was observed. .... 32
- Figure 2-26:** Schematic energy level diagram showing electron capture (process A and C) and thermal re-emission (process B) in a PVK/PBD device at high dye concentration with isolated dye molecules and excimer complexes. .... 33
- Figure 2-27:** Electroluminescence intensity of a PVK:PBD:C6 device as a function of C6 concentration at room temperature (solid squares) and at  $77 \text{ K}$  (open squares). .... 34

<b>Figure 2-28:</b> Photoluminescence intensity (dotted line) and electroluminescence intensity (solid line) for a PVK/PBD device as a function of dye concentration (C47). .....	34
<b>Figure 2-29:</b> Photoluminescence intensity (dotted line) and electroluminescence intensity (solid line) for a PVK/PBD device as a function of dye concentration (Nile red). .....	35
<b>Figure 2-30:</b> EL micrograph of a device (diameter 1.5 mm at 50 mA/cm <sup>2</sup> ) with inhomogeneous polymer film thickness due to fast solvent evaporation. The device was fabricated using chloroform as the solvent. The polymer film was deposited at 2000 rpm. ....	37
<b>Figure 2-31:</b> Polymer film thickness as a function of spin speed. ....	37
<b>Figure 3-1:</b> Patterning of the emissive layer using a shadow mask. ....	47
<b>Figure 3-2:</b> Use of “banks” to confine the polymer solution during the ink-jet process. ...	48
<b>Figure 3-3:</b> Fabrication of three colors using dry etching of organic layer. ....	49
<b>Figure 3-4:</b> Patterning of the emission color by locally printing of dye solution. ....	50
<b>Figure 3-5:</b> Dye Transfer Method. ....	51
<b>Figure 3-6:</b> RGB emission using white emitter and color filters. ....	52
<b>Figure 3-7:</b> RGB emission using color conversion materials. ....	53
<b>Figure 4-1:</b> Local dye transfer to device polymer layer using a large area dye source and a shadow mask [6].	59
<b>Figure 4-2:</b> Photoluminescence spectra of a PVK film after different process times at 100 °C in air. The dye C6 was transferred to a film of pure PVK (emission peak at 495 nm). ....	60
<b>Figure 4-3:</b> I-V characteristics and measured photo current of a control device (not exposed to any heat treatment, solid line), of a heat treated device (80 °C for one hour in vacuum, dashed line), and a device with C6 transferred by dye diffusion (80 °C for one hour in vacuum, dotted line). ....	62
<b>Figure 4-4:</b> Normalized PL spectra of PVK/PBD/bimane film with C6 transferred. The sample was annealed for three hours at 90 °C. ....	63
<b>Figure 4-5:</b> Electroluminescence spectra of a blue, green, and red device fabricated using the dye transfer method. Blue devices contained bimane from spin-coated film, green devices contained C6 (transferred) and bimane, and red devices contained Nile red (transferred) and bimane. After initial dye transfer at 70 °C, the samples were kept in vacuum at 70 °C for 12 hours. ....	64

**Figure 4-6:** I-V characteristics (solid symbols) and measured photo-current (open symbols) of standard C6 devices exposed to heat treatment at various temperatures for one hour in vacuum. .... 65

**Figure 4-7:** SIMS data of PVK film with C6 transferred at 70 °C from a PVK layer highly doped with C6. The profiles for carbon, and the sulfur isotopes 32-S and 34-S and shown. The dashed line represents the 34-S signal intensified according to the ratio of its natural abundance vs. 32-S. .... 67

**Figure 4-8:** SIMS analyses of a PVK/PBD film in which was C6 was transferred for one hour at 70 °C from a highly doped PVK layer as the dye source. Two analyses were performed after the sample was kept for two hours (solid line) and after three hours (dashed lines) in the vacuum chamber. The oxygen signal decreased due to outgassing, and the 32-sulfur signal decreased because due to less interference with oxygen. .... 68

**Figure 4-9:** SIMS profiles of PVK/PBD film with C6 deposited by thermal evaporation and then and annealed for 4 hours (triangles) and 8 hours (circles) at 92 °C in vacuum. Open symbols represent the carbon signature, closed symbol the sulfur-32 signal. For comparison, the profile of a non-annealed sample is also shown (squares). The reason for the anomalously large dye signal in the polymer film before the high-temperature anneal is not known, and may be due to excess water vapor or oxygen in the film. .... 69

**Figure 4-10:** Diffusion Depth Sensitive Photoluminescence (DDSP): The polymer film containing bimane was excited by UV from the front and the back side of the sample and the resulting emission spectrum recorded. .... 70

**Figure 4-11:** Ratio of C6/bimane PL emission of a PVK film containing 0.3% (by weight) bimane as a function of C6/bimane mass ratio. The C6 level is varied. The dashed line is a linear fit ( $k = 10.3 w$ ), and the dotted line is a quadratic fit ( $k = 2 w + 7.6 w^2$ ). .... 72

**Figure 4-12:** Computed uniformity coefficient  $h$  as a function of the diffusion length  $L$ . If  $h = 1$  the dye profile is flat in the polymer film. .... 74

**Figure 4-13:** Computed uniformity coefficient  $h$  as a function of the diffusion length  $L$ . The dye distribution was assumed to be Gaussian. The coefficient was calculated for different dye loads  $k = 1$  and  $k = 100$ . .... 76

**Figure 4-14:** Photoluminescence spectrum (before and after annealing at 90 °C for 6 hours) of a PVK-film containing bimane in which C6 was diffused. The film was spun-on on a sapphire substrate to allow for probing the top and the bottom of the PVK film separately. The C6 peak is more pronounced after the substrate was annealed at elevated temperatures. .... 77

**Figure 4-15:** Volume expansion of amorphous polymer below and above the glass transition temperature  $T_g$ . The dashed line represents the behavior of a crystal. The contribution

beyond that is due to free volume. .... 82

**Figure 5-1:** Microscopic and macroscopic processes during the solvent-vapor assisted anneal. .... 91

**Figure 5-2:** Experimental apparatus to anneal devices in saturated solvent-vapor. .... 92

**Figure 5-3:** PL spectra of PVK/PBD/C47 film on sapphire substrate in which C6 was diffused. The back side (open squares) denotes the excitation and emission through the sapphire substrate, the front side (solid squares) denotes these of the polymer layer. PL measurements were recorded before (solid lines) and after (dotted lines) the anneal for 10 min in air saturated with acetone at room temperature. .... 93

**Figure 5-4:** SIMS profiles of dye in a PVK:PBD sample exposed to air saturated with acetone for 10 min (diamonds). The dye profile of the untreated sample (triangles) and of a sample with dye contained in the spun-on film (squares) and also shown. .... 94

**Figure 5-5:** Comparison of the ratio of back/front emission of C6 vs. C47 for different anneal temperatures. The anneal in acetone vapor at room temperature for 10 min had approximately the same effect on the dye diffusion as a conventional anneal for 12 hours at 80 °C in vacuum. .... 95

**Figure 5-6:** Determination of the solvent uptake in the polymer film by in situ measurement of the thickness by ellipsometry. .... 96

**Figure 5-7:** Chemical structure of acetone. .... 97

**Figure 5-8:** I-V-curves and photo-current of samples with C6 contained in the spun-on PVK/PBD/C47 solution. The annealed sample (10 min in air saturated with acetone at room temperature, squares) showed a higher leakage current compared to the non-treated one (triangles). The external quantum efficiency of the annealed device dropped only slightly. .... 98

**Figure 5-9:** I-V-curves and photo-current of samples with C6 transferred by dye transfer method into the PVK/PBD/C47 film. The non-annealed sample (triangles) shows a very poor external quantum efficiency. It improved by nearly an order of magnitude after the sample was annealed in air saturated with acetone (squares) for 10 min at room temperature. .... 99

**Figure 5-10:** Schematic of the tube reactor. .... 101

**Figure 5-11:** Schematic interior of the anneal chamber. .... 101

**Figure 5-12:** Time response of the PVK:PBD film thickness in glass tube reactor. .... 102

**Figure 5-13:** Experimental set-up for measurement of the time response of the polymer

film thickness. A small metal cylinder has been placed on the sample stage in the glass tube reactor, and the gas inlet was directed into this enclosure. .... 103

**Figure 5-14:** Time response of the PVK:PBD film thickness in the small metal cylinder inside the glass tube reactor. The theoretical thickness response based only on the increase of solvent vapor is given as the dotted line. The fit for the actual measurement is shown as the dashed line. .... 104

**Figure 5-15:** Change in polymer film (PVK:PBD) thickness as a function of partial acetone vapor pressure. .... 105

**Figure 5-16:** Estimated glass transition temperature  $T_g$  of the PVK:PBD/solvent mixture as a function of partial pressure of acetone. .... 106

**Figure 5-17:** SIMS sulfur profile of a PVK:PBD sample with C6 transferred into a PVK film before (squares) and after (circles) acetone anneal. The sample was annealed in acetone vapor (87.4 torr) for 150 sec at room temperature. For comparison, a thermally annealed sample (4 hours at 92 °C) after the same initial transfer is also shown (triangles). .... 107

**Figure 5-18:** Diffusion coefficient of C6 in PVK:PBD in vacuum and in acetone vapor (87.4 torr). The diffusion coefficient increases by many orders of magnitude in solvent vapor. The referenced data points (a) was extracted from the dye diffusion experiment at 92 °C for 4 hour explained in Chapter 4.3.5, the data points (b) are extracted from lateral dye diffusion experiments discussed in Chapter 6.3.1. .... 108

**Figure 5-19:** SIMS profiles of sulfur and carbon in PVK:PBD after C6 was transferred and annealed at different partial pressures of acetone for 60 sec. The final dye profile is essentially flat in all cases, independent of the solvent vapor pressure. .... 109

**Figure 5-20:** SIMS profiles of sulfur of PVK:PBD samples annealed at different partial pressures of acetone for 30 sec. No difference in diffusion enhancement could be detected. .... 110

**Figure 5-21:** I-V-characteristics and photocurrent of PVK/PBD/C6 devices with the dye contained in the spun-on solution treated in acetone vapor (partial pressure 87 torr) for different times. .... 111

**Figure 5-22:** I-V-characteristic of PVK/PBD/C47 devices with C6 diffused into the polymer film for different times at acetone vapor pressure of 87 torr. The photocurrent of the device exposed to acetone vapor increased by nearly one order of magnitude. .... 112

**Figure 5-23:** Normalized EL spectra of a PVK/PBD/C47 device with C6 transferred into the polymer film. Before the anneal (solid line), emission occurred entirely from C47. After 60 sec anneal (dashed line) in acetone vapor (partial pressure 87 torr), the emission is shifted to C6. Nearly no emission from C47 was detected in a device annealed for 150 sec (dot-

ted line). ..... 113

**Figure 5-24:** External quantum efficiency (circles) and rectification ratio (squares) as a function of exposure time to acetone vapor (partial pressure 87 torr). Control devices (solid symbols) are devices with C6 contained in the spin-on solution, diffused devices (open symbols) are devices with transferred C6. .... 113

**Figure 5-25:** External quantum efficiencies of rectification ratio of control devices (dye contained in the spun-on solution) at different partial pressures of acetone after 4 min anneal. .... 115

**Figure 5-26:** SIMS profiles of sulfur and carbon in PVK/PBD samples with transferred C6 after different transfer times. .... 116

**Figure 5-27:** Total amount of C6 in a PVK/PBD film after transfer at 70 °C in vacuum for different times. .... 117

**Figure 5-28:** Plot of measured values of  $D$  vs.  $1/T$  (process temperature) and predicted values according to the WLF model (dotted line with common parameters; with fitted parameters dashed line). .... 119

**Figure 5-29:** Plot of measured values of  $D$  vs.  $1/T$  (process temperature) and predicted values according to the WLF model (dotted line with common parameters; with fitted parameters dashed line). The process temperatures of the solvent vapor data point are adjusted using the relation to account for the different glass transition temperatures in this case. .120

**Figure 6-1:** Electroluminescence micrograph of a device with a 50  $\mu\text{m}$  wide line of C6 transferred into a PVK/PBD/bimane film. .... 125

**Figure 6-2:** Micrograph of a damaged polymer film due to burr of the steel shadow mask. .... 126

**Figure 6-3:** Photoluminescence photograph of a substrate with two dyes transferred into polymer film (400  $\mu\text{m}$  wide lines). 126

**Figure 6-4:** Device fabrication process using local dye patterning with transferred photoresist. .... 129

**Figure 6-5:** Photoluminescence micrograph of a PVK/PBD/bimane film with C6 transferred from a dye source using a patterned Riston film as integrated diffusion mask. ....130

**Figure 6-6:** Electroluminescence micrograph of a PVK/PBD/bimane film with C6 transferred from a dye source using a patterned Riston film as integrated shadow mask. ....131

**Figure 6-7:** Device fabrication process with patterned dye source by dry etch of dye doped polymer film. .... 134

**Figure 6-8:** EL micrograph of a 3 mm high letter with 200  $\mu\text{m}$  lines of transferred Nile red ..... 135

**Figure 6-9:** Spatial PL intensity profiles before and after 4 hour anneal at 90  $^{\circ}\text{C}$  or 135  $^{\circ}\text{C}$  of substrates with C6 stripes patterns transferred into PVK/PBD film. .... 137

**Figure 6-10:** Photoluminescence micrograph of a stripe (300  $\mu\text{m}$  wide) of C6 transferred into a PVK/PBD blend after solvent anneal. The solvent anneal did not significantly increase the width of the dye-doped stripe. .... 139

**Figure 6-11:** PL intensity profiles of a PVK/PBD sample with a 300  $\mu\text{m}$  wide stripe of C6 transferred before (solid line) and after (dashed line) the anneal in acetone vapor (partial pressure 46.4 torr) for 180 sec. .... 140

**Figure 7-1:** Schematic of a passive matrix display. Devices are formed where the ITO stripe intersects with the cathode metal stripe. .... 143

**Figure 7-2:** Use of cathode separators to pattern organic layer and cathode. .... 144

**Figure 7-3:** Cathode patterning using a shadow mask during the metal evaporation. .... 145

**Figure 7-4:** Patterning of metal cathodes by dry etching of a blanket metal film. .... 146

**Figure 7-5:** Damage to the aluminum film after photoresist development when only a single aluminum layer was deposited. The small features ( $<100 \mu\text{m}$ ) are the desired photoresist patterns. .... 147

**Figure 7-6:** Device structure to avoid blistering of the aluminum film due to contact with water during the lithography process, and to reduce aluminum pinholes. .... 148

**Figure 7-7:** Micrograph of a sample with Al cathode lines fabricated with plasma etching. The width of the ITO lines and the Al lines is 20  $\mu\text{m}$ . Note some damage to the photoresist (on top of the cathode) from metal etching can be seen. .... 148

**Figure 7-8:** Electroluminescent micrograph of devices of different sizes fabricated with plasma etching of the cathodes. The ITO lines run horizontally, the aluminum lines vertically. Note the non-emissive zone in all samples along the edge of the aluminum line. The devices were exposed to air for approximately 4 hours. .... 149

**Figure 7-9:** Current-voltage characteristics and photo current of OLEDs with plasma etched cathode: 1000  $\mu\text{m}$  device (squares), 500  $\mu\text{m}$  device (circles), and 200  $\mu\text{m}$  (triangles). The devices were exposed to air for approximately 4 hours. .... 150

**Figure 7-10:** Growth of the non-emissive zone with time in air after (a) aluminum cathode (300 nm) patterning with plasma etching (circles), and (b) patterned cathode formation by

aluminum evaporation through a shadow mask (squares).  $\Delta L$  is the width of the non-emissive zone (inset). ..... 151

**Figure 7-11:** Growth of the non-emissive zone vs. exposure time to air for cathodes of different material and processing steps after cathode deposition. All cathodes were deposited using a shadow mask. .... 152

**Figure 7-12:** Electroluminescence micrographs of devices with Mg:Ag/Al cathode exposed to oxygen plasma for 4 min. The width of the non-emissive zone was 20  $\mu\text{m}$  after 11 min exposure to air, 23  $\mu\text{m}$  after one hour, 55  $\mu\text{m}$  after 12 hours, and 60  $\mu\text{m}$  after 15 hours. .... 153

**Figure 7-13:** Schematic process to form cathode separators using transferred photoresist. .... 154

**Figure 7-14:** Device with damage due to spray-adhesive (device size 80  $\mu\text{m}$  by 400  $\mu\text{m}$ ). .... 155

**Figure 7-15:** EL micrograph of an OLED feature fabricated using transferred photoresist. .... 155

**Figure 7-16:** EL micrographs of devices with adhesion promotion layer painted onto the Riston film before the lamination process. .... 156

**Figure 7-17:** Contamination of the emissive polymer layer due to contact with adhesive deposited on the Riston film. .... 157

**Figure 7-18:** Adhesion promotion using a very blanket thin metal layer deposited before the lamination of the Riston photoresist. A thick cathode metal film is evaporated after the Riston layer is deposited. .... 158

**Figure 7-19:** EL micrographs of device patterned with transferred Riston photoresist. A thin blanket silver film was deposited before the lamination process to promote the adhesion of the Riston film. Picture (b) is the fivefold magnified version of (a). .... 159

**Figure 7-20:** Cathode patterning by cathode metal lift off. .... 160

**Figure 7-21:** Micrograph of a cathode metal layer after lift-off process. .... 161

**Figure 7-22:** (a) SEM micrograph of section of a Riston photoresist laminated onto a PVK/PBD coated ITO/glass substrate; (b) insulation of separated devices due to the wedge-like structure of the photoresist. .... 162

**Figure 7-23:** SEM micrograph of a device with laminated Riston film. The edges of the film show thin protruding features. .... 163

**Figure 7-24:** Schematic of connected devices due to protruding Riston film. .... 164

**Figure 8-1:** PL images of the device after the dye transfer (left side: entire device 78 mm x 78 mm, right side: magnified detail). [images courtesy of Ke Long] ..... 168

**Figure 8-3:** Dye diffusion process for an integrated RGB device. .... 168

**Figure 8-4:** EL micrograph of a pixel with red, green and blue subpixel fabricated by dye transfer and cathode separators. [micrographs courtesy of Ke Long] ..... 169

## List of Tables

- Table 2-1:** HOMO levels, LUMO levels and wavelength of the peak emission of materials used in experiments. The wavelength of the peak emission was measured in devices with optimal dye concentration. .... 19
- Table 2-2:** Conversion Factor Q to obtain the external quantum efficiency. .... 23
- Table 2-3:** Film thickness and turn-on voltage of PVK/PBD devices fabricated with different solvents. Values for vapor pressure are taken from Ref. [70]. The turn-on voltage is in this case defined as the voltage at which the dark-current of the detector equal to the photo-current (see Figure 2-16). .... 38
- Table 4-1:** External quantum efficiencies of devices with diffused dye and control devices. .... 64
- Table 4-2:** Parameters of DDSP calculation. .... 74
- Table 5-1:** Device characteristics of devices annealed in acetone vapor (partial pressure: 87.4 torr) for 5 min. The turn-on voltage was defined as the point where the photo-current in the detector exceeded the dark current. The rectification ratio was determined at  $\pm 10$  V. .... 114
- Table 5-2:** Measured diffusivity D of C6 in PVK/PBD films. .... 118
- Table 5-3:** WLF parameter for different polymers ..... 120
- Table 6-1:** FWHM increase of stripes of transferred C6 before and after the anneal in acetone vapor for 180 sec. .... 139

# 1 Introduction

Designing the human-machine-interface in the age of microelectronics is a challenging job. Computers are able to process much more information than, for example, Leibnitz' multiplication machine invented in 1674 or the ENIAC computer in 1946. This huge amount of information has to be displayed in a way comprehensible to humans. The development of the computer coincided with the invention of television and its cathode ray tube (CRT). So it comes as no surprise that the CRT is the most common device used as the computer display. While the picture quality of CRTs has improved much over the years, due to the required vacuum tube the CRT is quite bulky, heavy and fragile. Clearly, in the age of wireless communication and computing, this device is far from being ideal. Liquid crystal displays (LCD) are now a common substitute for CRTs. These flat panel displays need much less space and power than CRTs. However, they are expensive to fabricate and, due to their glass components, are still very likely to break. Moreover, because of their non-emissive nature, they need either surrounding light (reflective mode) or a back light (transmissive mode). With these shortcomings of LCDs, it would be desirable to develop a display which is emissive (does not need a back light) and is based on plastic substrates rather than glass. In the last decade much research focused on organic light-emitting devices (OLEDs) which promise these properties. In this context, "organic" means that the materials used are based on carbon chemistry rather than conventional inorganic electronic materials.

## 1.1 Organic Light-Emitting Devices

Although the first OLED based on polymer was reported in 1983 by Partridge [1], OLEDs gained practical importance only in 1987 when C. W. Tang and S. A. VanSlyke fabricated a device based on small molecules with promising characteristics [2]. Since then, the field of organic electronics has attracted a tremendous amount of attention both from

industry and academia [3]. In 1990, Burroughes *et al.* fabricated devices based on the polymer poly(*p*-phenylene vinylene) (PPV) which is still one of the most often used polymers in OLEDs [4]. A further boost for polymer-based devices came when Fukuda *et al.* [5] obtained emission from polyfluorenes. As of today, this kind of polymers exhibits the most promising characteristics for commercial applications. Devices based on this kind of polymer have now efficiencies in excess of 20 lm/W and are broadly comparable to inorganic LEDs based on III-V semiconductors in terms of brightness and efficiencies. Also, lifetimes of more than 10,000 hours at 200 cd/m<sup>2</sup> have been reported [6][7].

The device structure of an OLED is surprisingly simple: sandwiched between two electrodes is a thin film of organic material. If an electric field is applied across the electrodes, electrons and holes are injected into states of the LUMO (lowest unoccupied molecular orbital) and HOMO (highest occupied molecular orbital), respectively. Light emission from the organic materials occurs when the molecule relaxes from the excited state to the ground state and emits of a photon. This process is analogous to what happens in inorganic crystalline semiconductors such as GaAs. In this case, an excited electron in the conduction band recombines with a hole in the valence band. The energy of the emitted photon is determined by the energy gap between the conduction and the valence bands (bandgap). Similarities and differences between the amorphous organic film and the crystalline semiconductor are discussed in more detail in Chapter 2.1.

## 1.2 Human Perception of Color and Brightness

Electromagnetic radiation with a wavelength between 380 nm and 780 nm is perceived as light by the human eye. We associate a certain wavelength range in this spectrum with a particular color. However, the retina of the human eye actually has only three different color receptors, called cones. (Another kind of receptor, called rods, only detect brightness.) [8] Each kind of cone has its distinct spectral response. The spectral resolution of the response is rather broad as shown in Figure 1-1. This spectral overlap between the response means that light of a certain wavelength is detected by more than one cone. The ratio of these responses is in turn associated with a color like red, blue, orange, yellow, turquoise or white. This means that the full range of colors can be simulated by just three colors, namely red, green and blue.

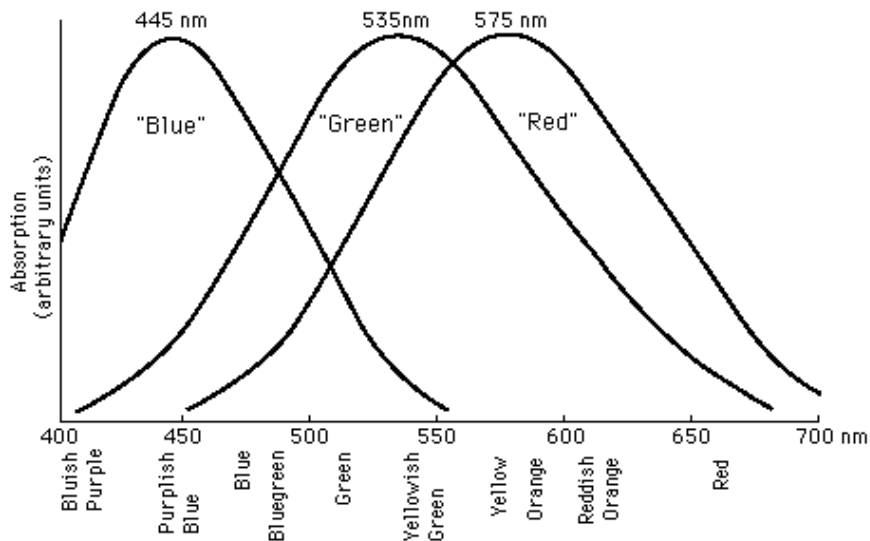


**Figure 1-1.** Spectral response of cones in the human eye.[9]

The human eye is well adapted to the environment, having the most sensitive response of color vision (photopic vision) in the yellow-green section of the spectrum which coincides with the emission peak of the sun. The sensitivity falls sharply towards either end of the spectrum as shown in Figure 1-2.

This curve has implications for the design of displays: To obtain the same impression of brightness in the red or in the blue compared to yellow/green, the device has to emit a much larger number of photons, requiring a higher driving current.

### 1.3 Full-Color Organic Displays

In a full-color display, each pixel of the display has to be capable of simulating the full range of colors to the observer. Therefore, the pixel is usually subdivided into three subpixels, with one subpixel emitting in the blue, one in the green and one in the red. While this concept is utilized in all color CRTs and LCDs, its implementation with organic light-emitting devices poses a variety of problems. In OLEDs, one option to achieve this would require patterned organic layers, so each subpixel is an OLED directly emitting the desired color. Because organic materials are very sensitive to water and oxygen, all patterning techniques used in conventional semiconductor fabrication (such as photolithography and wet etch) cannot be easily be applied to organic materials without damaging the device. Therefore, novel methods for the patterning process of organic thin films are needed.

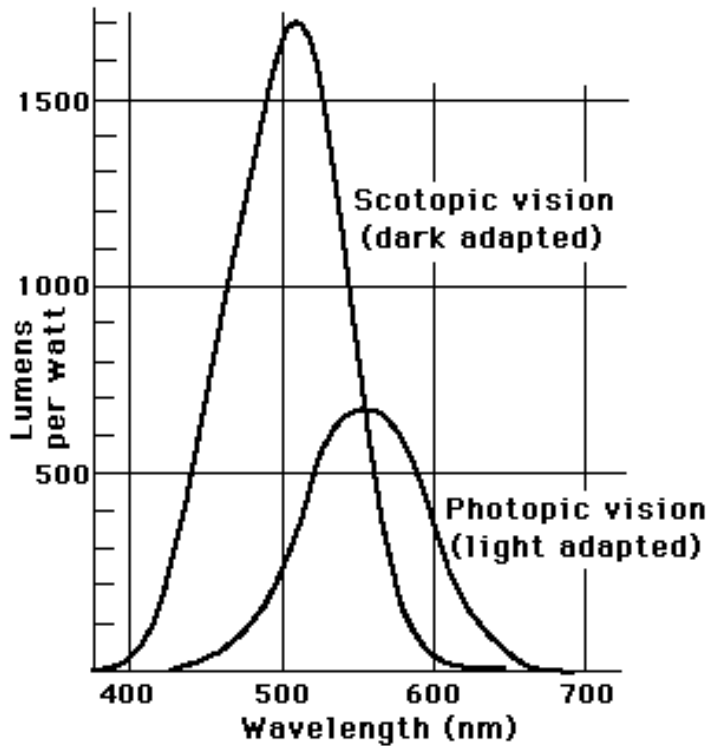


**Figure 1-2.** Spectral sensitivity of the human eye. Photopic vision refers to the response of the cones when sufficient illumination is present (day vision). Scotopic vision is the response of the rods which are more sensitive but are unable to distinguish color (night vision). [9]

## 1.4 Thesis Outline

The work introduced in this thesis focuses on the patterning aspect of organic light-emitting devices based on polymers. Two issues are discussed in depth: First patterning issues of the polymer film arising from the need to obtain subpixels emitting different colors are considered. In Chapter 2, the principle structure and characteristics of OLEDs will be discussed. An overview of patterning techniques is given in Chapter 3. Chapter 4 focuses on the dye diffusion technique and its underlying theory. In Chapter 5 we introduce a solvent-vapor anneal to enhance the diffusion of dye in the polymer film. The actual patterning process incorporating the dye diffusion method is discussed in Chapter 6. The second part of this thesis will focus on patterning methods for the cathode metal layer on top of the organic layer. In Chapter 7, a technique is described to pattern the cathode of OLEDs based on dry etching. Finally, Chapter 8 gives a summary and suggests topics for further work.

## 1.5 References

- [1] R. H. Partridge, "Electroluminescence from polyvinylcarbazole films. III. Electroluminescent devices", *Polymer* **24** (6), 748 (1983).
- [2] Tang, C. W. and S. A. VanSlyke. "Organic electroluminescent diodes." *Appl. Phys. Lett.* **51**(12): 913-915 (1987).
- [3] K. Chang, "Electronics Based on Plastic," in *The New York Times* (New York, October 17, 2000).
- [4] J. H. Burroughes, D. D. C. Bradley, A. R. Brown, R. N. Marks, K. Mackay, R. H. Friend, P. L. Burns, and A. B. Holmes, "Light-emitting diodes based on conjugated polymers", *Nature* **347**, 539 (1990).
- [5] M. Fukuda, K. Sawada, S. Morita, and K. Yoshino, "Novel characteristics of conducting poly(9-alkylfluorene), poly(9,9-dialkylfluorene) and poly(1,10-bis(9-alkylfluorenyl) alkane)", *Synthetic Metals* **41** (3), 855 (1991).
- [6] M. T. Bernius, M. Inbasekaran, J. O'Brien, and W. Wu, "Progress with light-emitting polymers", *Advanced Materials* **12** (23), 1737 (2000).
- [7] S. R. Forrest, "Active optoelectronics using thin-film organic semiconductors", *IEEE Journal on Selected Topics in Quantum Electronics* **6** (6), 1072 (2000).
- [8] J. D. Schanda, "Colorimetry," in *Handbook of Applied Photometry*, edited by C. DeCusatis (Optical Society of America and Springer-Verlag New York, Inc., New York, 1998), pp. 327.
- [9] Graphs obtained from "hyperphysics": <http://hyperphysics.phy-astr.gsu.edu/hbase/vision/colcon.html#c1>. Reproduced with kind permission from Rod Nave, Georgia State University.

# 2 Light-Emitting Devices based on Polymers

Organic devices can be based on small molecules or polymers. This chapter will outline the fundamental properties of conducting polymers used in polymer light-emitting devices. However, most of the discussed concepts apply to small molecules as well. Polymers are materials consisting of a chain of covalently bonded units. These units are known as monomers. The molecular weight of a polymer molecule can be very high, because the polymer chain can contain a very large number of monomers.

In Chapter 2.1 we describe briefly how polymers can conduct electricity. The absorption and emission of polymers and energy transfer mechanisms are discussed in Chapter 2.2 and Chapter 2.4. Chapter 2.5 focuses on electroluminescence of and the injection of charges into polymeric materials. The fundamental structure of a single layer OLED is given in Chapter 2.6, and the materials used are discussed in Chapter 2.7. The fabrication of devices is described in detail in Chapter 2.8. Chapter 2.9 is dedicated to the difference between photoluminescence and electroluminescence, while Chapter 2.10 focuses on the dependency of the OLED efficiency on the concentration of dye. The morphology of the polymer film and its impact on the device performance are discussed in Chapter 2.11.

## 2.1 Electrical Conduction in Polymers

In 1990, J. H. Burroughes *et al.* at Cambridge University published data on conductive polymers for light-emitting devices [1]. In 1991, Alan Heeger reported on polymers which demonstrated a high conductivity and presented a conclusive theory. For this research, he was awarded the Nobel prize in chemistry in 2000 [2][3].

Common polymers like polyethylene (the common plastic shopping bag, see Figure 2-1) have a very low electrical conductivity. The polymer only contains single bonds, i.e. the carbon atoms are bonded to the other atoms in the  $sp^3$ -configuration, as

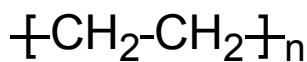


**Figure 2-1.** Chemical structure of polyethylene.

known from the diamond structure. All electron-orbitals only extend in the direction of the bond ( $\sigma$ -bonds). The two bonding orbitals interact and form a symmetric or asymmetric configuration (level splitting), see Figure 2-2. The symmetric state (characterized by a lower energy and therefore energetically preferred) is referred to as the bonding state. In this state, an actual bond is formed holding the molecule together. Because these  $\sigma$ -orbitals extend only in direction of the bonded atom, the probability to find an electron at the perimeter of the molecule is very small. In the bonded state, all electrons are localized in the states associated with the  $\sigma$ -orbitals and all these states are filled. Therefore, no electrical conduction is possible. The asymmetric state (characterized by a higher energy) leads to the destruction of the bond and is called anti-bonding state ( $\sigma^*$ ).

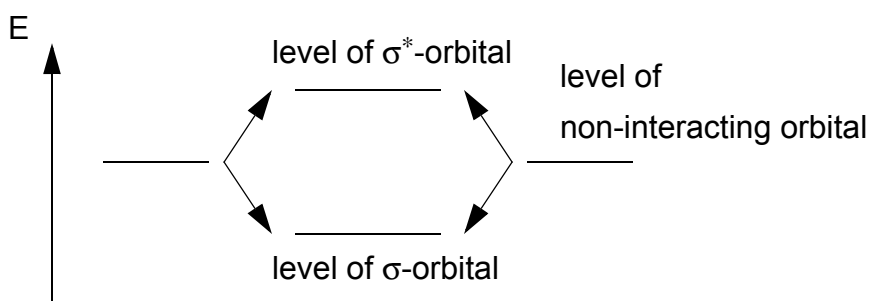


**Figure 2-2.** Energy levels of interacting molecular orbitals.

Now consider a bond formed in the  $sp^2$ -hybridization (usually referred to as “double bond”): In this case, in addition to the  $\sigma$ -bond in direction to the neighboring atom, the overlap of the  $p_z$  orbitals forms a bond ( $\pi$ -bond) which extends perpendicular to the  $\sigma$ -bond. A common polymer used in electroluminescent devices is poly(phenylene vinylene), PPV. The structure of PPV is shown in Figure 2-3(a). PPV is a conjugated polymer, i.e. the polymer backbone consists of alternating single and double bonds. Again, the interaction of orbitals leads to a symmetric and asymmetric state ( $\pi$  and  $\pi^*$ ). The structure of PPV also contains a benzene ring where each of the carbon atoms in the structure forms a  $\pi$ -orbital. The symmetric state of the orbitals is the lowest energy level (HOMO) of the structure as shown in Figure 2-3(b).

Analogous to a molecule bonded with a  $\sigma$ -bond, in a molecule in the ground state, all electrons are localized in the states associated with the  $\sigma$  and  $\pi$ -orbitals, and all of these states are filled. In contrast to the  $\sigma^*$ -bond, the molecule is not destroyed if the two atoms are bound in the  $\pi^*$  state. However, the geometrical configuration of the molecule can change. Because  $\pi$ -orbitals extend out of the plane of the molecule, the orbital can interact with another  $\pi$ -orbitals on a different molecules and electrical transport becomes possible, leading to a high electrical conductivity.

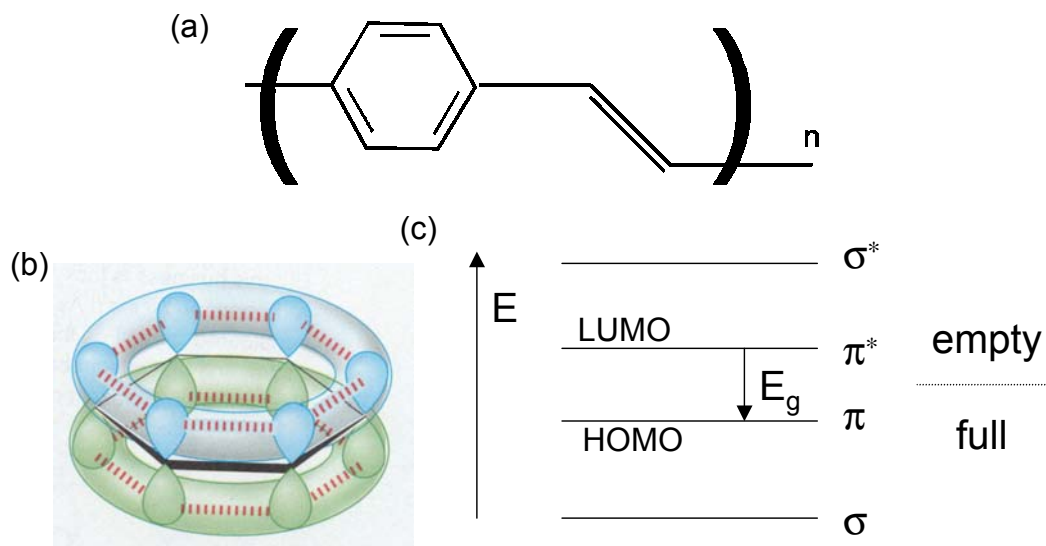


**Figure 2-3.** Chemical structure of PPV (a). The HOMO level of the benzene ring is the symmetric configuration of the  $\pi$ -orbitals [4](b). The energy diagram (c) shows the relative energy levels of the  $\sigma$  and  $\pi$  orbitals.

If the polymer chain contains double bonds, the electrical transport can occur along the polymer chain (intrachain transport) or between different polymer strands (interchain transport) [5][6][7].

In a non-excited molecule, all the low-energy states are occupied. If the molecule contains a “double bond”, the highest filled molecular orbital (HOMO) is a  $\pi$ -orbital. In this case, if an electron is promoted from the HOMO to the lowest unoccupied molecular orbital (LUMO), it has to overcome an energy gap  $E_g$  (see Figure 2-3(c)). These energy levels (HOMO and LUMO) are determined by molecular orbitals. In addition, vibrational modes (vibrations of the nuclei) lead to additional states above the LUMO and the HOMO levels.

The electron affinity of the molecule is correlated with the LUMO level. The HOMO level can be derived from the ionization potential, as shown in Figure 2-4.

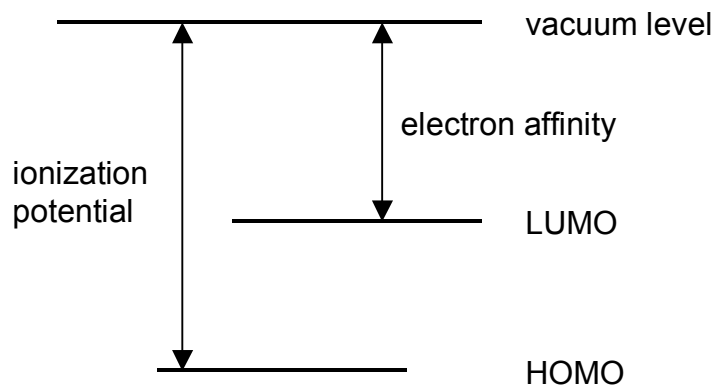


**Figure 2-4.** Relationship between HOMO, LUMO, ionization potential and electron affinity.

It is convenient to simply apply the band model (developed for conventional crystalline semiconductors like silicon) to polymeric materials by substituting the HOMO with valence-band and the LUMO with the conduction band. Although this concept is sufficient to explain many observations, the band model fails to predict many transport characteristics.

Because of the interaction of orbitals (level splitting) in a crystalline material and the close proximity of the atoms, a multitude of delocalized states very close to each other in energy are created. These states form a band of states over a wide energy range. In an amorphous polymer material, however, the interchain distances are much bigger and therefore, the interaction of the orbitals is much smaller. As a result, the states are much more localized and cannot be treated as bands. Based on this observation, several transport models have been developed [8][9][10][11][12][13][14][15].

## 2.2 Absorption and Emission

A molecule can be excited by absorption of a photon or a phonon, by dipole-dipole interactions with a neighboring molecule, or by injecting electrical charges. Light emission from the molecule can occur when an exciton radiatively recombines. An exciton is a bound state of an electron and a hole, leading to a zero net charge. Excitons can be treated

as quasi-particles capable of diffusion. The average distance of the electron and the corresponding hole is the radius of the exciton. Due to the small orbital overlap in polymeric systems, excitons are localized (Frenkel excitons), i.e. their radius is small (less than 5 Å) compared to the intermolecular distances. In contrast, excitons in an inorganic crystal are delocalized and have a radius of 40 to 100 Å (Wannier excitons) [16].

An exciton can be localized on one polymer chain (intrachain exciton), or between two polymer chains (interchain excitons). Interchain excitons have in general a much smaller photoluminescence efficiency [17].

Absorption and emission phenomena in polymers usually do not involve the whole polymer chain because more distant units do not interact. In addition, geometrical factors such as bends in the polymer chain limit the interaction. The term conjugation length is used to describe the effective interaction length of the polymer. It can be assumed that only segments within this length contribute to absorption or emission of the polymer. In most cases, the conjugation length of polymers is between 11 and 20 monomer units [18][19][20].

If the emission is caused by absorption of photons, the process is referred to as photoluminescence (PL); emission caused by charge injection is called electroluminescence (EL).

### **2.2.1 Photoluminescence and Franck-Condon-Shift**

When an electron in the ground state absorbs a photon of energy  $E_A$ , it is promoted from the lowest ground state of the HOMO ( $S_0$ ) to the corresponding vibronic sublevel of the LUMO ( $S_1$ ) determined by the energy of the absorbed photon (Figure 2-5). The position of the nuclei remains unchanged during this process because the time is too short to allow for their relocation ( $\sim 10^{-15}$ s), although the electronic distribution has changed. After this, the electron relaxes non-radiatively down to the lowest vibrational sub-level of the LUMO ( $\sim 10^{-13}$ s). Because of the time needed for this process, the nuclei rearrange themselves. ( $\Delta r$  represents the increase in distance between the nuclei.) The electron then relaxes to the HOMO state by emission of a photon of energy  $E_B$ . Because of the changed geometrical configuration and the energy loss due to the vibronic levels, the emitted photon has a lower

energy than the absorbed one. This energy shift between the absorbed and emitted photon is referred to as the Franck-Condon-Shift [16].

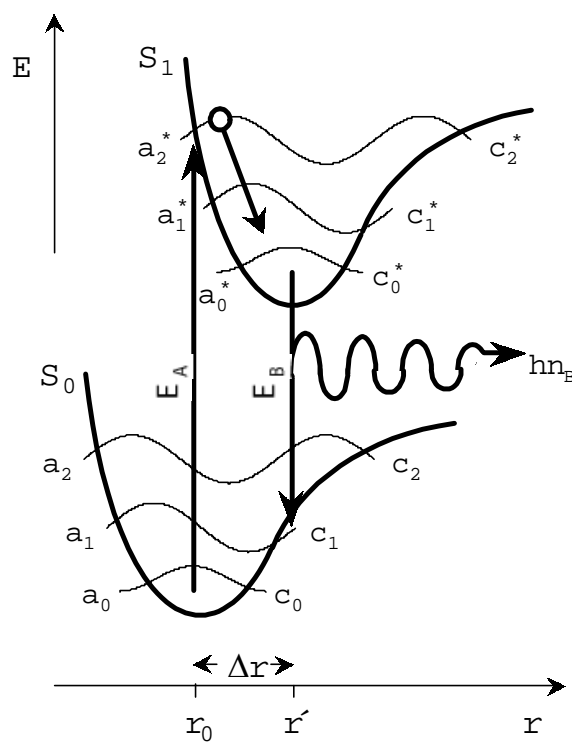


**Figure 2-5.** Franck-Condon-Shift in a diatomic molecule,  $r$  represents the interatomic distance [21].

Because the vibrational structure of the ground state and the excited state are very similar, the absorption and emission spectra have often mirror-like corresponding peaks. If a photon is absorbed, an electron is in most cases excited from the lowest vibrational level of the ground state to a certain vibronic level of the excited state (transition  $E_A$  in Figure 2-5) depending on the energy of the absorbed photon. Each peak in the absorption spectrum corresponds to a transition to a certain vibronic state (see Figure 2-13 for PVK). The emission of the photon is the opposite process where the electron relaxes in most cases from the lowest vibronic level of the excited state to a certain vibronic level in the ground state. This feature is illustrated in Figure 2-6 showing the absorption and emission spectrum of a green emitting polymer (2-Methoxy-5-(2'-ethylhexyloxy)-1,4-phenylenevinylene copolymer).

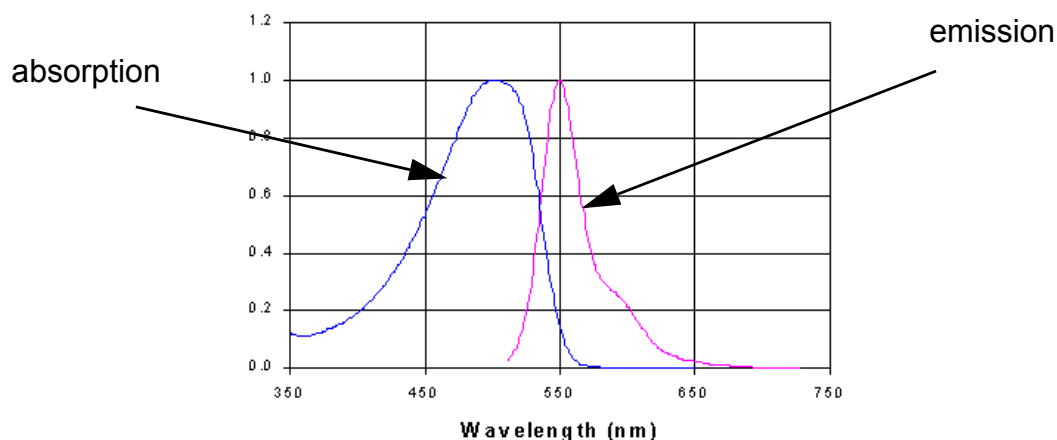


**Figure 2-6.** Absorption and emission spectra of 2-Methoxy-5-(2'-ethylhexyloxy)-1,4-phenylenevinylene copolymer [22].

## 2.3 Energy Transfer

Beside the observed absorption and emission of one moiety, excited molecules can transfer energy and electrical charges to neighboring molecules.

### 2.3.1 Förster Transfer

Förster transfer describes the migration of energy by resonant coupling of electrical dipoles from an excited molecule (donor) to a non-excited molecule (acceptor) as shown in Figure 2-7 [23]. The mechanical equivalent to this process are coupled pendulums where the amplitude of one pendulum increases while the amplitude of the other one decreases due to energy migration. Because of its electrostatic (Coulombic) character, Förster transfer can occur over relatively long distances (30 to 100 Å).

A missing electron (hole) in the ground state and an electron in the higher energy level with antiparallel spin form a singlet exciton. A molecular orbital can be occupied by two electrons with opposite spin. Therefore, for the electron to be able to relax from the higher energy level, its spin has to be the opposite of the electron already occupying the ground state. Because of that, only singlet excitons contribute to this transfer. Due to spin conservation, the created exciton on the acceptor has to be a singlet, too [16]. Förster transfer is a very fast process ( $\sim 10^{-9}$ s).

For efficient Förster transfer, the emission spectrum of the donor and the absorption spectrum of the acceptor have to overlap sufficiently.

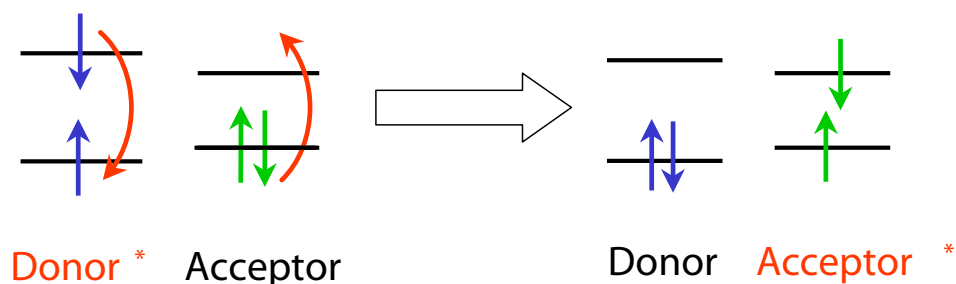


Figure 2-7. Förster transfer [21].

### 2.3.2 Dexter Transfer

In contrast to excitation by Förster transfer, which does not involve any transport of charge, a molecule can be excited if an exciton diffuses from donor to acceptor as (Figure 2-8) by transferring an electron and a hole at the same time [24]. Because the transfer rate is proportional to the overlap of molecular orbitals, Dexter transfer is limited to relatively short distances ( $\sim 10$  Å) and is attenuated exponentially with intermolecular distance. Due to spin conservation, only singlet-singlet or triplet-triplet transfer is allowed [16].

Also for efficient Dexter transfer, the emission and absorption spectra have to overlap sufficiently.

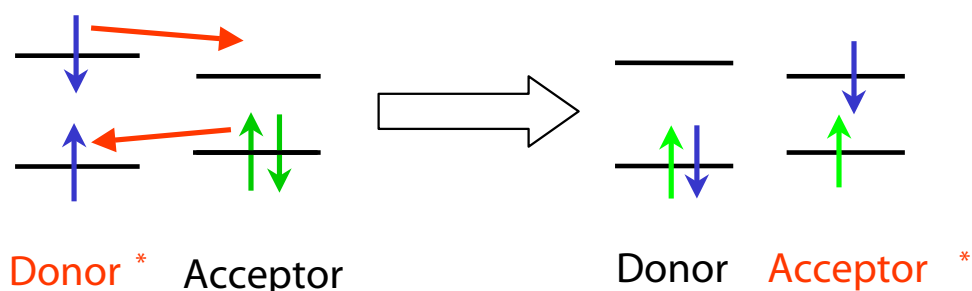


Figure 2-8. Dexter transfer [21].

## 2.4 Charge Transfer

Electrical conduction is based on carrier transport due to an external electric field. This means that in a polymeric material, the charge carrier has to be transferred from one

molecular orbital to another molecular orbital. The transfer probability is proportional to the square of the overlap integral of the electronic wave function of these orbitals. In addition, the energy difference between these states is of great importance for the transfer: If the difference is too big (much more than  $kT$ ), the carrier is “trapped” in the state with lower energy, because its thermal energy is insufficient to transfer to the energetically higher state. In case the difference in energy between the states is on the order of  $kT$ , the carrier might be able to overcome the energy difference and thus move from one molecule to the next.

Given a sufficient orbital overlap between the molecules, electrical charge can be transferred from a higher energy level to a lower one on a different molecule. As an example, Figure 2-9 shows a molecule A with an additional electron in the LUMO (negatively charged) whereas molecule B has a hole in the HOMO (positively charged). The electron and the hole can be transferred at different times to a dye molecule where they recombine. This fact impacts the emission characteristics of doped polymer devices as discussed in detail in Chapter 2.9.

## 2.5 Electroluminescence and Charge Injection

In the context of this work, excitation by injection of electric charge is the most important mechanism. If an electron is injected into a polymeric material by means of an external electric field, it will have to occupy a LUMO state because all states below the HOMO are occupied. In this case, no emission can occur because the excited electron is unable to relax. Therefore, to obtain emission from the material, electrons and holes have to be injected at the same time. Both carriers then travel through the material in opposite direction under the influence of the external electric field. For fluorescent materials, the emission of a photon occurs when singlet excitons, formed by the coulombic interaction of electrons and holes with opposite spin states, radiatively decay to the molecular ground state. The region where this process occurs is referred to as the recombination zone. In the ideal case, all injected electrons recombine with a hole, i.e. the same number of electrons and holes has to be injected. The concept of “balanced injection” of carriers is an important aspect for the choice of materials (see Chapter 2.6.2) [25]. A significant disadvantage of fluorescent EL compared to PL is that emission can only occur from singlet excitons, lim-

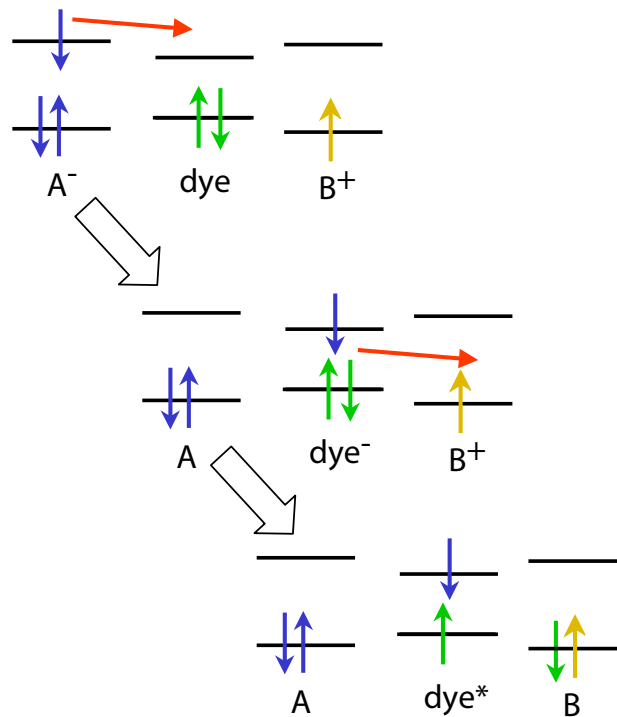


**Figure 2-9.** Excitation by charge transfer: From a negatively charged molecule A an electron is transferred to a dye molecule. Similarly, a hole is transferred from a positively charged molecule B. After these transfers, the dye molecule is left in an excited state.

iting the electroluminescence efficiency (emitted photons per injected electron) in fluorescent materials to less than 25% [26]. Theoretically, the PL efficiency can be unity because in this case all electron-hole pairs form singlet excitons.

Recently, phosphorescent materials have been investigated for use in OLEDs [27]. Due to spin-orbit coupling of a heavy metal ion in the emissive molecule, the transition probability from a triplet state becomes dominant. Using triplet states as well as singlet states by phosphorescent materials will increase the upper efficiency limit of fluorescence. Devices with very high efficiencies have been demonstrated [28].

## 2.6 Single Layer OLED

The device structure of a single layer polymer light-emissive device is intriguingly simple: A polymer film is sandwiched between two electrodes. Applying a electric field across the polymer will eventually lead to injection of charges into the film as shown in Figure 2-10. As mentioned in 2.5, the choice of material is of great importance for balanced

charge injection and thus for the device efficiency. The work function of materials used as contacts should closely match the HOMO or LUMO level of the electroactive material to provide a good contact. In addition, at least one of the electrodes has to be transparent to allow emitted photons to escape.

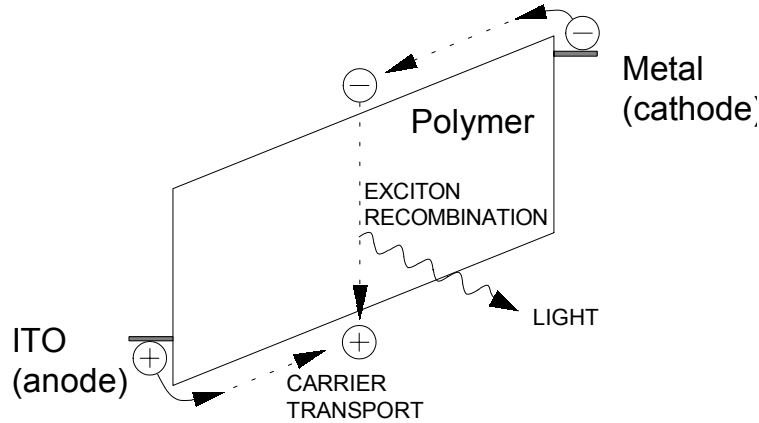


**Figure 2-10.** Band diagram of an OLED.

### 2.6.1 Indium-Tin-Oxide

Commonly used as the transparent and hole injecting contact (anode) is indium-tin-oxide (ITO). The material is transparent, conductive and has a reasonably high work function (4.5 to 5 eV). Indium oxide ( $\text{In}_2\text{O}_3$ ) is a wide band-gap semiconductor. To modify the conductivity of the material, indium oxide is degenerately doped with tin. To obtain films,  $\text{In}_2\text{O}_3$  and  $\text{SnO}_2$  are usually simultaneously sputtered onto transparent substrates such as glass in a molar ratio of 91% : 9%. Because ITO is non-stoichiometric, the electronic properties depend on the preparation and cleaning processes used. An oxygen plasma treatment can increase the work function by as much as 0.5 eV and thus increase the efficiency of the device [29][30][31].

### 2.6.2 Cathode Materials

The material used as a cathode should have a low work function, like alkali metals, for good electron-injecting properties. However, all of these metals, for example lithium, are also more likely to react with either the emissive material or with the surrounding atmosphere leading to device degradation. The device stability can be enhanced by using alloys containing these metals in a matrix of more stable metals like silver or aluminum.

### 2.6.3 Device Structure

The basic structure of a single layer device is shown in Figure 2-11: The ITO film is deposited as a blanket film on the glass substrate. If needed, the film can be easily patterned using conventional photolithography and wet-etching (see Chapter 2.8.1.1). The polymer layer is formed by spin-coating from solution. The resulting film is usually about 100 nm thick. The thickness strongly depends on the spin speed and the concentration of the polymer in the solvent as described in more detail in Chapter 2.11. The cathode metal layer is deposited by thermal evaporation. Several techniques to pattern the metal cathode are introduced in Chapter 7. In most cases in this thesis, however, the metal was evaporated through shadow masks to form the desired pattern.

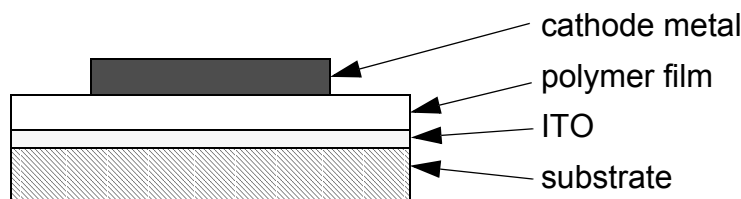


**Figure 2-11.** Structure of a single layer polymer light-emitting device.

## 2.7 Organic Materials

### 2.7.1 Electron and Hole Transport Materials

The electroactive polymer used in most experiments reported in this thesis is poly-(9-vinyl-carbazole) (PVK). In contrast to conjugated polymers (such as poly(*p*-phenylene vinylene), PPV), where the polymer-backbone consists of carbon-carbon bonds with  $\pi$ -orbitals, PVK has a fully saturated backbone, i.e. none of the carbon-carbon bonds is a double bond. The chemical structure of PVK is shown in Figure 2-12. The optical and electrical characteristics of PVK are mainly defined by the carbazole side-groups attached to the inactive polymer backbone [32]. This property is illustrated in Figure 2-13. The PVK and the carbazole monomer have very similar absorption spectra. The PVK we used has a molecular weight of 1,100,000 g/mole. It was obtained from Aldrich, Milwaukee, IL) and usually used as received. In some cases, the PVK was purified by dissolving it in chloroform (500 mg PVK in 10 ml solvent). After the solution was mixed with methanol (10 ml),

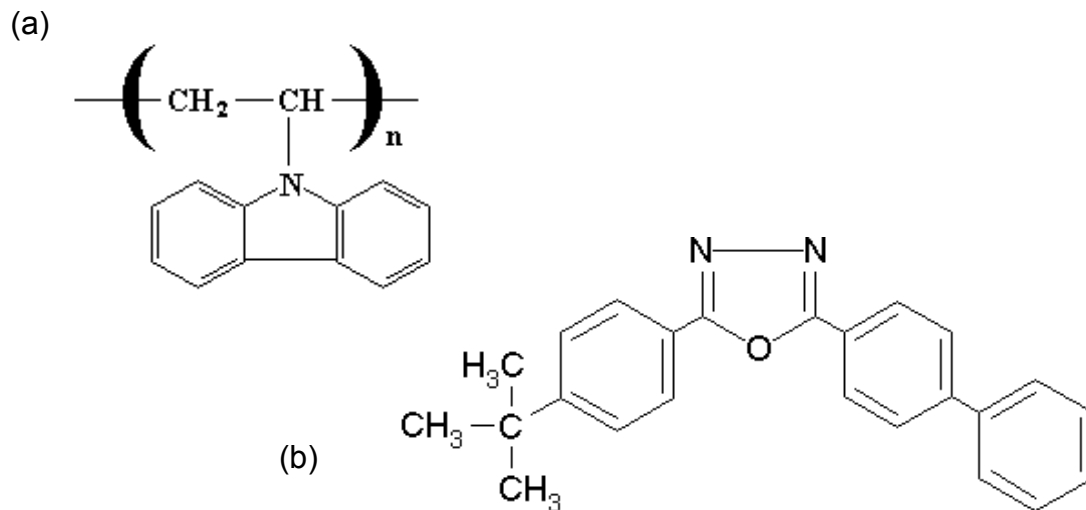


**Figure 2-12.** Chemical structure of (a) poly-(9-vinyl-carbazole) (PVK) and (b) 2-(4-Biphenyl)-5-(4-*tert*-butyl-phenyl)-1,3,4-oxadiazole (PBD)

the polymer precipitated. The polymer flakes were then filtered out and dried in vacuum at 70 °C for 3 hours.

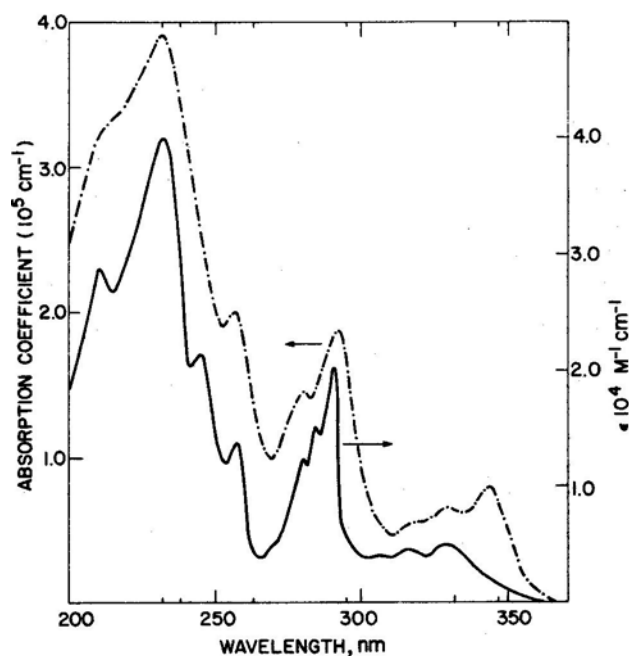


**Figure 2-13.** Absorption spectra of a solid PVK film (dotted line) and of a solution of N-isopropylcarbazole in hexane (solid line) [32].

Polymers tend to have a low electron affinity and high hole mobility [33]. To improve the performance of the device by tuning the ratio of injected electrons and holes and emission properties, multilayer devices have been reported [34]. This method is especially appealing for devices based on small molecules because different layers of material can be thermally deposited successively. Polymer blends represent a different approach: By blending different materials (polymers as well as small molecules) in solution, the transport characteristics and emissive properties of the organic film can be changed [35]. To compensate for the lack of electron-transport in PVK, a small molecule with electron transporting properties 2-(4-Biphenyl)-5-(4-*tert*-butyl-phenyl)-1,3,4-oxadiazole (PBD, also obtained from Aldrich and used as received) was added to the polymer solution. The concentration of PBD in PVK for optimum EL efficiency in one specific case was established to be 28.6% by weight in the final film [36]. The HOMO and LUMO levels along with the peak of the emission spectrum of these materials are listed in Table 2-1.

**Table 2-1.** HOMO levels, LUMO levels and wavelength of the peak emission of materials used in experiments. The wavelength of the peak emission was measured in devices with optimal dye concentration.

	HOMO [eV]	LUMO [eV]	peak emission [nm]	reference
PVK	5.54	2.04	380	[37]
PBD	6.6	2.7	390	[38]
C47	5.37	2.49	420	[37]
C6	5.39	2.93	495	[37]
Nile red	5.3	3.49	600	[37]
bimane			435	[40]

### 2.7.2 Emissive Materials

Due to the energy transfer mechanisms (outlined in Chapter 2.3), the introduction of guest molecules with HOMO-LUMO energy levels between those of the host material and with high fluorescence efficiency (emitted photons per absorbed photons) can enhance the performance of the device as well as tune the emissive color. Materials with a high fluorescence efficiency are called dyes or chromophores. This concept of dye-doping was first introduced by Tang *et al.* [39]. In our experiments, we doped the PVK/PBD blend using the following dyes: Coumarin 47 (C47, Lambda Physik, Göttingen, Germany) for blue devices, Coumarin 6 (C6, also obtained from Lambda Physik) for green and Nile red (obtained from

Aldrich, Milwaukee). In some experiments the dye 9,10-Dioxa-*syn*-dimethylbimane (bimane, obtained from M.E. Thompson, University of Southern California, Los Angeles) was used [40]. The HOMO and LUMO levels of these materials are also given in Table 2-1, and the chemical structures are shown in Figure 2-14.

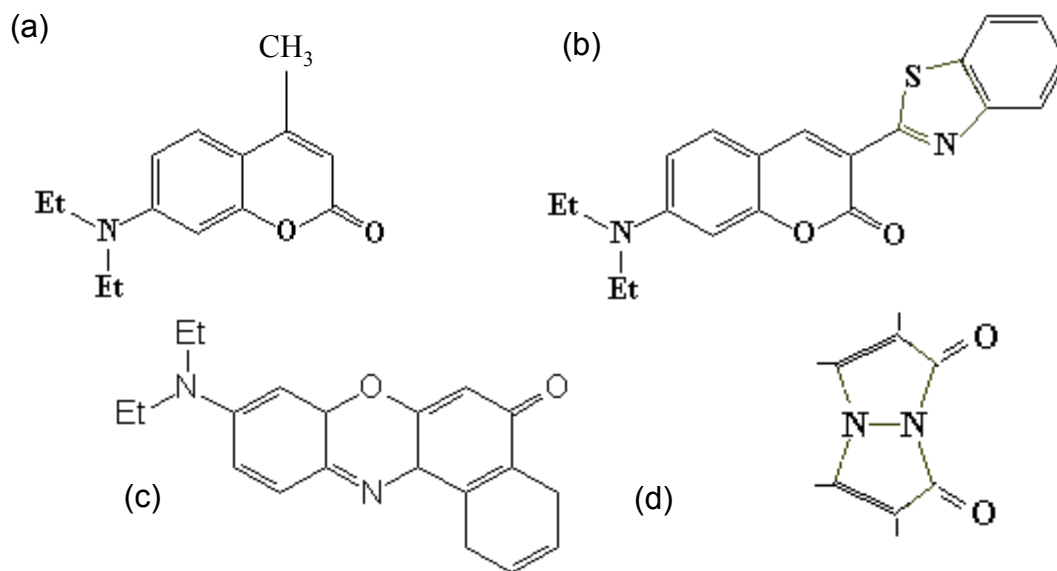


**Figure 2-14.** Chemical structure of (a) Coumarin 47, (b) Coumarin 6, (c) Nile red, and (d) bimane

The electroluminescence efficiency of the device increased drastically when a dye was incorporated into the polymer matrix. Best results were obtained for C6. The device efficiency depends strongly on the dye concentration as discussed in more detail in Chapter 2.10. The following weight ratios PVK:PBD:dye for optimal device performance were established: For C47: 100:40:1, for C6: 100:40:0.3, for Nile red: 100:40:0.2 [37][41], and for bimane: 100:40:0.2 [42].

## 2.8 Device Fabrication and Characterization

Specific fabrication processes pertaining to patterning are described in more detail in later chapters. However, some of the processing steps are common to all fabricated devices. For the sake of brevity, the fabrication process of a “standard” single layer OLEDs is outlined at this time. If not mentioned otherwise, the discussed devices were fabricated using the following procedures:

## **2.8.1 Device Fabrication**

Devices were fabricated on ITO-coated glass substrates. The coated glass sheets were obtained from Applied Films Corp., Longmont, Colorado. The ITO film is about 1200Å thick (resulting in a sheet resistance of  $30\Omega/\square$ ), and has a RMS roughness of about 25Å. The glass substrate is 1.1mm thick.

### **2.8.1.1 Patterning of ITO substrate**

In case a patterned ITO film was required, the film was etched after conventional photolithography using the following wet-etch solution: 50 ml deionized (DI) water, 45 ml HCl and 5 ml  $H_3NO_4$ . The films were etched for about 2 min at elevated temperatures (about 50 °C; lowest setting on the hotplate). After the etch, the conductivity was measured to ensure the complete removal of the ITO layer.

### **2.8.1.2 Substrate Cleaning**

The substrate was cleaned in an automatic cleaning process by first brushing the surface using a soap solution (Tergitol and deionized (DI) water), second by cleaning the surface with a high pressure DI water jet, and finally by blowing the substrate dry with a nitrogen jet. This was done in a Photomask Cleaner (Ultra-t Equipment Co. Inc., Model 602).

### **2.8.1.3 Oxygen Plasma Treatment**

The substrate (with the ITO side up) was then transferred into a parallel plate reactor (10" diameter) for the oxygen treatment to raise the work function of the ITO [30]. The following process parameters were used: oxygen flow: 25 sccm, plasma power: 25 W, chamber pressure: 150 mTorr, process time: 4 min.

### **2.8.1.4 Polymer Deposition**

The polymer layer was then deposited onto the ITO substrate by spin coating in a nitrogen-filled glove box. The polymer solution contained 100 mg PVK, 40 mg PBD, and the appropriate amount of dye in 7.0 ml chlorobenzene. The dye was added from a pre-mixed dye solution with a dye concentration of 1 mg dye per 1 ml chlorobenzene. Using a disposable pipette, the polymer solution was dropped onto the substrate which was placed on the spinner chuck. In contrast to photoresist, the PVK solution has a very low viscosity.

To obtain a uniform polymer film, it was necessary to cover the whole surface of the device with polymer solution before spinning. A spin speed of 2000 rpm yielded films 800 to 1000 Å thick. The dependency of the morphology and the film thickness will be the focus of a later section (Chapter 2.11). During the 60-sec spin cycle, the solvent evaporated and the sample was then transferred into the evaporator. Since the evaporator was not connected to the glove box, the sample was exposed to air for a brief period of time.

### **2.8.1.5 Cathode Metal Deposition**

A shadow mask with 2 mm<sup>2</sup> holes was often used to pattern the cathode during the evaporation of the cathode metal. A recessed notch in the sample holder made sure that the shadow mask never made contact with the polymer film. After the pump down cycle, the metal was evaporated at a starting pressure below 10<sup>-6</sup> Torr. However, depending on the metal used, the pressure could rise considerably during the evaporation process. Magnesium often lead to a pressure of close to 10<sup>-5</sup> Torr before it decreased again. The most commonly used cathode was an alloy of silver and magnesium. In this case, these metals evaporated simultaneously. The evaporation rate and film thickness was controlled automatically using independent crystal monitors as the sensors. Each of the crystal monitors was placed in close proximity to the metal source to be able to control the evaporation rate independently for each source. The film was deposited with an evaporation rate of 7Å/sec for magnesium and 0.7 Å/sec for silver, resulting in a film of approximately 1 part of silver to 10 parts (by weight) of magnesium to obtain a stable alloy. The total thickness of the Mg:Ag film was 500 Å. A capping layer (again 500 Å) of pure silver was then evaporated to protect the Mg:Ag layer from corrosion. The sample was rotated during the evaporation with a speed of about 12 rpm.

After the cathode deposition, the finished sample was transferred back into the glove box for electrical characterization.

### **2.8.2 Device Characterization**

To contact the device on the probe station, a needle probe was lowered onto the ITO substrate. The soft polymer film was easily scratched off by the needle, so one could make good contact with the ITO as the anode. The cathode metal islands was contacted with a

thin gold wire to avoid mechanical damage to the cathode, which would cause short-circuited devices.

We used a Hewlett-Packard 4145B semiconductor parameter analyzer to measure the current-voltage characteristics (I-V) of the device. A large-area silicon photodetector (detector area 50 mm<sup>2</sup>) in close proximity to the OLED was used to measure the light output of the device. The OLED drive current  $I_D$  and the short-circuited photocurrent  $I_{ph}$  was simultaneously recorded. The external quantum efficiency  $\eta_{ext}$  of the device was obtained by calculating the following expression where  $Q$  is a wavelength dependent con-

$$\eta_{ext} = \frac{I_{ph}}{I_D} \cdot Q \quad (2-1)$$

version factor. This factor was determined by geometrical considerations and accounting for the response of the photodetector [37]. The value of  $Q$  was first established for a green device containing the dye C6. For other colors,  $Q$  was adjusted based on the wavelength of the emission maximum of the device and the response of the photodetector. This approach introduced a small error by assuming that all the light was emitted at this wavelength. The value of the conversion factor  $Q$  for different dyes is given in Table 2-2.

**Table 2-2.** Conversion Factor  $Q$  to obtain the external quantum efficiency.

dye (peak wavelength)	$Q$ [%]
C 47 (420 nm)	279
C 6 (495 nm)	220
Nile red (600 nm)	188
bimane (435 nm)	268

Emission spectra were measured with a Photo Science 650 spectrometer. In addition, CIE-color coordinates and brightness were extracted at the same time. The experimental set-up required the sample to be taken out of the glove box. We therefore always recorded the I-V characteristics before measuring the spectrum of the device. In Figure 2-15, the normalized EL spectra for the different dyes are shown. No emission from the PVK or the PBD could be detected. Therefore, the energy transfer to the dyes is very efficient.

Figure 2-16 shows a typical I-V curve of a fabricated OLED along with the photocurrent. The current stops rising at 0.5 mA because the current compliance was set to 0.5 mA.

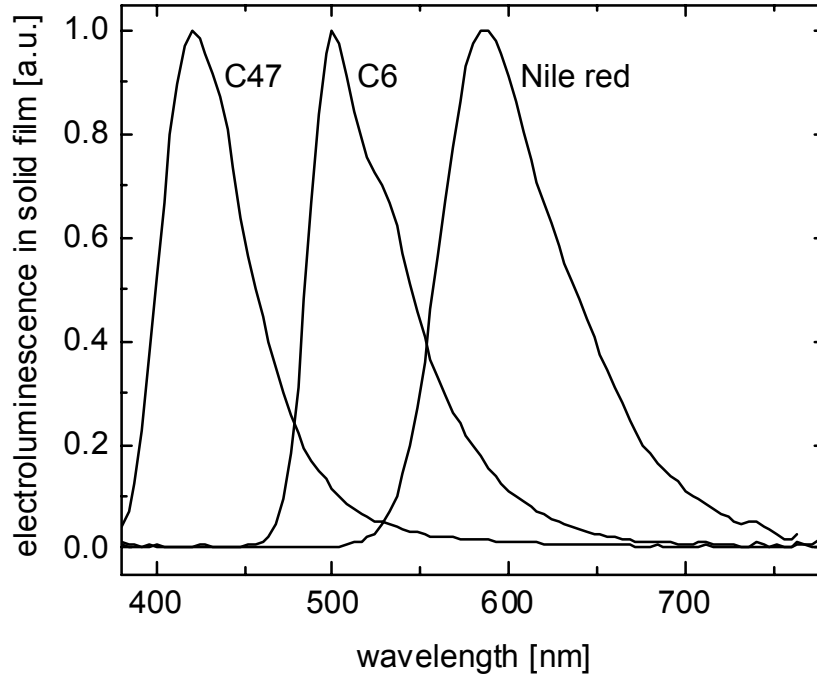


**Figure 2-15.** Electroluminescence spectra of standard PVK/PBD devices doped with either C47, C6 or Nile red.

## 2.9 Electroluminescence versus Photoluminescence

The integration of multiple dyes in the polymer film has been the focus of research to either obtain white emitting OLEDs [43][44][45][46][47][48][49][50] or to enhance the efficiency of a dopant by introducing an assist dopant which increases the transfer probability [51][52].

Because of the different excitation mechanisms of photoluminescence and electroluminescence, the emission spectra can be quite different when a single or multiple dyes are present. Figure 2-18 shows the EL (at 50 mA/cm<sup>2</sup>) and the PL spectrum at room temperature of a device with 0.3 mg C47 (blue) and 0.3 mg Nile red added to the PVK/PBD/chlorobenzene solution. The photoluminescence spectrum was recorded under UV illumination ( $\lambda = 254$  nm). Whereas the EL spectrum is dominated by the emission from the Nile Red, the PL spectrum shows two distinct peaks, one from each of the dyes. To first order, the

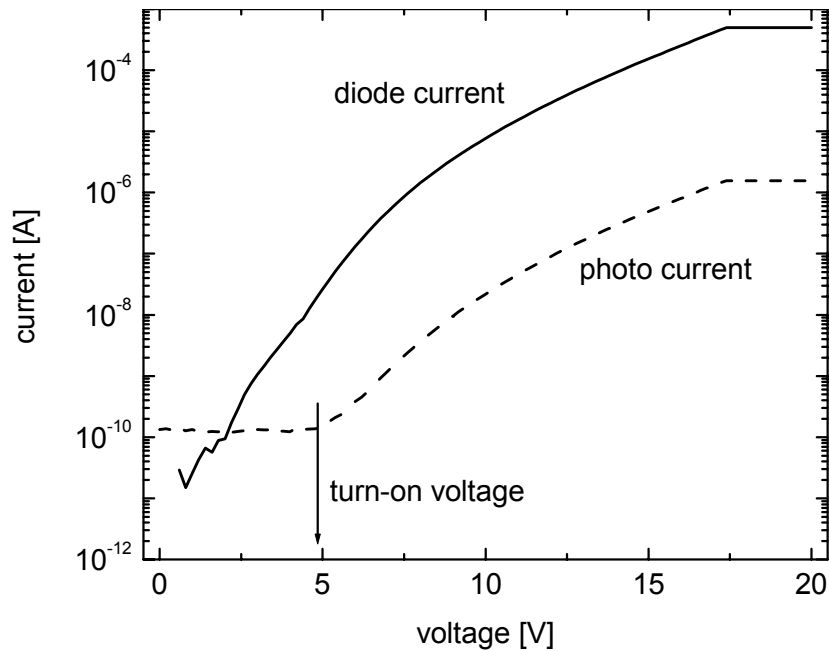


**Figure 2-16.** Current-voltage characteristics of a standard PVK:PBD:C6 device. The detected photocurrent is also shown. The device area was  $2 \text{ mm}^2$  and the thickness of the polymer film was  $800 \text{ \AA}$ .

EL spectrum does not depend on the current density over a range from  $5 \text{ mA/cm}^2$  to  $500 \text{ mA/cm}^2$  (Figure 2-17). Qualitatively similar results were seen with C6 and Nile red mixtures, where again the EL occurs almost exclusively from the dye with the longer emission wavelength. Other research groups have reported similar observations [48][53].

Excitation of the dye can be accomplished by either energy transfer or sequential charge transfer from the host to the dye. In the case of energy transfer, an exciton is formed at a host molecule, which is then transferred to the dye by either resonant coupling or by coherent charge exchange (Förster or Dexter transfer, respectively) [16]. For excitation by charge transfer, electrons and holes from the host are sequentially trapped by the dye, resulting in exciton formation on the dye and then photon emission due to exciton decay.

Because the dye concentration is very low in the polymer film, the photoluminescence process begins with the creation of singlet excitons in the host polymer. That the emission occurs from both dyes but not from PVK implies that (i) the excitons created on the PVK are transferred to the dye much faster than the radiative lifetime of an exciton on PVK, and (ii) that once captured on the dye, no exchange of excitons between the dyes

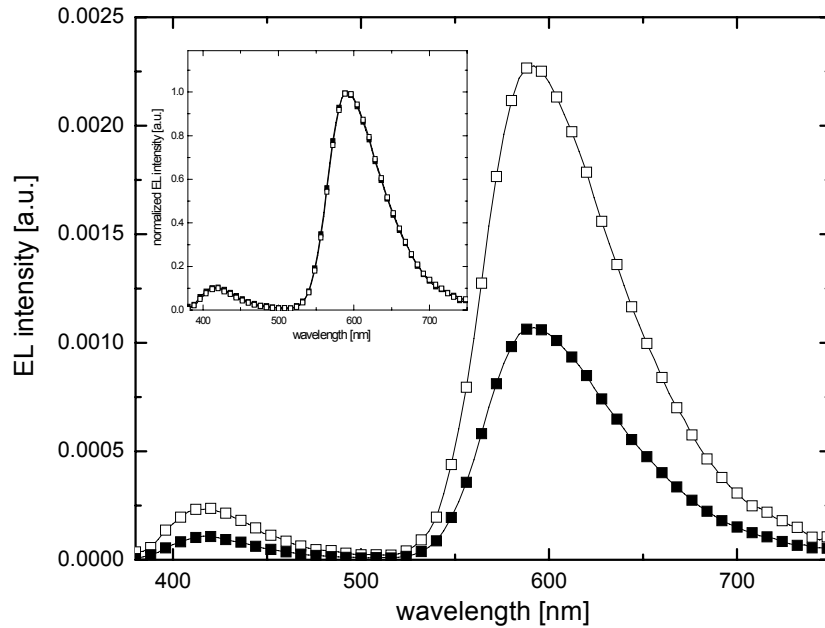


**Figure 2-17.** EL spectra of PVK/PBD devices containing the dyes C47 and Nile red at 50 mA/cm<sup>2</sup> (closed symbols) and 100 mA/cm<sup>2</sup> (open symbols). The inset shows the normalized spectra of these devices. No spectral change could be detected.

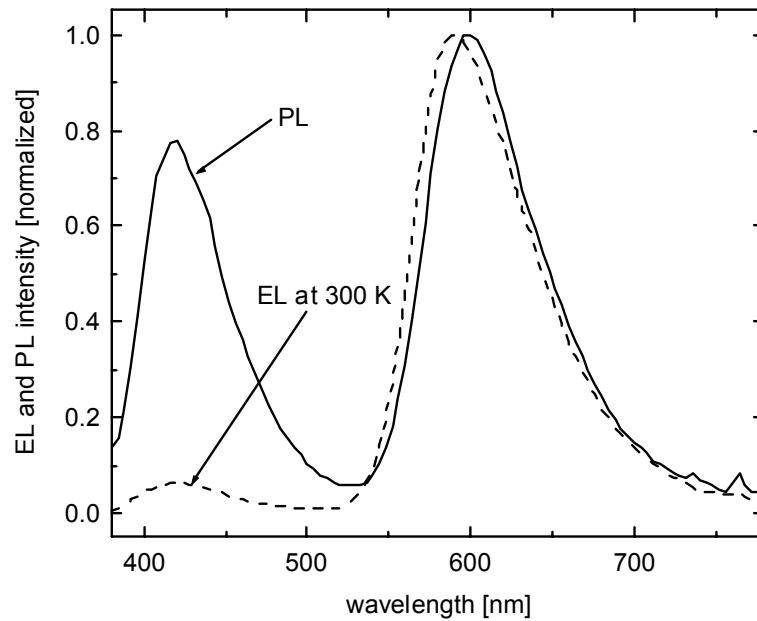


**Figure 2-18.** Photoluminescence (solid line) and electroluminescence (dashed line, 50 mA/mm<sup>2</sup>) of a PVK/PBD film containing the dyes C47 and Nile red. [54]

occurs (which would otherwise lead to emission from the dye with the longest emission wavelength only). This process is shown in Figure 2-19. Excitons on the dyes presumably do not interact because either they are too far apart or the spectral overlap for Förster or

Dexter is insufficient. For an efficient Förster transfer, these emission and absorption spectra have to overlap sufficiently which is not the case as shown in Figure 2-20 (see also Chapter 2.3). Thus excitons captured by a dye (by Förster or Dexter transfer) lead to PL from that dye [57].

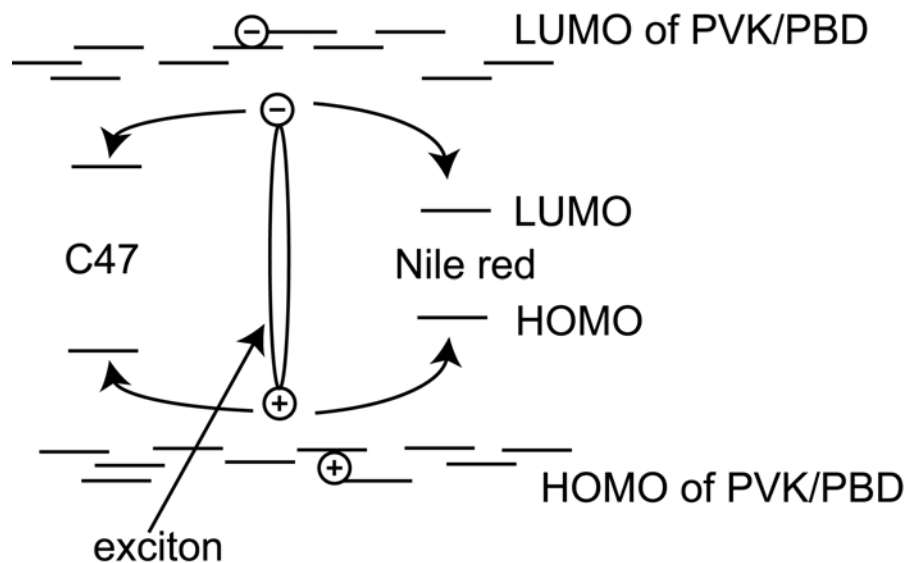


**Figure 2-19.** Process of excitonic transfer to both dyes in PL. The HOMO and LUMO states are represented by lines, and the small offset between the lines for the host HOMO and LUMO states shows the interaction of the orbitals resulting in a small shift in energy.

That the EL spectrum is very different from the PL spectrum means that singlet excitons are not created in EL in the host, implying that the sequential capture of electrons and holes (and exciton formation followed by light emission) occurs directly on the dye. Similar observations have been reported elsewhere [58]. Because the EL spectrum shows emission primary from the dye with the longest wavelength, we hypothesize that the lifetime of the first captured carrier (electron in a LUMO state or hole in a HOMO state) is long compared to the exciton lifetime. These first-captured carriers cannot recombine until a singlet exciton is formed, i.e. an electron and a hole of opposite spin are captured by the same molecule. Therefore the initially trapped carrier could be thermally re-emitted back to the host (Figure 2-21, process B) before the complimentary carrier is trapped and move relatively freely because of the small energy difference between the host states. Eventually, it will be re-captured by either dye after transport through the host. The release of carriers from the dye states will be slowest for dye states with the largest energy difference to the

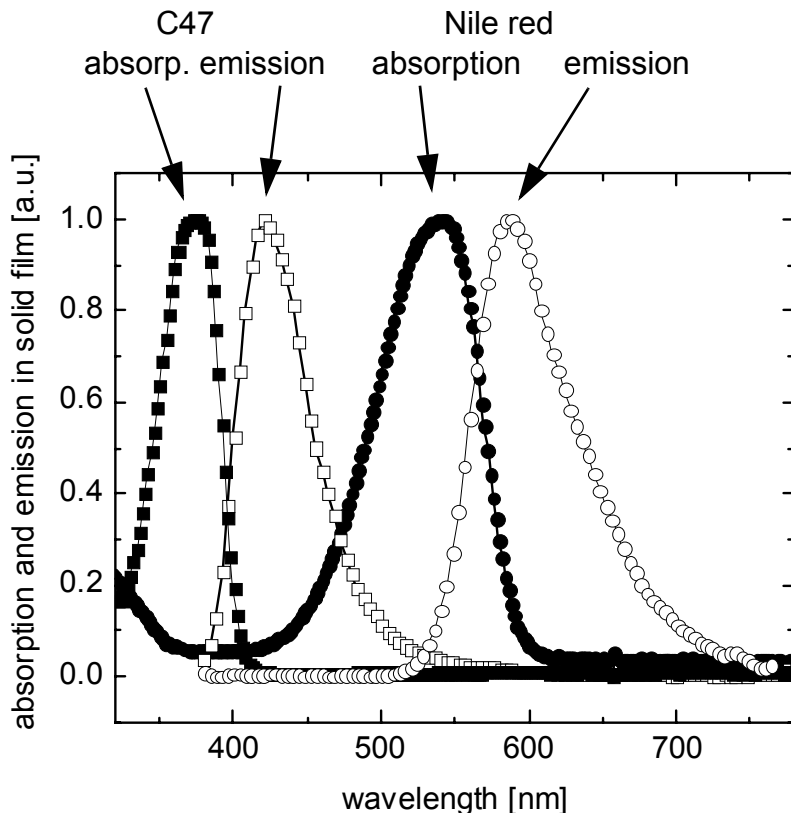


**Figure 2-20.** Absorption and emission spectra of C47 and Nile Red [56] in solid film.

relevant host HOMO/LUMO levels. Therefore the accumulation of carriers in these deep states will occur, leading to the eventual capture of the opposite carrier, and exciton formation followed by light emission. Assuming a level alignment such that the dye with the lowest exciton energy has its HOMO/LUMO levels farthest from the host level (see Figure 2-21), light emission will preferably occur from the dye with the longest wavelength. Therefore, in EL, nearly all emission was observed from Nile red. (Figure 2-21 arbitrary assumes that the initially trapped carrier is an electron.)

In support of this model, the EL emission from C47 increased significantly when the device was cooled (Figure 2-22). This implies that carriers, which were re-emitted from a C47 level in liquid nitrogen (process B in Figure 2-21) at 300 K to be re-trapped by a Nile red state (process C), could not escape from the C47 level at lower temperatures. This, in turn, increases the probability that a singlet exciton can be formed on a C47 molecule, explaining the increased emission from this dye at lower temperatures.

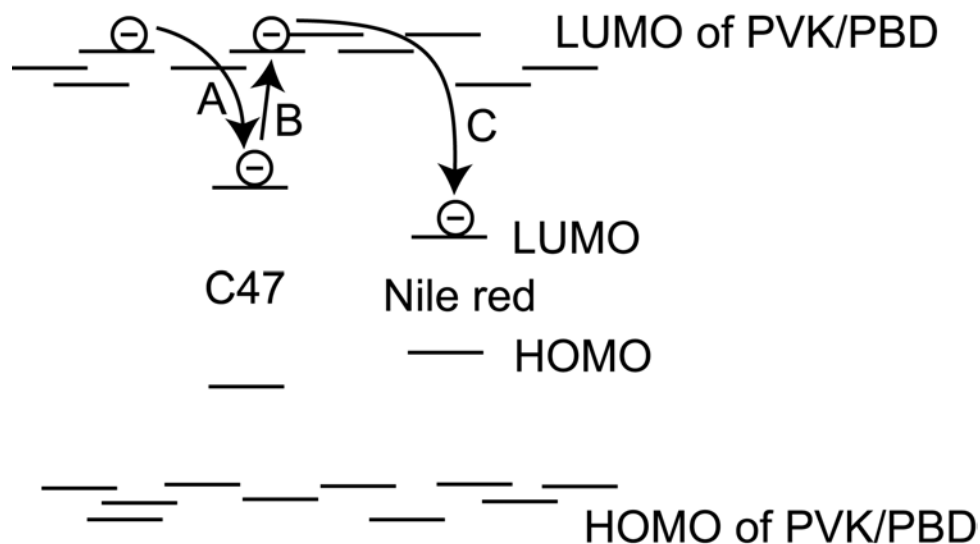


**Figure 2-21.** Schematic energy level diagram showing electron capture (process A and C) and thermal re-emission (process B) in a PVK/PBD device containing C47 and Nile red [54].

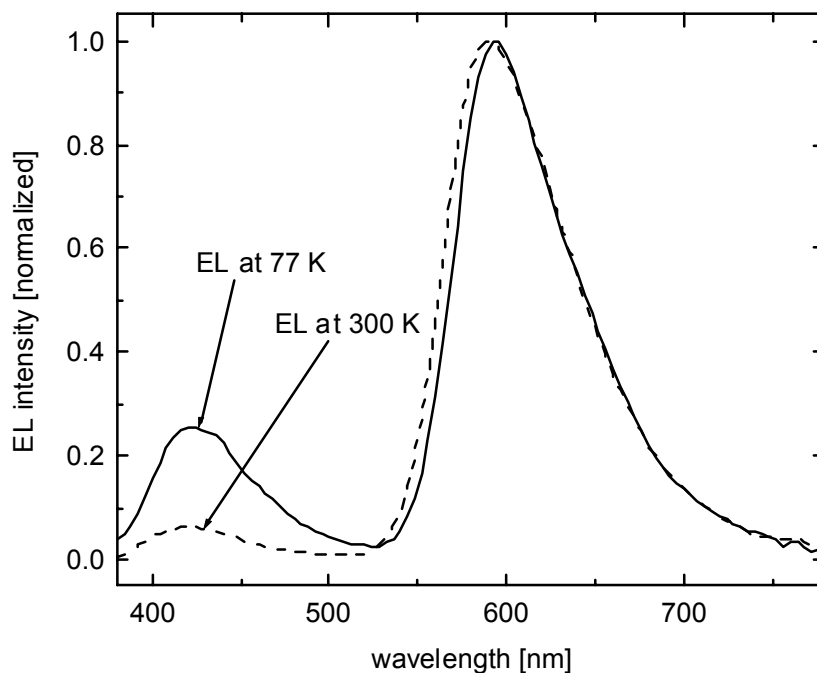


**Figure 2-22.** Normalized electroluminescence ( $50 \text{ mA/cm}^2$ ) spectrum at room temperature (dashed line), and at 77 K (solid line) of a PVK/PBD device containing the dyes C47 and Nile red.[54]

Detailed studies of the temperature dependence of the emission spectra remain to be carried out. It is possible that the EL from the dye with the wider energy gap at room

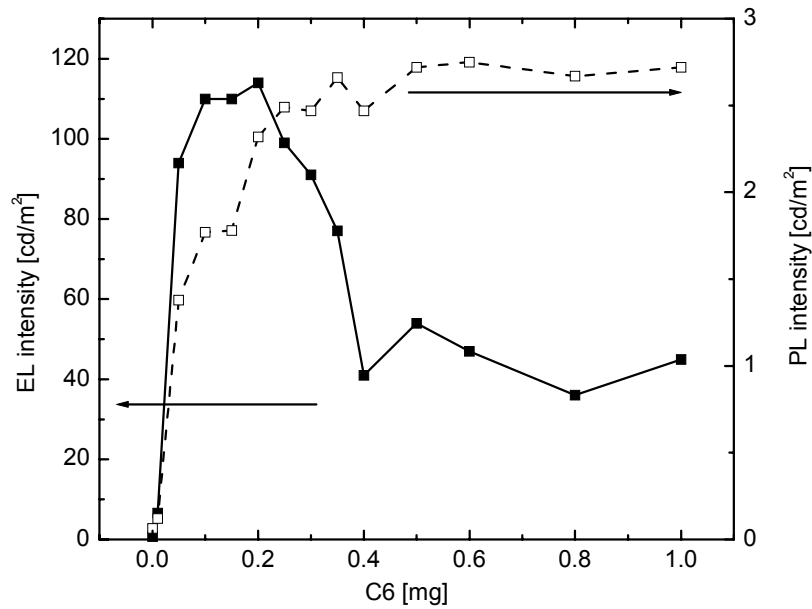
temperature is due to exciton formation in the host, and subsequent transfer to both dyes for emission in PL.

## 2.10 Efficiency versus Dye Concentration

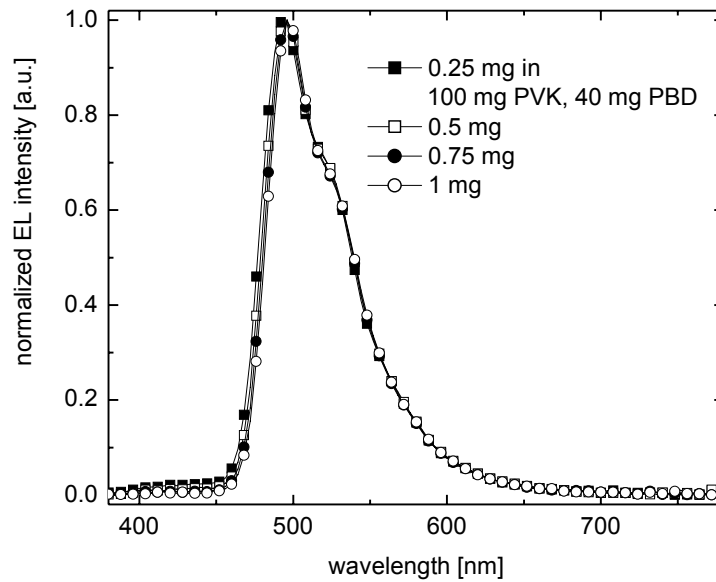
Incorporating molecules with a very high photoluminescence quantum yield (chromophores, dyes) into a host material to enhance the light output of an OLED has first been demonstrated by C.W. Tang [39]. This way, the device can be optimized by choosing a material emitting efficiently in the desired wavelength as a dopant and using the host material for charge or exciton transport. However, the performance of the device is strongly dependent on the concentration of the dye [41]. Figure 2-23 shows the EL luminance at a constant current (1 mA) of a PVK/PBD/C6 device (100mg : 40mg : x, where x is the x-axis in Figure 2-23). The luminance increases with dye concentration, reaches a maximum value and decreases again for higher dye concentrations. The initial increase in luminance is understandable because more excitons can be formed on the dye due to the increased number of dye molecules. In addition, the emission from the host decreases, indicating that more charges are getting trapped on the dye. Along with the EL luminance of the device, the PL luminance of the polymer film under constant illumination ( $\lambda=254$  nm) is also shown. The PL luminance also shows the initial increase due to the fact that more excitons are able to transfer to the dye. In contrast to the EL luminance, the PL luminance decreases only slightly at higher dye concentrations. The effect of EL luminescence quenching at higher dye concentrations has been reported earlier [35][37][53][58][59][60][61][62][63][64][65]. However, the striking difference between PL and EL intensity as a function of dye concentration has not previously explained.

Figure 2-24 shows normalized EL spectra (at 50 mA/cm<sup>2</sup>) for different concentrations of C6. The spectrum is dominated by the emission from the dye at very low concentrations and remains relatively unchanged thereafter.

One could argue, that because the chance that an electron and a hole are captured by the same dye molecule is less likely for an increasing number of possible sites, the probability of exciton formation decreases. Since the excess carriers have a limited lifetime, they will recombine non-radiatively. According to this argument, the EL efficiency should



**Figure 2-23.** Photoluminescence intensity (dotted line) and electroluminescence (at 50 mA/cm<sup>2</sup>) intensity (solid line) for a PVK/PBD device as a function of dye concentration (C6).



**Figure 2-24.** Normalized EL spectra (at 50 mA/cm<sup>2</sup>) of PVK/PBD devices with different C6 concentration.

recover with increasing carrier density, i.e. higher device current. However, we did not observe such a superlinear increase in EL luminance with device current as shown in Figure 2-25.

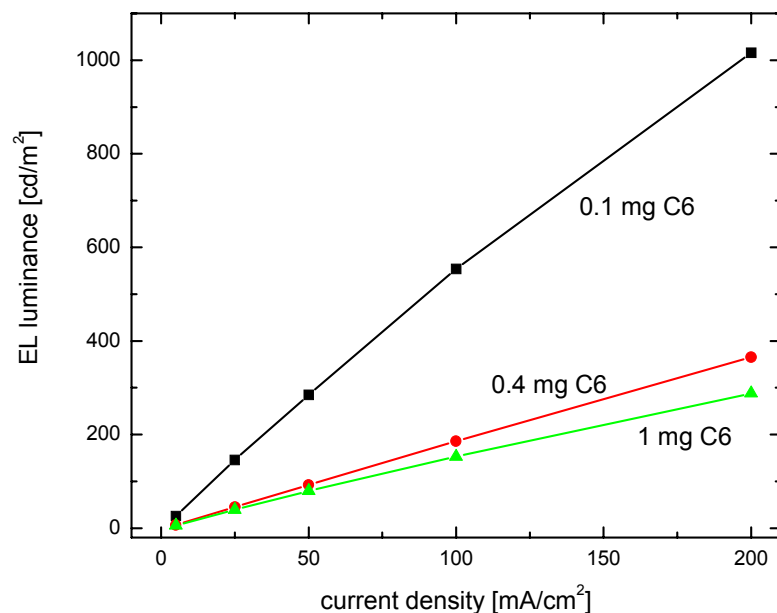


**Figure 2-25.** Luminance as a function of current density of a PVK:BPBD:C6 device with different dye concentrations. No superlinear increase in luminance was observed.

It is well known that dyes aggregate and form excimer states at high dye concentrations [58]. In this case, the exciton is delocalized over several molecules due to the increased intermolecular interaction [49][50][66]. These states decay with a much smaller radiative efficiency, an effect referred to as “dye self-quenching”. In addition, the emission spectrum is red-shifted compared to the emission of a single dye molecule. However, if this were the only effect at high dye concentrations, the EL and PL would be reduced similarly, which is not observed.

This difference in EL and PL efficiency at high dye concentrations may be explained using the same “two-dye” model (Figure 2-21), but with levels of an isolated dye (efficient light emitters) and dye-dye complexes (excimers, which are inefficient light emitters) representing the two separate sets of levels (Figure 2-26).

At high dye concentrations, in PL singlet excitons are captured and immediately decay both on the C6 dye and on the C6 excimer, which explains the slight reduction of PL intensity. As shown before, the main excitation mechanism in EL is sequential charge capture. Analogous to the argument that the dye with the smallest bandgap dominates the EL spectrum, most of the excitons will in this case form at an excimer site with a low radiative efficiency, even if there are only a relatively small number of them. Due to this mechanism,

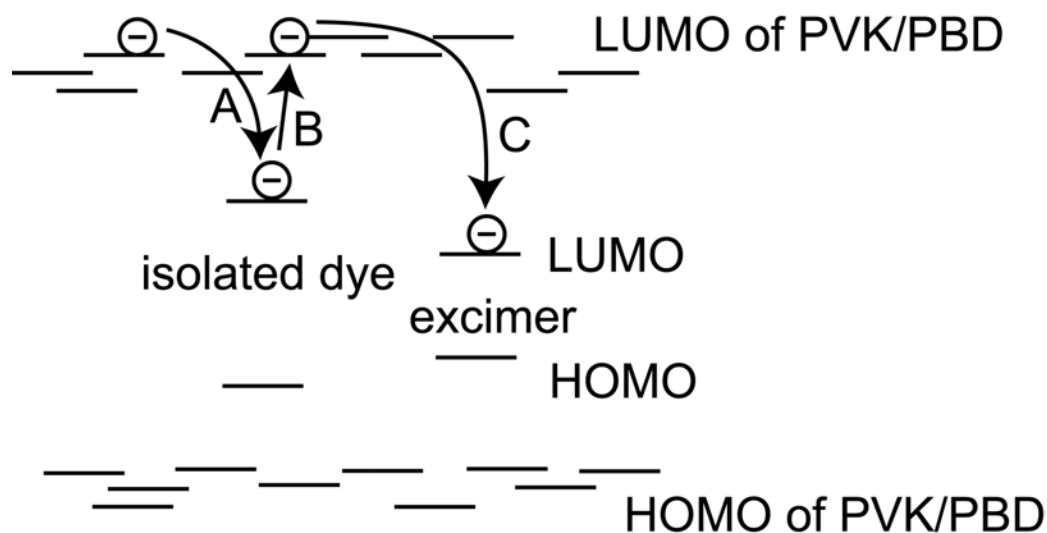


**Figure 2-26.** Schematic energy level diagram showing electron capture (process A and C) and thermal re-emission (process B) in a PVK/PBD device at high dye concentration with isolated dye molecules and excimer complexes. [54]

the EL efficiency decays faster than the PL efficiency at high dye concentrations. The EL spectra of devices with various C6 concentrations immersed in liquid nitrogen ( $9 \text{ mA/cm}^2$ ; shown in Figure 2-27) supports this argument. Due to reduced re-emission and thus less chance of excited carriers reaching the excimer, the EL intensity decay with dye concentration was much slower for the cooled device with a peak efficiency observed at a dye concentration of 0.5 mg (in 100 mg PVK and 40 mg PBD) vs. 0.1 mg for a room temperature device. The absolute efficiency of the cooled device was also higher than the room temperature device. This may be due to reduced de-trapping from emissive sites (to be captured on non-radiative sites). But it could also be due to other changes in the device at low temperatures (such as carrier mobilities etc.).

Similar results were obtained with other dyes: Figure 2-28 shows the characteristics for a PVK:PBD:C47 device (100mg : 40mg : x in the final film) and Figure 2-29 those of a PVK:PBD:NR device (100mg : 40mg : x). In both cases, the luminance was measured at room temperature and at a diode current of  $50 \text{ mA/cm}^2$ .

## 2.11 Surface Morphology of the Polymer Film

In addition to the choice of material and their composition, the polymer deposition process has a significant impact on the device performance. One major advantage of poly-

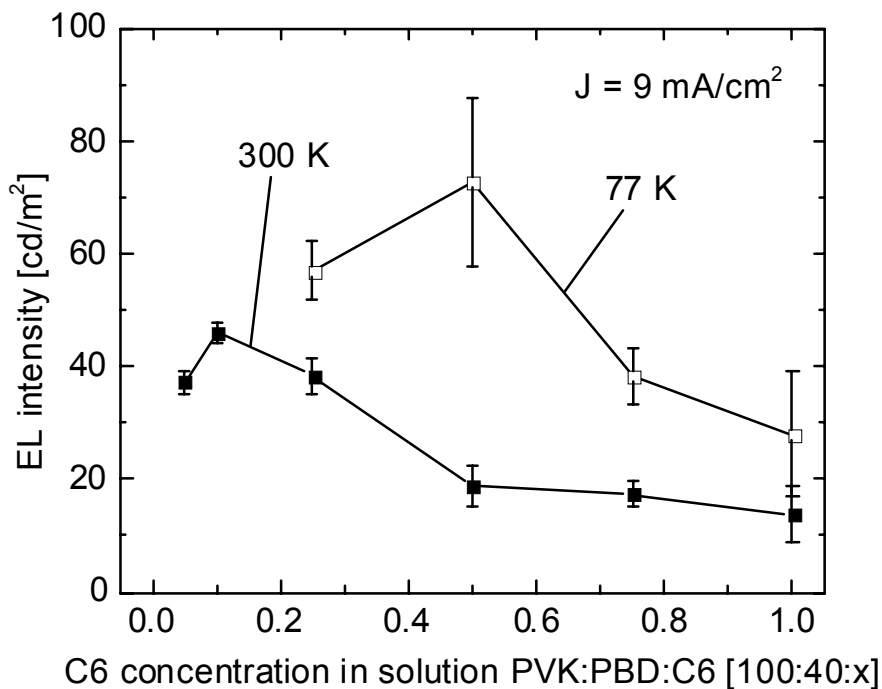


**Figure 2-27.** Electroluminescence intensity of a PVK:PBD:C6 device as a function of C6 concentration at room temperature (solid squares) and at 77 K (open squares). [54]

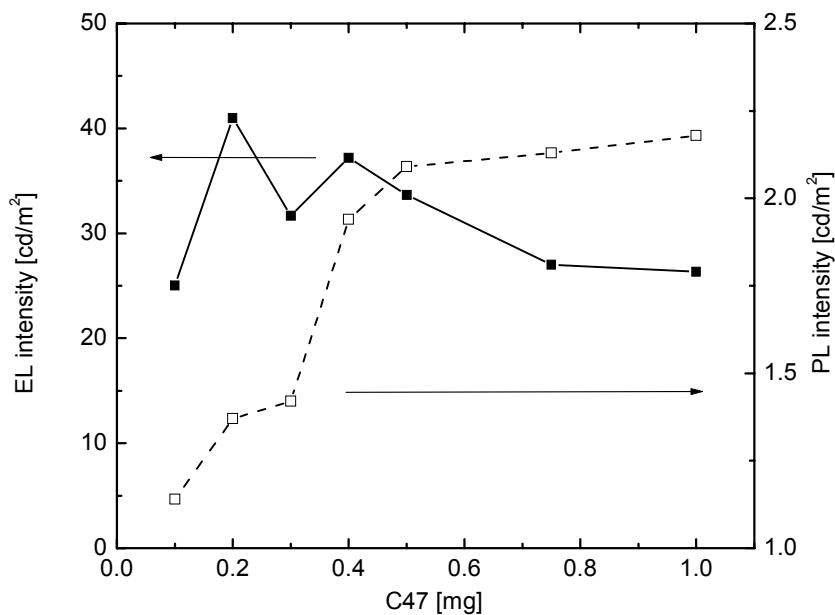


**Figure 2-28.** Photoluminescence intensity (dotted line) and electroluminescence intensity (solid line) for a PVK/PBD device as a function of dye concentration (C47).

mer-based OLEDs over those based on small molecules is the fact that the polymer can be deposited by spin-coating, a potentially very cost-effective processing step. In the micro-

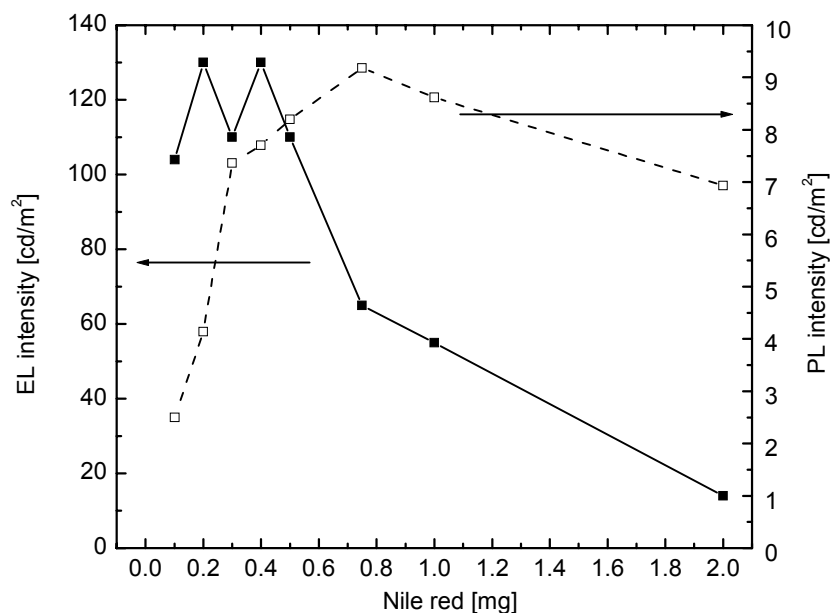


**Figure 2-29.** Photoluminescence intensity (dotted line) and electroluminescence intensity (solid line) for a PVK/PBD device as a function of dye concentration (Nile red).

electronics industry, spin-coating is a very common technique to deposit photoresist or spin-on glass. A few drops of polymer solution are dropped onto the substrate which is subsequently rotated horizontally at high speed. Due to radial force on the liquid, it spreads out wetting the whole surface of the substrate. While forming a film, the solvent evaporates leaving a homogeneous polymer film behind. Obviously, the spin speed is of major importance on the resulting film thickness. The thickness  $d$  of the film can be estimated using the following equation [67][68], where  $C_0$  is the initial polymer concentration,  $\nu_0$  is the initial

$$d = \frac{C_0 \sqrt[4]{\nu_0 D_0}}{\sqrt{\Omega}} \quad (2-2)$$

kinematic viscosity of the solution,  $D_0$  is the solute diffusivity, and  $\Omega$  is the spin speed. The ramping time, i.e. the time from the start of the process until the spinner has reached its nominal speed, does not have a major influence [69]. However, this equation does not take the evaporation of the solvent during the spin-coating process into account. The choice of solvent has a major influence on the film thickness: For solvents with low vapor pressure (i.e. the surrounding air will take up only a small amount of solvent before being saturated), the evaporation process will take longer than for solvents with a high vapor pressure. For

the same spin speed and polymer concentration, the film thickness will therefore be thinner for a low vapor pressure solvent (such as toluene) than for a high vapor pressure solvent (such as chloroform). Since the polymer solution containing the PVK is very dilute (typically 100 mg polymer in 7 ml solvent), the viscosity is very close to that of the pure solvent and thus very low. Because of the low viscosity and the wetting properties of the solution and the substrate, the solution does not spread out evenly while spinning. It was therefore necessary to cover the whole surface with the polymer solution before spinning.

Beside the work function lowering effect of the oxygen plasma in the ITO (see Chapter 2.8), the treatment also decreased the contact angle, i.e. the solution spreads out more evenly than on the pristine ITO surface.

Beside the spin speed and the concentration of the solution, the choice of solvent has an impact not only on the thickness of the polymer film but also on the morphology of the deposited film. During the spin process, the mass transport is caused by radial forces. But the solution is also exposed to tangential forces while the substrate is accelerated. The resulting forces cause the solution to exhibit a radial wave-like profile. If the solvent is evaporating too fast, this pattern is “frozen in”. The resulting film shows a radial pattern of hills and valleys leading to a non-uniform electric field distribution in the device. Figure 2-30 shows the EL micrograph of a device which was fabricated using chloroform as the solvent (PVK:PBD:bimane) at 2000 rpm where the ripples in the emission profile are caused by the thickness variations. The problem was alleviated using a more dilute polymer/chloroform solution and spinning at a lower speed. For this, we used a solution with 75 mg PVK in 7 ml chloroform. A spin speed for an 800 Å thick polymer film was obtained to be 600 rpm. Using a solvent with lower vapor pressure (such as chlorobenzene or dichloroethane), however, solved the problem completely. Because the solvent evaporates more slowly, the substrate acceleration phase is concluded before the solvent evaporates completely. Because of that, the radial waves subside during the constant spin speed phase.

Figure 2-31 shows the obtained film thickness as a function of the spin speed for different solvents, chloroform ( $\text{CHCl}_3$ ) and tetra-hydrofuran (THF,  $\text{C}_4\text{H}_8\text{O}$ ). The viscosity of the THF-solution is slightly lower than that of the  $\text{CHCl}_3$ -solution resulting in thinner films at similar spin speeds.

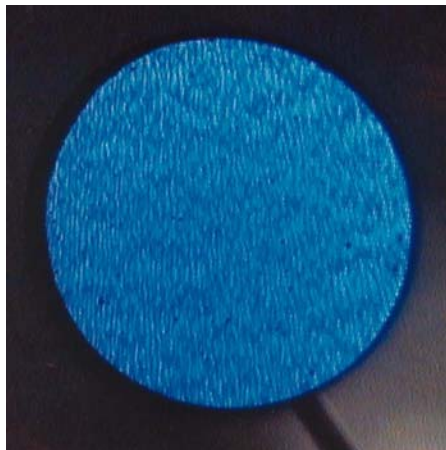


**Figure 2-30.** EL micrograph of a device (diameter 1.5 mm at 50 mA/cm<sup>2</sup>) with inhomogeneous polymer film thickness due to fast solvent evaporation. The device was fabricated using chloroform as the solvent. The polymer film was deposited at 2000 rpm.

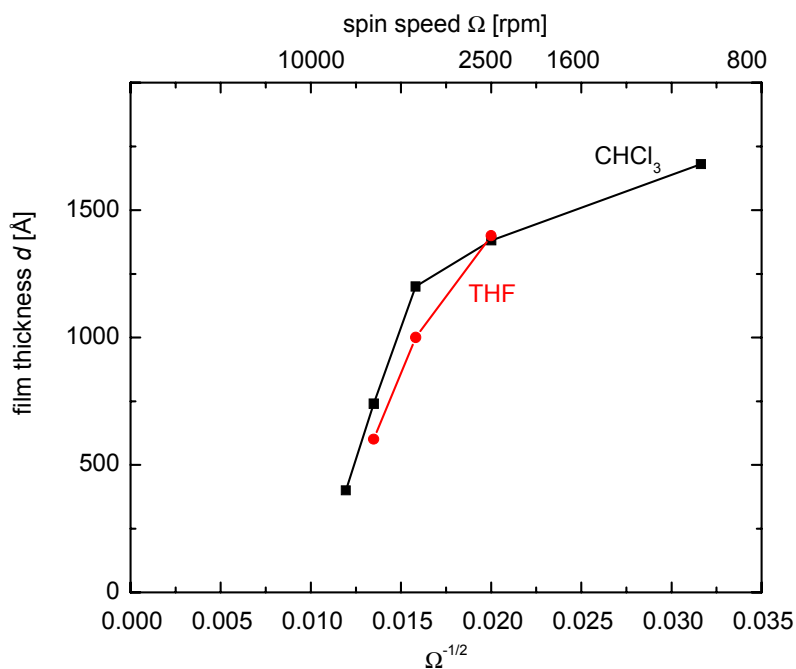


**Figure 2-31.** Polymer film thickness as a function of spin speed.

Table 2-3 lists the experimentally obtained polymer film thickness for different solvents at a spin speed of 4000 rpm for 60 sec. Because chloroform has such a high vapor pressure, it evaporates very fast resulting in thick polymer films. Toluene, on the other hand, evaporates much slower, yielding thin polymer films. The turn-on voltage decreases with film thickness. To analyze the electric field across the polymer film at the turn-on volt-

age, we divided the turn-on voltage by the film thickness. Except for tetrahydrofuran, we obtained a nearly constant value of 52 MV/m. This constant electric field is consistent with the simple model of carrier injection with barriers at the contacts and a trap free polymer film.

**Table 2-3.** Film thickness and turn-on voltage of PVK/PBD devices fabricated with different solvents. Values for vapor pressure are taken from Ref. [70]. The turn-on voltage is in this case defined as the voltage at which the dark-current of the detector equal to the photo-current (see Figure 2-16).

solvent	vapor pressure [kPa] at room temp.	polymer concentration [mg/ml]	film thickness [Å]	turn-on voltage [V]	electrical field at turn-on voltage [MV/m]
chloroform	26	13.3	1080	5.4	50
chloroform	26	15.4	1250	6.2	49
tetrahydrofuran	22	13.3	900	7.1	79
dichloroethane	10.6	13.3	800	4.4	55
toluene	3.8	13.3	550	3.1	56

The dependence of the turn-on voltage on the solvent and spin speed was reported earlier [71][72][73]. The fact that devices fabricated from THF solution displays the highest electric field at the turn-on voltage, is in agreement with the observation discussed in [71], that non-aromatic solvents tend to form polymer/metal or polymer/ITO interfaces with higher injection barriers.

## 2.12 Summary

In summary, we fabricated single layer OLEDs using PVK as the host polymer and hole transport material, and PBD as electron transport material. These devices were doped with an appropriate dye to change the emission color. The details of the fabrication process have been outlined in detail.

The difference in EL and PL device performance was investigated in detail. In addition, the device characteristics as a function of dye concentration has been explored. A carrier transport model has been introduced which can explain these observations.

The surface morphology of the polymer film and the device performance dependent on the solvent used during the spin-coating process have been discussed and a solvent has been chosen for our device fabrication.

## 2.13 References

- [1] J. H. Burroughes, D. D. C. Bradley, A. R. Brown, R. N. Marks, K. Mackay, R. H. Friend, P. L. Burns, and A. B. Holmes, "Light-emitting diodes based on conjugated polymers", *Nature* **347**, 539 (1990).
- [2] C. K. Chiang, C. R. Fincher, Jr., Y.W. Park, A. J. Heeger, H. Shirakawa, E. J. Louis, S. C. Gau and A. G. MacDiarmid, "Electrical Conductivity in Doped Polyacetylene", *Phys. Rev. Lett.* **39** 1098 (1977).
- [3] A.J. Heeger, "Semiconducting and Metallic Polymers: New Science with Potential for New Technology", *Comments Sol. State Phys.* **10** 53 (1981).
- [4] M. Jones, Jr., *Organic Chemistry*, 1st ed. (W.W. Norton & Company, New York, 1997).
- [5] J. A. Reedijk, H. C. F. Martens, H. B. Brom, and M. A. J. Michels, "Dopant-induced crossover from 1D to 3D charge transport in conjugated polymers", *Physical Review Letters* **83** (19), 3904 (1999).
- [6] B. J. Schwartz, T. Q. Nguyen, J. Wu, and S. H. Tolbert, "Interchain and intrachain exciton transport in conjugated polymers: ultrafast studies of energy migration in aligned MEH-PPV/mesoporous silica composites", *Synthetic Metals* **116** (1-3), 35 (2001).
- [7] J. Cornil, J. P. Calbert, D. Beljonne, R. Silbey, and J. L. Bredas, "Interchain interactions in pi -conjugated oligomers and polymers: a primer", *Synthetic Metals* **119** (1-3), 1 (2001).
- [8] W. D. Gill, "Drift mobilities in amorphous charge-transfer complexes of trinitrofluorenone and poly-n-vinylcarbazole", *Journal of Applied Physics* **43** (12), 5033 (1972).
- [9] H. Bässler, "Charge transport in disordered organic photoconductors. A Monte Carlo simulation study", *Physica Status Solidi B* **175** (1), 15 (1993).
- [10] F. Pfister, "Hopping transport in a molecularly doped organic polymer", *Physical Review B (Solid State)* **16** (8), 3676 (1977).

- [11] H. Schon, C. Kloc, and B. Batlogg, "Universal crossover from band to hopping conduction in molecular organic semiconductors", *Phys. Rev. Lett.* **86** (17), 3843 (2001).
- [12] I. G. Romijn, W. F. Pasveer, H. C. F. Martens, H. B. Brom, and M. A. J. Michels, "Hopping transport in polythiophene versus poly(phenylene vinylene)", *Synthetic Metals* **119** (1-3), 439 (2001).
- [13] S. D. Baranovskii, H. Cordes, F. Hensel, and S. Yamasaki, "On the description of charge carrier transport in disordered organic solids", *Synthetic Metals* **119** (1-3), 57 (2001).
- [14] P. M. Borsenberger, E. H. Magin, and S. A. Visser, "Charge trapping in molecularly doped polymers", *Japanese Journal of Applied Physics, Part 1: Regular Papers & Short Notes & Review Papers* **37** (4A), 1945 (1998).
- [15] M. Van der Auweraer, F. C. De Schryver, P. M. Borsenberger, and H. Bassler, "Disorder in charge transport in doped polymers", *Adv. Mat.* **6** (3), 199 (1994).
- [16] M. Pope and C. E. Swenberg, *Electronic processes in organic crystals and polymers*, 2nd ed. (Oxford University Press, New York, 1999).
- [17] S. Tretiak, A. Saxena, R. L. Martin, and A. R. Bishop, "Interchain Electronic Excitation in Poly(phenylenevinylene) (PPV) Aggregates", *J. Phys. Chem. B* **104** (30), 7029 (2000).
- [18] P. Argyrakis, M. V. Kobryanskii, M. I. Sluch, and A. G. Vitukhnovsky, "Influence of conjugated polymer chain length on luminescence properties of ordered polymer films", *Synthetic Metals* **91** (1-3), 159 (1997).
- [19] H. Kuzmany and J. Kurti, "The physical meaning of the conjugation length in polymers", *Synthetic Metals* **21** (1), 95 (1987).
- [20] L. Bredas, "Relationship between band gap and bond length alternation in organic conjugated polymers", *Journal of Chemical Physics* **82** (8), 3808 (1985).
- [21] Graphic reproduced with kind permission by Vladimir Bulovic, Massachusetts Institute of Technology (2001).
- [22] Graph obtained from H. W. Sands Corporation, Jupiter, Florida (2001).

- [23] T. Förster, *Ann. Phys.* **2** (6), 55 (1948).
- [24] D. L. Dexter, "A Theory of Sensitized Luminescence in Solids", *J. Chem. Phys.* **21** (5), 836 (1953).
- [25] J. R. Sheats, H. Antoniadis, M. Hueschen, W. Leonard, J. Miller, R. Moon, D. Roitman, and A. Stocking, "Organic Electroluminescent Devices", *Science* **273**, 884 (1996).
- [26] M. A. Baldo, D. F. O'Brien, M. E. Thompson, and S. R. Forrest, "Excitonic singlet-triplet ratio in a semiconducting organic thin film", *Physical Review B* **60** (20), 14422 (1999).
- [27] M. A. Baldo, D. F. O'Brien, Y. You, A. Shoustikov, S. Sibley, M. E. Thompson, and S. R. Forrest, "Highly efficient phosphorescent emission from organic electroluminescent devices", *Nature* **395** (6698), 151 (1998).
- [28] M. E. Thompson, S. Lamansky, P. Djurovich, D. Murphy, F. Abdel-Razzaq, S. R. Forrest, M. Baldo, P. E. Burrows, C. Adachi, T. X. Zhou, L. Michalski, K. Rajan, and J. J. Brown, "High efficiency organic electrophosphorescent devices", *Proceedings of SPIE - The International Society for Optical Engineering* **4105**, 119 (2001).
- [29] D. J. Milliron, I. G. Hill, C. Shen, A. Kahn, and J. Schwartz, "Surface oxidation activates indium tin oxide for hole injection", *J. Appl. Phys.* **87** (1), 572 (2000).
- [30] C. C. Wu, C. I. Wu, J. C. Sturm, and A. Kahn, "Surface modification of indium tin oxide by plasma treatment: an effective method to improve the efficiency, brightness, and reliability of organic light emitting devices", *Appl. Phys. Lett.* **70** (11), 1348 (1997).
- [31] F. Nuesch, L. J. Rothberg, E. W. Forsythe, Q. T. Le, and Y. Gao, "A photoelectron spectroscopy study on the indium tin oxide treatment by acids and bases", *Appl. Phys. Lett.* **74** (6), 880 (1999).
- [32] J. M. Pearson and M. Stolka, *Poly(N-vinyl carbazole)* (Gordon and Breach, New York, 1981).
- [33] M. T. Bernius, M. Inbasekaran, J. O'Brien, and W. Wu, "Progress with light-emitting polymers", *Adv. Mat.* **12** (23), 1737 (2000).

- [34] C. Adachi, T. Tsutsui, and S. Saito, "Organic electroluminescent device having a hole conductor as an emitting layer", *Appl. Phys. Lett.* **55** (15), 1489 (1989).
- [35] G. Yu, H. Nishino, A. J. Heeger, T.-A. Chen, and R. D. Rieke, "Enhanced electroluminescence from semiconducting polymer blends", *Synthetic Metals* **72** (3), 249 (1995).
- [36] C. C. Wu, J. C. Sturm, R. A. Register, J. Tian, E. P. Dana, and M. E. Thompson, "Efficient Organic Electroluminescent Devices Using Single-layer Doped Polymer Thin Films with Bipolar Carrier Transport Abilities", *IEEE Trans. Electron Devices* **44** (8), 1269 (1997).
- [37] C. C. Wu, "Light-Emitting Devices Based on Doped Polymer Thin Films," Doctoral Thesis, Princeton University, 1997.
- [38] T. Granlund, L. A. A. Pettersson, M. R. Anderson, and O. Inganäs, "Interference phenomenon determines the color in an organic light emitting diode", *J. Appl. Phys.* **81** (12), 8097 (1997).
- [39] C. W. Tang, S. A. VanSlyke, and C. H. Chen, "Electroluminescence of doped organic thin films", *J. Appl. Phys.* **65** (9), 3610 (1989).
- [40] T. G. Pavlopoulos, J. H. Boyer, I. R. Politzer, and C. M. Lau, "Laser action from syn-(methyl,methyl)bimane", *J. Appl. Phys.* **60** (11), 4028 (1986).
- [41] C. C. Wu, J. C. Sturm, R. A. Register, and M. E. Thompson, "Integrated three-color organic light-emitting devices", *Appl. Phys. Lett.* **69** (21), 3117 (1996).
- [42] F. Pschenitzka and J. C. Sturm, "Three-color organic light-emitting diodes patterned by masked dye diffusion", *Appl. Phys. Lett.* **74** (13), 1913 (1999).
- [43] J. Thompson, R. I. R. Blyth, M. Mazzeo, M. Anni, G. Gigli, and R. Cingolani, "White light emission from blends of blue-emitting organic molecules: A general route to the white organic light-emitting diode?", *Appl. Phys. Lett.* **79** (5), 560 (2001).
- [44] Y. Qiu, L. Duana, X. Hua, D. Zhanga, M. Zhengb and F. Baib, "Electroluminescence enhancement by blending PVK with an alternating copolymer containing triphenylamine and phenylene units", *Synthetic Metals* **123** (1), 39 (2001).

- [45] T.-W. Lee, O. O. Park, H. N. Cho, J.-M. Hong, C. Y. Kim, and Y. C. Kim, "White emission from a ternary polymer blend by incomplete cascade energy transfer", *Synthetic Metals* **122** (2), 437 (2001).
- [46] G. Giro, M. Cocchi, J. Kalinowski, P. Di Marco, and V. Fattori, "Multicomponent emission from organic light emitting diodes based on polymer dispersion of an aromatic diamine and an oxadiazole derivative", *Chemical Physics Letters* **318** (1-3), 137 (2000).
- [47] C.-I. Chao and S.-A. Chen, "White light emission from exciplex in a bilayer device with two blue light-emitting polymers", *Appl. Phys. Lett.* **73** (4), 426 (1998).
- [48] E. J. W. List, G. Leising, N. Schulte, D. A. Schluer, U. Scherf, and W. Graupner, "White light emission from a polymer-macromolecule blend system due to energy and charge transfer", *Japanese Journal of Applied Physics, Part 2 (Letters)* **39** (7B), L760 (2000).
- [49] J. Feng, F. Li, W. Gao, S. Liu, Y. Liu, and Y. Wang, "White light emission from exciplex using tris-(8-hydroxyquinoline)aluminum as chromaticity-tuning layer", *Appl. Phys. Lett.* **78** (25), 3947 (2001).
- [50] Y.-Z. Lee, X. Chen, M.-C. Chen, S.-A. Chen, J.-H. Hsu, and W. Fann, "White-light electroluminescence from soluble oxadiazole-containing phenylene vinylene ether-linkage copolymer", *Appl. Phys. Lett.* **79** (3), 308 (2001).
- [51] Y. Hamada, H. Kanno, T. Tsujioka, T. Hisakazu, and T. Usuki, "Red organic light-emitting diodes using an emitting assist dopant", *Appl. Phys. Lett.* **75** (12), 1682 (1999).
- [52] B. W. D'Andrade, M. A. Baldo, C. Adachi, J. Brooks, M. E. Thompson, and S. R. Forrest, "High-efficiency yellow double-doped organic light-emitting devices based on phosphor-sensitized fluorescence", *Appl. Phys. Lett.* **79** (7), 1045 (2001).
- [53] M. Uchida, C. Adachi, T. Koyama, and Y. Taniguchi, "Charge carrier trapping effect by luminescent dopant molecules in single-layer organic light emitting diodes", *J. Appl. Phys.* **86** (3), 1680 (1999).
- [54] F. Pschenitzka, J. C. Sturm, "Excitation mechanisms in dye-doped organic light-emitting devices", *Appl. Phys. Lett.* **79** (26), 4354 (2001).

- [55] F. Pschenitzka and J. C. Sturm, “Three-color doping of polymer OLEDs by masked dye diffusion”, *Proc. Mat. Res. Soc.* **558**, 513 (2000).
- [56] Absorption spectra of C47 and Nile red were measured by Xuezhong Jiang, Department of Materials Science and Engineering, University of Washington, Seattle, WA.
- [57] D. V. Roberts, B. P. Wittmershaus, Y.-Z. Zhang, S. Swan, and M. P. Klinosky, “Efficient excitation energy transfer among multiple dyes in polystyrene microspheres”, *J. Lumin.* **79**, 225 (1998).
- [58] A. A. Shoustikov, Y. You, and M. E. Thompson, “Electroluminescence Color Tuning by Dye Doping in Organic Light-Emitting Diodes”, *IEEE Journal of Selected Topics in Quantum Electronics* **4** (1), 3 (1998).
- [59] J. Kalinowski, L. C. Picciolo, H. Murata, and Z. H. Kafafi, “Effect of emitter disorder on the recombination zone and the quantum yield of organic electroluminescent diodes”, *J. Appl. Phys.* **89** (3), 1866 (2001).
- [60] S. Tasch, E. J. W. List, C. Hochfilzer, G. Leising, P. Schlichting, U. Rohr, Y. Geerts, U. Scherf, and K. Müllen, “Efficient red- and orange-light-emitting diodes realized by excitation energy transfer from blue-light-emitting conjugated polymers”, *Phys. Rev. B* **56** (8), 4479 (1997).
- [61] H. Murata, C. D. Merritt, and Z. H. Kafafi, “Emission mechanism in rubrene-doped molecular organic light-emitting diodes: direct carrier recombination at luminescent centers”, *IEEE Journal of Selected Topics in Quantum Electronics* **4** (1), 119 (1998).
- [62] J. Kalinowski, G. Giro, M. Cocchi, V. Fattori, and P. Di Marco, “Unusual disparity in electroluminescence and photoluminescence spectra of vacuum-evaporated films of 1,1-bis ((di-4-tolylamino) phenyl) cyclohexane”, *Appl. Phys. Lett.* **76** (17), 2352 (2000).
- [63] E. Gautier-Thianche, C. Sentein, J.-M. Nunzi, A. Lorin, C. Denis, and P. Raimond, “Coumarin concentration effect on PVK-based blue light-emitting diodes”, *Synthetic Metals* **91** (1-3), 323 (1997).
- [64] J.-M. Nunzi, A. Gautier-Thianche, A. Lorin, C. Denis, P. Raimond, and C. Sentein, “Concentration effects on charge transport in dye doped polymer light emitting diodes”, *Proceedings of the SPIE - The International Society for Optical Engineering* **3281**, 302 (1998).

- [65] P. A. Lane, L. C. Palilis, D. F. O'Brien, C. Giebeler, A. J. Cadby, D. G. Lidzey, A. J. Campbell, W. Blau, and D. D. C. Bradley, "Origin of electrophosphorescence from a doped polymer light emitting diode", *Physical Review B (Condensed Matter and Materials Physics)* **63** (23), 235206/1 (2001).
- [66] H. Ogawa, R. Okuda, and Y. Shirota, "Tuning of the emission color of organic electroluminescent devices by exciplex formation at the organic solid interface", *Applied Physics A: Materials Science & Processing* **67** (5), 599 (1998).
- [67] C. J. Lawrence, "The mechanics of spin coating of polymer films", *Phys. Fluids* **31** (10), 2786 (1988).
- [68] D. B. Hall, P. Underhill, and J. M. Torkelson, "Spin coating of thin and ultrathin polymer films", *Polymer Engineering and Science* **38** (12), 2039 (1998).
- [69] M. Cecchi, H. Smith, and D. Braun, "Method to optimize polymer film spin coating for polymer LED displays", *Synthetic Metals* **121** (1-3), 1715 (2001).
- [70] *CRC Handbook of Chemistry and Physics*, edited by D. R. Lide, 75th ed. (CRC Press, Boca Raton, 1994).
- [71] J. Liu, Y. Shi, L. Ma, and Y. Yang, "Device performance and polymer morphology in polymer light emitting diodes: The control of device electrical properties and metal/polymer contact", *J. Appl. Phys.* **88** (2), 605 (2000).
- [72] Y. Shi, J. Liu, and Y. Yang, "Device performance and polymer morphology in polymer light emitting diodes: The control of thin film morphology and device quantum efficiency", *J. Appl. Phys.* **87** (9), 4254 (2000).
- [73] T.-Q. Nguyen, R. C. Kwong, M. E. Thompson, and B. J. Schwartz, "Higher efficiency conjugated polymer-based LEDs by control of polymer film morphology and interchain interactions", *Synthetic Metals* **119** (1-3), 523 (2001).

# 3 Patterning Techniques of the Emissive Layer for Full-Color Organic Displays

To convey the impression of a single mixed color to the observer, red, green and blue emitters have to be in close proximity. Although many display products are low-content displays, high-resolution products like computer screens are the ultimate application for OLED displays. Although cones provide color vision in the human eye, at the point of the highest spatial resolution on the retina (fovea), the vast majority of the receptors are rods, which only detect brightness. To fully utilize the capability of the eye, the pixel pitch of the display's image on the retina should equal the pitch of the rods on the retina. At the fovea, the density of rods is about 150,000 rods/mm<sup>2</sup> [1], and the average distance between two cones at this point is therefore about 2.6 μm. Considering the optics of the eye, the angle between two pixels should be about 20 sec of an arc. In fact, neurological image processing starts in the retina where the nerve cells connected to the rods can actually block each other and thereby enhance the contrast and resolution [2]. However, measurements show that the practical limit of the spacial resolution of the human eye is about 40 lines per degree [1]. Thus, for a computer screen (assuming the observer is about 40 cm away from the screen) the distance between pixels should not exceed 0.1 mm where each pixel consists of three subpixels emitting in the red, green, and blue. The required fine pattern along with the large area of the display poses a unique fabrication problem for OLED displays.

This chapter reviews some of the suggested technologies to achieve full-color displays with its advantages and disadvantages.

The technology of dye transfer into electroactive polymers, which is the main focus of this work, will be briefly outlined. It will be discussed in detail in the following chapters.

## 3.1 Patterning Techniques using Materials Emitting Different Colors

### 3.1.1 Direct Deposition of Red, Green, and Blue Emitters

The most straightforward approach to obtain emission from red, green and blue subpixels is the direct deposition of material emitting this color. The efficiency of this method is optimal because no external filtering is necessary. However, a concern is a long-term color shift due to different aging characteristics of different emissive materials.

#### 3.1.1.1 Shadow mask

The shadow mask technique is the simplest patterning method where the emitting material is thermally evaporated onto the device substrate through a shadow mask [3][4][5]. This technology requires vacuum processing and the alignment in the vacuum environment is problematic. The shadow mask must be in close contact with the substrate in order to reproduce small feature sizes accurately which poses a risk of mechanically damaging the device. In addition to the high fabrication cost of a shadow mask, the feature sizes are limited due to stability requirements of the mask. The process is shown in Figure 3-1. After the deposition of the first emitting material, the shadow mask is shifted

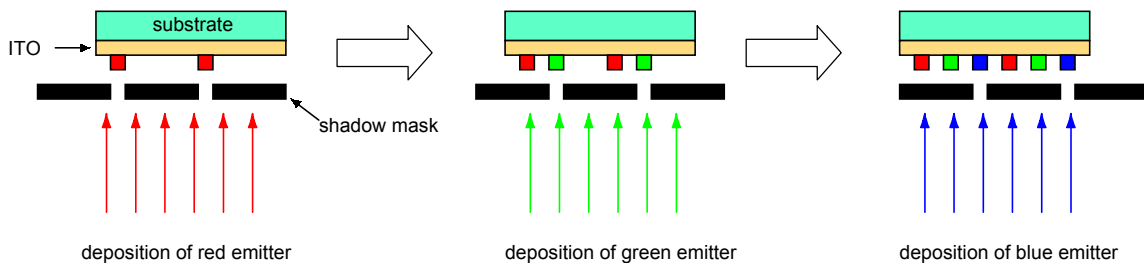


**Figure 3-1.** Patterning of the emissive layer using a shadow mask.

followed by the evaporation of the second emitting material. This procedure is repeated until all three materials are deposited. In addition, the cathode material can be deposited directly after the emissive layer has been formed without breaking the vacuum.

In February 2001, Sony Corp. demonstrated a full-color display (800 by 600 pixels) with a 13.1 inch diagonal fabricated using this technology [6].

Because materials with high molecular weight can not be deposited by thermal evaporation this method is not applicable to polymer-based OLEDs.

### 3.1.1.2 Ink-Jet Printing of Polymers

Since polymers have good film-forming properties, they can be deposited by spin-coating onto the device substrate. However, in this case, the film is homogeneous and is only capable of emitting a single color. To locally deposit different polymer material, ink jet printing has been demonstrated to be a viable technology [7]. In this case, a small drop of the solution with the proper polymer is deposited onto the substrate. The drying properties of the drop are of major concern because an uneven morphology leads to a non-uniform emission pattern and ultimately to early degradation of the device [8][9]. Careful choice of materials can alleviate the problem.

In addition to the choice of materials, the use of a substrate pre-patterned with “banks” has been reported [10][11]. As shown in Figure 3-2, a material is deposited onto the substrate. The “banks” confine the solution and helps to form a more uniform polymer film.

Among other companies, Seiko-Epson and Toshiba have decided to pursue this approach. In June 2001 Seiko-Epson demonstrated their ink-jet printed 2.5-inch display with 150 by 200 pixels. Toshiba showed a very similar product [6].

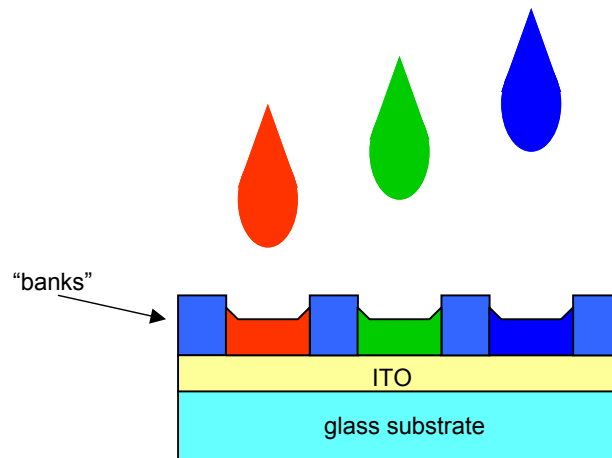


**Figure 3-2.** Use of “banks” to confine the polymer solution during the ink-jet process.

### 3.1.1.3 Screen Printing

Recently, the deposition of the polymer film by screen printing has been demonstrated [12][13]. Analogous to the conventional screen printing technology used in the printing industry, the polymer solution is applied through a shadow mask (stencil) onto the substrate by squeezing the solution through the openings of the mask. This process has the potential of low fabrication costs. For a full-color display, three successive deposition steps have to be carried out. This process bears the risk of mechanically damaging the already deposited polymer features during the following printing steps resulting in short circuited devices.

### 3.1.1.4 Dry Etching

Using oxygen plasma to locally etch away the organic layer after deposition has been utilized to fabricate a three color device [14]. After the first deposition by spin-coating of a polymer solution, the cathode was evaporated at places where devices with the respective emission color were desired as shown in Figure 3-3(a) using a shadow mask. The subsequent dry etching step removed the polymer layer where it was not protected by the cathode metal layer (b). Before the next polymer layer could be spun-on, the existing device had to be completely encapsulated to avoid damage to the already deposited polymer layer due to sensitivity to solvents. To this end, a second metal layer was evaporated (c). Subsequently, a second polymer layer was spun-on, and the procedure was repeated until a three color device was fabricated (d).

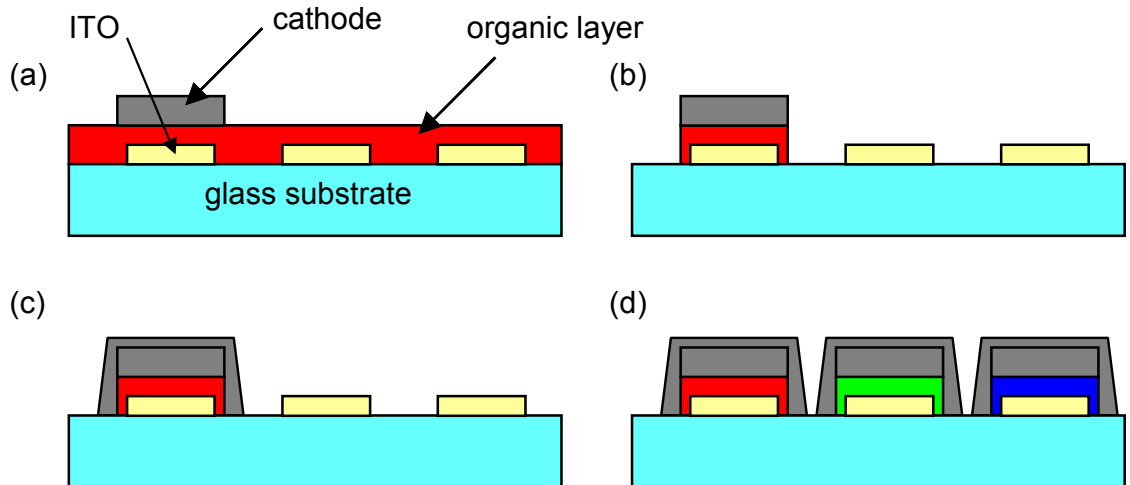


**Figure 3-3.** Fabrication of three colors using dry etching of organic layer.

Because of the cumbersome fabrication process, this approach has little potential to be utilized in an industrial environment; unless the patterning is done by a printing process. However, the technology would still require many steps and therefore be relatively expensive.

### 3.1.2 Direct Emission of RGB by Local Dye Doping

#### 3.1.2.1 Ink-Jet Printing of Dye Solution

As outlined in Chapter 2.3, the emission color can be tuned by introducing a small amount of dye into the host material [15]. To avoid the problem of non-uniformities caused by the drying of ink-jet printed droplets, a dye-containing solution (which does not dissolve the polymer) is printed using ink-jet technology onto a substrate previously coated with a uniform polymer layer as shown in Figure 3-4. The dye then diffuses into the polymer layer

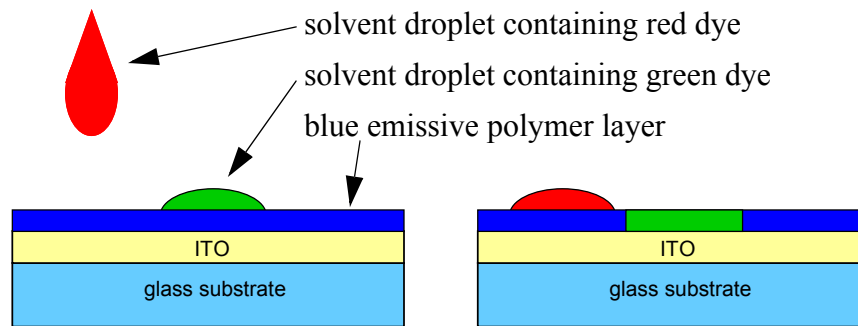


**Figure 3-4.** Patterning of the emission color by locally printing of dye solution.

during the evaporation of the solvent and thereby changes the emissive color of the polymer film. The emission of the dye has to be of longer wavelength than the host material to allow for energy transfer from the host to the dye [16]. However, due to the drying properties of the solvent droplet and mass transport within the droplet, the lateral distribution of the dye still needs to be optimized [17].

#### 3.1.2.2 Dye Transfer Method

The idea of introducing a small amount of dye into a previously deposited layer is also the basis for the dye transfer method. In this case, the dye is locally transferred over a large area into the polymer film and thus changes the emission color of the device [18].

During this process, the dye desorbs from a source substrate containing the dye and travels

to the emissive polymer film. A mask sandwiched in between the dye source substrate and the device substrate defines the dyed pattern as shown in Figure 3-5. The mask may be integrated in the display plate or into the dye source plate (see Chapter 6.2). Alternatively, the

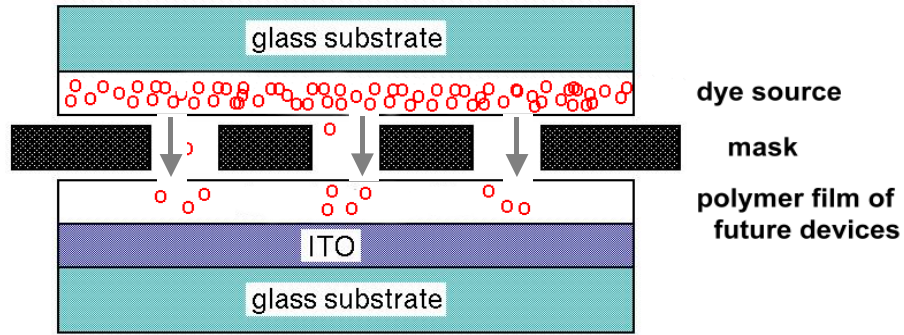


**Figure 3-5.** Dye Transfer Method. [16]

dye source itself may be patterned (see Chapter 6.2). After the device substrate has been patterned to locally emit different colors, a metal cathode is thermally evaporated. As with the use of different emitting materials, the color stability of the display is an issue, because the dyes used have different aging characteristics resulting in a long-term color shift. However, devices fabricated using this process can be very efficient, because no external filtering is necessary.

The main focus of this thesis is on the process of dry patterned dye transfer. Chapter 4 discusses the dye transfer and its underlying concepts, whereas Chapter 5 and Chapter 6 concentrate on the technological details.

### 3.1.3 Photobleaching

A very promising technology of photobleaching was introduced by Kido *et al.* [30]. Mixing a photosensitive dye in the spin-on polymer solution, the dye was locally and selectively deactivated by UV radiation using a conventional photo mask to define the pattern. Therefore, the dye emits in its respective color when it was not irradiated with UV, and the emission occurs from the host when the dye has been bleached. So far, the stability of the dye has been insufficient. In addition, only a two-color device have been demonstrated because of the lack of suitable photosensitive dyes.

## 3.2 Patterning Techniques using a Uniform Emissive Material

### 3.2.1 RGB emission by white emission and color filtering

Conventional liquid crystal displays (LCD) operate by locally blocking white light from a back light. The white light passing through each of three subpixels is then filtered to emit red, green, and blue. The idea has its equivalent in the white-emitting OLED [19][20][21][22], where each of the subpixels is subsequently filtered in the same fashion as shown in Figure 3-6. The advantage of this method is the use of very reliable color filter technology and a uniform aging characteristics. But due to the filtering, the efficiency of the device is lower than direct emitting devices.

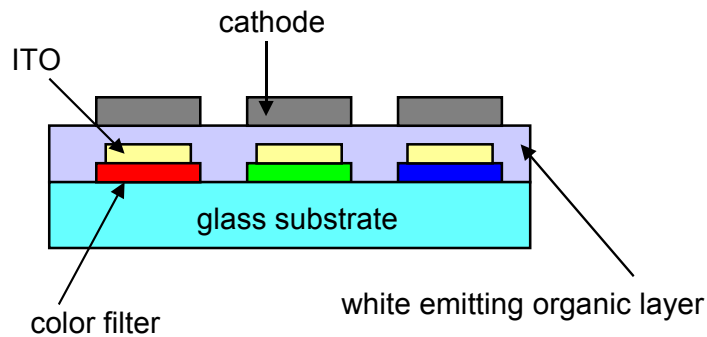


**Figure 3-6.** RGB emission using white emitter and color filters.

### 3.2.2 Emission of RGB with color converting materials

Applying the well understood idea of converting light of a short wavelength to light of a longer wavelength [23] to OLEDs, the blue photon can be changed to red or green by color converting materials (CCM). In the same fashion as white light is filtered by color filters, the blue emission is converted into green and red emission by converting material in front of the emitting subpixel (see Figure 3-7) [24][25]. Again, due to the limited efficiency of the conversion process, green and especially red devices have lower efficiencies than direct emitter. In addition, although the aging of the emission layer is uniform, the aging characteristics of the conversion material is not.

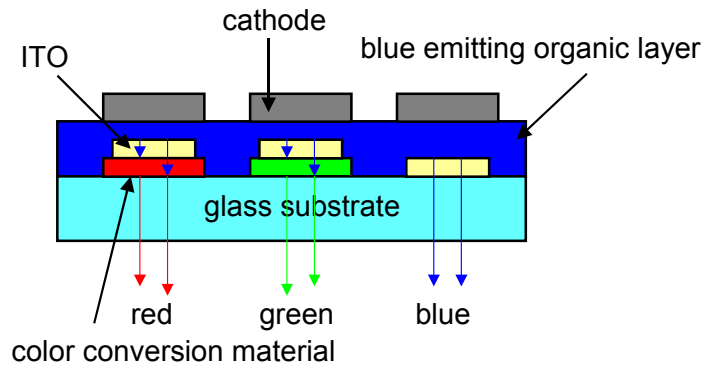


**Figure 3-7.** RGB emission using color conversion materials.

### 3.2.3 Microcavity

Because the thickness of the emission layer is of the order of the emitted wavelength of the light, the thickness of the film can be used to tune the emission color in a certain range by constructive or destructive interference [26]. While this method can increase the color purity of the emission, it is not possible to efficiently cover the full range of the visible spectrum with only one emissive material [27][28][29]. In addition, due to the geometrical configuration of the device, a spectral shift depending on the viewing angle is also problematic.

### 3.2.4 Stacked OLED

The concept to stack transparent or semi-transparent red, green, and blue-emitting devices on top of each other has been realized by Forrest *et al.* [31][32][33][34]. In the area of a single device, the structure could therefore emit the full range of color. But because the devices are stacked in a way that the cathode of the blue emitting sub-device is the anode of the green one to minimize the number of layers, the addressing scheme is very difficult. Furthermore, patterning of all layers to directly contact the intermediate layers is problematic. Although this approach is very simple and elegant, so far, no display has been fabricated due to the complicated fabrication process and operation scheme.

### 3.3 References

- [1] D. A. Atchison and G. Smith, *Optics of the human eye* (Oxford; Boston: Butterworth-Heinemann, Oxford; Boston: Butterworth-Heinemann, 2000).
- [2] T. N. Cornsweet, *Visual Perception* (Academic Press, New York, 1970).
- [3] Y. Iketsu, E. Kitazume, T. Tanaka, E. Nishigaki, S. Ootsuki, and K. Mizoguchi, "Multicolor organic electroluminescent QVGA display devices with patterned lateral three-color emitters", *Proceedings of SPIE - The International Society for Optical Engineering* **3476**, 226 (1998).
- [4] P. F. Tian, P. E. Burrows, and S. R. Forrest, "Photolithographic patterning of vacuum-deposited organic light emitting devices", *Appl. Phys. Lett.* **71** (22), 3197 (1997).
- [5] P. F. Tian, V. Bulovic, P. E. Burrows, G. Gu, S. R. Forrest, and T. X. Zhou, "Precise, scalable shadow mask patterning of vacuum-deposited organic light emitting devices", *J. Vac. Sci. Technol. A* **17** (5), 2975 (1999).
- [6] EE Times "Organic LEDs shine at display meeting" by David Lieberman, June 25, 2001.
- [7] T. R. Hebner, C. C. Wu, D. Marcy, M. H. Lu, and J. C. Sturm, "Ink-jet printing of doped polymers for organic light emitting devices", *Appl. Phys. Lett.* **72** (5), 519 (1998).
- [8] S.-C. Chang, J. Bhanathan, and Y. Yang, "Dual-color polymer light-emitting pixels processed by hybrid inkjet printing", *Appl. Phys. Lett.* **73** (18), 2561 (1998).
- [9] J. Bharathan and Y. Yang, "Polymer electroluminescent devices processed by inkjet printing: Polymer light-emitting logo", *Appl. Phys. Lett.* **72** (21), 2660 (1998).
- [10] T. Shimoda, S. Kanbe, H. Kobayashi, S. Seki, H. Kiguchi, I. Yudasaka, M. Kimura, S. Miyashita, R. H. Friend, J. H. Burroughes, and C. R. Towns, "Multicolor Pixel Patterning of Light-Emitting Polymers by Ink-Jet Printing," presented at the SID, 1999 (unpublished).
- [11] H. Kobayashi, S. Kanbe, S. Seki, H. Kiguchi, M. Kimura, I. Yudasaka, S. Miyashita, T. Shimoda, C. R. Towns, J. H. Burroughes, and R. H. Friend, "A novel RGB multi-color light-emitting polymer display", *Syn. Met.* **111**, 125 (2000).

- [12] J. Birnstock, J. Blassing, A. Hunze, M. Scheffel, M. Stossel, K. Heuser, G. Wittmann, J. Worle, and A. Winnacker, "Screen-printed passive matrix displays based on light-emitting polymers", *78* (24), 3905 (2001).
- [13] D. A. Pardo, G. E. Jabbour, and N. Peyghambarian, "Application of Screen Printing in the Fabrication of Organic Light-Emitting Devices", *Adv. Mater.* **12** (17), 1249 (2000).
- [14] C. C. Wu, J. C. Sturm, R. A. Register, and M. E. Thompson, "Integrated three-color organic light-emitting devices", *Appl. Phys. Lett.* **69** (21), 3117 (1996).
- [15] C. W. Tang, S. A. VanSlyke, and C. H. Chen, "Electroluminescence of doped organic thin films", *J. Appl. Phys.* **65** (9), 3610 (1989).
- [16] T. R. Hebner and J. C. Sturm, "Local tuning of organic light-emitting diode color by dye droplet application", *Appl. Phys. Lett.* **73** (13), 1775 (1998).
- [17] C. F. Madigan, T. R. Hebner, J. C. Sturm, R. A. Register, and S. Troian, "Lateral dye distribution with ink-jet dye doping of polymer organic light emitting diodes", *Mater. Res. Soc. Symp. Proc.* **624**, 211 (2000).
- [18] F. Pschenitzka and J. C. Sturm, "Three-color organic light-emitting diodes patterned by masked dye diffusion", *Appl. Phys. Lett.* **74** (13), 1913 (1999).
- [19] J. Kido, M. Kimura, and K. Nagai, "Multilayer White Light-Emitting Organic Electroluminescent Device", *Science* **267**, 1332 (1995).
- [20] J. Kido, H. Shionoya, and K. Nagai, "Single-layer white light-emitting organic electroluminescent devices based on dye-dispersed poly(*N*-vinylcarbazole)", *Appl. Phys. Lett.* **67** (16), 2281 (1995).
- [21] S. Tasch, E. J. W. List, O. Ekstrom, W. Graupner, and G. Leising, "Efficient white light-emitting diodes realized with new processable blends of conjugated polymers", *Appl. Phys. Lett.* **71** (20), 2883 (1997).
- [22] C.-I. Chao and S.-A. Chen, "White light emission from exciplex in a bilayer device with two blue light-emitting polymers", *Appl. Phys. Lett.* **73** (4), 426 (1998).

- [23] P. Schlotter, R. Schmidt, and J. Schneider, "Luminescence conversion of blue light emitting diodes", *Applied Physics A (Materials Science Processing)* **64** (4), 417 (1997).
- [24] A. Niko, S. Tasch, F. Meghdadi, C. Brandstaetter, and G. Leising, "Red-green-blue emission of parahexaphenyl devices with color-converting media", *J. Appl. Phys.* **82** (9), 4177 (1997).
- [25] C. Hosokawa, M. Matsuura, M. Eida, K. Fukuoka, H. Tokailin, and T. Kusumoto, "Full-color organic EL display", *Journal of the Society for Information Display* **6** (4), 257 (1998).
- [26] A. Dodabalapur, L. J. Rothberg, and T. M. Miller, "Electroluminescence from organic semiconductors in patterned microcavities", *Electronic Letters* **30** (12), 1000 (1994).
- [27] R. H. Jordan, L. J. Rothberg, A. Dodabalapur, and R. E. Slusher, "Efficiency enhancement of microcavity organic light emitting diodes", *Appl. Phys. Lett.* **69** (14), 1997 (1996).
- [28] D. G. Lidzey, D. D. C. Bradley, S. J. Martin, and M. A. Pate, "Pixelated multicolor microcavity displays", *IEEE Journal on Selected Topics in Quantum Electronics* **4** (1), 113 (1998).
- [29] Y. Fukuda, T. Watanabe, T. Wakimoto, S. Miyaguchi, and M. Tsuchida, "An organic LED display exhibiting pure RGB colors", *Synthetic Metals* **111-112**, 1 (2000).
- [30] J. Kido, S. Shirai, Y. Yamagata, and G. Harada, "Multicolor polymer electroluminescent devices", presented at *Mat. Res. Soc. Symp.* (San Francisco, CA, 1999).
- [31] S. R. Forrest, P. E. Burrows, Z. Shen, G. Gu, V. Bulovic, and M. E. Thompson, "Stacked OLED (SOLED): A new type of organic device for achieving high-resolution full-color displays", *Synthetic Metals* **91** (1-3), 9 (1997).
- [32] P. E. Burrows, Z. Shen, and S. R. Forrest, "Saturated full color stacked organic light emitting devices", *SID Conference Record of the International Display Research Conference*, 318 (1997).
- [33] G. Gu, V. Khalfin, and S. R. Forrest, "High-efficiency, low-drive-voltage, semitransparent stacked organic light-emitting device", *Appl. Phys. Lett.* **73** (17), 2399 (1998).

- [34] G. Parthasarathy, G. Gu, and S. R. Forrest, “Full-color transparent metal-free stacked organic light emitting device with simplified pixel biasing”, *Advanced Materials* **11** (11), 907 (1999).

# 4 Dye Transfer by Thermal Processing

The basic operation of OLED color patterning by local transfer of dye has been already outlined in Chapter 3.1.2. This chapter focuses in detail on the transfer of the dye from a dye source to the device, the subsequent thermally-driven diffusion of the dye in the device polymer film, and the obtained device characteristics. This chapter elaborates on these transfer processes themselves without any patterning. Chapter 5 describes the use of a solvent vapor to increase the diffusion of dye in the device polymer layer. Actual patterning approaches to locally change the emission color of a device are given in Chapter 6.

Chapter 4.1 gives the basic concept of masked dye transfer, and shows how it can be used to change the emissive color of the device. A method to create the dye source plate and carry out the whole process in air is demonstrated.

Chapter 4.2 presents the electroluminescence performance of dye-transferred devices, and the necessity of annealing after the initial dye transfer to distribute the dye throughout the polymer film. The ability to re-distribute the dye without damaging the polymer is raised as a key challenge to this thesis.

Chapter 4.3 and Chapter 4.4 introduce two methods to determine the distribution of dye in the polymer film, and results and limitations of these methods are presented.

The theory of diffusion in polymers and the concept of glass transition is discussed in Chapter 4.5 and Chapter 4.6.

## 4.1 Concept of Large-Area Dye Transfer

The concept of dye doping (see Chapter 2.10) where a small amount of dye is incorporated in a matrix to change the emission color and to increase the efficiency of the device is a widely utilized method [1][2][3][4][5]. We suggested the use of a large area dopant

source, which provided the dye to be transferred, and a shadow mask to locally pattern the emission color of the device [6]. The mask is sandwiched between the device substrate and the dye source as shown in Figure 4-1. The transfer is then carried out at elevated temper-

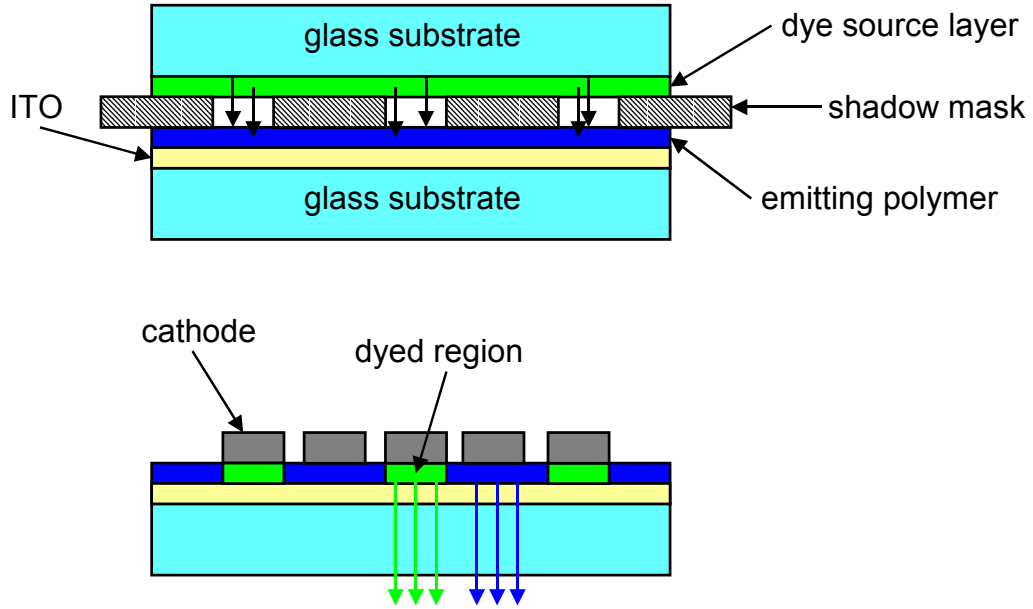


**Figure 4-1.** Local dye transfer to device polymer layer using a large area dye source and a shadow mask [6].

atures to enhance the transfer process. The dyed regions are subsequently capped with a cathode metal layer. If the dye has been properly chosen, the resulting device emits now only at the characteristic wavelength of the dye.

Figure 4-2 shows the photoluminescence spectra of a film which has been processed in this fashion: A film of pure PVK was held at 100 °C in an oven in air for different times during the transfer of the dye C6. The distance between the two substrates was about 50  $\mu\text{m}$ . The dye source was a substrate with a layer of pure C6 deposited by thermal evaporation. After a process time of 15 min, the spectrum shows an emerging C6 peak. The C6 emission dominated the spectrum after 30 min.

This process can be repeated with different masks and dyes to create separate regions of polymer emitting different colors. Integrated RGB devices fabricated with this technique are discussed in Chapter 8.1. It will also be shown that integrated RGB devices can be achieved with only two transfer steps.

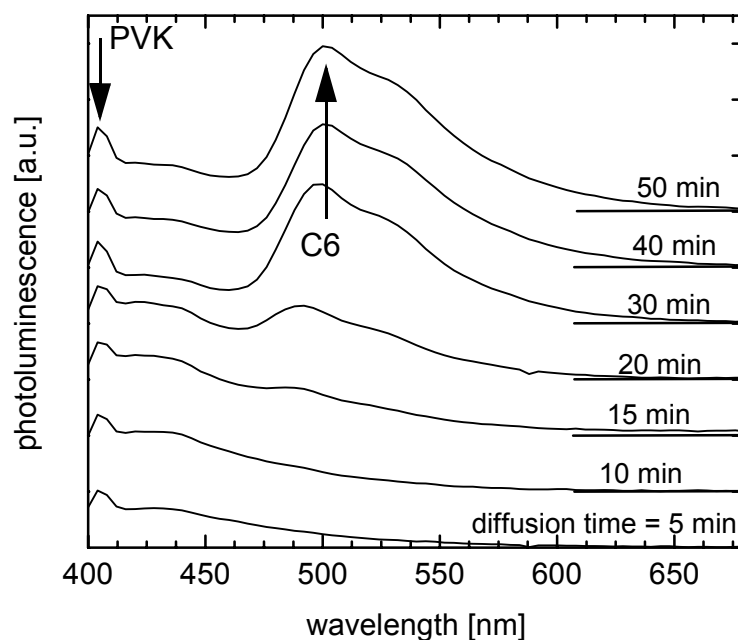


**Figure 4-2.** Photoluminescence spectra of a PVK film after different process times at 100 °C in air. The dye C6 was transferred to a film of pure PVK (emission peak at 495 nm) [6].

The process of large-area dye transfer outlined in this chapter has significant technological advantages over other patterning methods: The simultaneous processing over the whole area of the display offers a high throughput in the production process. In addition, the technology is compatible with roll-to-roll processing which could further improve the productivity.

However, this method also poses some problems. The shadow mask has to be precisely aligned to avoid “color-bleeding”. A method to replace the shadow mask by photolithographic means is discussed in Chapter 6.2. In addition, for the dye to be active, it must be diffused into the polymer layer rather than being accumulated at the polymer surface. To achieve this, we designed a post-transfer anneal step which is discussed in the next section.

## 4.2 EL Performance of Devices with Transferred Dye and Post-Dye-Transfer Annealing

### 4.2.1 Performance of the Device with Transferred Dye

Performing the dye transfer process on glass/ITO substrates (cleaned and oxygen-plasma-treated) and using the standard PVK/PBD mixture, we fabricated devices which we expected to emit according to the dye transferred. In addition to samples with transferred C6, we also prepared samples with Nile red transferred into the polymer film. In both cases, the transfer time was one hour at 80 °C in air. A cleaned glass slide with a heavily doped PVK layer (50% dye by weight in the final film) served as the dye source. After thermal evaporation of the Mg:Ag (10:1) cathode, the devices were tested and the efficiency was calculated. The efficiency was very low, but more surprisingly, the emission color did not change to the characteristic emission of the transferred dye. The external quantum efficiency of the devices did not exceed 0.05% for any device, and the emission was mainly from the PVK/PBD film. The I-V characteristics and the measured photocurrent are shown in Figure 4-3. For comparison, a control device with C6 contained in the spun-on film and not exposed to any heat treatment is also presented. Whereas the I-V curves for these devices are similar, the measured photo current is more than one order of magnitude less than that of the control device. To discern if this poor performance is caused by the heat treatment during the transfer process, we exposed a control device to the same heat treatment as a device undergoes during the transfer process (80 °C for one hour in vacuum). The device did not suffer considerable damage due to the heat treatment; neither the I-V curve nor the photo current show significant degradation as shown in Figure 4-3.

For a change in electroluminescence emission, the dye has to be in or close to the recombination zone of the device. It is known, because of the good hole transport property of PVK and the higher injection barrier for electrons, that the recombination zone in our devices is rather close to the cathode [8]. However, due to cathode quenching [9], it is unlikely that excitons will radiatively recombine very close to the cathode layer. The absorption length of UV light in the PVK/PBD layer is much greater than the distance from the cathode to the recombination zone. As a result, the PL spectrum is less sensitive to the location of the dye than the EL. Under these considerations and because the PL spectrum

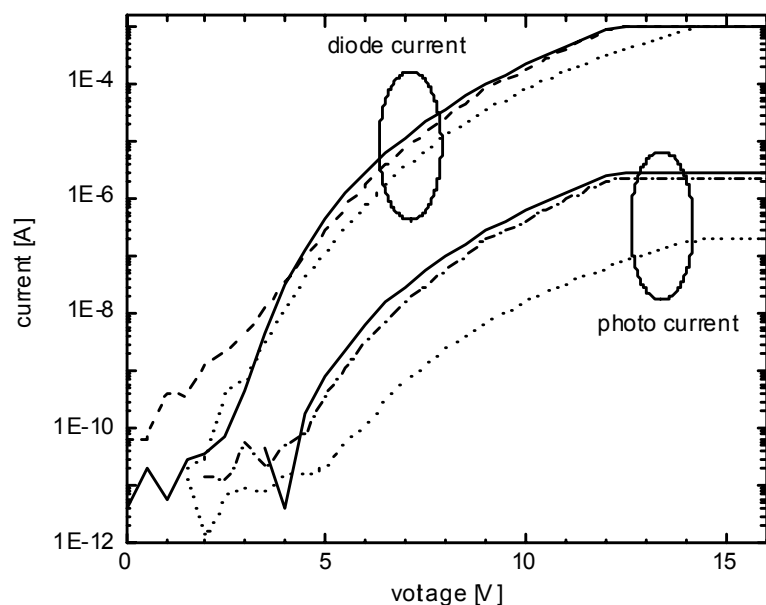


**Figure 4-3.** I-V characteristics and measured photo current of a control device (not exposed to any heat treatment, solid line), of a heat treated device (80 °C for one hour in vacuum, dashed line), and a device with C6 transferred by dye diffusion (80 °C for one hour in vacuum, dotted line) [7].

was dominated by the transferred dye under UV light, we could rule out the possibility that not enough dye was transferred.

From these results we concluded, that the dye probably accumulates on the surface or very close to the surface of the polymer layer. It may be that the very high concentration of dye in the near surface (which is where the EL occurs) leads to dye-dye complexes (excimer) which prevent emission from the dye (while PL can occur from a deeper layer). It is therefore necessary to drive the dye deeper into the bulk of the polymer film. The first approach to accomplish this was to expose the device to a high temperature treatment for an extended period of time after the initial dye transfer.

#### 4.2.2 Photoluminescence and Post-Dye-Transfer Annealing

The process of introducing a dye molecule into the target film consists basically of four steps: the dye must desorb from the source film, travel to the surface of the target film, and absorb on the surface (and not re-evaporate) and finally diffuse into the film. If the diffusion is slow compared to the desorption and transfer process, the transferred dye will pile up on top of or very near to the surface of the target polymer film. Thus annealing of the

sample after the dye source plate and the mask are removed might increase the photoluminescence as more dye diffuses into the film. Figure 4-4 shows the normalized PL spectra of a PVK/PBD/bimane film in which C6 was transferred at 80 °C for one hour in vacuum. The dye source substrate was a thin film of pure dye deposited by thermal evaporation on a glass substrate held at a distance of 50 μm to the polymer film. The film was then annealed at 90 °C for 3 hours in vacuum. The relative intensity of the C6 emission compared to the bimane emission increases after the anneal process, indicating that more dye is active in the emission process which previously was piled up on the surface of the polymer film.

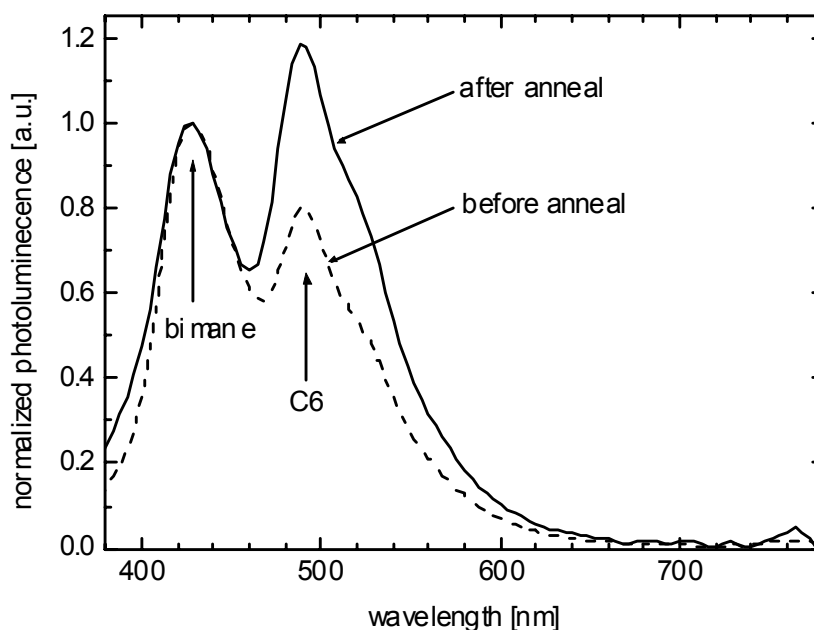


**Figure 4-4.** Normalized PL spectra of PVK/PBD/bimane film with C6 transferred. The sample was annealed for three hours at 90 °C.

### 4.2.3 Electroluminescence and Post-Dye-Transfer Annealing

After the device substrates with dyes diffused into the polymer were exposed to the heat treatment (three hours at 90 °C), a metal cathode was thermally evaporated (Mg:Ag, 10:1). Table 4-1 shows the external quantum efficiencies of devices fabricated this way in comparison to control devices with dye contained in the spin-on solution. In addition, Figure 4-5 shows the normalized EL spectra of device with bimane contained in solution and C6 or Nile red added by dye transfer. The emission is now clearly controlled by the diffused dye with only little emission from bimane. However, the efficiencies of the

devices were still quite low and the turn-on voltage was high compared to control samples with dye contained in the spin-on solution.

**Table 4-1.** External quantum efficiencies of devices with diffused dye and control devices [6]

	control device	diffused dye device
Blue (bimane)	0.25%	0.1%
Green (C6)	1%	0.4%
Red (Nile red)	0.6%	0.13%

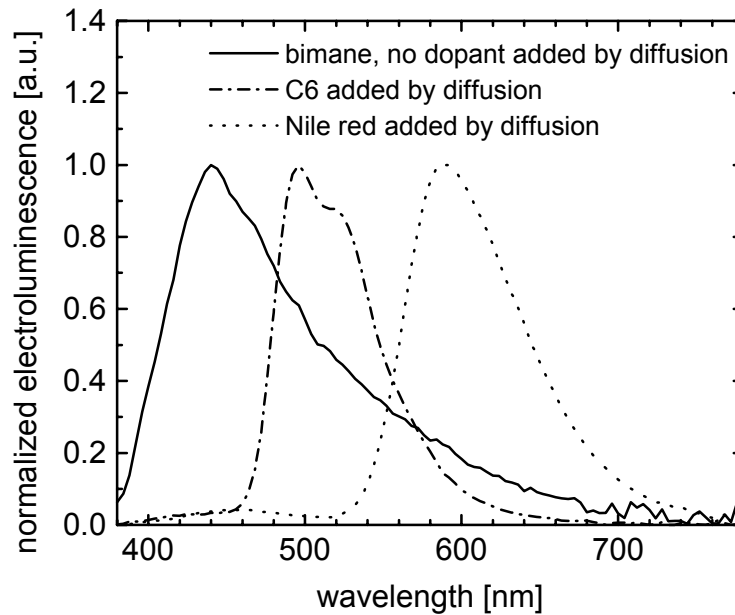


**Figure 4-5.** Electroluminescence spectra of a blue, green, and red device fabricated using the dye transfer method. Blue devices contained bimane from spin-coated film, green devices contained C6 (transferred) and bimane, and red devices contained Nile red (transferred) and bimane. After initial dye transfer at 70 °C, the samples were kept in vacuum at 70 °C for 12 hours. [6]

To investigate the reason for this poor performance, we exposed control samples with dye contained in solution (standard C6 device, see Chapter 2.8) to different temperatures in vacuum or air. Figure 4-6 shows the I-V curves and the measured photo-current of standard C6 samples (0.2% C6 in the final PVK/PBD film), which were exposed to different temperatures for one hour in vacuum. The turn-on voltage increased significantly from about 5 V for the non-treated sample to about 13 V for the sample kept at 115 °C for one hour. In addition, the efficiency of the devices was negatively impacted. The characteristics

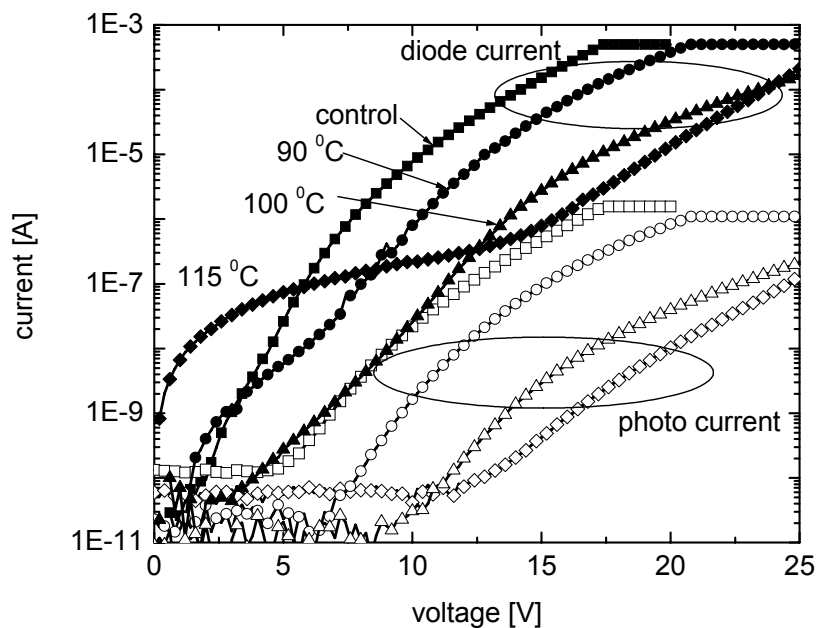


**Figure 4-6.** I-V characteristics (solid symbols) and measured photo-current (open symbols) of standard C6 devices exposed to heat treatment at various temperatures for one hour in vacuum.

of devices kept in air were even more degraded than those of devices kept in vacuum during the heat treatment.

These results clearly explain why the characteristics of devices with diffused dye have a lower efficiency. It also prohibits utilizing heat treatment as annealing step to drive the dye further into the bulk of the polymer film above 80 °C.

The damage due to heat treatment is very dependent on the polymer used. For MEH-PPV it has been reported [10] that annealing of a device at the glass transition temperature at 210 °C for several hours actually increased the efficiency because of the increased interchain interaction.

In Chapter 5, we show that exposing the device polymer to a solvent vapor can increase the diffusion of dye in the polymer by several orders of magnitude, so that a satisfactory dye re-distribution can be achieved at low processing temperatures.

## 4.3 Secondary Ion Mass Spectroscopy

### 4.3.1 Method for Probing the Dye Profile by SIMS

We employed Secondary Ion Mass Spectroscopy (SIMS) to determine the dye concentration profile in polymer films with transferred dye. Using a high energy ion beam (Cesium, 2 keV) targeted onto the polymer film, the molecules are destroyed on impact of the ions and the mass of the resulting ions of the debris is analyzed (ion counts per second). Because only the surface layer of the film is being destroyed and analyzed, repeated sputtering with the ion beam at the same spot yields depth information of the material composition of the film. The analyses were performed at Evans East in West Windsor, NJ.

### 4.3.2 Sulfur as Marker for C6 and Oxygen Interference

Figure 4-7 show SIMS data of a sample with C6 transferred into PVK at 70 °C for one hour. Because C6 is the only material containing sulfur, the element can be used as a tracer to indicate the distribution of C6. In this plot, the counts per second for carbon, oxygen, sulfur-32 and sulfur-34 are presented. The thickness of the polymer layer (850 nm by ellipsometry) was higher than the SIMS data showed (650 nm) because the sputter rate was not well calibrated in this case. The sulfur count increases at the polymer/ITO interface due to oxygen interference from the ITO ( $^{16}\text{O}_2^+$  is interpreted as  $^{32}\text{S}^+$ ). The profiles of the two sulfur isotopes are not perfectly proportional. Considering the natural abundance of sulfur-34 of 4.4%, the adjusted curve (sulfur-34 \* 22.5) is shown as a dotted line. The reason for this discrepancy was found to from oxygen in the polymer which increased the  $^{32}\text{S}^+$  signal. To avoid this interference, we observed that leaving the samples in the vacuum chamber prior to the analysis for several hours outgassing significantly reduced the amount of oxygen trapped in the film and, in turn, decreased the interference between the sulfur and oxygen signal. This is shown in Figure 4-8, where the same sample (a PVK/PBD film doped with C6 from a highly doped PVK film as dye source, dye transfer at 70 °C in vacuum for one hour) was analyzed twice, one time after approximately two hours in the vacuum chamber (solid lines) and then again after one additional hour (dashed lines). In the case where the sample was kept longer in the vacuum chamber, the oxygen signal is reduced due to outgassing of oxygen. At the same time, the 32-sulfur signal decreased as

well. However, the  $^{34}\text{S}$  signal remained constant, indicating that the decrease in  $^{32}\text{S}$  sulfur is due to the reduced interference from oxygen. In the following experiments reported in this thesis, the SIMS analyses were carried out after the sample was left in the vacuum chamber over night to minimize the influence of oxygen.

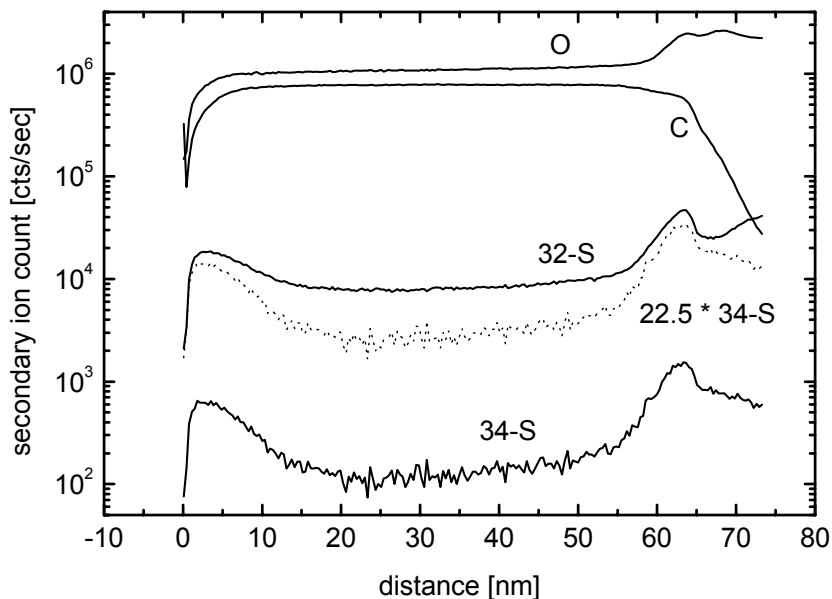


**Figure 4-7.** SIMS data of PVK film with C6 transferred at  $70^\circ\text{C}$  from a PVK layer highly doped with C6. The profiles for carbon, and the sulfur isotopes  $^{32}\text{S}$  and  $^{34}\text{S}$  and shown. The dashed line represents the  $^{34}\text{S}$  signal intensified according to the ratio of its natural abundance vs.  $^{32}\text{S}$ . The discrepancy between this signal and the  $^{32}\text{S}$  signal is due to oxygen interference.

### 4.3.3 Resolution Limit of SIMS

To establish a lower limit to the resolution of the SIMS analysis, we evaporated a very thin film of C6 ( $20\text{ \AA}$ ) onto a glass substrate spin-coated with a PVK layer. The sample was then analyzed without further treatment to ensure that the dye did not significantly diffuse into the PVK layer.

During the SIMS analysis, the heavy ions bombard the surface of the sample. Most of the debris will desorb from the surface on impact. However, some atoms are driven deeper into the film due to the momentum of the ion. This phenomenon is well understood and is usually referred to as the “knock-on effect”. We expected this effect to be particularly significant because of the low atomic number of the constituents of the polymeric material.

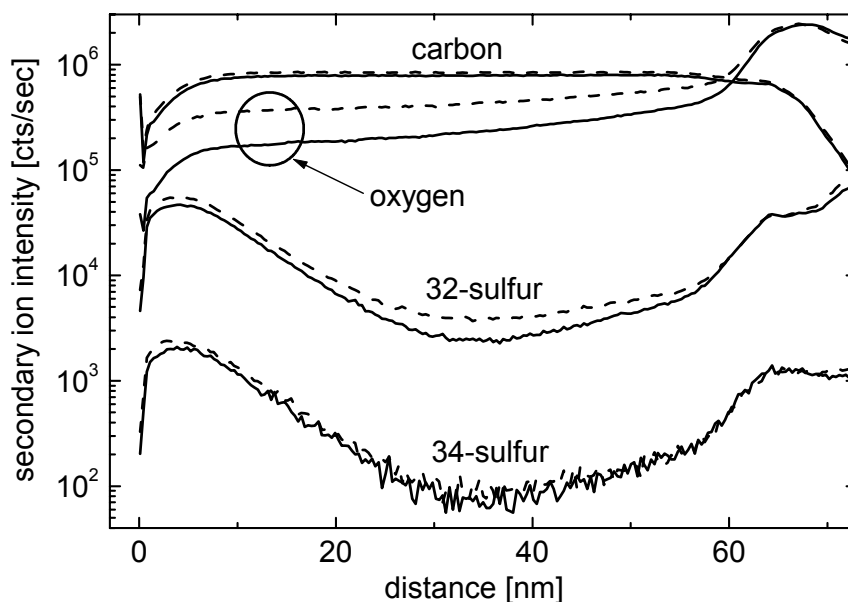


**Figure 4-8.** SIMS analyses of a PVK/PBD film in which was C6 was transferred for one hour at 70 °C from a highly doped PVK layer as the dye source. Two analyses were performed after the sample was kept for two hours (solid line) and after three hours (dashed lines) in the vacuum chamber. The oxygen signal decreased due to outgassing, and the 32-sulfur signal decreased because due to less interference with oxygen.

The SIMS profile of the sample is given in Figure 4-9 (squares) and is very similar to the one shown in Figure 4-7. From this observation, the SIMS resolution limit was determined to be 17 nm/decade. No useful information can therefore be obtained by SIMS if the dye concentration changes within 20 nm by more than a decade.

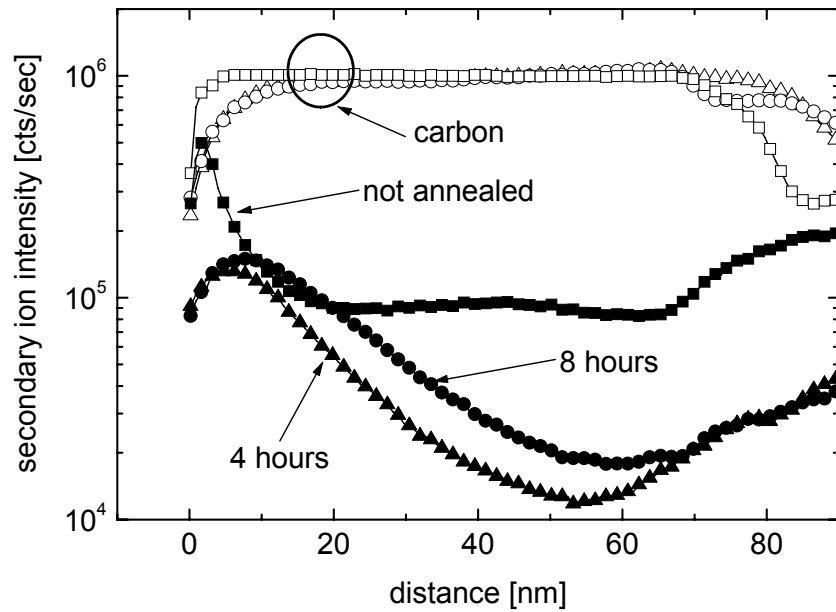
#### 4.3.4 Dye Profiles Before Annealing

Figure 4-7 and Figure 4-8 show that the dye is indeed accumulated on top of the polymer film or very close to the surface of the film after the transfer at 70 °C. It has been reported [11], that the diffusivity is enhanced near the surface of a polymer film due to extra free volume because of changes in the packing density. Therefore the dye may enter the polymer film during the initial transfer step at 70 °C, but does not substantially diffuse into the bulk of the layer.

#### 4.3.5 Dye Profiles after High-Temperature Annealing

SIMS was used to track the motion of dye during high-temperature annealing. In this case, the samples were prepared by evaporating a thin film of C6 on a sample with a

previously spun-on polymer layer (100 mg PVK, 40 mg PBD in 7 ml chlorobenzene, resulting in a 850 Å thick film). The PVK/PBD film was not intentionally heated during the evaporation. The samples were then annealed at 92 °C for 4 hours and for 8 hours. The resulting SIMS profiles are pictured in Figure 4-9. After annealing, the penetration of C6 into the PVK layer is still clearly limited. This result is in agreement with that obtained using Diffusion-Depth-Sensitive Photoluminescence (see Chapter 4.4). From the data of Figure 4-9, the diffusion coefficient in the standard PVK/PBD blend was estimated from the graph to be  $10^{-17}$  cm<sup>2</sup>/s.



**Figure 4-9.** SIMS profiles of PVK/PBD film with C6 deposited by thermal evaporation and then annealed for 4 hours (triangles) and 8 hours (circles) at 92 °C in vacuum. Open symbols represent the carbon signature, closed symbol the sulfur-32 signal. For comparison, the profile of a non-annealed sample is also shown (squares). The reason for the anomalously large dye signal in the polymer film before the high-temperature anneal is not known, and may be due to excess water vapor or oxygen in the film. [12]

The results of the thermal damage observed in I-V characteristics (see Chapter 4.2.3) together with this outcome pose the challenge. Device performance considerations do not permit a heat treatment at temperatures higher than 80 °C. At the same time, the dye does not diffuse sufficiently at temperatures below 92 °C in a reasonable time.

## 4.4 Diffusion-Depth-Sensitive Photoluminescence

Because SIMS is very expensive and has a slow turnaround, and because it is only applicable to dyes with chemical elements other than those found in the host (other than C, N, O), a rapid general method of estimating the dye profile and diffusion coefficient was sought.

Therefore we developed the technique to independently probing the photoluminescence at the top and the bottom of the polymer film after the dye diffusion.

### 4.4.1 Introduction to Diffusion-Depth-Sensitive Photoluminescence

Because the absorption length at the excitation wavelength of 254 nm is about 50 nm in PVK (less than the 100 nm thickness of the PVK film [13]), we were able to probe the front and the back of the PVK film separately as shown in Figure 4-10. This required the use of sapphire substrates, which are nearly transparent to UV light at this wavelength.

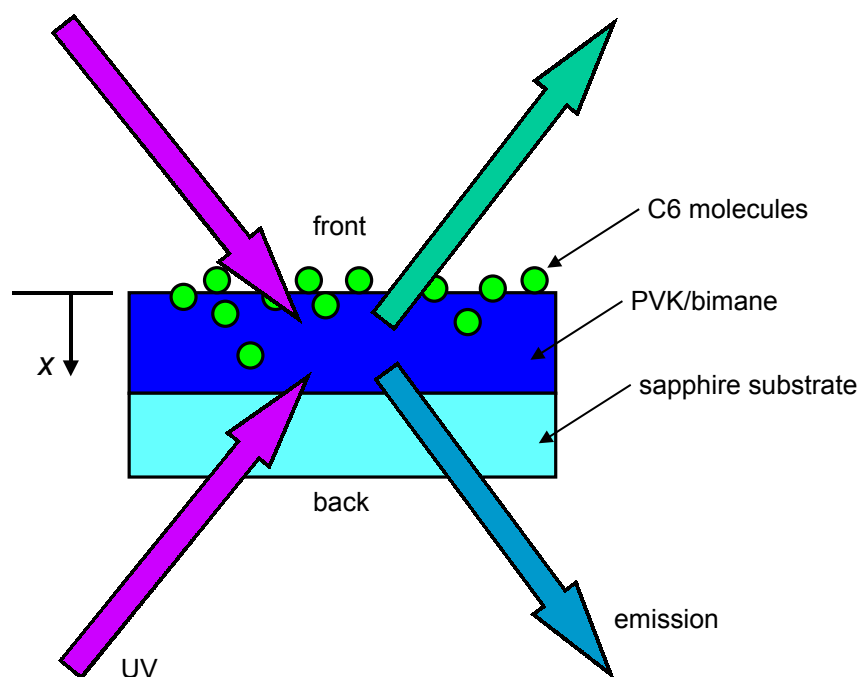


**Figure 4-10.** Diffusion Depth Sensitive Photoluminescence (DDSP): The polymer film containing bimane was excited by UV from the front and the back side of the sample and the resulting emission spectrum recorded.

#### 4.4.2 Quantitative Analysis

Our goal is to use this method to extract quantitative data on the dye profile. To this end we developed a quantitative model for extraction of  $D$  from the photoluminescence spectra. We expect that the actual dye profile will not be a simple solution of a Gaussian distribution (as for diffusion from a limited source) or a complimentary error function (as for diffusion from an unlimited source) (see Chapter 4.2, [14]). Because the dye diffuses from a very thin layer with a high concentration of dye on the surface of the polymer film into the bulk, the dye profile is likely to be a superposition of the two solutions. Knowing the absorption length of UV light by PVK (see Figure 2-13), it is possible to compute the diffusion length from the ratio of the intensity peak of the dyes on the front side in relation to the ratio on the back side. This approach assumes that the ratio of the emission peaks of bimane and C6 is a unique function of their mass ratio. To show this, we recorded PL spectra under UV illumination (215 nm) of a PVK film containing the dyes bimane (0.3% by weight in final film) and the appropriate amount of C6 in the spin-on solution. The C6/bimane emission ratio  $k(w) = \frac{I_{C6}}{I_{bimane}}$ , where  $w$  is the C6/bimane mass ratio and  $I$  is the peak intensity of the emission of the respective dye, is a linear function of the C6/bimane ratio for low C6 concentrations. At higher C6 concentrations, the function becomes super-linear as shown in Figure 4-11

Using the absorption length  $a$  of UV light (at 215 nm) in PVK, one can describe the local UV intensity  $I_{UV}$  within the polymer film by (refer to Figure 4-10)

$$I_{UV}(x) = I_0 \exp\left(-\frac{x}{a}\right) \quad (4-1)$$

where  $I_0$  is the incident UV intensity at the surface. The measured PL C6/bimane intensity ratio  $k_{\text{front}}$  from the front side (i.e. the polymer side) is therefore

$$k_{\text{front}} = \int_0^r I_{UV}(x) k(w(x)) dx \quad (4-2)$$

where  $r$  is the thickness of the polymer film and  $w(x)$  is the local C6/bimane mass ratio. Given the dye concentration  $g(x)$ , this ratio can also be written as

$$w(x) = \frac{C_0 g(x)}{c_{\text{bimane}}} = \kappa g(x) \quad (4-3)$$

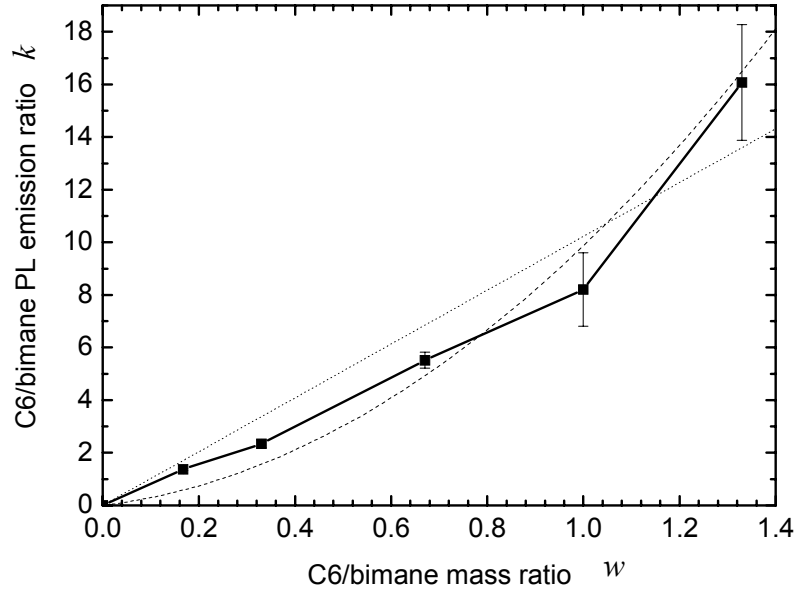


**Figure 4-11.** Ratio of C6/bimane PL emission of a PVK film containing 0.3% (by weight) bimane as a function of C6/bimane mass ratio. The C6 level is varied. The dashed line is a linear fit ( $k = 10.3 w$ ), and the dotted line is a quadratic fit ( $k = 2 w + 7.6 w^2$ ) [15].

where  $C_0$  is the total amount of C6 transferred and  $c_{\text{bimane}}$  is the bimane concentration in the film, which is constant because bimane is contained in the spin coated film. Approximating the function  $k(w)$  by a quadratic expression

$$k(w) = \alpha w + \beta w^2 \quad (4-4)$$

and substituting Equation (4-3) and Equation (4-4) in Equation (4-2) yields

$$k_{\text{front}} = \int_0^r I_{\text{UV}}(x) (\kappa \alpha g(x) + \beta \kappa^2 g^2(x)) dx \quad (4-5)$$

A similar expression can be obtained for the emission  $k_{\text{back}}$  from the backside of the substrate. Because we measure the ratio between the bimane and the C6 peak, the measurement is not influenced by absorption due to the sapphire substrate.

$$k_{\text{back}} = \int_0^r I_{\text{UV}}(r-x) (\kappa \alpha g(x) + \beta \kappa^2 g^2(x)) dx \quad (4-6)$$

We define now  $h$ , the dye uniformity coefficient [12], which is the quotient of the dye emission ratios  $k_{\text{front}}$  and  $k_{\text{back}}$ .

$$h = \frac{k_{\text{front}}}{k_{\text{back}}} = \frac{\int_0^r I_{\text{UV}}(x)(\kappa\alpha g(x) + \beta\kappa^2 g^2(x)) dx}{\int_0^r I_{\text{UV}}(r-x)(\kappa\alpha g(x) + \beta\kappa^2 g^2(x)) dx} \quad (4-7)$$

Substituting Equation (4-1) yields

$$h = \frac{k_{\text{front}}}{k_{\text{back}}} = \frac{\int_0^r \exp\left(-\frac{x}{a}\right)(\alpha g(x) + \beta\kappa g^2(x)) dx}{\int_0^r \exp\left(-\frac{r-x}{a}\right)(\alpha g(x) + \beta\kappa g^2(x)) dx} \quad (4-8)$$

For low C6 concentrations, a linear approximation of  $k(w)$  is sufficient ( $\beta=0$ ). In this case, Equation (4-7) can be simplified to

$$h = \frac{k_{\text{front}}}{k_{\text{back}}} = \frac{\int_0^r \exp\left(-\frac{x}{a}\right)g(x) dx}{\int_0^r \exp\left(-\frac{r-x}{a}\right)g(x) dx} \quad (4-9)$$

Assuming  $g(x)$  to be a Gaussian distribution (see Chapter 4.2)

$$g(x) = \frac{1}{\sqrt{\pi L}} \exp\left(-\frac{x}{L}\right)^2 \quad (4-10)$$

or a distribution governed by the complimentary error function,

$$g(x) = \text{erfc}\left(\frac{x}{2L}\right) \quad (4-11)$$

where  $L$  is the diffusion length, we computed  $h$  for different values of  $L$  based on Equation (4-9), as shown in Figure 4-12. The used MATLAB routine is given in the appendix

(Chapter 9.1). The parameter used in this calculation are listed in Table 4-2. If  $h = 1$ , the dye distribution is uniform throughout the film.

**Table 4-2.** Parameters of DDSP calculation

	variable in Equation (4-8)	MATLAB variable	value
UV absorption coefficient	$a$	abs	500 Å
polymer film thickness	$r$	n	1000 Å
	$\alpha$	alpha	10 (linear fit) 2 (quadratic fit)
	$\beta$	beta	0 (linear fit) 10 (quadratic fit)
	$\kappa$	kappa	1 or 100 cm <sup>3</sup>

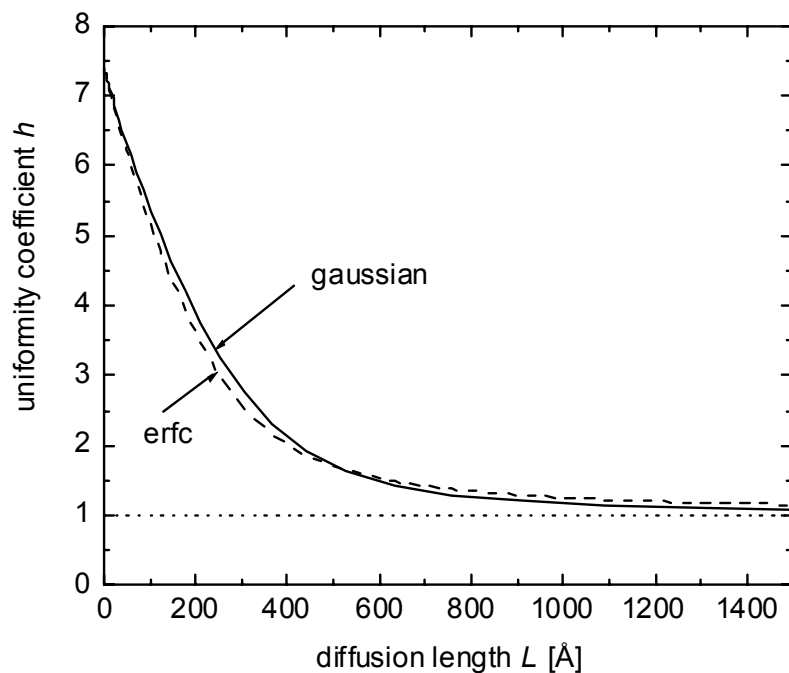


**Figure 4-12.** Computed uniformity coefficient  $h$  as a function of the diffusion length  $L$ . If  $h = 1$  the dye profile is flat in the polymer film.

#### 4.4.3 Limitations

The first source of error is introduced by neglecting excitonic diffusion. After being created on PVK, excitons are free to diffuse. Because of that, the place of creation does not necessarily coincide with the place of emission. This effect “smears out” the measurement,

leading to a higher diffusion length  $L$ . However, the diffusion is limited by the exciton lifetime on a dye molecule, which is very short. The maximum error is therefore about the mean distance between two dye molecules. For moderate doping level, this distance is  $\sim 10$  Å.

If the dye concentration is higher than that of bimane, the C6 emission grows super-linear with C6 concentration (see Figure 4-11). In this case, the assumption that  $\beta=0$  in Equation (4-9) is no longer valid. Depending on the dopant source used, the concentration of the transferred dye can be significantly higher than the bimane concentration. For example, if the dye source consists of a polymer film doped with 30% C6 and the bimane concentration in the PVK/PBD film is 0.3%, the C6 concentration in the device polymer film after the transfer process can be as much as 100 times higher than the concentration of bimane. Based on the parameters extracted from a quadratic fit of data shown in Figure 4-11 ( $\alpha = 2$ ,  $\beta = 7$  in Equation (4-4)), Figure 4-13 shows the impact of the increased C6 concentration with  $\kappa=100$  compared to the linear case with  $\beta = 0$  in case of a Gaussian distribution. For the same value of  $L$ ,  $h$  is increased for high dye concentrations, due to the non-linear C6/bimane emission ratio at high C6 doping levels.

As can be seen in Figure 4-13, the introduced error due to the quadratic term in  $k$  is relatively small and should not have a significant impact on the results of the measurements.

The technique also assumes that all transferred dye molecules are accessible to excitation by excitonic transfer from the PVK/PBD film. For this transfer to be possible, the dye molecules have to be in close proximity to the polymer strands. If dye molecules are piled up at the surface of the film after the initial dye transfer, this assumption is not valid because the accumulated dye will not be active in the photoluminescence process before the anneal due to the limited exciton diffusion length, surface recombination [16] and creation of excimer states (see Chapter 2.10). During the anneal process, the dye molecules move into the bulk of the polymer film and can thus be excited by exciton transfer from the PVK. This effective increase in the C6 amount is not accounted for in the model based on Equation (4-8).

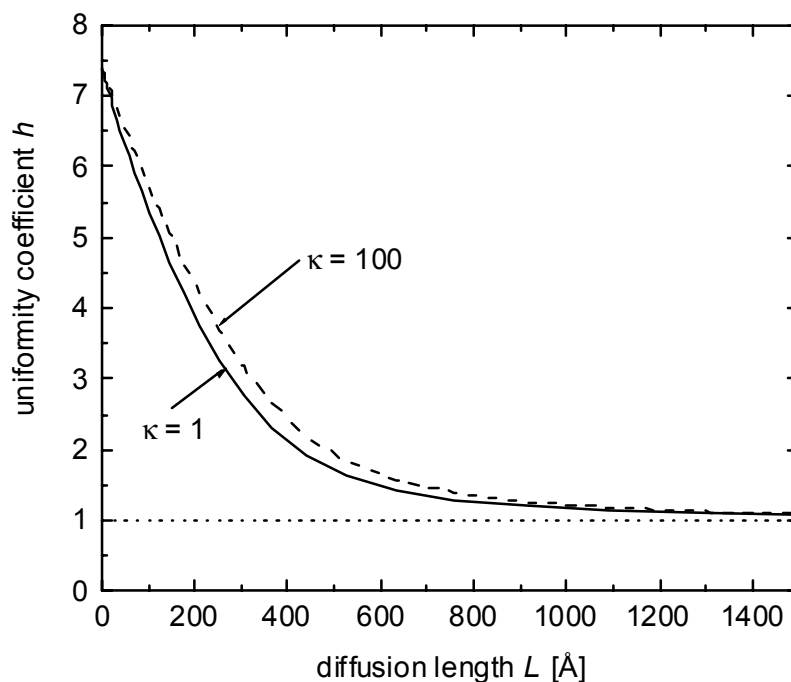


**Figure 4-13.** Computed uniformity coefficient  $h$  as a function of the diffusion length  $L$ . The dye distribution was assumed to be Gaussian. The coefficient was calculated for different dye loads  $\kappa = 1$  and  $\kappa = 100$ .

Comparing these three sources of error, the last one is certainly the most important, because the introduced error can render the measurement meaningless.

#### 4.4.4 Experimental Results

Figure 4-14 shows the effect of annealing a sample of PVK film (spun onto a transparent sapphire substrate), originally doped in solution with bimane, after C6 was transferred into it by the described process for one hour at 90 °C from a highly doped PVK film as the dye source. Before the anneal, the PL spectrum of the surface (excited from the front) shows a shoulder at about 500 nm corresponding to the emission of C6. However, the emission peak of bimane at 435 nm is still much more pronounced. The PL spectrum from the back side does not show any emission from C6 at all. This shows that the C6 diffused only into the front of the polymer film. After the sample was annealed at 90 °C for six hours in vacuum, the C6 peak becomes stronger. On the front surface, C6 emission now surpasses the intensity of bimane, whereas on the back side only a small shoulder due to the C6 emission emerged. From this we conclude, that the dye indeed diffuses deeper into the PVK

layer during annealing, but that the C6 concentration is still much higher at the front of the film compared to the back. However, calculating  $h$  for these spectra, we observed in this case that  $h_{\text{before}} < h_{\text{after}}$  ( $h_{\text{before}} = 1.39$ ,  $h_{\text{after}} = 2.62$ ), which means that the dye is less uniformly distributed after the anneal process than before. This result can only be explained if dye was activated during the anneal process.

Due to this limitation, quantitative data of the dye diffusivity in polymer films extracted using this method are very unreliable.

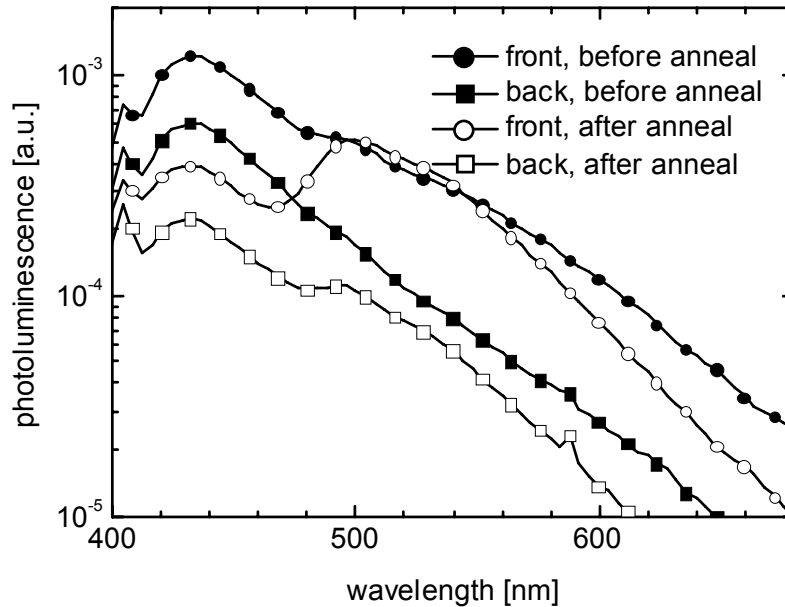


**Figure 4-14.** Photoluminescence spectrum (before and after annealing at 90 °C for 6 hours) of a PVK-film containing bimane in which C6 was diffused. The film was spun-on on a sapphire substrate to allow for probing the top and the bottom of the PVK film separately. The C6 peak is more pronounced after the substrate was annealed at elevated temperatures. [6]

## 4.5 Modelling of Dye Transport in Polymers

To fabricate efficient devices using the dye-transfer technique, the amount of dye transferred into the device polymer film and the dye concentration profile within this film has to be finely controlled. It is therefore important to identify the crucial process parameters and estimate their impact using established theories. Diffusion can be described in a simple differential equation. As a reference, Fick’s laws of diffusion are briefly reviewed in the beginning of this section. However, properties of materials and interfaces are not

accounted for in these equations. In addition, polymers show a variety of properties which are unknown in crystalline materials. We therefore will outline a basic approach to diffusion in polymers based on the free volume theory.

### 4.5.1 Fick's Laws of Diffusion

Diffusion is the redistribution of particles due to a concentration gradient. In a homogeneous medium, the particle flux is proportional to the concentration gradient with  $D$  being the proportionality factor referred to as the diffusion coefficient. Fick's first law describes the diffusion in a homogeneous, isotropic medium [17]:

$$\vec{j} = -D \vec{\nabla} c \quad (4-12)$$

where  $\vec{j}$  is the particle flux, and  $c$  the concentration of the diffusant. Because of mass conservation

$$-\vec{\nabla} \cdot \vec{j} = \frac{\partial c}{\partial t} \quad (4-13)$$

Equation (4-12) can be written as (Fick's second law):

$$\frac{\partial c}{\partial t} = D \nabla^2 c \quad (4-14)$$

These equations assume that the properties of the medium do not change during the diffusion process and are independent of the location. In the one-dimensional case, Equation (4-14) can be simplified to

$$\frac{\partial c}{\partial t} = D \frac{\partial^2 c}{\partial x^2} \quad (4-15)$$

## 4.5.2 Solutions of Diffusion Equations

### 4.5.2.1 Diffusion with Constant Amount of Dopant

If the total amount of dopant is conserved during the diffusion process, the boundary condition can be written as

$$S = \int_0^{\infty} c(x, t) dx \quad (4-16)$$

where  $S$  is the total amount of dopant. If the initial distribution of dye can be described by a  $\delta$ -function, the solution of Equation (4-15) is then a Gaussian distribution of the dopant given by [14]

$$c(x, t) = \frac{S}{\sqrt{\pi Dt}} \exp\left(-\frac{x^2}{4Dt}\right) \quad (4-17)$$

#### 4.5.2.2 Unlimited Source

The boundary condition

$$c(0, t) = c_s \quad (4-18)$$

represents the case in which the surface concentration of the dopant  $c_s$  is held constant during the diffusion. The resulting diffusion profile is given by the complementary error function defined as

$$\operatorname{erfc} x = 1 - \operatorname{erf} x = 1 - \frac{2}{\sqrt{\pi}} \int_0^x \exp(-w^2) dw = \frac{2}{\sqrt{\pi}} \int_x^\infty \exp(-w^2) dw \quad (4-19)$$

which can be interpreted as the superposition of infinite Gaussian distributions. The solution to the diffusion equation Equation (4-15) is in this case given by [14]

$$c(x, t) = c_s \operatorname{erfc}\left(\frac{x}{2\sqrt{Dt}}\right) \quad (4-20)$$

#### 4.5.3 Diffusion in Polymers - Free Volume Theory

Because of the importance of the diffusivity  $D$ , as we have seen in previous chapters, it is necessary to investigate the nature of diffusion in polymers in more detail.

In most cases, polymers form glasses below the glass transition temperature. A glass is a solid with random orientation of the molecules because the material was cooled fast enough so that no crystallization of the polymer could occur. The glass transition temperature  $T_g$  of the polymer is the temperature where the polymer sections are able to move cooperatively. The glass transition is a shift from the glassy state to a more viscous state, and it is accompanied by an increase in specific heat and thermal expansion [18].

Because of the intrinsic disorder of the glass (below and above the glass transition), the occupied volume is bigger than that of the crystalline form. The difference is referred to as “free volume” [19],

$$V_f = V_0 - V_c \quad (4-21)$$

where  $V_f$  is the free volume,  $V_0$  is the measured volume of the polymer and  $V_c$  is the volume in its crystalline form. The “fractional free volume”  $f$  is defined as

$$f = \frac{V_f}{V_0} \quad (4-22)$$

Treating the polymer chains like Brownian spheres and neglecting the interaction between the chains, the diffusivity  $D$  of small particle in the polymer matrix was predicted to behave according to the Stokes-Einstein-Equation: where  $k$  is the Boltzmann constant,  $T$

$$D = \frac{kT}{3\pi d\eta} \quad (4-23)$$

the temperature,  $d$  the “diameter” of the polymer, and  $\eta$  the shear viscosity of the polymer. Since it is impossible to assign a diameter to an elongated structure like a polymer, the diffusion was empirically modeled based on the radius of gyration of the polymer segment using the unknown proportionality factor  $\kappa$ .

$$D = \frac{kT}{\xi} \quad \text{with} \quad \xi = \kappa\eta \quad (4-24)$$

Measuring the volume and the viscosity of polymers [20], the following dependency was found ( $V_c$  and  $V_f$  measured at the same temperature)

$$\eta = a \cdot \exp\left(b \frac{V_c}{V_f}\right) \quad (4-25)$$

with  $b \approx 1$ . Therefore

$$\ln \xi = \ln \kappa + \ln a + b \frac{V_c}{V_f} \approx \ln(\kappa a) + \frac{V_c}{V_f} \quad (4-26)$$

and with

$$\frac{V_c}{V_f} = \frac{V_0 - V_f}{V_f} \quad (4-27)$$

follows

$$\ln \xi = \ln(\kappa a) - 1 + \frac{1}{f} \quad (4-28)$$

Using Equation (4-24), the diffusion coefficient can be written as

$$\ln D = \ln kT - \ln \xi \quad (4-29)$$

For two sets of measurements

$$\begin{aligned} \ln D_1 &= \ln kT_1 - \ln \xi_1 \\ \ln D_2 &= \ln kT_2 - \ln \xi_2 \end{aligned} \quad (4-30)$$

a temperature shift factor  $a_T$  can be defined as

$$\ln a_T = \ln \frac{D_2}{D_1} = \ln \frac{T_2}{T_1} + \ln \frac{\xi_2}{\xi_1} \quad (4-31)$$

In all cases of interest  $\ln \frac{T_2}{T_1} \ll \ln \frac{\xi_2}{\xi_1}$ , and therefore  $a_T$  can be expressed as

$$\ln a_T = \ln \frac{\xi_2}{\xi_1} = \frac{1}{f_1} - \frac{1}{f_2} \quad (4-32)$$

If  $T_2$  is chosen to be  $T_g$ ,  $a_T$  becomes

$$\ln a_T = \frac{1}{f_1} - \frac{1}{f_{Tg}} \quad (4-33)$$

The accelerated volume increase above  $T_g$  is due to added free volume superimposed on the volume increase due to ordinary thermal expansion. The linear approximation of the thermal expansion coefficient  $\alpha_1$  above  $T_g$  can be written as

$$\alpha_1 = \alpha_g + \alpha_f \quad (4-34)$$

where  $\alpha_g$  is the contribution of the expansion due ordinary thermal expansion and  $\alpha_f$  the

contribution due to added free volume as shown in Figure 4-15.

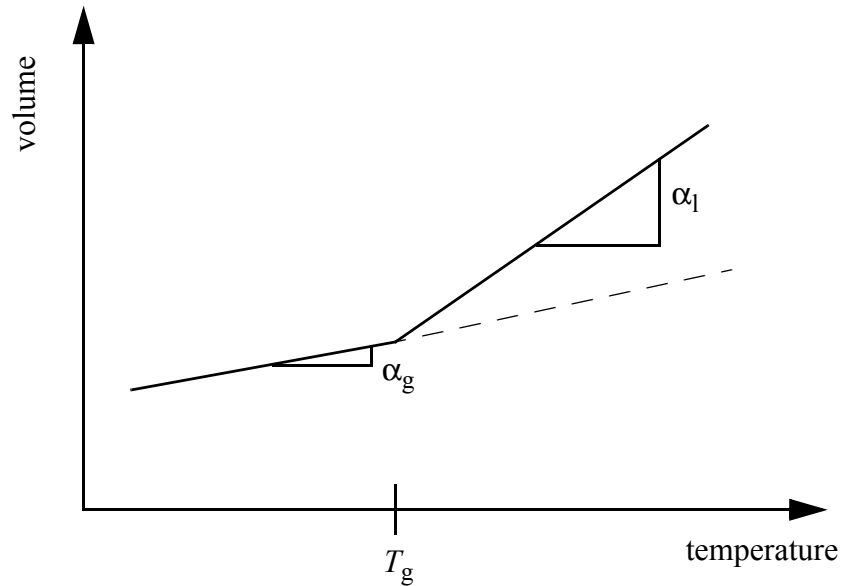


**Figure 4-15.** Volume expansion of amorphous polymer below and above the glass transition temperature  $T_g$ . The dashed line represents the behavior of a crystal. The contribution beyond that is due to free volume. [18]

Using this linear approximation, the expression for the fractional free volume can be expressed as

$$f = \frac{V_f}{V_0} = \frac{V_f(T_g) + \alpha_f V_0 (T - T_g)}{V_0} = f_{T_g} + \alpha_f (T - T_g) \quad (4-35)$$

Substituting Equation (4-35) into Equation (4-33) yields

$$\begin{aligned} \ln a_T &= \frac{1}{f_{T_g} + \alpha_f (T - T_g)} - \frac{1}{f_{T_g}} \\ &= \frac{-\frac{1}{f_{T_g}} (T - T_g)}{\frac{f_{T_g}}{\alpha_f} + T - T_g} \end{aligned} \quad (4-36)$$

The equation Equation (4-36) has the same form as the equation empirically developed by William, Landel and Ferry (WLF-equation) [21][22]:

$$\log a_T = \frac{-c_1 (T - T_g)}{c_2 + T - T_g} \quad (4-37)$$

The values for  $c_1$  and  $c_2$  are quite similar for a wide variety of polymers. Often quoted values are  $c_1 = -17.44$  and  $c_2 = 51.6$  K [23][24]. Knowing the diffusion coefficient at the glass transition temperature  $D_g$ , the temperature dependence of the diffusivity is predicted as [23]

$$\log D(T) = \frac{-c_1 (T - T_g)}{c_2 + T - T_g} + \log D_g \quad (4-38)$$

This model is only valid above and around  $T_g$ . The model describes the effect of free volume on the diffusivity which has an appreciable impact only at temperatures around and above  $T_g$ .

In Chapter 5.5, we will use this model to explain the findings with regard to the diffusivity of dye in the PVK/PBD matrix.

## 4.6 Glass Transition in Mixed Systems

According to Equation (4-38), the diffusivity  $D$  is mainly determined by the difference between the process temperature  $T$  and the glass transition temperature  $T_g$ . It is therefore of great importance to examine the relationship between the polymer blend and the glass transition temperature  $T_g$ . In a material system consisting of different components with different  $T_g$ , the  $T_g$  of the blend will be a function of the mass fraction of the component and its  $T_g$ .

### 4.6.1 Fox Equation

From the WLF-equation Equation (4-38), we can determine the free-volume-fraction  $f$  at  $T_g$ . Comparing Equation (4-36) with Equation (4-37) yields the following relationship:

$$f_{T_g} = \frac{\log e}{c_1} = \frac{0.434}{17.44} = 0.025 \quad (4-39)$$

Under the assumption the constants  $c_1$  and  $c_2$  do not depend on the chemical structure of the polymer, this result indicates that the polymer at its glass transition has 2.5% free volume. The glass transition can therefore be regarded as iso-free-volume-state.

The Simha-Boyer-Rule [25] states that the product of the thermal expansion due to the added free-volume and the glass transition temperature is constant.

$$\alpha_f T_g = \gamma = \text{const} \approx 1500 \quad (4-40)$$

In a system consisting of different materials, the free volume of the different components adds up. Therefore, where  $\Phi_i$  is the volume fraction of component  $i$

$$f_{\text{blend}} = \sum_i \Phi_i (f_{T_g} + \alpha_{fi} (T - T_{gi})) \quad (4-41)$$

$$1 = \sum_i \Phi_i \quad (4-42)$$

and  $T_{gi}$  its glass transition temperature. At  $T = T_g$  of the blend,  $f_{\text{blend}}$  is  $f_{T_g}$ , and Equation (4-41) can therefore be written as

$$0 = \sum_i \Phi_i \alpha_{fi} (T_{g \text{ blend}} - T_{gi}) \quad (4-43)$$

Using the Simha-Boyer-Rule Equation (4-40) yields

$$0 = \sum_i \Phi_i \left( \frac{\kappa}{T_{gi}} T_{g \text{ blend}} - \kappa \right) = \sum_i \Phi_i \left( \frac{T_{g \text{ blend}} - T_{gi}}{T_{gi}} \right) \quad (4-44)$$

which, using Equation (4-42), can be simplified to

$$\frac{1}{T_{g \text{ blend}}} = \sum_i \frac{\Phi_i}{T_{gi}} \quad (4-45)$$

This result is very similar to the empirical equation reported by Fox *et al.* [26]

$$\frac{1}{T_{g \text{ blend}}} = \sum_i \frac{w_i}{T_{gi}} \quad (4-46)$$

where  $w_i$  is the mass fraction of component  $i$ , rather than the volume fraction  $\Phi_i$  in Equation (4-45). If the density of all components is the equal, both equations are equivalent.

The Fox equation Equation (4-46) is a very good approximation for the glass transition temperature  $T_{g \text{ blend}}$  of a mixed system if the intermolecular interactions between the different moieties is weak [22].

#### **4.6.2 Prediction for PVK/PBD**

The glass transition temperature of the PVK:PBD blend (100:40 by weight) was measured to be 120 °C [27]. The weight fraction of PVK in the solid film of the PVK/PBD-blend used in this thesis is therefore 0.71, and the one of PBD 0.29. Using Fox' equation Equation (4-46) and assuming that the  $T_g$  of pure PVK is 473 K [28], we calculated  $T_g$  of the PBD component to be 278 K.

### **4.7 Diffusivity of C6 in PVK/PBD Films**

At a temperature of 92 °C (i.e. below the glass transition of PVK/PBD), the diffusivity of C6 in the polymer blend was measured to be approximately  $10^{-17}$  cm<sup>2</sup>/s (see Figure 4-9). Using DDSP, some further measurements of the diffusivity vs. temperature were obtained. Because these results are related to the work on Solvent Vapor Anneal (Chapter 5) or Patterned Dye Diffusion (Chapter 6), these results are given in their respective context.

### **4.8 Summary**

The fundamental principle of the dye transfer technique has been shown to achieve the desired shift in emission color. However, the efficiency of the devices is very low due to that fact that the dye is not sufficiently homogeneously distributed in the polymer film. During the transfer, the dye molecules accumulate at the surface of the film and thus quench the luminescence. Thermal anneal of the polymer film after the initial dye transfer to obtain a more uniform dye distribution has been demonstrated. At the same time, thermal damage to the polymer film due to the thermal anneal has a detrimental effect on the device performance. It is therefore necessary to find another way to obtain a homogeneous dye distribution without significantly increasing the process temperature.

## 4.9 References

- [1] S. Tasch, E. J. W. List, C. Hochfilzer, G. Leising, P. Schlichting, U. Rohr, Y. Geerts, U. Scherf, and K. Müllen, “Efficient red- and orange-light-emitting diodes realized by excitation energy transfer from blue-light-emitting conjugated polymers”, *Phys. Rev. B* **56** (8), 4479 (1997).
- [2] A. A. Shoustikov, Y. You, and M. E. Thompson, “Electroluminescence Color Tuning by Dye Doping in Organic Light-Emitting Diodes”, *IEEE Journal of Selected Topics in Quantum Electronics* **4** (1), 3 (1998).
- [3] Y. Armada, H. Kana, T. Tsujioka, T. Hisakazu, and T. Usuki, “Red organic light-emitting diodes using an emitting assist dopant”, *Appl. Phys. Lett.* **75** (12), 1682 (1999).
- [4] D. F. O'Brien, C. Giebeler, R. B. Fletcher, A. J. Cadby, L. C. Palilis, D. G. Lidzey, P. A. Lane, D. D. C. Bradley, and W. Blau, “Electrophosphorescence from a doped polymer light emitting diode”, *Synth. Met.* **116**, 379 (2001).
- [5] M. D. McGehee, T. Bergstedt, Z. Chi, A. P. Saab, M. B. O'Regan, G. C. Bazan, V. I. Srdanov, and A. J. Heeger, “Narrow bandwidth luminescence from blends with energy transfer from semiconducting conjugated polymers to europium complexes”, *Advanced Materials* **11** (16), 1349 (1999).
- [6] F. Pschenitzka and J. C. Sturm, “Three-color organic light-emitting diodes patterned by masked dye diffusion”, *Appl. Phys. Lett.* **74** (13), 1913 (1999).
- [7] F. Pschenitzka and J. C. Sturm, “Patterned dye diffusion using transferred photoresist for polymer OLED displays”, *Proceedings of SPIE - The International Society for Optical Engineering* **4105**, 59 (2001).
- [8] K. Long, M.-H. Lu, F. Pschenitzka, and J. C. Sturm, “Novel Three-Color Polymer Light-Emitting Devices for Passive-Matrix Flat Panel Display”, *Device Research Conference* , 179 (2001).
- [9] A. L. Burin and M. A. Ratner, “Exciton migration and cathode quenching in organic light emitting diodes”, *Journal of Physical Chemistry A* **104** (20), 4704 (2000).
- [10] T.-Q. Nguyen, R. C. Kwong, M. E. Thompson, and B. J. Schwartz, “Improving the performance of conjugated polymer-based devices by control of interchain interactions and polymer film morphology”, *Appl. Phys. Lett.* **76** (17), 2454 (2000).

- [11] K. C. Tseng, N. J. Turro, and C. J. Durning, "Molecular mobility in polymer thin films", *Phys. Rev. E* **61** (2), 1800 (2000).
- [12] F. Pschenitzka and J. C. Sturm, "Solvent-enhanced dye diffusion in polymer thin films for color tuning of organic light-emitting diodes", *Appl. Phys. Lett.* **78** (17), 2584 (2001).
- [13] J. M. Pearson and M. Stolka, *Poly(N-vinyl carbazole)* (Gordon and Breach, New York, 1981).
- [14] S. M. Sze, *Semiconductor Devices: Physics and Technology* (John Wiley & Sons, New York, 1985).
- [15] F. Pschenitzka and J. C. Sturm, "Three-color doping of polymer OLEDs by masked dye diffusion", *Proc. Mat. Res. Soc.* **558**, 513 (2000).
- [16] D. Z. Garbuzov, V. Bulovic, P. E. Burrows, and S. R. Forrest, "Photoluminescence efficiency and absorption of aluminum-tris-quinolate (Alq<sub>3</sub>) thin films", *Chemical Physics Letters* **249** (5-6), 433 (1996).
- [17] A. L. Ruoff, *Introduction to Material Science* (Prentice-Hall, Inc., Eaglewood Cliffs, New Jersey, 1973).
- [18] D. Turnbull and M. H. Cohen, "Free-Volume Model of the Amorphous Phase: Glass Transition", *J. Chem. Phys.* **34** (1), 120 (1961).
- [19] R. A. Register, lecture notes of course "Solid-State Properties of Polymers", taught at Princeton University, Department of Chemical Engineering.
- [20] A. K. Doolittle, "Studies in Newtonian Flow. II. The Dependence of the Viscosity of Liquids on Free Space", *Journal of Applied Physics* **22** (12), 1471 (1951).
- [21] M. L. Williams, R. F. Landel, and J. D. Ferry, "The Temperature Dependence of Relaxation Mechanisms in Amorphous Polymers and Other Glass-forming Liquids", *Am. Chem. Soc.* **77**, 3701 (1955).
- [22] J. D. Ferry, *Viscoelastic properties of polymers*, 2 ed. (Wiley, New York, 1970).

- [23] T. E. Shearmur, D. W. Drew, A. S. Clough, M. G. D. v. d. Grinten, and A. t. Slark, "Study of dye diffusion using Rutherford backscattering", *Polymer* **37** (13), 2695 (1996).
- [24] A. T. Slark and J. O'Kane, "Solute Diffusion in Relation to the Glass Transition Temperature of Solute-Polymer Blends", *Eur. Polym. J.* **33** (8), 1369 (1997).
- [25] Simha, Boyer, *Journal of Chemical Physics*, 37, 1003 (1962).
- [26] T. G. Fox, *Bull. Am. Phys. Soc.* **1**, 123 (1956).
- [27] measured by differential scanning calorimetry (DSC), personal communication with X. Jiang and R. Register, Princeton University (1999).
- [28] Adrich, technical information on PVK, obtained from [www.aldrich.com](http://www.aldrich.com) (2001).

# 5 Solvent-Vapor-Assisted Dye Diffusion

As shown in the previous chapter, the diffusivity of dye in the polymer film is mainly governed by the difference between the process temperature and the glass transition of the polymer composite. In the previous chapter, we saw that the diffusion of dye in a PVK/PBD blend ( $T_g = 120$  °C) at the temperature of 90 °C was not enough to distribute the transferred dopant uniformly throughout the polymer film. Increasing the process temperature has a negative effect on the device performance and was therefore not a viable approach for increasing the dye diffusion. We therefore pursued an approach where we temporarily lowered the glass transition temperature of the film to let the dye diffuse at room temperature. This way we obtained devices with dye-doped polymer layer without having to compromise the device characteristics due to high temperature processing.

In Chapter 5.1, the basic concept of solvent-vapor-assisted dye diffusion is discussed. Chapter 5.2 focuses on device annealing in saturated solvent vapor, and Chapter 5.3 describes the process in a atmosphere with a controlled amount of solvent vapor. The amount of transferred dye is very important for the device performance. The results to optimize this aspect of the process are given in Chapter 5.4.

A comparison of experimental results for the diffusivity of dye in PVK/PBD with the WLF-model is discussed in Chapter 5.5.

A brief summary of the findings is given in Chapter 5.6.

## 5.1 Basic Concept of Dye Diffusion Enhancement in Solvent Vapor

According to the modified WLF-equation, Equation (4-27), based on the free volume theory of diffusion in polymers outlined in Chapter 4.3, the diffusion coefficient  $D$

$$\log D(T) = \frac{-c_1 (T - T_g)}{c_2 + T - T_g} + \log D_g \quad (5-1)$$

depends mainly on the molecular volume of the diffusant and on the difference between the process temperature  $T$  and the glass transition temperature  $T_g$  while assuming  $c_1$  and  $c_2$  to be parameters independent of the polymer.

To enhance the diffusion, either the process temperature has to be increased or the glass transition temperature of the polymer has to be decreased. The degradation of the OLED performance caused by the high temperature anneal (see Chapter 4.2.3), prohibits the increase of the process temperature. On the other hand, a high  $T_g$  is desirable for device stability: Due to power dissipation, the operating temperature of the OLED can be quite high. If the operating temperature rises close to  $T_g$ , the device degrades very quickly. Because of the poor heat conduction of the glass substrate, the device temperature can easily exceed 80 °C [1]. To employ a polymer with a low  $T_g$  is consequently counterproductive.

We were therefore looking for a method to temporarily lower  $T_g$  during the dye-patterning process. From the Fox' equation (see Chapter 4.4), it is known that  $T_g$  can be changed by mixing the polymer with material with a different  $T_g$ . For example, pure PVK has a  $T_g$  of about 220 °C. Mixing this polymer with PBD (29% by weight in final film) lowers  $T_g$  of the mixture to about 120 °C due to the low  $T_g$  of PBD. The Fox' equation does not take any molecular interactions of the mixed substances into account. However, the measured values of  $T_g$  are often in very good agreement with the predictions [2].

Mixing a solvent into the polymer film has a similar effect. Because the glass transition temperature of common organic solvents is very low, the combined  $T_g$  of the polymer-solvent-system is lowered as well and, in effect, the diffusion is enhanced. To introduce the solvent into the polymer film, we exposed the polymer to solvent vapor.

During this process, the entropy of mixing of the solvent and the polymer leads to an uptake of solvent into the polymer and thus to a swelling of the film. The solvent was eliminated after the anneal process by drying the polymer film in nitrogen and the polymer regains its original higher  $T_g$  [3][4][5][6][7]. These macroscopic and microscopic processes are pictured in Figure 5-1

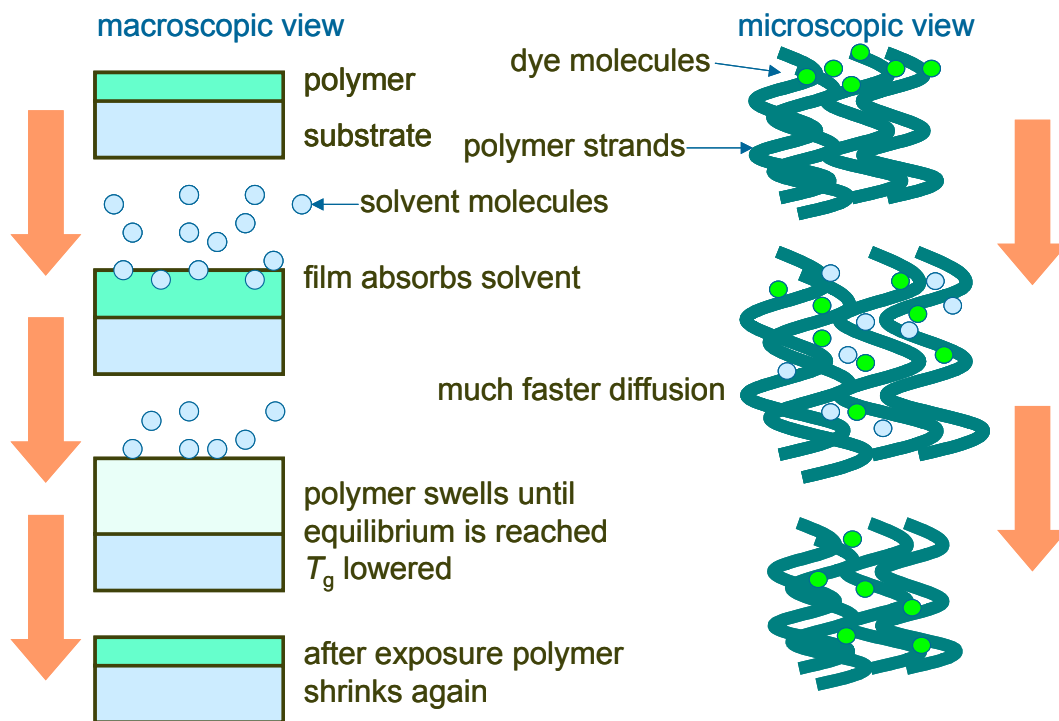


**Figure 5-1.** Microscopic and macroscopic processes during the solvent-vapor assisted anneal.

## 5.2 Annealing in Saturated Solvent-Vapor

### 5.2.1 Experimental Apparatus

To investigate the dye diffusion using this technique, we fabricated devices with transferred dye, which were subsequently annealed in solvent atmosphere. The polymer film (PVK/PBD/C47) was spun-on onto ITO substrates prepared by the standard procedure (see Chapter 2.8). The dye source substrate was a glass slide with a spun-on layer of the polymer Vylon 103 (obtained from Toyoba, molecular weight 20,000 - 25,000 g/mole, glass transition temperature 47 °C) containing C6 (2% by weight in the final film). The polymer was dissolved in chloroform (18 mg/ml) and spun on at 2000 rpm resulting in

films approximately 1200 Å thick. The initial transfer of C6 was carried out by placing the device substrate and the dye source substrate into direct contact at 64 °C for one hour in vacuum. After the transfer, the dye is still located on the surface of the polymer film. To lower the temperature required for dopant diffusion, we then studied the dye diffusion in air saturated with acetone vapor. Beside the dye-diffused device, a control sample was created in which the dye C6 was already mixed into the PVK/PBD/C47 solution (0.2% by weight in final film) before spin-coating.

During the anneal process, the samples were placed on a little tripod in a glass container as shown in Figure 5-2. The glass container was filled with acetone, however, the samples did not come into direct contact with the solvent. The container was then covered so that the air inside the container became saturated with acetone.

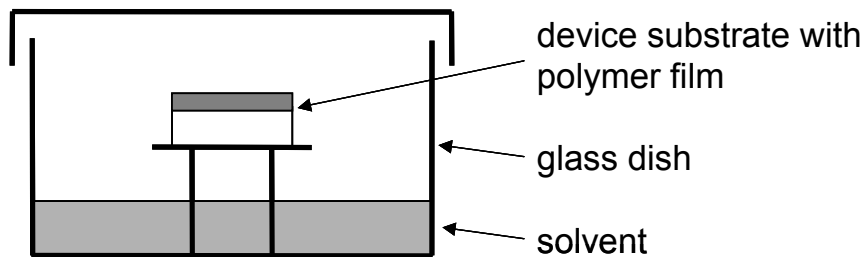


**Figure 5-2.** Experimental apparatus to anneal devices in saturated solvent-vapor.

### 5.2.2 Dye Diffusion Characterization by Photoluminescence and SIMS

Inspecting the samples after the initial C6 transfer under UV excitation, the sample annealed in air saturated with acetone for 10 min at room temperature, showed a stronger C6-emission than the not annealed sample, indicating more "active" dye and suggesting less "inactive" dye piled up at the surface after the anneal. To investigate this observation further, the PVK/PBD/C47 solution was spun-on onto a sapphire for Diffusion Depth Sensitive Photoluminescence. Figure 5-3 shows the spectra (normalized with respect to the C47 emission peak) from the front and the back after the initial transfer of C6 at 64 °C, and then again after annealing the sample in air saturated with acetone for 10 min at room temperature. After the dye transfer, the C6 emission is stronger from the front vs. the back of the film because of the higher concentration of C6 at the polymer surface. After the solvent-enhanced diffusion, the C6 emission increased relative to the C47 emission for both sides.

However, the increase is much more pronounced for the emission from the sapphire side. This result demonstrates that the dye is indeed significantly diffusing into the polymer film during the brief exposure to acetone vapor.

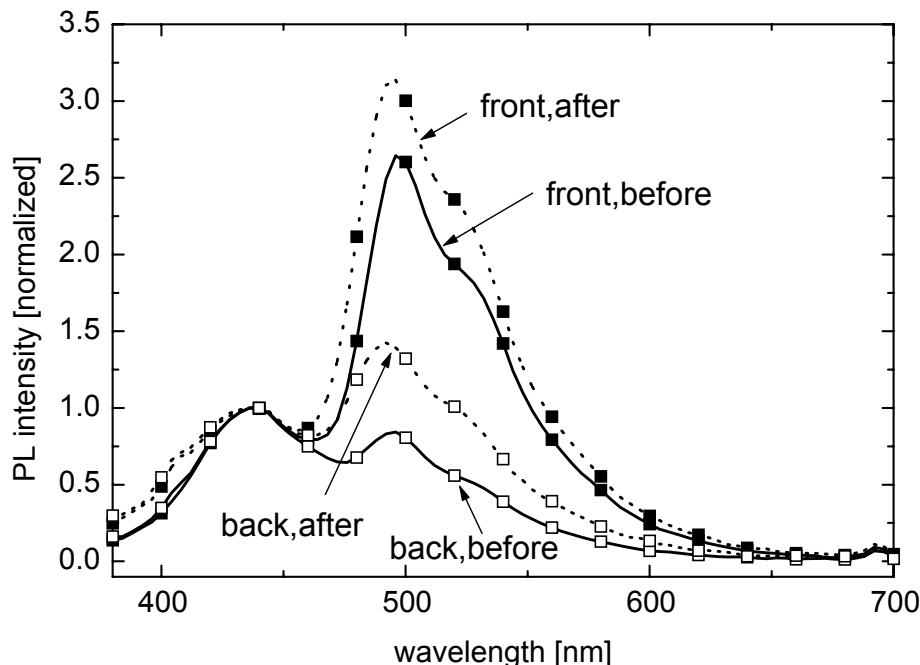


**Figure 5-3.** PL spectra of PVK/PBD/C47 film on sapphire substrate in which C6 was diffused. The back side (open squares) denotes the excitation and emission through the sapphire substrate, the front side (solid squares) denotes these of the polymer layer. PL measurements were recorded before (solid lines) and after (dotted lines) the anneal for 10 min in air saturated with acetone at room temperature. [8]

Figure 5-4 shows SIMS profiles of dye after the initial dye transfer as described above and after the additional anneal in acetone vapor, along with the control sample to establish an absolute reference level for C6. The polymer layer of the control samples contained C6 (100 mg PVK, 40 mg PBD, 0.3 mg C6) and was about 20 nm thicker than that of the other two samples. All samples were outgassed in the vacuum chamber before the analysis to reduce the interference of oxygen with sulfur. The sulfur signature differs greatly for all samples: The control sample shows a uniform sulfur profile. As expected, the sample with C6 diffused into the polymer film without the anneal process shows a high concentration of sulfur at the surface with the characteristic slope of 17 nm/decade (resolution limit of SIMS, see Chapter 4.3.3). The actual profile is probably much narrower than the mea-

sured one due to the "knock-on" effect from the  $\text{Cs}^+$  primary beam. The rise of the sulfur count at about 80 nm is due to  $\text{O}_2$  interference from the ITO substrate. The sample was then annealed at 35 °C for 10 min in air saturated with acetone. In contrast to the profile shown in Figure 4-9, after the anneal at 92 °C for many hours, the dye profile is now flat after only 10 min. This result shows that the dye diffusion is indeed drastically enhanced due to the presence of the acetone vapor, consistent with the DDSP data shown in Figure 5-3.

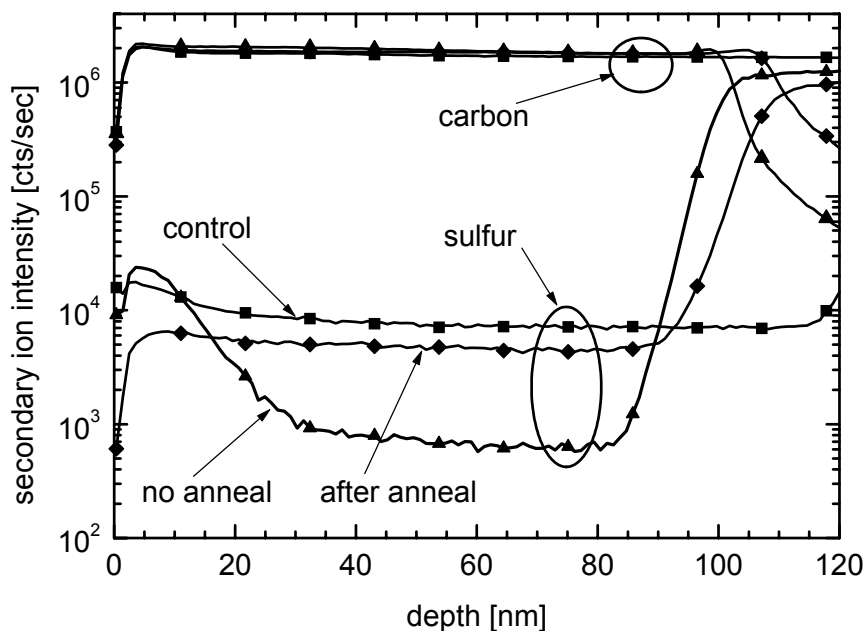


**Figure 5-4.** SIMS profiles of dye in a PVK:PBD sample exposed to air saturated with acetone for 10 min (diamonds). The dye profile of the untreated sample (triangles) and of a sample with dye contained in the spun-on film (squares) and also shown. [8]

Figure 5-5 shows a comparison of the uniformity coefficient  $h$  (defined in Chapter 4.4) from DDSP at different anneal temperatures after the initial dye transfer and then after different anneal processes. In the case of anneal in solvent vapor, after the initial dye transfer  $h$  is about 4, indicating that the concentration of C6 is higher at the surface of the polymer film. Using conventional anneal for 12 hours at 80 °C,  $h$  decreased to 1.6. However, solvent-anneal at room temperature yielded the same  $h$  after only 10 min. From this  $h$ , a the calculated  $L$  of approximately 55 nm can be obtained from Figure 4-12, which corresponds to a diffusivity  $D$  of  $5 \cdot 10^{-14} \text{ cm}^2/\text{s}$ . Given the limitations of the DDSP method (outlined in Chapter 4.4.3), the actual diffusivity is likely to be higher.

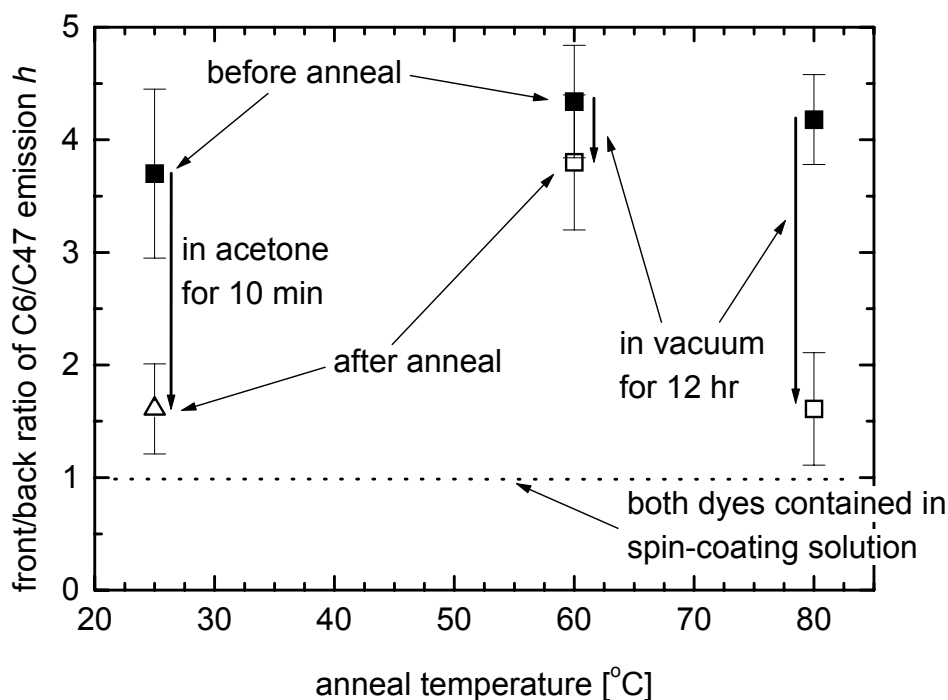


**Figure 5-5.** Comparison of the ratio of back/front emission of C6 vs. C47 for different anneal temperatures. The anneal in acetone vapor at room temperature for 10 min had approximately the same effect on the dye diffusion as a conventional anneal for 12 hours at 80 °C in vacuum. [8]

### 5.2.3 Volume Expansion Measurements of Polymer Films

If a polymer is exposed to a solvent, the solvent diffuses into the polymer matrix and thereby causes the polymer to swell. The addition of small solvent molecules into the polymer film increases the average interchain distance and weakens the molecular interaction between the polymer molecules, allowing the polymer molecule to move more freely [6]. When diffusing into glassy polymers at temperatures well below  $T_g$ , a sharp penetration boundary is often observed [9][10]. This penetration boundary moves into the pristine polymer and leaves the swollen polymer behind. We expect that the diffusion coefficient of this polymer-solvent system is increasing with increasing solvent concentration [11]. It has been reported that the dye diffusivity can be scaled quantitatively to the solvent diffusivity because of the high mobility and small concentration of dye in the solvent [6][12]. After the exposure to solvent vapor, the film is dried in pure nitrogen and regains its original  $T_g$  and film thickness before the exposure to the solvent.

To confirm the proposed diffusion enhancement mechanism, the polymer thickness was measured *in situ* during the anneal process by ellipsometry [13]. The glass substrate with a spun-on layer of PVK:PBD (100:40 by weight) was kept in a glass Petri dish in air saturated with acetone as shown in Figure 5-6. A narrow slit was cut into the lid of the dish to allow the incident and the reflected laser beam reach the sample and detector without passing through the glass. The initial thickness of the film was measured to be  $790 \text{ \AA} \pm 25 \text{ \AA}$  and the thickness while exposed to acetone vapor was  $1010 \text{ \AA} \pm 40 \text{ \AA}$  - an increase in thickness of 27%. After the film was exposed to acetone vapor, it was dried in air. The thickness of the dried film was measured to be  $792 \text{ \AA} \pm 30 \text{ \AA}$ .

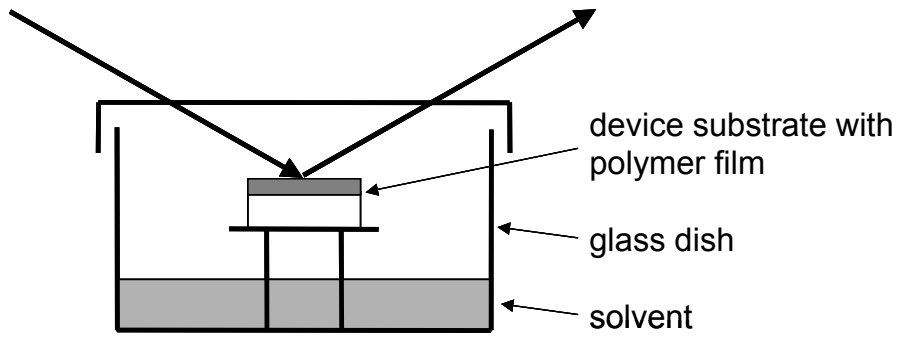


**Figure 5-6.** Determination of the solvent uptake in the polymer film by *in situ* measurement of the thickness by ellipsometry.

Fox' equation (see Chapter 4.4) describes the glass transition temperature  $T_g$  of a polymer blend as the inverse average of glass transition temperature  $T_{gi}$  weighted with the volume fraction  $w_i$  of the component  $i$  of the material system

$$T_g = \left( \sum_i \frac{w_i}{T_{gi}} \right)^{-1} \quad (5-2)$$

with

$$\sum_i w_i = 1 \quad (5-3)$$

By measuring the change in thickness during the exposure, and thus the volume fraction of the solvent, we can estimate the change in  $T_g$  of the polymer-solvent-system. The  $T_g$  of the solvent can be approximated by [14][3]

$$T_{g, \text{ solvent}} = \frac{2}{3} T_{m, \text{ solvent}} \quad (5-4)$$

where  $T_{m, \text{ solvent}}$  is the melting temperature of the solvent. This approximation is valid for a wide variety of solvent, in particular for solvents with a symmetric molecular structure like acetone (Figure 5-7).

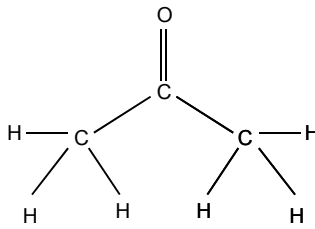


**Figure 5-7.** Chemical structure of acetone.

As already mentioned in Chapter 4.6.2,  $T_g$  of PVK is 473 K, and  $T_g$  of PVK/PBD has been measured to be 278 K. Assuming the glass transition temperature of PBD to be 278 K (see Chapter 4.6.2), we can calculate  $T_g$  of the PVK/PBD/acetone system. The melting point of acetone is 178 K, thus the approximated  $T_g$  of acetone is 119 K. The volume fraction of acetone in the swollen PVK:PBD:acetone film in the case of 27% expansion is  $0.27/1.27 = 0.213$ . Because PVK and PBD have nearly the same density ( $1.2 \text{ g/cm}^3$ , [15]), the volume fraction of PVK is given by  $0.71 * 1/1.27 = 0.56$ , and the one of PBD by  $0.29 * 1/1.27 = 0.228$ . Based on this data, the calculated value of  $T_g$  of the polymer-solvent mixture is 264 K.

This result indicates that we lowered the glass transition temperature of the PVK/PBD sufficiently so that the process temperature (in this case room temperature) is well above the glass transition temperature. As pointed out in Chapter 5.1, this condition is the major prerequisite for an efficient diffusion process for the redistribution of dye within the polymer film.

## 5.2.4 Device Performance after Anneal in Saturated Acetone Vapor

Standard OLEDs were then fabricated by the standard procedure with PVK/PBD/C47 films either subject to only the dye transfer step at 64 °C or with the additional solvent vapor anneal in acetone vapor. Control samples with a spun-on PVK/PBD/C47/C6 solution (with and without exposure to solvent) served as a reference.

The I-V-curves along with the measured photocurrent of the control devices are shown in Figure 5-8. The untreated sample shows a much lower current at low voltages than the solvent-treated sample. The amount of light emitted by the sample exposed to solvent vapor is only slightly lower than that of the unexposed one, indicating that the treatment does not damage the polymer film significantly. The external quantum efficiency dropped from 0.9% for the pristine device to 0.61% for the treated device.

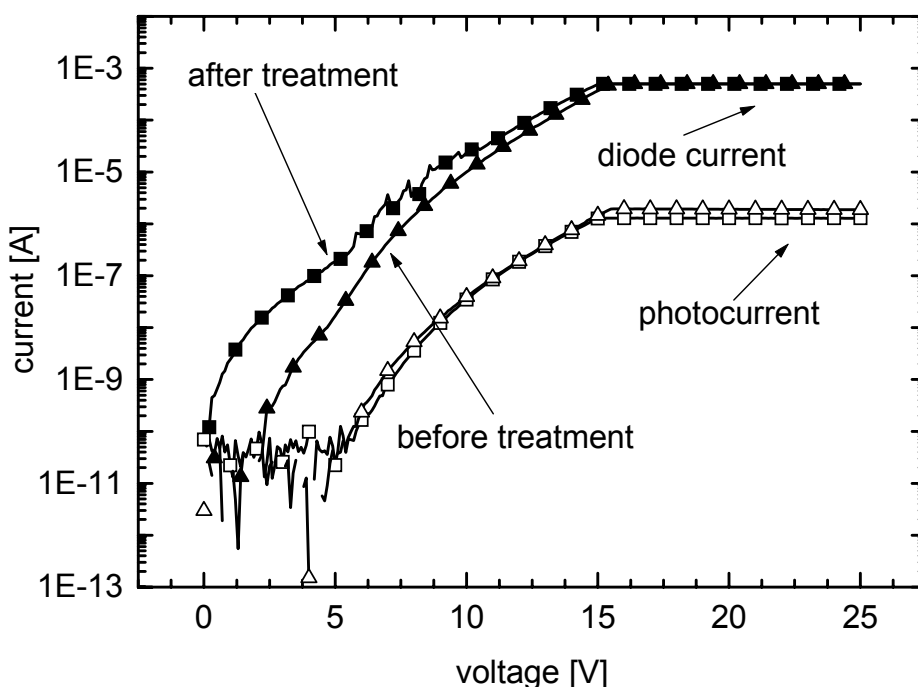


**Figure 5-8.** I-V-curves and photo-current of samples with C6 contained in the spun-on PVK/PBD/C47 solution. The annealed sample (10 min in air saturated with acetone at room temperature, squares) showed a higher leakage current compared to the non-treated one (triangles). The external quantum efficiency of the annealed device dropped only slightly. [8]

The samples with C6 diffused into the PVK/PBD/C47 film were prepared in exactly the same way as for the SIMS analysis (see Chapter 4.3). As with the control samples, the

solvent-vapor-processed sample shows a higher current at low voltages (Figure 5-9). But the photocurrent increased drastically for the treated sample, and the emission changed from blue to green. The external quantum efficiency rose from 0.07% for the device with C6 only diffused into the polymer film but without the subsequent anneal step to 0.54% for the annealed device. For comparison, results for C6 diffused devices with a thermal anneal for 4 hours at 80 °C were 0.3%. In this case, the turn-on voltage (defined as the point where the photo-current exceeds the dark-current of the photodetector) increased to approximately 9 V due to the high temperature process, vs. only approximately 4 V after the solvent-vapor-treatment

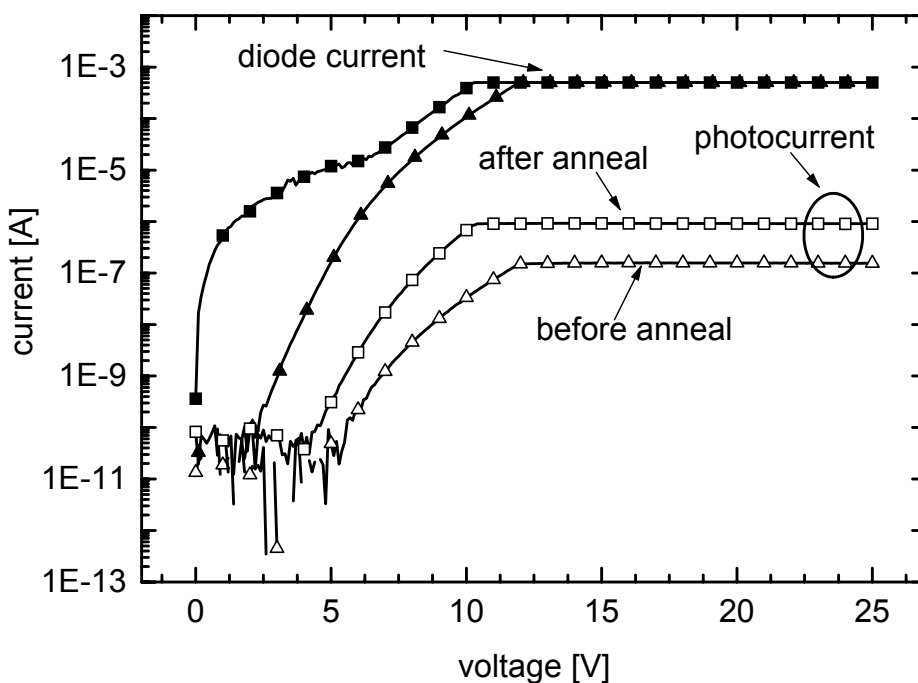


**Figure 5-9.** I-V-curves and photo-current of samples with C6 transferred by dye transfer method into the PVK/PBD/C47 film. The non-annealed sample (triangles) shows a very poor external quantum efficiency. It improved by nearly an order of magnitude after the sample was annealed in air saturated with acetone (squares) for 10 min at room temperature. [8]

### 5.2.5 Discussion

These results show clearly that the technique of solvent-assisted dye diffusion works in principle. Both, the SIMS data and the device performance suggest that the dye is nearly uniformly distributed throughout the polymer film after the solvent-vapor-anneal. The device performance of control devices with dye added to the spin-on solution did not

suffer substantially due to the solvent treatment and the characteristics of devices with transferred dye improved remarkably after solvent-vapor-anneal - far more than with the high-temperature-anneal. We therefore decided to investigate the solvent-vapor process in more detail.

## 5.3 Controlled Partial Pressure Annealing

### 5.3.1 Experimental Apparatus

To investigate the correlation between the solvent uptake and the dye diffusion in the polymer film, we constructed a tube reactor which allows us to adjust the partial pressure of the solvent. The reactor chamber is a 18-inch-long glass cylinder with 6 inch diameter. A gas wash bottle containing the solvent is used to add it to dry nitrogen by bubbling the nitrogen gas through it. The resulting gas mixture can be diluted with nitrogen or forming gas. Both flow rates are monitored by flow meters. Figure 5-10 shows the schematic of the tube reactor. The chamber contains the sample stage which is equipped with a resistive heater and a thermocouple thermometer. In addition, a optical fiber reflectance spectrometer (F-20, Filmetrics Inc., San Diego, CA) allowed *in situ* monitoring the thickness of the polymer film. The schematic interior of the chamber is shown in Figure 5-11.

The acetone uptake in dry nitrogen using a bubbler was measured to be 100 ml acetone per hour at a nitrogen flow of 4 l/min. This corresponds approximately to 130 ml gaseous acetone per liter nitrogen or to 87.4 torr partial pressure.

### 5.3.2 Volume Expansion Measurements of Polymer Films

#### 5.3.2.1 Time Dependence

Because the diffusivity  $D$  is dependent on the swelling of the polymer film, it is necessary to know how fast the film absorbs the solvent and, in turn, how fast  $D$  changes. As a result, it must be decided if  $D$  can be assumed as constant during the diffusion process or if a time-dependence has to be taken into account.

Figure 5-12 shows the thickness of a PVK/PBD film exposed to 10 ml gaseous acetone per liter nitrogen (equal to a partial pressure of acetone of 7.5 torr). The chamber was initially filled with dry nitrogen. The measurement started when the acetone/nitrogen mix-

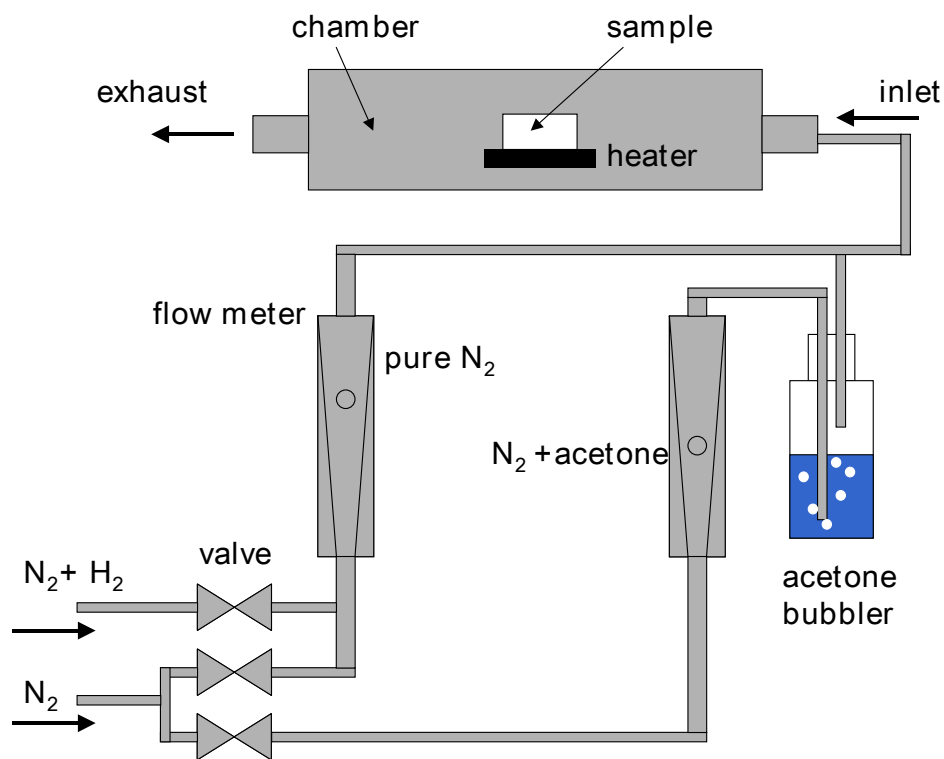


Figure 5-10. Schematic of the tube reactor.

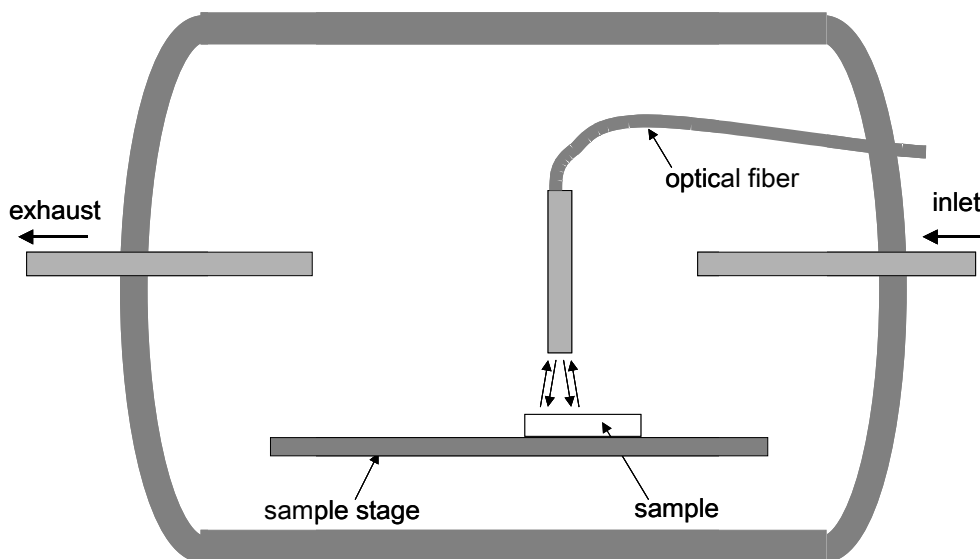
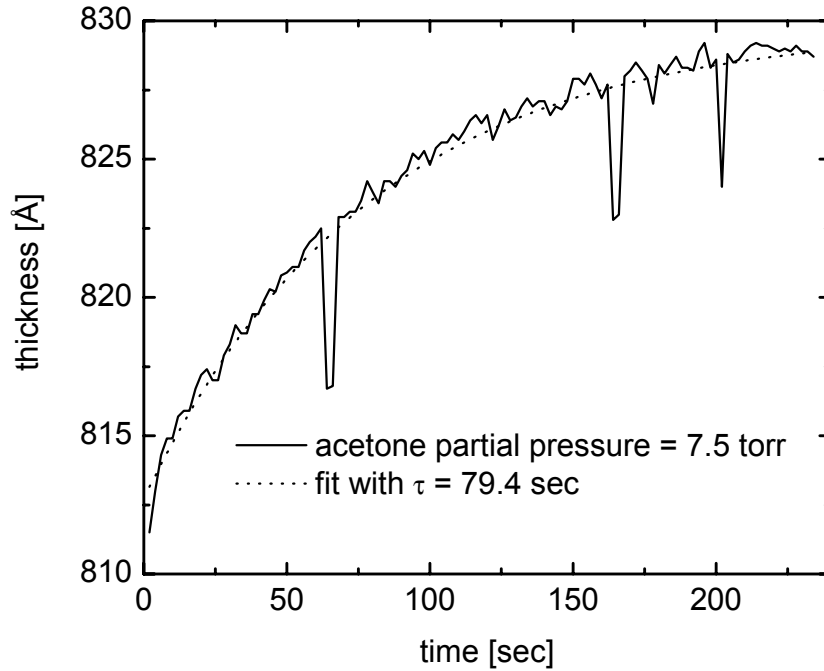


Figure 5-11. Schematic interior of the anneal chamber.

ture was lead into the chamber with a flow of 6 liters per minute. The initial thickness of the film was measured to be 812 Å. Because of the big volume of the glass tube (8.6 liters), the acetone vapor concentration increases quite slowly, and the measured thickness of the polymer film grows accordingly.



**Figure 5-12.** Time response of the PVK:PBD film thickness in glass tube reactor.

The exponential fit of this curve has a time constant  $\tau = 79.4$  sec. The time constant for the partial pressure of acetone is given by

$$\tau = \frac{\text{volume}}{\text{flow rate}} = \frac{8.6 \text{ liter}}{6 \text{ liters/min}} = 86 \text{ sec} \quad (5-5)$$

The slight discrepancy between the theoretical value and the measured value of  $\tau$  can be explained by the fact that the sample was placed in the vicinity of the gas outlet within the glass tube. Therefore, the partial pressure of acetone is likely to be somewhat higher at this position than the average value in the chamber.

The measurement shows that the time constant of the actual swelling process is very small. This fact has been validated by measuring the thickness of the polymer in a smaller volume as shown in Figure 5-13. In this case, a small metal cylinder was placed inside the glass tube and the gas inlet was directed into this cylinder. Because the time constant in this

cylinder is much smaller ( $\tau = 0.355$  sec with a cylinder volume of  $35.5 \text{ cm}^3$ ), the measurement of the polymer film thickness yielded the final film thickness much faster as shown in Figure 5-14. The delay in thickness increase compared to the solvent vapor increase with a time constant  $\tau = 0.355$  sec can be attributed to the swelling characteristics of the film. The residual delay of approximately 0.6 sec could be due to a delay in absorption of the solvent vapor by the polymer film, or due to the fact that the vapor confinement to the small volume was not perfect.

After the film was dried in pure nitrogen, the film thickness decreased to a value very close to its initial value. In most cases, the final thickness was slightly less (up to  $5 \text{ \AA}$ ) than the initial thickness which might be due to decreased free volume (denser packing) of the polymer film after the anneal. The rate of thickness decrease was not investigated in detail, but it roughly is correlated to the partial pressure of the solvent vapor in the same fashion as the rate of increase as discussed above.

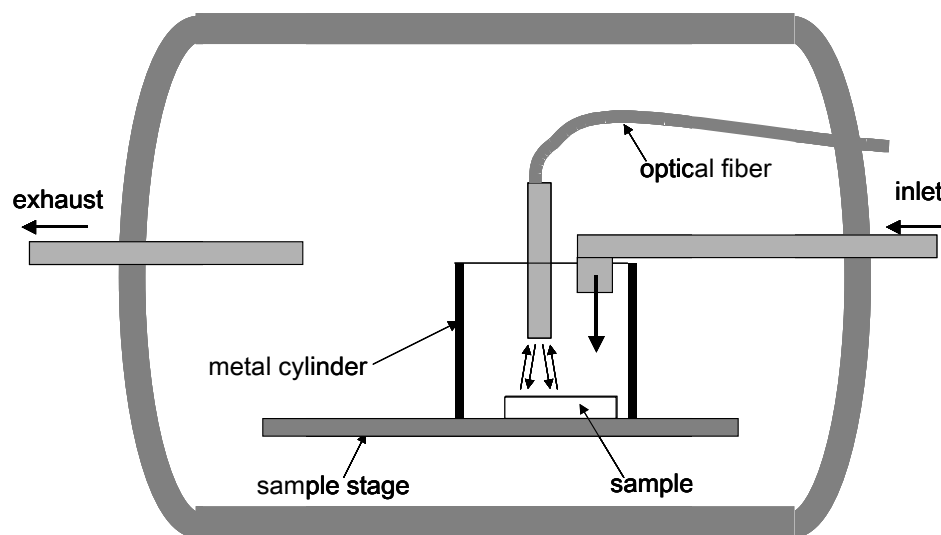


**Figure 5-13.** Experimental set-up for measurement of the time response of the polymer film thickness. A small metal cylinder has been placed on the sample stage in the glass tube reactor, and the gas inlet was directed into this enclosure.

### 5.3.2.2 Effects of Partial Pressure of the Solvent Vapor

Due to the uptake of solvent in a solvent atmosphere, the polymer film swells up. This process provides additional free volume, lowers the glass transition temperature  $T_g$

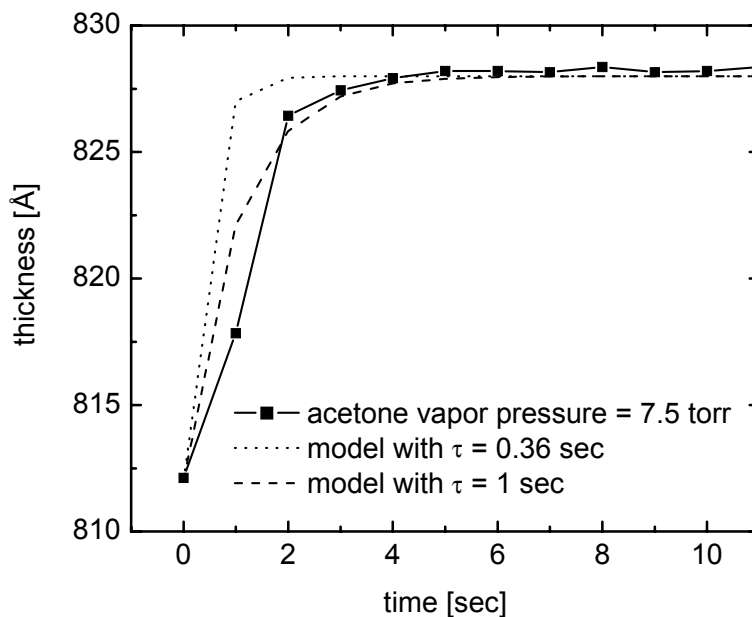


**Figure 5-14.** Time response of the PVK:PBD film thickness in the small metal cylinder inside the glass tube reactor. The theoretical thickness response based only on the increase of solvent vapor is given as the dotted line. The fit for the actual measurement is shown as the dashed line.

and the increases thus the diffusivity  $D$  in the film (see Chapter 5.2.3). The amount of swelling is therefore a suitable indicator of the change in  $T_g$  [17].

Figure 5-15 shows the change in thickness of a PVK:PBD film as a function of partial acetone vapor pressure at room temperature. The vapor pressure of acetone is 184 torr [18]. In the case of acetone saturated vapor, the glass tube was sealed and a small amount of liquid acetone was poured into the chamber. The liquid acetone did not come into contact with the polymer film. During the measurement, some liquid acetone remained at the bottom of the tube. A change in thickness of 32% was observed in air saturated with acetone vapor. This measurement result is slightly different from the result obtained by ellipsometry in air saturated with acetone vapor (Chapter 5.2.3) which was 27% change in thickness. Beside measurement errors, the ellipsometry result is lower because of the experimental set-up: The narrow slit in the glass Petri dish to let the laser beam pass in and out also allowed the acetone vapor to escape the enclosure. Therefore, the partial pressure of acetone was likely to be lower during the measurement by ellipsometry than in the glass tube during the measurement by reflectance spectroscopy.

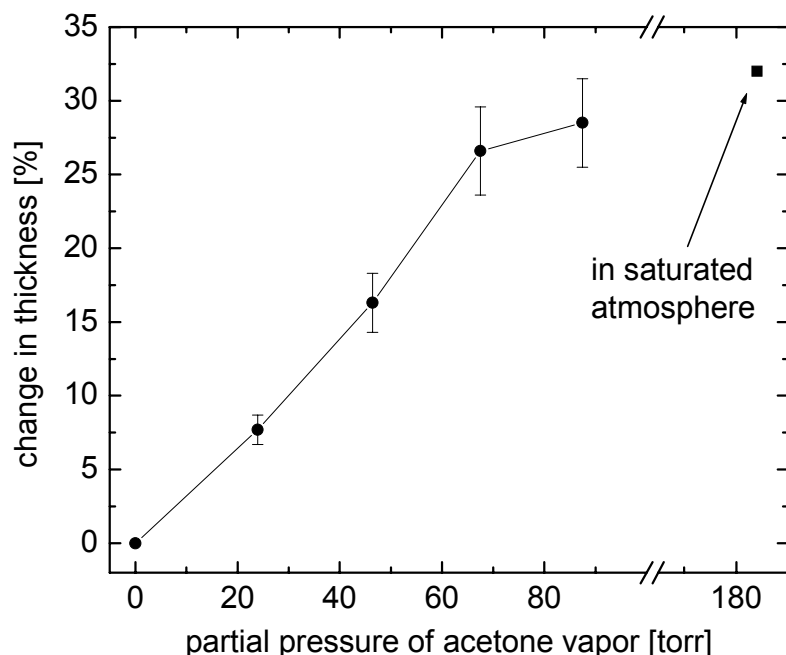


**Figure 5-15.** Change in polymer film (PVK:PBD) thickness as a function of partial acetone vapor pressure.

The increase in thickness is linear at low partial pressures of acetone. At higher partial pressures, the increase slows down until it reaches the maximum value in a saturated environment.

The estimated values for the glass transition temperature  $T_g$  for the PVK:PBD/solvent mix based on the measured thickness of the film and the calculation outlined in Chapter 5.2.3 as a function of the partial acetone vapor pressure are shown in Figure 5-16.

### 5.3.3 Dye Profile after Anneal at Low Partial Pressure of Solvent Vapor

#### 5.3.3.1 Partial Pressure of Acetone of 87.4 torr

Figure 5-17 shows the SIMS profile of a sample (with C6 previously transferred) before and after the solvent anneal for 150 sec at room temperature in a nitrogen atmosphere with partial pressure of acetone of 87.4 torr (equals 130 ml gaseous acetone per liter nitrogen). For comparison, the dye profile of a thermally annealed sample for 4 hours at 92 °C is also shown. Before the anneal we observed a dye profile governed by the SIMS resolution limit. After the anneal process, the dye distribution was essentially flat throughout the film. The diffusion coefficient during the anneal process was at least  $10^{-11}$  cm<sup>2</sup>/s, higher

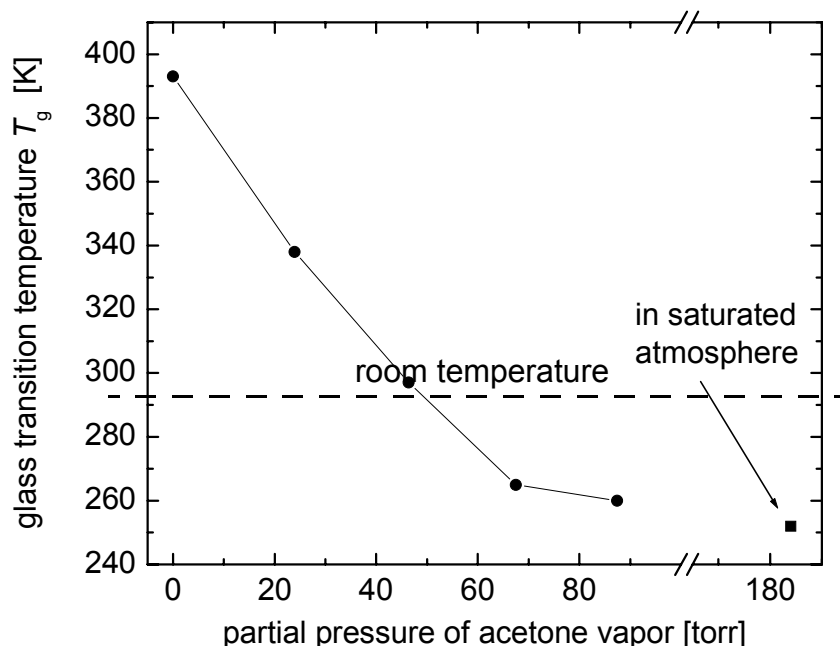


**Figure 5-16.** Estimated glass transition temperature  $T_g$  of the PVK:PBD/solvent mixture as a function of partial pressure of acetone.

than the diffusion coefficient at 135 °C in vacuum as shown in Figure 5-18. In agreement with this observation is the estimated  $T_g$  derived from *in situ* thickness measurements of the polymer film by reflectance spectrometry: The thickness of the PVK/PBD film increased by 28.5% in the acetone vapor (87.4 torr partial pressure). Based on Equation (5-2), the glass transition temperature  $T_g$  of this blend is therefore 260 K.

This lowering of  $T_g$  leads to a remarkable increase of the diffusion coefficient. If the dependence of  $D$  on temperature for the thermal diffusion experiments at 90 and 130 °C is used to predict the diffusion coefficient due to thermal effects at 25 °C, the solvent vapor treatment leads to a  $10^{25}$  increase in diffusivity. A quantitative model of  $D$  vs.  $T$  including the effect of  $T_g$  will be presented in Chapter 5.5.

#### **Partial Pressure of Acetone Vapor below 87.4 torr**

As shown in Figure 5-16, the exposure to acetone vapor leads to depression of the glass transition temperature  $T_g$  of the polymer. The anneal process was carried out at room temperature (20 °C). If the partial pressure of acetone exceeds approximately 50 torr,  $T_g$  is lower than the process temperature. In this case, the WLF equation applies and we expect a large increase in diffusivity of the polymer.

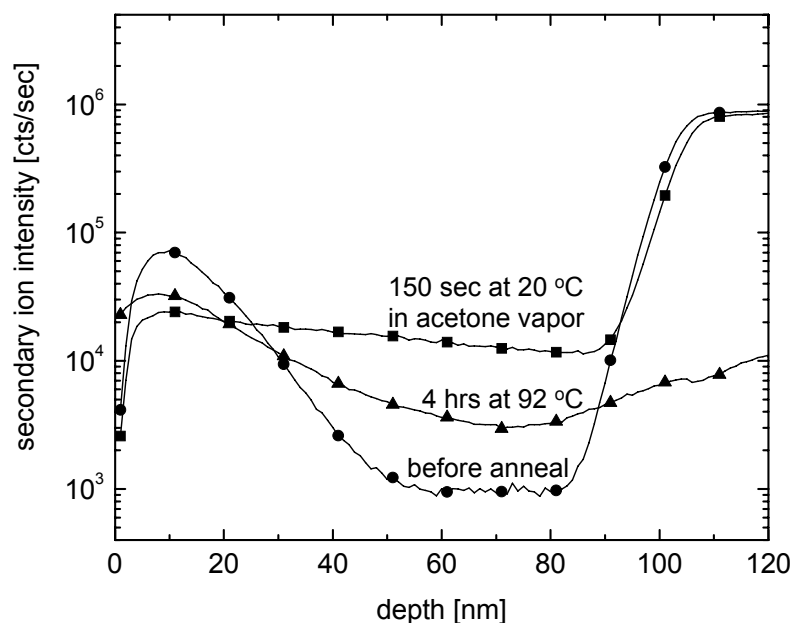


**Figure 5-17.** SIMS sulfur profile of a PVK:PBD sample with C6 transferred into a PVK film before (squares) and after (circles) acetone anneal. The sample was annealed in acetone vapor (87.4 torr) for 150 sec at room temperature. For comparison, a thermally annealed sample (4 hours at 92 °C) after the same initial transfer is also shown (triangles). [5]

To investigate the diffusivity in detail, we performed SIMS analysis on samples with the dye C6 transferred from a dye source by the described technique. The polymer solution (100 mg PVK, 40 mg PBD in 7 ml chlorobenzene) was deposited by spin-coating at 2000 rpm on silicon substrates. The dye source was a glass slide with a spun-on layer of C6 doped (4% by weight in the final film) vylon film. The initial dye transfer was carried out by placing both substrates in direct contact at 70 °C for one hour in vacuum.

The samples were then annealed in acetone vapor for 60 seconds in the small metal cylinder at different partial pressures of acetone. The resulting sulfur profiles obtained by SIMS are shown in Figure 5-19. Although some samples (#1 and 2) were annealed at acetone concentrations that result in a  $T_g$  lower than the process temperature, all of the sulfur profiles are essentially flat and no information about the diffusivity can be deduced from these measurements. Interestingly, even the samples where the expected  $T_g$  exceeds the process temperature show a flat profile. The considerable spread in the amount of dye in the film after the anneal can have several reasons: First, the amount of dye transferred to the PVK/PBD film varies from sample to sample due to slightly different process temper-

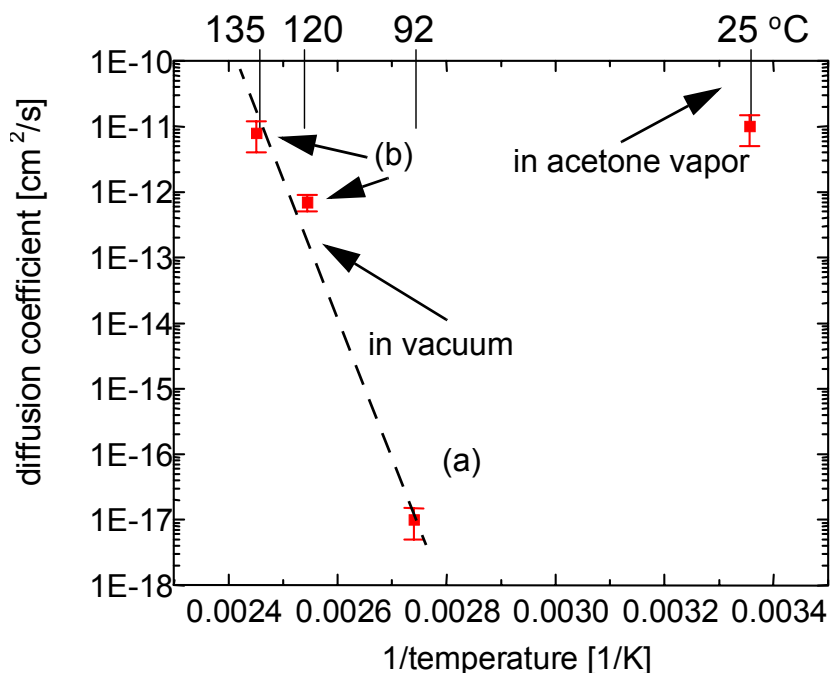


**Figure 5-18.** Diffusion coefficient of C6 in PVK:PBD in vacuum and in acetone vapor (87.4 torr). The diffusion coefficient increases by many orders of magnitude in solvent vapor. The referenced data points (a) was extracted from the dye diffusion experiment at 92°C for 4 hour explained in Chapter 4.3.5, the data points (b) are extracted from lateral dye diffusion experiments discussed in Chapter 6.3.1 [5].

atures in the vacuum oven. Although this is possible, the result presented in Chapter 5.4 shows that the dye transfer process scales very well with time. Secondly, the exposure to solvent vapor does not only lead to enhanced diffusion within the polymer film, but also to higher probability that the dye molecule can escape from the film. This claim is supported by the result of *in situ* measurements of the PL intensity of a sample exposed to acetone vapor. The intensity decreased much faster than a sample which was not exposed to the acetone vapor.

To obtain data on the diffusivity of the PVK/PBD film, we repeated this experiment with lower partial pressures of acetone and a shorter process time. The initial dye transfer was similar, although in this case we used a dye source with a Vylon film which only contained 1% (by weight in the final film) of C6. The samples were annealed for only 30 seconds at room temperature. The resulting data are shown in Figure 5-20. A control sample was included which was not exposed to any solvent anneal. Slight differences in the slope of the sulfur concentration can be obtained from the figure. However, the sample with the

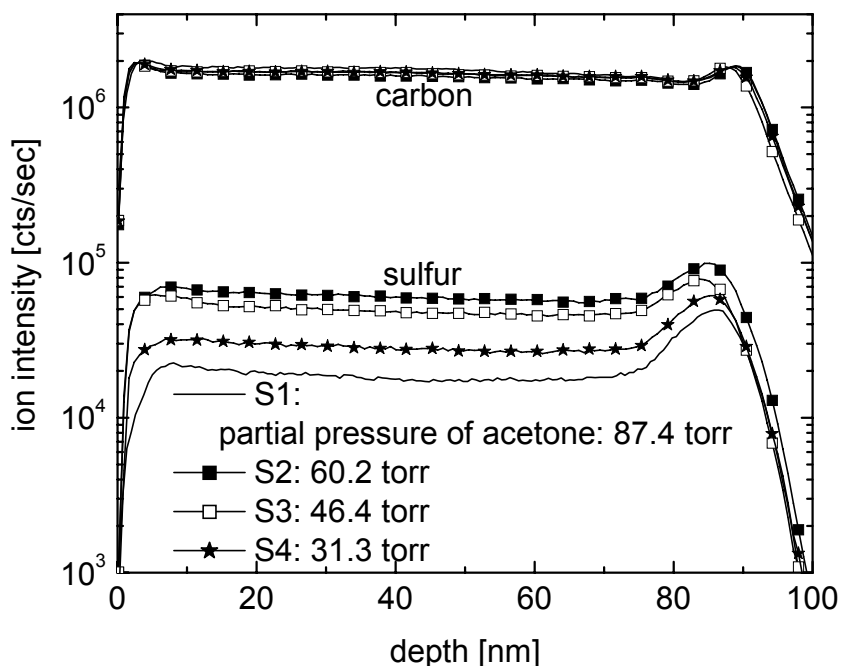


**Figure 5-19.** SIMS profiles of sulfur and carbon in PVK:PBD after C6 was transferred and annealed at different partial pressures of acetone for 60 sec. The final dye profile is essentially flat in all cases, independent of the solvent vapor pressure.

steepest slope should be the control sample because it was not annealed and the profile is entirely due to the resolution of the SIMS measurement. But instead it is the control sample which shows the shallowest slope of all the samples which leads us to believe that the observed difference is not due to the anneal process but rather experimental errors. Samples #2 and #4 show a very similar behavior but were not displayed for the sake of clarity.

More interestingly, even sample #6 in Figure 5-20 which was annealed at a higher acetone concentration than sample #4 in Figure 5-19, shows no enhanced diffusion. The only different process parameter between these samples is the process time. The obtained dye profile can therefore not be explained by simple diffusion theory. We suggest the following explanation: The diffusion of solvent into the polymer film is a very fast process. However, the dye can only diffuse within the film once it is dissolved in the solvent. The time needed to dissolve the dye is the limiting step in the anneal process. Once the dye is dissolved, it can redistribute in a very short time. In this regime, the diffusivity of dye and solvent are likely to be linearly correlated [19], although it is expected to be much lower than acetone because of the molecular volume of C6 is much bigger than that of acetone [7].

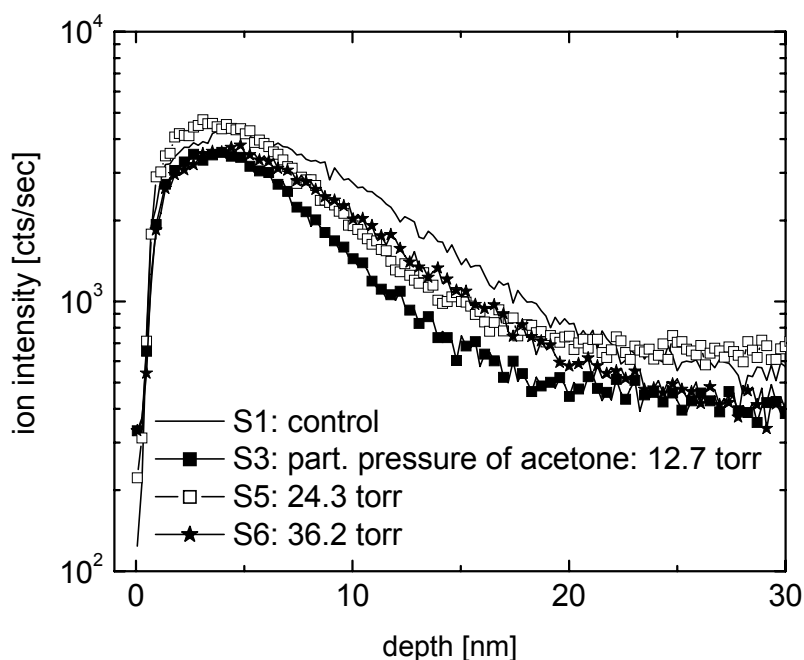


**Figure 5-20.** SIMS profiles of sulfur of PVK:PBD samples annealed at different partial pressures of acetone for 30 sec. No difference in diffusion enhancement could be detected.

Further work is necessary to understand the surprisingly large difference between the data in Figure 5-19 (60 sec anneal) and Figure 5-20 (30 sec anneal).

### 5.3.4 Device Performance after Anneal at Low Partial Pressure of Acetone

#### 5.3.4.1 Partial Pressure of Acetone of 87 torr

##### Devices with dye contained in solution (control devices)

To investigate the device characteristics of a solvent annealed PVK/PBD/C6 device, we exposed a standard PVK/PBD/C6 devices (with dye contained in solution) with a thermally evaporated Mg:Ag cathode to acetone vapor in the tube reactor. The I-V-characteristics along with the photo-current of these devices are shown in Figure 5-21. These devices were subjected to the anneal in acetone vapor (partial pressure 87 torr) at room temperature without dye being added by the dye transfer step. The forward bias characteristics of the devices do not change significantly even after a 10 min anneal in acetone vapor. However, the rectification ratio at  $\pm 10$  V decreased by roughly one order of magnitude after 10 min anneal (see also Figure 5-24).

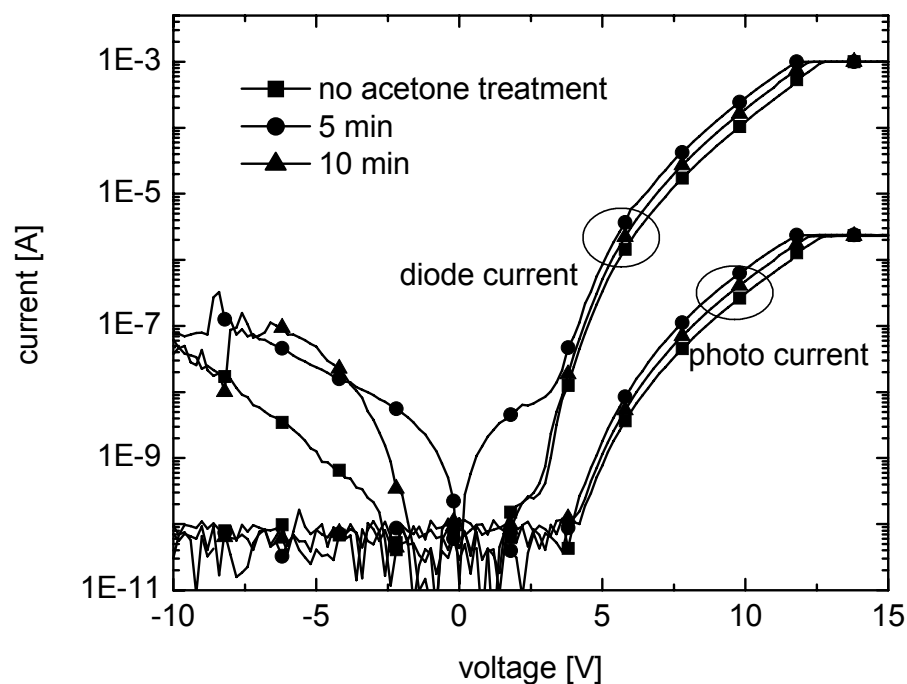


**Figure 5-21.** I-V-characteristics and photocurrent of PVK/PBD/C6 devices with the dye contained in the spun-on solution treated in acetone vapor (partial pressure 87 torr) for different times. [5]

### Devices with transferred dye

For devices fabricated using the dye transfer method we obtained very promising results, which is shown in Figure 5-22. The C6 dye was transferred from a dye source consisting of a glass substrate with a spun-on nylon layer doped with C6 (4% in the final film). The transfer was carried out at 70 °C for one hour in vacuum. The device polymer layer was also deposited by spin-coating from a solution containing 100 mg PVK, 40 mg PBD and 0.3 mg C47 in 7 ml chlorobenzene. As expected, the non-treated sample shows a very low photocurrent and thus a low quantum efficiency because the dye is still accumulated at the surface of the polymer film and is not active in the emission process. This is supported by the electroluminescence spectrum, which only shows emission from C47 as shown in Figure 5-23. After 60 sec acetone anneal in a nitrogen-solvent-mixture (87 torr partial pressure of acetone), the external quantum efficiency increases and the EL emission is shifted to green, indicating that C6 is moving into the polymer film. However, a small C47 peak is still observed in the EL spectrum, which may be due to insufficient dye in the recombination zone of the device. After a 4 min anneal, the dye is now homogeneously distributed

throughout the polymer film. The emission originates now entirely from C6 and the external quantum efficiency improved by nearly an order of magnitude. The external quantum efficiency of these devices is comparable to those of devices with dye contained in the spin-on solution as shown in Figure 5-24. In addition to the external quantum efficiency, the rectification ratio  $r$  (determined at  $\pm 10$  V) is presented. The decrease of  $r$  for the control device is significant and exponential in nature and due to the increased current in reverse bias. The reason for the decrease of the rectification ratio has not been investigated. It can be argued, that a limited crystallization of the polymer increases the carrier mobility in the polymer and thus the conductivity of the film [16].

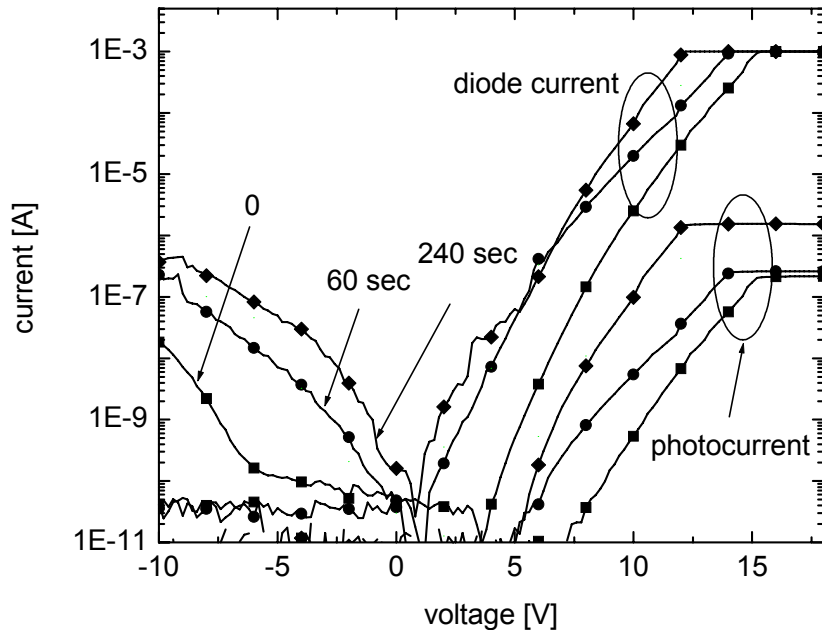


**Figure 5-22.** I-V-characteristic of PVK/PBD/C47 devices with C6 diffused into the polymer film for different times at acetone vapor pressure of 87 torr. The photocurrent of the device exposed to acetone vapor increased by nearly one order of magnitude. [5]

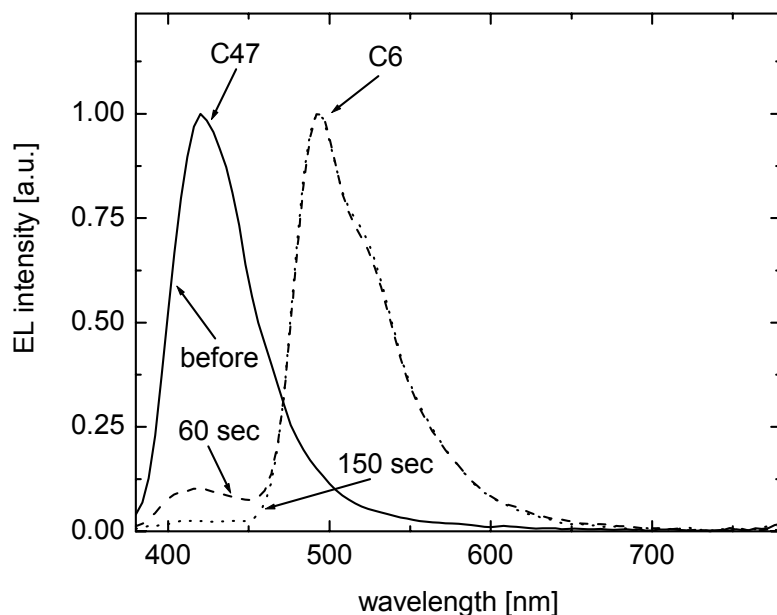


**Figure 5-23.** Normalized EL spectra of a PVK/PBD/C47 device with C6 transferred into the polymer film. Before the anneal (solid line), emission occurred entirely from C47. After 60 sec anneal (dashed line) in acetone vapor (partial pressure 87 torr), the emission is shifted to C6. Nearly no emission from C47 was detected in a device annealed for 150 sec (dotted line).

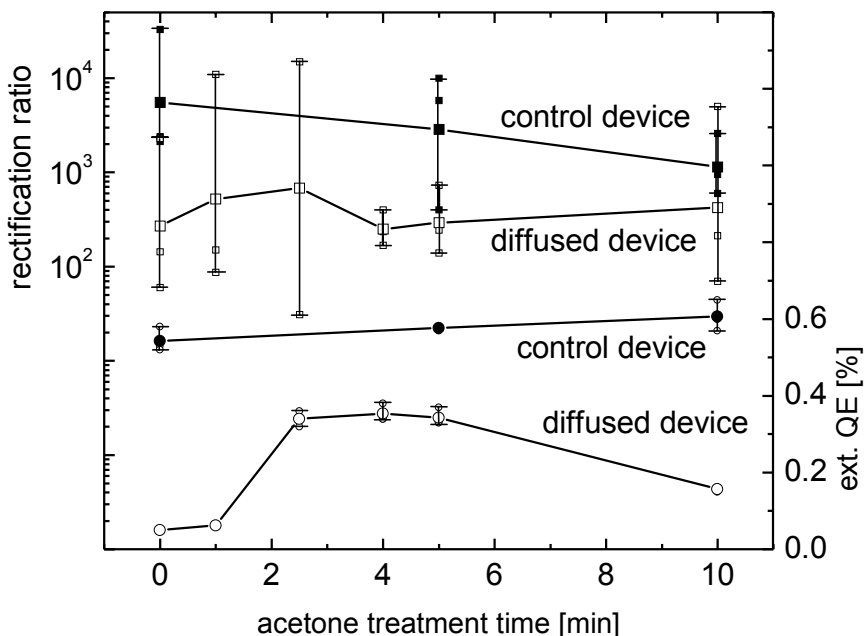


**Figure 5-24.** External quantum efficiency (circles) and rectification ratio (squares) as a function of exposure time to acetone vapor (partial pressure 87 torr). Control devices (solid symbols) are devices with C6 contained in the spin-on solution, diffused devices (open symbols) are devices with transferred C6.

Table 5-1 summarizes the performance for control devices and devices with transferred dye before and after anneal in acetone solvent vapor.

**Table 5-1.** Device characteristics of devices annealed in acetone vapor (partial pressure: 87.4 torr) for 5 min. The turn-on voltage was defined as the point where the photo-current in the detector exceeded the dark current. The rectification ratio was determined at  $\pm 10$  V.

	control device		device with transferred dye	
	before anneal	after anneal	before anneal	after anneal
$\eta_{\text{ext}}$	0.54%	0.61%	0.07%	0.54%
$V_{\text{turn-on}}$	5.5 V	5.5 V	5.5 V	4.5 V
rectification ratio	5000	2000	300	300
$V$ at 50 mA/cm <sup>2</sup>	15 V	15 V	13 V	10 V

#### 5.3.4.2 Dependence of the Device Performance on Partial Pressure of Acetone

From these results presented in Figure 5-19 we can infer that the dye is homogeneously distributed throughout the polymer film even after the anneal process at a partial pressure of acetone of 31.3 torr. Since the anneal process time had a major impact on the rectification ratio (see Figure 5-24), we investigated the quantum efficiencies and the rectification ratio of control devices (with dye contained in the spun-on solution) at different acetone vapor concentrations to determine optimal process parameter for the solvent anneal process.

Standard C6-devices were exposed to acetone vapor for 4 min (in the small metal cylinder placed within the reactor) before a standard Mg:Ag was thermally evaporated. After this, the samples were transferred into the glove box and characterized. The results are presented in Figure 5-25.

The external quantum efficiency did not change considerable with acetone vapor concentration. However, the rectification ratio (determined at  $\pm 10$  V) decreases significantly. In a passive matrix, the rectification ratio determines the size of the display [20]. It should therefore be maintained as high as possible. Further work is necessary to obtain more quantitative data to determine the optimal process parameters. But the dye profile of the sample annealed at a partial pressure of acetone of 31.3 torr for 60 sec (see Figure 5-19) shows that the rectification ratio can be further improved by reducing the process time and reducing the solvent concentration.

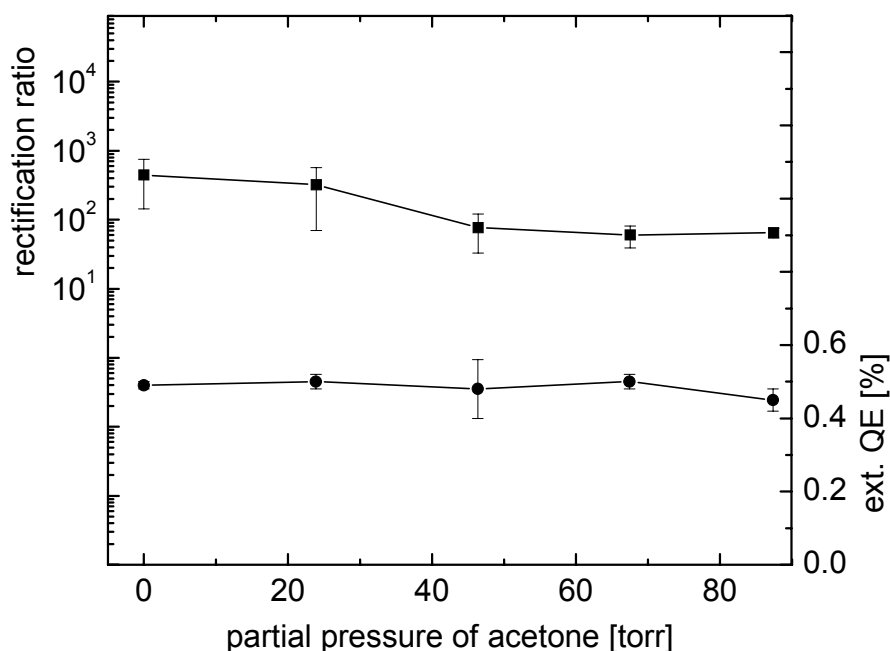


**Figure 5-25.** External quantum efficiencies of rectification ratio of control devices (dye contained in the spun-on solution) at different partial pressures of acetone after 4 min anneal.

## 5.4 Dye Concentration Control

The efficiency of an OLED is strongly dependent on the dye concentration (see Chapter 2.10). It is therefore of major importance to transfer the optimal amount of dye into the device polymer film. Depending on the transfer process, there are two basic approaches for the dye control during the transfer process.

In the case when the dye source layer consists of pure dye or a very high concentration of dye in a polymer matrix, the amount of dye transferred is mainly dependent on the process temperature and, to a lesser degree, the process time. Whereas the amount of dye transferred is a weak function in time, we observed that the transfer process is very sensitive to changes in temperature. This is not surprising because some of the parameters (like  $T_g$ ) all depend exponentially on the temperature.

To investigate the dependence of the dye amount transferred on the process time, we performed SIMS on samples after different process times. The sulfur profiles obtained by SIMS are shown in Figure 5-26. A PVK/PBD film (100 mg PVK, 40 mg PBD in 7.5 ml chlorobenzene) was spun-on at 4000 rpm onto cleaned glass substrates, which were then

kept in direct contact at 73 °C in vacuum under a pressure of 1500 Pa with the dye source substrate (100 mg C6 per ml chloroform spun-on at 2000 rpm on glass substrates, no polymer used). Again, the dye did not diffuse into the polymer film but accumulated on top or very close to the surface of the film. The total amount of dopant is given by integral of the profile. Because the dye source only consisted of a thin layer of pure dye, the C6 molecules

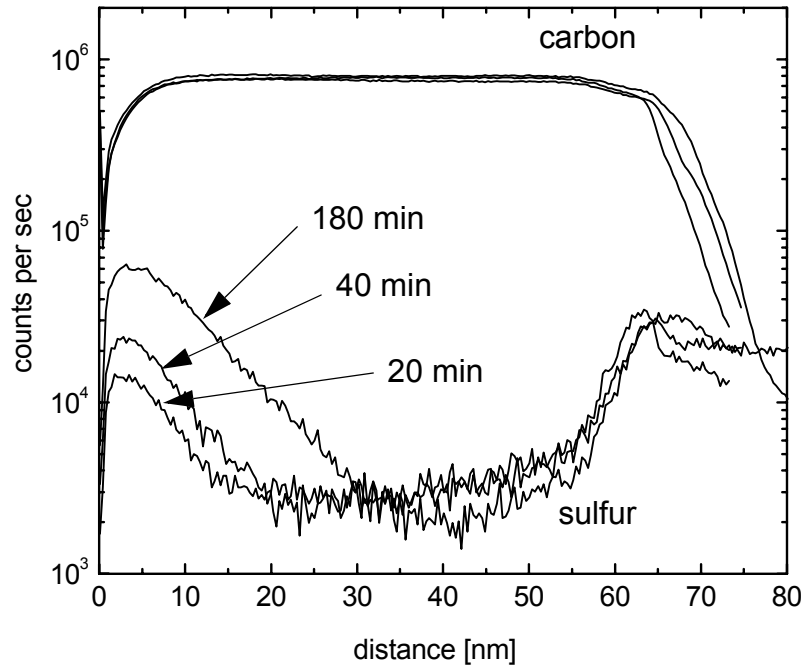


**Figure 5-26.** SIMS profiles of sulfur and carbon in PVK/PBD samples with transferred C6 after different transfer times.

did not have to diffuse out of the polymer matrix but rather just desorb from the glass substrate. The measured integrated amount of dye vs. time is shown in Figure 5-27. The control device with 0.3% C6 in PVK/PBD in Figure 5-4 on page 94 served as a reference for the dye/carbon ratio. Also shown in the graph is an exponential fit with a time constant of 70 min. The data shows that the diffusion source is clearly limited.

However, due to the sensitivity of this process especially to temperature, we were looking for a more robust technique to control the amount of transferred dye. Using a dye-doped polymer film with a doping level similar to the desired doping level in the device was reported by Wu *et al.* [21]. Because the doping level of the dye source is limited to a low value, the amount of transferred dye is restricted as well. Depending on the affinity of

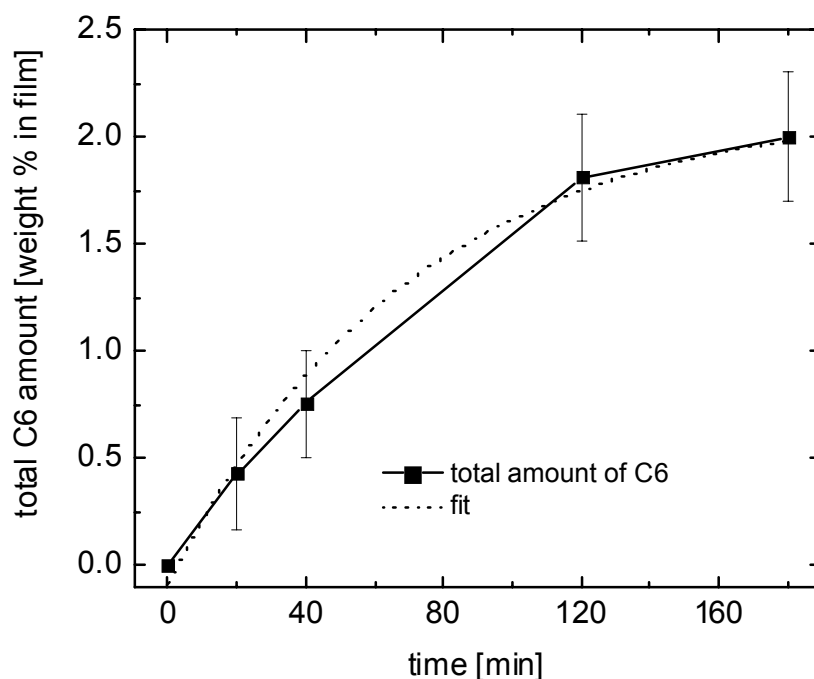


**Figure 5-27.** Total amount of C6 in a PVK/PBD film after transfer at 70 °C in vacuum for different times.

the dye to the polymer, the concentration in the device polymer film can actually be significantly higher or lower than in the dye source film after the thermal equilibrium is reached [22][23][24]. This problem can be avoided by using either the same polymer for the dye source and the device. In this case, the dye affinity is the same on both sides and a normal dye diffusion can be assumed [21]. Most of the later experiments, however, were done using a dye doped Vylon 103 film (obtained from Toyoba with a glass transition temperature of 47 °C) containing C6 (2% by weight in the final film). The low glass transition temperature of this polymer ensured that the transfer process is limited by the diffusion of the dye into the PVK. This dye source concentration yielded good efficiencies (see Figure 5-4 and Figure 5-24). However, fine tuning of the dye concentration is likely to further increase the efficiency of the device.

## 5.5 Model for Diffusivity of C6 in PVK:PBD

Table 5-2 list measurements of  $D$  of C6 in PVK:PBD films (71.4% PVK in the final film) along with the process temperature, the calculated glass transition temperature of the polymer film during the experiment, the difference between these temperatures, and the

respective experiment. It also includes measurements obtained from dye pattern stability which will be discussed in detail in Chapter 6.3. These data points are included here since in this section we compare all data on dye diffusion in PVK/PBD in this thesis to a universal model.

**Table 5-2.** Measured diffusivity  $D$  of C6 in PVK/PBD films.

$D$	$T$ (process temp)	$T_g$	$T - T_g$	experiment
$10^{-17} \text{ cm}^2/\text{s}$	365 K	393 K	-28 K	thermal anneal, no solvent (Chapter 4.3.5)
$10^{-11} \text{ cm}^2/\text{s}$	293 K	260 K	33 K	solvent anneal at 87.4 torr, (Chapter 5.3.3.1)
$7 \cdot 10^{-13} \text{ cm}^2/\text{s}$	393 K	393 K	0	lateral diffusion (thermal, no solvent) (Chapter 6.3.1)
$8 \cdot 10^{-12} \text{ cm}^2/\text{s}$	408 K	393 K	15 K	lateral diffusion (thermal, no solvent) (Chapter 6.3.1)
$4 \cdot 10^{-9} \text{ cm}^2/\text{s}$	293	293	0	lateral diffusion (solvent) (Chapter 6.3.2)

Assuming  $T_g$  of the PVK/PBD film to be = 393 K,  $D$  can be modelled using the WLF-equation (see Chapter 4.5.3, Equation 4-38 on page 83) and the common values for

$$\log D(T) = \frac{-c_1 (T - T_g)}{c_2 + T - T_g} + \log D_g \quad (5-6)$$

$c_1 = 17.4$  and  $c_2 = 52$  K. This approach is not valid for the diffusivity data obtained from experiments in solvent vapor because  $T_g$  is different in this case. The data of the diffusivity  $D$  vs.  $1/T$  are shown in Figure 5-28 along with the predicted value of  $D$  (dotted line).  $D_g$ , the diffusion coefficient at the glass transition temperature, was an adjustable parameter and chosen to be  $7 \cdot 10^{-13} \text{ cm}^2/\text{s}$  since we had a measured data point for  $D$  at  $T_g$  (393 K).

While the overall trend of the data is consistent with the standard WLF-model, the fit is poor. The data actually suggest that the parameter  $c_1$  is too large and  $c_2$  is too small. Adjusting these parameters to  $c_1 = 13$  and  $c_2 = 130$  K results in a much better fit (dashed line). While these parameters are dependent on the polymer, the diffusivity for most polymers can be sufficiently described by the “universal values” ( $c_1 = 17.4$  and  $c_2 = 52$  K).

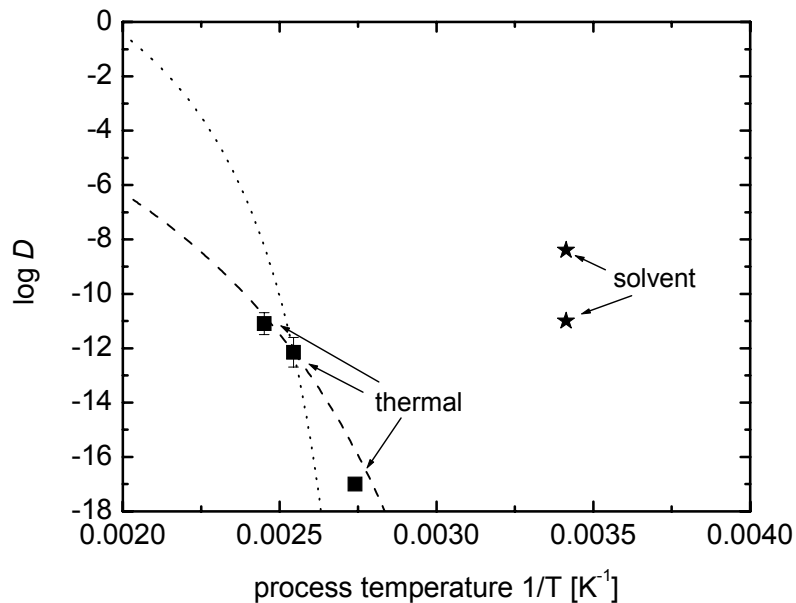


**Figure 5-28.** Plot of measured values of  $D$  vs.  $1/T$  (process temperature) and predicted values according to the WLF model (dotted line with common parameters; with fitted parameters dashed line).

Shown in Table 5-3 are values of parameters for different polymers. Most of these values are in good agreement with the “universal values”. However, for some polymers these values differ significantly.

According to the WLF model, the diffusivity  $D$  is entirely dependent on the difference between the process temperature  $T$  and the glass transition temperature  $T_g$ . This fact allows us to compare the measured diffusivity for both cases, the thermal anneal and the solvent-vapor anneal. We therefore rescaled the process temperature  $T$  in the case of solvent-vapor according to the equation  $T_{\text{process (rescaled)}} - T_g = T_{\text{process solvent}} - T_{g \text{ solvent}}$ , where  $T_g$  is the glass transition temperature of the dry PVK/PBD film (393 K),  $T_{\text{process solvent}}$  is the process temperature during the solvent treatment (293 K), and  $T_{g \text{ solvent}}$  is the predicted glass transition temperature of the polymer film in the solvent vapor. Figure 5-29 shows the data with the two adjusted data points of solvent-vapor diffusion. The data point  $D = 4 \cdot 10^{-9} \text{ cm}^2/\text{s}$  (lateral diffusion in solvent vapor) is likely to be an outlier due to dye transport in the vapor phase (as discussed in Chapter 6.3.2).

From this we conclude, that the extracted parameter for the  $c_1$  - and  $c_2$  - value for PVK/PBD blends are very different than those for most polymers. The difference in the fit-

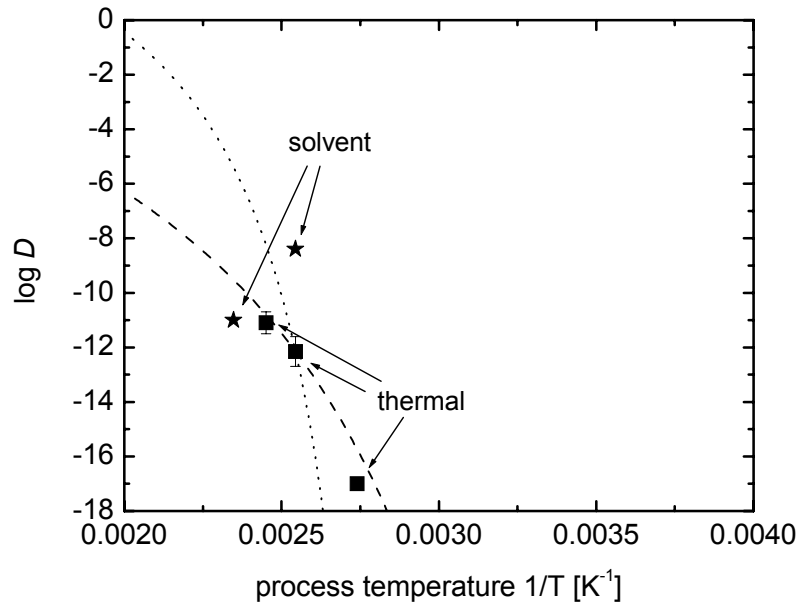


**Figure 5-29.** Plot of measured values of  $D$  vs.  $1/T$  (process temperature) and predicted values according to the WLF model (dotted line with common parameters; with fitted parameters dashed line). The process temperatures of the solvent vapor data point are adjusted using the relation  $T_{\text{process (rescaled)}} - T_g = T_{\text{process solvent}} - T_{g \text{ solvent}}$  to account for the different glass transition temperatures in this case.

ting parameter may be due to the presence of the PBD and the fact that this blend material might contain crystalline grains. Although the fit of the data is quite convincing and the values not unrealistic, they should be confirmed by other means.

**Table 5-3.** WLF parameter for different polymers [2]

polymer	$c_1$	$c_2$
natural rubber	16.7	53.6 K
polystyrene	14.5	50.4 K
polyurethane elastomer	15.6	32.6 K
polyisobutylene	16.6	104 K

That all of the data points (excepting the case with spurious surface transport of dye) both with and without solvents present can be fitted by a single model tells us about the diffusion of dye in the solvent vapor case. That is, like in the standard thermal diffusion model, the diffusion is controlled solely by the difference between the process temperature  $T$  and the glass transition temperature  $T_g$ .

## 5.6 Summary

The anneal of the device in acetone solvent vapor after the initial dye transfer has been demonstrated to achieve a very homogeneous dye distribution in the polymer film with raising the process temperature. This process allowed us to eliminate the high temperature anneal and its negative effects on the device performance described in the previous chapter. Using the solvent vapor anneal method, devices with efficiencies comparable to control devices have been obtained. However, the rectification ratio decreased substantially for the annealed device.

The fundamental interaction of the solvent and the PVK/PBD and its effect on diffusion has been studied. Significant dopant diffusion occurs already at low partial pressures of solvent and at short processing times, leading to less device degradation. The reduction of the glass transition temperature by the solvent appears to be the main mechanism for the enhanced diffusion, with the difference between the process temperature and the glass transition temperature as critical parameters. Additional work is required to further quantify these results.

## 5.7 References

- [1] J. C. Sturm, W. Wilson, and M. Iodice, "Thermal effects and scaling in organic light-emitting flat-panel displays", *IEEE Journal on Selected Topics in Quantum Electronics* **4** (1), 75 (1998).
- [2] R. A. Register, lecture notes of course "Solid-State Properties of Polymers", taught at Princeton University, Department of Chemical Engineering.
- [3] D.-Y. Khang and H. H. Lee, "Room-temperature imprint lithography by solvent vapor treatment", *Appl. Phys. Lett.* **76** (7), 870 (2000).
- [4] D.-Y. Khang, H. Yoon, and H. H. Lee, "Room-temperature imprint lithography", *Advanced Materials* **13** (10), 749 (2001).

- [5] F. Pschenitzka, K. Long, and J. C. Sturm, "Solvent-enhanced Dye Diffusion in Polymer Thin-Films for OLED Application", *Mat. Res. Soc. Symp. Proc.* **665**, C9.5 (2001).
- [6] S. Pickup, F. D. Blum, W. T. Ford, and M. Periyasamy, "Transport of small molecules in swollen polymer beads", *Journal of the American Chemical Society* **108** (14), 3987 (1986).
- [7] M. Lohfink and H. Sillescu, "Tracer diffusion in polymer and organic liquids close to the glass transition", *AIP Conference Proceedings* (256), 30 (1992).
- [8] F. Pschenitzka and J.C. Sturm, "Solvent-enhanced dye diffusion in polymer thin films for color tuning of organic light-emitting diodes", *Appl. Phys. Lett.* **78** (17), 2584 (2001).
- [9] T. Alfrey, E. F. Gurnee, and W. G. Lloyd, "Diffusion in Glassy Polymers", *J. Polym. Sci.* **C12** (12), 249 (1966).
- [10] T. K. Kwei and H. M. Zupko, "Diffusion in glassy polymers. I", *J. Polym. Sci. A-2, Polym. Phys.* **7** (5), 867 (1969).
- [11] J. Crank and G. S. Park, *Diffusion in polymers* (Academic Press, London, New York, 1968).
- [12] T. S. Frick, W. J. Huang, M. Tirrell, and T. P. Lodge, "Probe diffusion in polystyrene/toluene solutions", *Journal of Polymer Science, Part B: Polymer Physics* **28** (13), 2629 (1990).
- [13] J. S. Papanu, D. W. Hess, A. T. Bell, and D. S. Soane, "In situ ellipsometry to monitor swelling and dissolution of thin polymer films", *Journal of the Electrochemical Society* **136** (4), 1195 (1989).
- [14] D. W. v. Krevelen, *Properties of polymers : their correlation with chemical structure, their numerical estimation and prediction from additive group contributions*, 3rd, completely rev. ed ed. (Elsevier, Amsterdam; New York, 1990).
- [15] Aldrich, technical information on PVK, obtained from [www.alrich.com](http://www.alrich.com) (2001).
- [16] J. H. Schön, C. Kloc, R. A. Laudise, and B. Batlogg, "Surface and bulk mobilities of oligothiophene single crystals", *Appl. Phys. Lett.* **73** (24), 3574 (1998).

- [17] C. C. McDowell, B. D. Freeman, and G. W. McNeely, "Acetone sorption and uptake kinetic in poly(ethylene terephthalate)", *Polymer* **40** (12), 3487 (1999).
- [18] *CRC Handbook of Chemistry and Physics*, edited by D. R. Lide, 75th ed. (CRC Press, Boca Raton, 1994).
- [19] T. S. Frick, W. J. Huang, M. Tirrell, and T. P. Lodge, "Probe diffusion in polystyrene/toluene solutions", *Journal of Polymer Science, Part B: Polymer Physics* **28** (13), 2629 (1990).
- [20] D. Braun, "Crosstalk in passive matrix polymer LED displays", *Synth. Met.* **92**, 107 (1998).
- [21] C.-c. Wu, C.-c. Yang, H.-h. Chang, C.-W. Chen, and C.-C. Lee, "Finite-source dye-diffusion thermal transfer for doping and color integration of organic light-emitting devices", *Appl. Phys. Lett.* **77** (6), 794 (2000).
- [22] R. A. Hann and N. C. Beck, "Dye diffusion thermal transfer (D2T2) color printing", *Journal of Imaging Technology* **16** (6), 238 (1990).
- [23] K. Shinozaki and H. Hirano, "Dye - polymer affinity and its effect on thermal dye-transfer printing", *Journal of Imaging Science and Technology* **38** (6), 571 (1994).
- [24] V. V. Krongauz and W. F. Mooney, "Real-Time monitoring of diffusion between laminated polymer films", *Polymer* **35** (5), 929 (1994).

# 6 Patterning Approaches using Local Dye Transfer

In the previous chapter, the dye transfer aspect of the dye transfer method has been discussed in detail, and a fabrication process resulting in OLEDs with efficiencies comparable to conventional devices with dye contained in the spin-on solution has been introduced.

For the application of this technology in full-color display production, the color-changing dye has to be transferred into the polymer film of the device in a well defined pattern to obtain the red, green and blue emitting sub-pixels. This chapter focuses on the patterning technology developed for full-color OLED displays.

In Chapter 6.1 we discuss the use of a diffusion mask to obtain the desired pattern. Chapter 6.2 focuses on the implementation of a patterned dye source to eliminate the need for an additional shadow mask. The stability of the dye pattern is the topic of Chapter 6.3. A summary will be given in Chapter 6.4.

## 6.1 Patterning Approaches using a Diffusion Mask

### 6.1.1 “Scotch Tape” Method

As shown in Figure 3-5 on page 51 [1], the first approach of patterned dye transfer from the dye source substrate to the device substrate relied on a separate mask layer sandwiched between the two substrates during the transfer process. Only where the mask has openings, the dye is allowed to desorb from the dye source layer and absorb at the surface of the polymer layer of the device.

Initial results were obtained by using a highly doped polymer solution (100 mg C6, 100 mg PVK dissolved in 6.5 ml chloroform spun on at 4000 rpm on glass). Part of the dye source substrate were then covered with regular office adhesive tape (3M, 50  $\mu\text{m}$  thick,

“ScotchTape”). The dye transfer into a standard device (PVK/PBD/bimane layer on a ITO coated glass substrate) was carried out by placing both substrates in direct contact at 95 °C for 10 min. The pattern was transferred with good resolution, and feature sizes down to 50  $\mu\text{m}$  were accomplished (as shown in the electroluminescence micrograph in Figure 6-1).

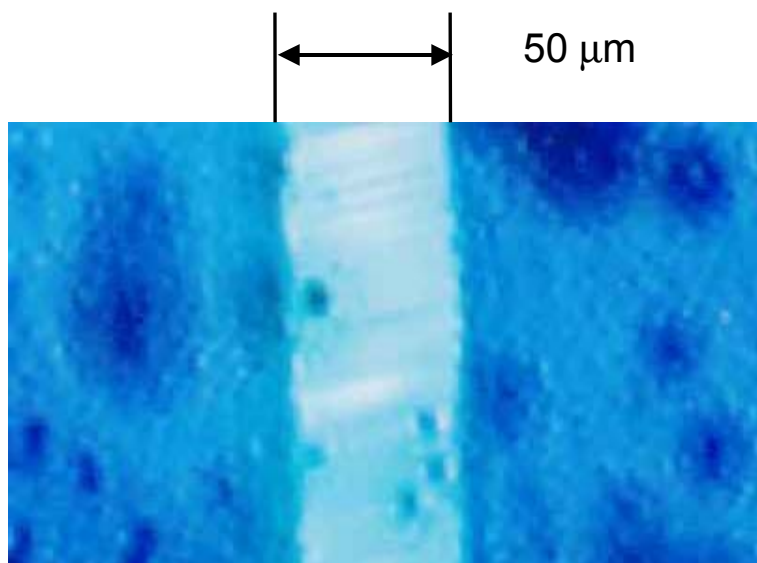


**Figure 6-1.** Electroluminescence micrograph of a device with a 50  $\mu\text{m}$  wide line of C6 transferred into a PVK/PBD/bimane film.

### 6.1.2 Stainless Steel Mask

After these promising results, we used a laser drilled stainless steel shadow mask (302 stainless steel, manufactured by Rache Corp., Camorillo, CA) in an attempt to fabricate a three-color display. The size of the mask was 51 mm by 39 mm with a thickness of 0.1 mm. Twenty slits (each 24 mm by 0.4 mm with a pitch of 1.5 mm) were laser-drilled into the steel foil. Figure 6-2 shows a photoluminescence photograph of a glass substrate with a spun-on PVK/PBD/bimane film with C6 (right side) and Nile red (left side) transferred into the film. The transfer was carried out at 70 °C in a vacuum oven for one hour using two dye source substrates simultaneously. The sample was not further processed with high temperature or solvent anneal.

However due to the laser-drilling of the steel mask, the edge of the openings in the mask retained some burr, which, when placed in contact with the device substrate, mechanically damaged the soft polymer film. These scratches (as shown in Figure 6-3) resulted in

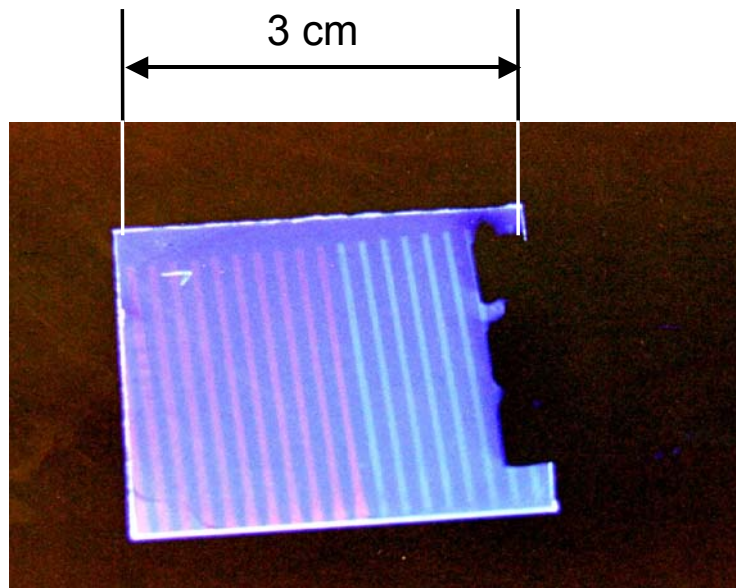


**Figure 6-2.** Photoluminescence photograph of a substrate with two dyes transferred into polymer film (400  $\mu\text{m}$  wide lines).

short circuited devices. Because short circuited devices are a major failure cause in a passive matrix display [2], the approach to use a stainless steel shadow mask was terminated.

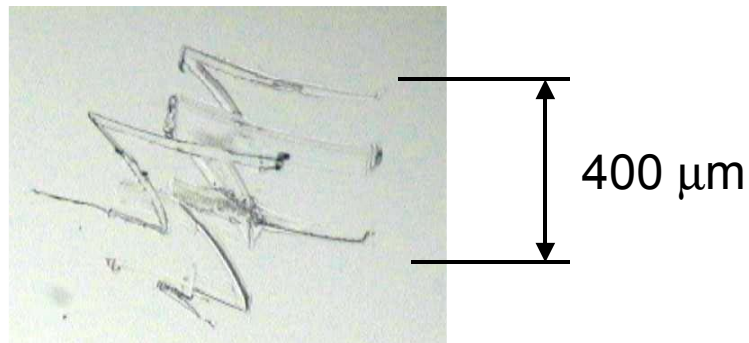


**Figure 6-3.** Micrograph of a damaged polymer film due to burr of the steel shadow mask.

### 6.1.3 Silicone and Polyurethane Mask

To eliminate the damage to the device polymer film, the mask had to be soft and at the same time demonstrate dimensional stability. We therefore fabricated a silicone mask (Silicone Rubber RTV 615, obtained from GE Silicones, Waterford, NY) which exhibited the desired softness. The mask was molded in a teflon form with the same geometry as the stainless steel mask. No damage to the polymer layer could be detected after the transfer

step. However, the transfer was very inefficient due to the increased thickness of the mask (0.4 mm). In addition, the silicone mask was too flexible, and it was impossible to keep the distance between the lines constant when placing the mask onto the device substrate.

To increase the stability of the mask, we then fabricated the mask with polyurethane (EP21LV, obtained from Master Bond, Inc., Hackensack, NJ) using the aforementioned teflon mold. The resulting shadow mask was more rigid (depending on the mixing ratio of the two components), but the thickness could not be reduced compared to the silicone mask without breaking the mask when separating it from the mold. In addition due to cohesive forces between the mold and the polyurethane precursor, the mask showed considerable deformation at the edge the openings, which damaged the device polymer film in the same fashion as the stainless steel mask.

We therefore decided not to employ a separate shadow mask in the patterning process but rather integrate the mask into the dye source substrate. In addition, we wanted to incorporate the versatility of conventional photolithography into the patterning process.

## **6.1.4 Transferred Photoresist (“RISTON”)**

### **6.1.4.1 Riston Photoresist**

Using dry photoresist, which can be laminated onto the surface before being patterned, is a common technology in printed circuit board manufacturing. To avoid the mixing of the two layers after the spin-on process of the photoresist onto the dye source matrix (Chapter 6.2.1), we used the dry photoresist Riston CM 206 (manufactured by DuPont) which can be laminated onto the surface and thus does not dissolve the polymer layer underneath.

The Riston photoresist consists of a 18  $\mu\text{m}$  thick photosensitive polymer film, sandwiched between a flexible capping and a more rigid backing foil. To use this product in the conventional way, the capping foil is removed, and the remaining layers are laminated under pressure at room temperature onto the metal layer of the circuit board. After this, the circuit board is exposed to UV light through an appropriate mask. This is followed by the development in  $\text{K}_2\text{CO}_3$  (1% by weight in water) after the backing foil is removed, leaving

only the photosensitive layer on the circuit board. During the development, all non-exposed areas are being removed (negative photoresist) [3].

Analogous to the described process, the Riston film was in this experiment laminated onto the cleaned glass substrate previously coated using either a solution of PVK and C6 or a solution of Vylon 103 and C6 (100 mg polymer, 100 mg C6 in 6.5 ml chloroform) after the flexible Riston capping foil was removed. The Riston film adhered to the Vylon film much better than to the PVK film. The lamination was carried out with a commercially available laminator (Model PL12A, obtained from ALPS Inc., Lonoke, AR) at 90 °C (reading of the thermometer attached to the laminator). The substrate was then exposed to UV light (30 sec), the remaining backing foil was removed and the photoresist developed. However, the dye-doped film blistered off again during the development step.

We therefore decided to eliminate any exposure of the dye-doped film to wet processing by patterning the resist before its lamination onto the dye source substrate, instead of transferring the pristine photoresist.

#### **6.1.4.2 Patterned Riston-Mask and Laminated Technology**

To transfer the patterned photoresist, we exposed the Riston film to UV light for 30 sec without previously removing any support foils. During the exposure, the Riston film was “glued” to a bare silicon wafer by a very small amount of water to avoid that the Riston film moves during processing in the mask aligner. After the exposure, the capping foil was removed and the remaining photoresist mounted to the remaining support foil was then developed in  $K_2CO_3$  (1% by weight in water). Because the photoresist layer does not adhere very strongly to the support foil, care has to be taken when rinsing it in DI water. Running water damaged the pattern by washing off many of the small features of photoresist. The film was then dried in air with the photoresist side up to protect it from sticking to the support material.

The film was then laminated onto the dye source substrate consisting of a cleaned glass slide and a spun-on dye-doped polymer layer (either PVK or Vylon). Because the Riston film did lose much of its sticking properties during the patterning process, the lamination temperature had to be raised considerably. In addition, many runs through the laminator helped to make the Riston layer stick to the dye source substrate. For the dye source

with the PVK layer as the polymer matrix, the lamination temperature was about 150 °C, for the Vylon dye source, this temperature was about 120 °C. The process is shown in Figure 6-4.

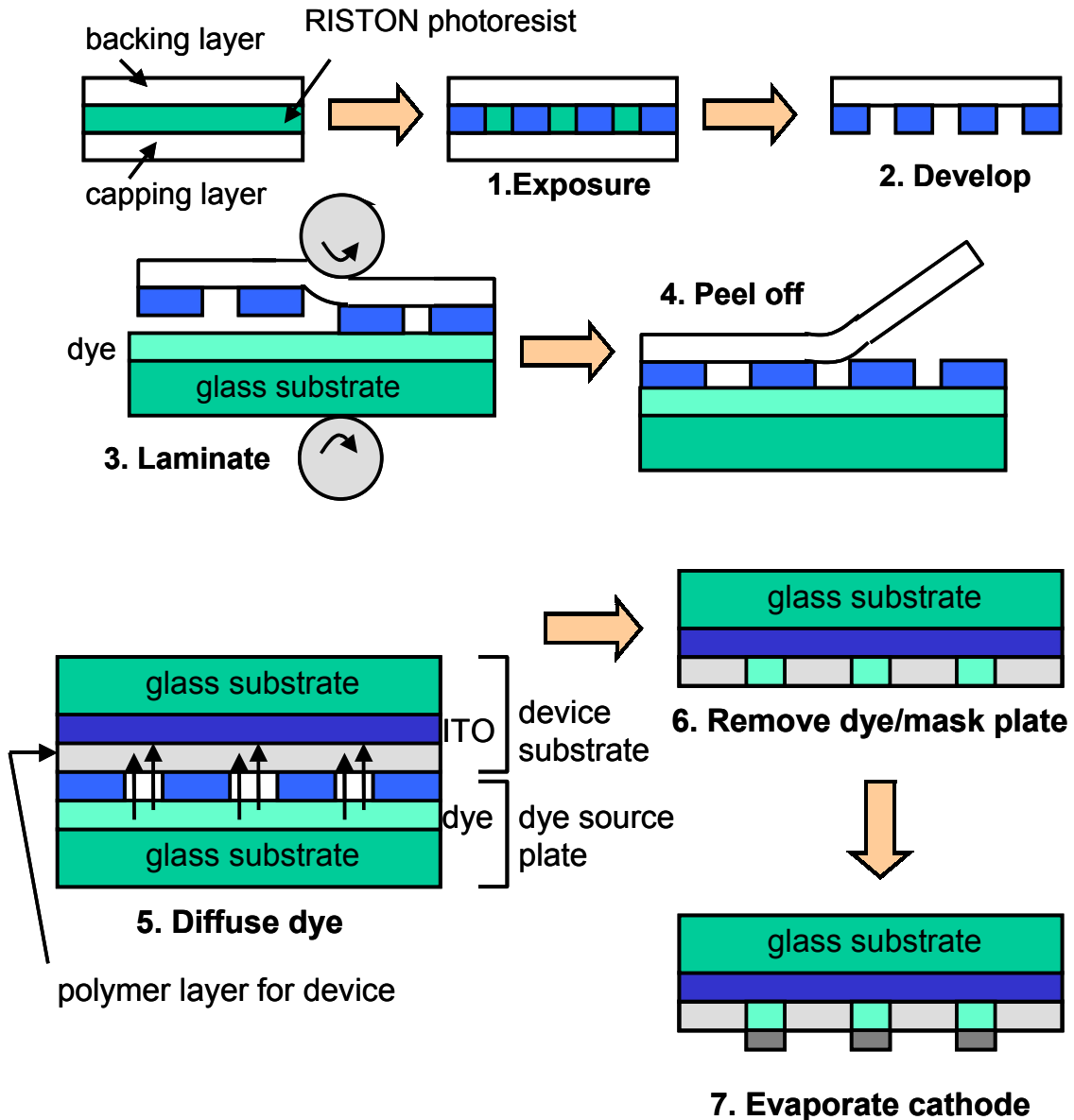


**Figure 6-4.** Device fabrication process using local dye patterning with transferred photoresist. [4]

#### 6.1.4.3 Dye Transfer Experiments

Using this patterning process, very small feature sizes were obtained. Figure 6-5 shows a photoluminescence micrograph of dyed lines (C6 transferred into a PVK/PBD/

bimane film). The pattern was obtained by transferring dye from a dye source substrate, consisting of a glass substrate with a highly doped PVK layer (50% in the final film), with a laminated and patterned Riston photoresist with 20  $\mu\text{m}$  lines (with a pitch of 40  $\mu\text{m}$ ). The diffusion was carried out 70  $^{\circ}\text{C}$  in vacuum for one hour. The micrograph was recorded

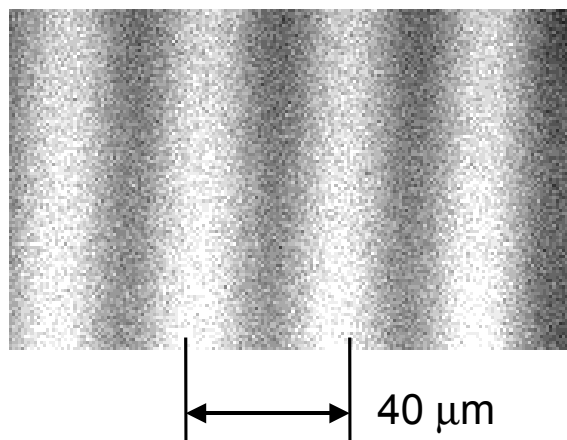


**Figure 6-5.** Photoluminescence micrograph of a PVK/PBD/bimane film with C6 transferred from a dye source using a patterned Riston film as integrated diffusion mask.

under laser excitation at 466 nm using a photomultiplier detector (Department of Molecular Biology, Princeton University). At this wavelength, only the C6 molecules are excited, but not the bimane. Therefore, all the emission is caused by the transferred dye.

Figure 6-6 shows the electroluminescence micrograph of a PVK/PBD/bimane device with C6 transferred by the described process. The feature size of this device is of much lower resolution than in case of the photoluminescence, because our measurement set-up does not allow to record electroluminescence micrographs at this scale. The figures show the successful application of patterning with transferred and pre-patterned photoresist.

However, we observed an overall luminescence quenching in areas where the Riston film was in contact with the polymer film of the device. The reason for this quenching effect was not further investigated. It could either be that dye diffuses out of the device film and into the Riston film, or that additives in the Riston film (such as plasticizers) diffuse during the transfer process into the device polymer layer and cause the observed quenching.

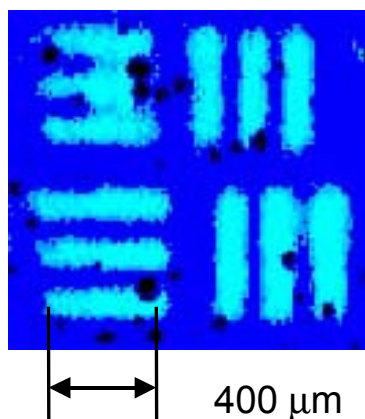


**Figure 6-6.** Electroluminescence micrograph of a PVK/PBD/bimane film with C6 transferred from a dye source using a patterned Riston film as integrated shadow mask.

## 6.2 Patterned Dye Source

Because of practical difficulties applying the technologies utilizing diffusion masks described in the previous section, we also investigated using a patterned dye source.

### 6.2.1 Photoresist Patterning of Dye Source Layer

The idea to deposit a layer of photoresist by spin-coating onto the dye source layer, evolved out of the effort to integrate the shadow mask into the dye source substrate. A cleaned glass sample with a spun-on polymer layer (100 mg PVK, 100 mg C6 in 6.5 ml chloroform) was spin-coated with the photoresist AZ5214-E. The photoresist seemed to dissolve the dye source layer because the resulting film did not retain the strong yellow color of the dye source layer characteristic of highly concentrated C6.

After exposure to UV light (30 sec), the sample was the developed (AZ 400, 1: 3.5 in DI water). During this step, the film blistered off completely from the glass substrate.

Considering these results, we decided to use the photoresist not as a blocking layer analogous to the steel shadow mask, but rather as the matrix holding the dye to be transferred.

### 6.2.2 Doped Photoresist

The direct approach to combine photolithography and dye transfer was pursued by mixing the dye into the liquid photoresist, and process the photoresist as usual to obtain a

patterned dye source layer. In this case, no blocking layer between the dye source substrate and the device substrate is needed.

However, the dye C6 did not dissolve sufficiently in the photoresist used (AZ 5214-E). Moreover, acetone, chloroform and other good solvents for C6 are also good solvents for the photoresist. Mixing a small amount of a C6/acetone solution into the liquid photoresist (100 mg C6 dissolved in 2 ml chloroform mixed in 6 ml AZ 5214-E) resulted, after the spin coating on a glass substrate, in a polymer layer which demonstrated a strong yellow tint characteristic of C6 at high dye concentrations. However, the PL emission of the film was very weak due to concentration quenching of C6 and due to the fact that no energy transfer from the polymer to the dye is possible because the photoresist is not electroactive.

After the exposure of the doped photoresist to UV light, the film blistered off during the development step (developer AZ 400, 1: 3.5 in DI water). To enhance the adhesion properties of the photoresist layer, the glass was first coated with adhesion promoter HMDS before the deposition of the doped photoresist. However, the film adhesion of these samples did not show any improvement. In a different approach, the cleaned glass slide was treated with oxygen plasma (same process parameter as for the ITO treatment, see Chapter 2.8.1.3). The resulting samples demonstrated significantly reduced blistering, however, the damage could not be completely eliminated. Samples exposed to UV light for 30 sec showed the best pattern definition.

The dye patterned source was then placed in direct contact with a standard device substrate (PVK/PBD/bimane), and the dye transfer was carried out at 60 °C for 90 min in vacuum. Not enough dye diffused out of the photoresist layer, probably because of the high glass transition temperature  $T_g$  of the photoresist.

To lower the  $T_g$  of the photoresist, we mixed a small amount of plasticizers di(n-butyl)phthalate (DBP) and di(2-ethylhexyl)phthalate (DEP) into the liquid doped-photoresist solution. However, the resulting films were sticky and could not be used as dye sources, since these substrates could not be removed from the target device film.

Although this approach was abandoned after these results, this method still holds some technological potential to pattern the dye source layer.

### 6.2.3 Dry-Etched Dye Source using a Laminated Photoresist Mask

To avoid any contact of the device substrate with the Riston photoresist, we designed a variation of the described process. Instead of using the transferred photoresist as a shadow mask, this layer served as an etching mask in which the dye-doped layer was patterned by oxygen plasma etching.

The dye source substrate was a cleaned glass slide with a spun-on either a Vylon/C6 film (for green, 100 mg Vylon, 100 mg C6 in 10 ml chloroform spun on at 2000 rpm) or Vylon/Nile red (for red, 84 mg Vylon, 10 mg Nile red, in 8.4 ml chloroform at 2000 rpm). After the photoresist was transferred by the same technique as described earlier, the substrate was then exposed to an oxygen plasma in the same parallel plate reactor as for the ITO treatment. The following process parameters were used: oxygen flow: 25 sccm, plasma power: 75 W, chamber pressure: 150 mTorr, process time: 4 min. The Vylon film was etched completely whereas the Riston film did not show any damage due to the oxygen plasma.

As mentioned earlier, the Riston photoresist is designed for patterning printed circuit boards and as such it adheres very well to metal surfaces. The Riston film could easily be removed from the dye source substrate by laminating a cleaned aluminum foil at 120 °C onto the substrate. After the substrate was allowed to cool down for 2 min, the aluminum foil was removed from the substrate with the Riston film attached to the aluminum foil. As a result, only the patterned doped Vylon layer was left on the glass substrate.

The dye source substrate and the device substrate (glass with a patterned ITO layer, oxygen plasma treated) was then placed in direct contact under a pressure of 1500 Pa for 90 min and held at 70 °C in air. The pressure was applied by placing a small steel cylinder on top of the two substrates. The fabrication process is pictured in Figure 6-7.

Figure 6-8 shows an electroluminescence micrograph of a 3 mm high letter “P” with stripes of Nile red transferred into PVK/PBD film. The outline of the letter is defined by previously patterned ITO. A blanket Mg:Ag cathode was deposited after the deposition of the polymer film and the transfer process. The 200 μm bright stripes are lines where the dye Nile red was transferred into the polymer film. The polymer film itself emits only very weakly in the blue.

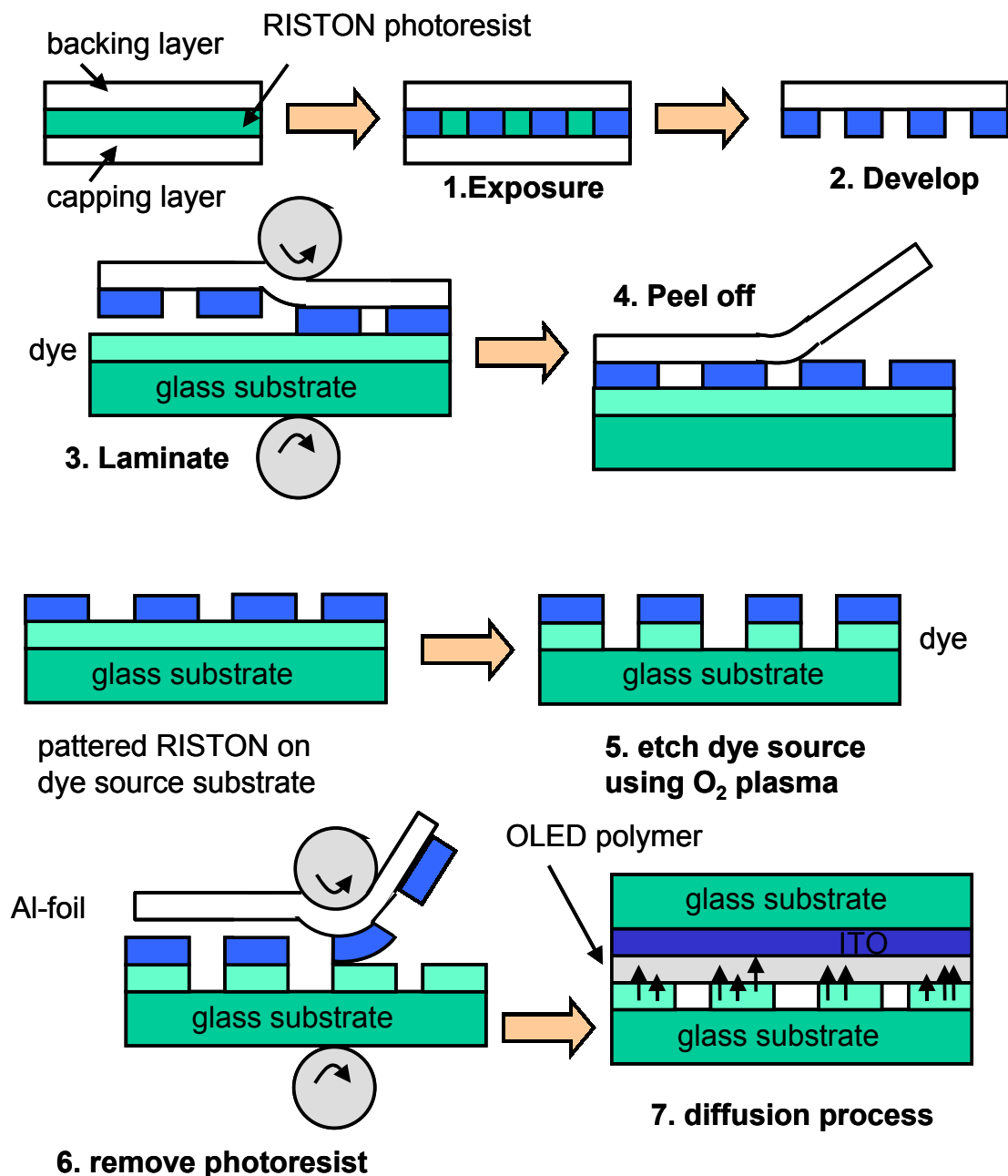


**Figure 6-7.** Device fabrication process with patterned dye source by dry etch of dye doped polymer film. [4]

This method eliminates any quenching due to the Riston film. However, the lateral resolution is limited due to the fact that no barrier is provided to keep the dye from diffusing laterally during the transfer process. Further work in this area is necessary.

In addition, the dye concentration is hard to control because the dye diffuses into the Riston film during the lamination process and the lift-off. The surface of the dye source

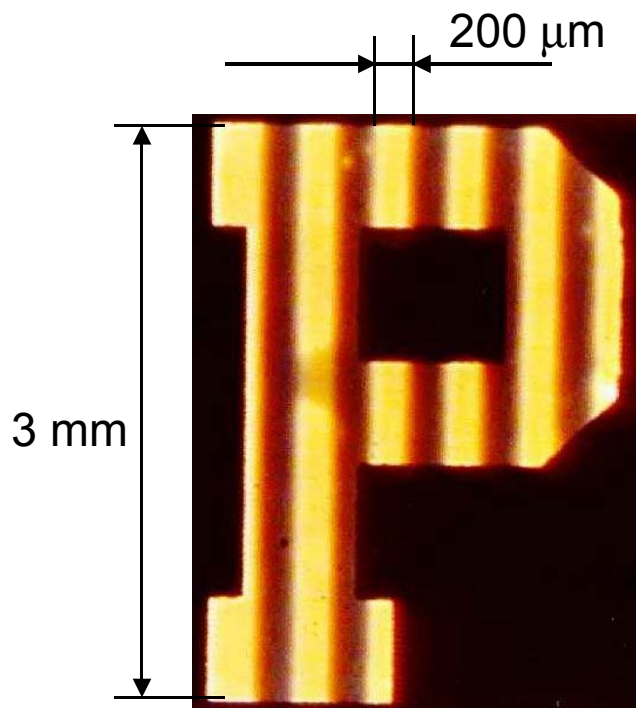


**Figure 6-8.** EL micrograph of a 3 mm high letter with 200  $\mu\text{m}$  lines of transferred Nile red layer is therefore depleted of dye compared to the bulk of the film [5]. To compensate this effect, the dye concentration of the dye source solution had to be significantly increased. Whereas the optimal dye concentration of C6 in the dye source film was 2% by weight for a Vylon film not patterned and in direct contact with the device polymer film, the optimal concentration for a Vylon film patterned by Riston lift-off is about 8% by weight.

### 6.3 Stability of Transferred Dye Pattern

The stability of the dye pattern is of major importance in full color displays. If the dye diffuses laterally from its original position, the color purity of neighboring sub-pixels is negatively effected, i.e. the dye is “bleeding”. We investigated the lateral dye diffusion under elevated temperature and while exposing the polymer film to solvent vapor. Whereas in the latter case we expose the device substrate to a solvent vapor to drive the dye into the device polymer film (see Chapter 5) during the fabrication process, the thermal enhanced diffusion of dye is of great concern in the context of long-term stability of the device at elevated operating temperatures due to the power dissipation or storage.

### 6.3.1 Thermal Stability of the Dye Pattern

It is expected that the diffusivity of dye is high above the glass transition temperature  $T_g$  and very small below it [6][7]. For the PVK/PBD blend used in this experiment,  $T_g$  is approximately 120 °C. To investigate the stability, we transferred C6 in a pattern of 20  $\mu\text{m}$  and 40  $\mu\text{m}$  pitch into a PVK/PBD film at 70 °C (see Chapter 6.1.4.3). The films were annealed at different temperatures and the change in PL vs. distance along the surface was used as evidence of lateral dye diffusion in the polymer. Initially, we observed anomalously high diffusion rates, which were found to be due to evaporation of dye, followed by gas phase transport and re-deposition onto undoped areas some distance away. To eliminate this effect, a 600 Å thick layer of  $\text{SiNO}_x$  was deposited on the polymer surface at 50 °C by Plasma Enhanced Chemical Vapor Deposition (PECVD). This solved the anomalous diffusion problem, and also helped to reduce any polymer degradation due to contact with air and water vapor at the annealing temperature. The photoluminescence image was taken using a fluorescence microscope. The samples were then annealed for four hours at 90 °C, 105 °C, 120 °C, or 135 °C in nitrogen. After anneal, a PL image was taken at the same spot, and compared to the one taken before the anneal (Figure 6-9). We were unable to detect any lateral diffusion of the dye at annealing temperatures below 120 °C, but samples annealed at higher temperatures showed a slight lateral diffusion. By modelling the evolution of these profiles, the diffusion coefficient of dye was extracted and found to be  $D = 7 \cdot 10^{-13} \pm 2 \cdot 10^{-13} \text{ cm}^2/\text{s}$  for 120 °C and  $D = 8 \cdot 10^{-12} \pm 4 \cdot 10^{-12} \text{ cm}^2/\text{s}$  for 135 °C. This value of  $D$  at 135 °C is comparable to reported diffusivities of dye in polystyrene [8]. However, it is difficult to compare these results because of the differences in the polymer and the dye in our work vs. theirs. For example, a dye volume increase by a factor of 10 can result in a decrease of  $D$  by nine orders of magnitude [9]. On the other hand, the observed diffusivity on the polymer/air interface is known to be much higher than in the bulk of the material. This can explain why these results are higher than those reported about the bulk diffusivity in polymers [10].

The lower limit for the dye diffusion coefficient within experimental resolution is  $10^{-13} \text{ cm}^2/\text{s}$ . Therefore, no change could be detected at temperatures of 90 °C and 105 °C.

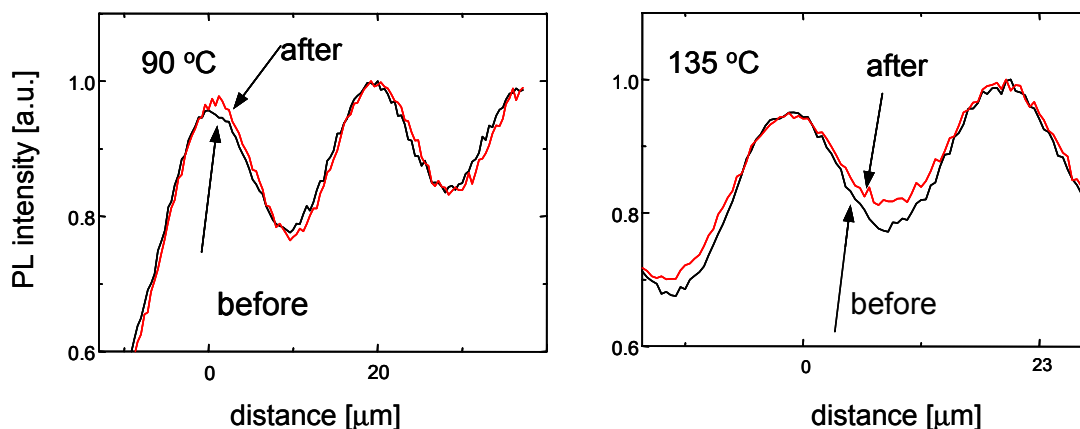


**Figure 6-9.** Spatial PL intensity profiles before and after 4 hour anneal at 90 °C or 135 °C of substrates with C6 stripes patterns transferred into PVK/PBD film. [4]

These results for diffusivity vs. temperature are modelled using the WLF model (see Chapter 4.5 on page 77 and Chapter 5.5 on page 117).

The operating or storage temperature should never exceed the glass transition temperature  $T_g$  of the emissive polymer for stability reasons. If we assume, for arguments sake, that the device is held at  $T_g$  (120 °C), what is the time needed for a dye in pixel to bleed into another pixel if the pixels are 1  $\mu\text{m}$  apart? Note that this distance is much smaller than for any practical display applications. Using the relationship  $L = \sqrt{Dt}$ , it will take 115 days for this to happen.

This result clearly indicates, that the dye pattern is very stable thermally. At normal operating temperatures, this time span will be significantly longer. For state of the art devices, the lifetime of a device is the smaller than this diffusion time.

### 6.3.2 Stability of Dye Pattern during Solvent Vapor Anneal

In contrast to the thermal stability of the dye pattern, the stability of the pattern during the solvent anneal is only of importance during the fabrication process. After the device substrate with the polymer film was exposed to solvent vapor to diffuse the dye into the bulk of the polymer film (see Chapter 5), the film is dried in pure nitrogen. All solvent is removed from the polymer film at this time and it regains its pre-solvent treatment properties like thickness and glass transition temperature  $T_g$ . That means, after the solvent treat-

ment, only the thermal dye diffusion has an impact on the stability, and this has already been shown to be very small.

Two solutions containing either PVK only (100 mg PVK in 7 ml chlorobenzene) or a PVK/PBD blend (100 mg PVK, 40 mg PBD in 7 ml chlorobenzene) were spun-on onto cleaned glass substrates at 2000 rpm. A dye source with a pattern of 300  $\mu\text{m}$  wide lines was fabricated using the plasma etching procedure outlined in Chapter 6.2.3. The dye source layer was Vylon with 8% of C6 (by weight in final film). The two substrates were placed in direct contact and held at 70  $^{\circ}\text{C}$  for one hour in vacuum. The samples were then transferred into the reactor for acetone solvent treatment. During the anneal process, a smaller glass slide was placed on the polymer film, which partially covered the sample. This glass slide locally prevented the solvent vapor from swelling up the PVK film. After the anneal, we investigated the difference in width of dye stripe by photoluminescent microscopy at the border between the exposed section of the sample and the section protected by the cover slide. The pictures were taken with an excitation wavelength of 488 nm, thus only exciting the C6 but not the PVK or the PVK/PBD blend. The micrograph of a 300  $\mu\text{m}$  wide stripe is shown in Figure 6-10. The sample with a PVK/PBD film was exposed to acetone vapor (65 ml per liter nitrogen) for 180 sec.

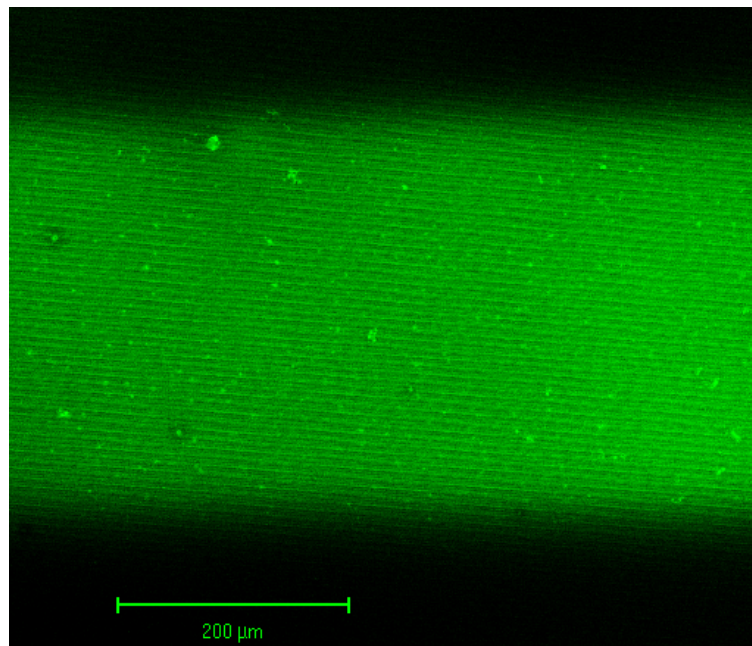


**Figure 6-10.** Photoluminescence micrograph of a stripe (300  $\mu\text{m}$  wide) of C6 transferred into a PVK/PBD blend after solvent anneal. The solvent anneal did not significantly increase the width of the dye-doped stripe.

The pictures were then analyzed by measuring the full-width-half-maximum of the photoluminescence intensity of the micrographs. The results are summarized in Table 6-1.

**Table 6-1.** FWHM increase of stripes of transferred C6 before and after the anneal in acetone vapor for 180 sec.

sample #	polymer film	acetone concentration	FWHM increase
1	PVK/PBD blend	65 ml per liter $\text{N}_2$	8 $\mu\text{m} \pm 3 \mu\text{m}$
2	PVK/PBD blend	43 ml per liter $\text{N}_2$	2 $\mu\text{m} \pm 2 \mu\text{m}$
3	PVK only	65 ml per liter $\text{N}_2$	9 $\mu\text{m} \pm 4 \mu\text{m}$
4	PVK only	43 ml per liter $\text{N}_2$	3 $\mu\text{m} \pm 3 \mu\text{m}$

All samples independent of the polymer material showed a slight increase in width after a solvent anneal. The two PL intensity profiles of a PVK/PBD film exposed to solvent vapor (65 ml acetone per liter nitrogen) for 180 sec are shown in Figure 6-11. From these profiles a diffusion coefficient was estimated to be  $D = 4 \cdot 10^{-9} \text{ cm}^2/\text{s}$ . Because the glass transition temperature  $T_g$  of a PVK/PBD film at this acetone concentration is 297 K (see Figure 5-16 on page 106), this result is orders of magnitude higher than expected from results presented above. The reason for this discrepancy could be the transport of dye in the

gas phase as in the previous section or it could be surface diffusion. That this increase is to first order independent of the composition of the polymer film, supports a model of surface or gas transport. Capping with a nitride layer was not possible from a technological point of view since OLED cathodes are to be put on the surface of the polymer film after the dye diffusion.

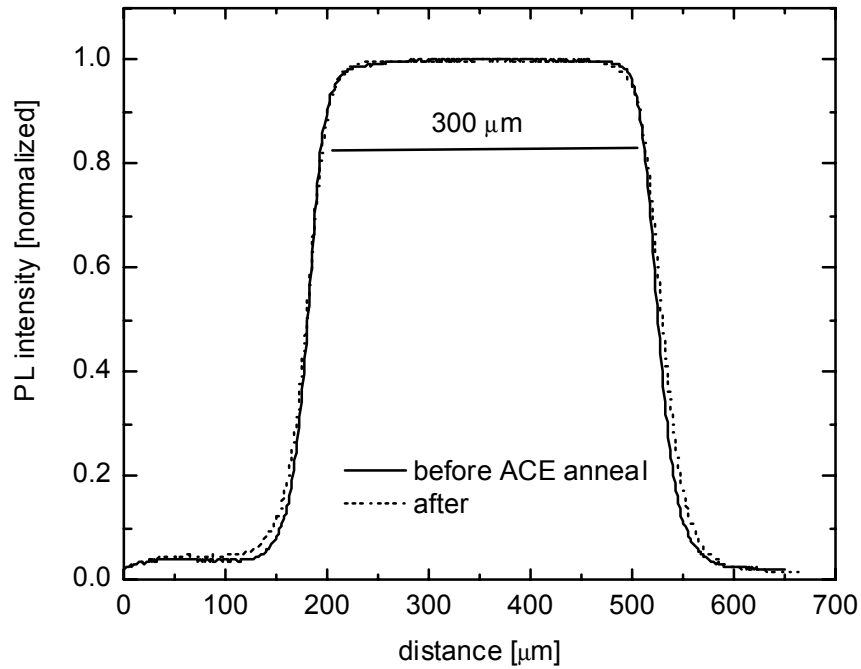


**Figure 6-11.** PL intensity profiles of a PVK/PBD sample with a 300  $\mu\text{m}$  wide stripe of C6 transferred before (solid line) and after (dashed line) the anneal in acetone vapor (partial pressure 46.4 torr) for 180 sec.

Since it is not possible to eliminate the anomalous transport of dye molecules, the solvent anneal is limiting the resolution of the display. However, except for microdisplay application, the stability of the dye pattern during the solvent exposure exceeds the required resolution for high-resolution computer screens with a pixel pitch of about 100  $\mu\text{m}$  when the solvent anneal is limited to 120 sec.

## **6.4 Summary**

The results given in this chapter demonstrate that patterning of OLEDs by local dye diffusion is a viable technology. Best results have been obtained using a dye source patterned by dry-etching. Integrated three-color devices fabricated with this technique will be discussed in Chapter 8.1.

## 6.5 References

- [1] F. Pschenitzka and J. C. Sturm, "Three-color organic light-emitting diodes patterned by masked dye diffusion", *Appl. Phys. Lett.* **74** (13), 1913 (1999).
- [2] D. Braun, "Crosstalk in passive matrix polymer LED displays", *Synth. Met.* **92**, 107 (1998).
- [3] DuPont Inc., Riston® - Aqueous-Processable Photopolymer Film, General Processing Guide. Document # DS97-41, obtained from [www.dupont.com/pcm](http://www.dupont.com/pcm) (1997).
- [4] F. Pschenitzka and J. C. Sturm, "Patterned dye diffusion using transferred photoresist for polymer OLED displays", *Proceedings of SPIE - The International Society for Optical Engineering* **4105**, 59 (2001).
- [5] Ke Long, Min-Hao Lu, Florian Pschenitzka and J.C. Sturm, "Novel Three-Color Polymer Light-Emitting Devices for Passive-Matrix Flat Panel Display", Digest of the 59th Device Research Conference, 179-180 (2001).
- [6] A. T. Slark and P. M. Haddgett, "The effect of specific interactions on dye transport in polymers above the glass transition", *Polymer* **40**, 4001 (1999).
- [7] J. C. Selser, "Diffusion of Dye Molecules in Polymers above and below the Glass transition Temperature Studies by Holographic Grating Technique", *Macromolecules* **18**, 587 (1985).
- [8] D. B. Hall and J. M. Torkelson, "Small molecule probe diffusion in thin and ultrathin supported polymer films", *Macromolecules* **31** (25), 8817 (1998).
- [9] D. Ehlich and H. Sillescu, "Tracer diffusion at the glass transition", *Macromolecules* **23** (6), 1600 (1990).
- [10] K. C. Tseng, N. J. Turro, and C. J. Durning, "Molecular mobility in polymer thin films", *Phys. Rev. E* **61** (2), 1800 (2000).

# 7 Cathode Patterning

For a display with high information density, the size of the pixels has to be sufficiently small. In a passive matrix display, the width of the intersecting ITO and cathode metal lines define the size of the basic pixel (see Figure 7-1).

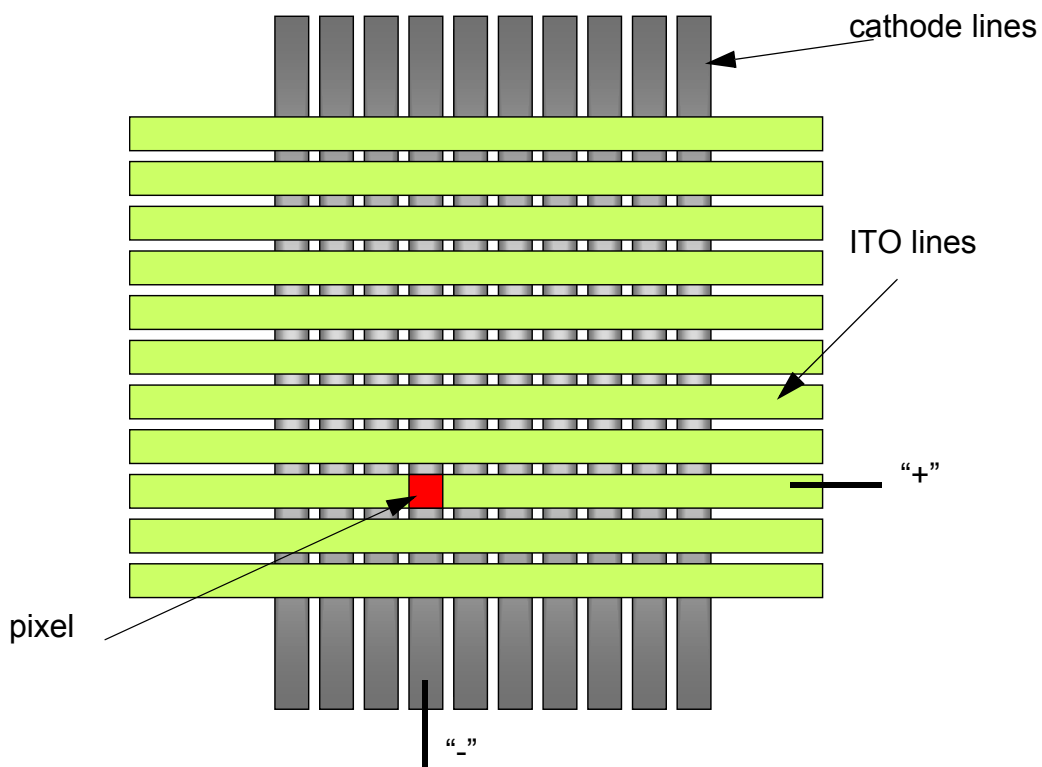


**Figure 7-1.** Schematic of a passive matrix display. Devices are formed where the ITO stripe intersects with the cathode metal stripe.

The ITO layer can be easily patterned using conventional photolithograph and wet etch (see Chapter 2.8.1.1) with very good resolution. The electroactive polymer layer is subsequently deposited on top of the patterned ITO substrate.

The organic material (polymer as well as small molecules) is very sensitive to water vapor, oxygen and organic solvents [1][2][3][4]. Because of this shortcoming, patterning

processes of the cathode covering the organic layer have generally been confined to technologies which do not rely on photolithography and/or wet etching.

For a system of materials based on small molecules, both, the organic layer and the cathode metal, are usually thermally evaporated. In this case, fine cathode lines can be created using the "cathode separators" technique: Pillars of insulating photo-processable materials are formed on the substrate prior to the evaporation of the organic material and the cathode metal. The pillar then serves as a separator between the individual devices [5][6] as shown in Figure 7-2.

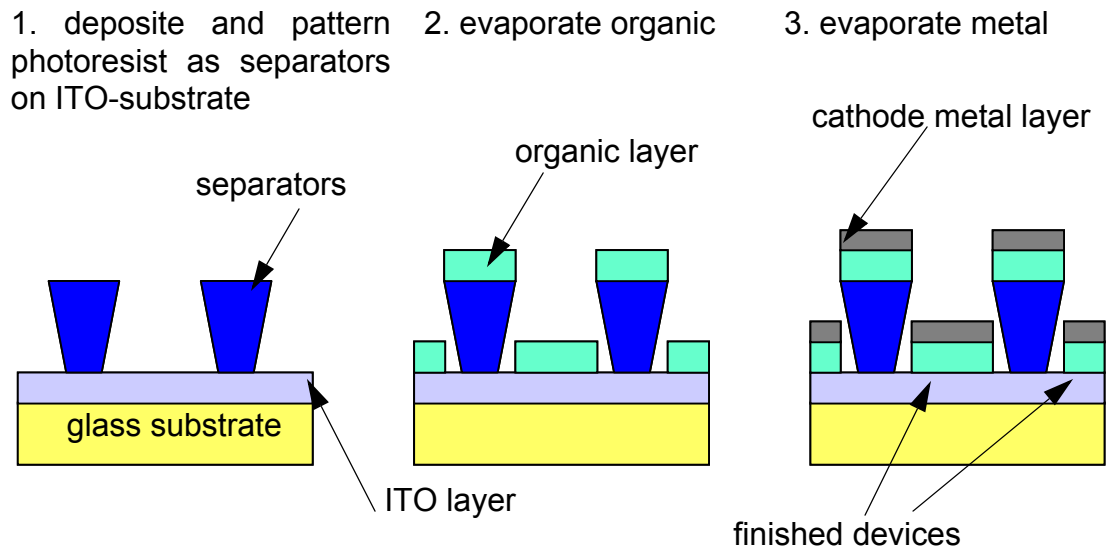


**Figure 7-2.** Use of cathode separators to pattern organic layer and cathode.

For polymer-based organic materials, the organic layer is usually deposited by spin-coating from a solution, forming a uniform film on the substrate. Since it is best done on planar substrates, spin-coating on pre-patterned surfaces with tall features is problematic. The pre-deposited separators could also be sensitive to the solvents used in spin-coating, and intermixing of the emissive polymer with the photoresist polymer could result in degradation of the device performance.

Shadow masks (as shown in Figure 7-3) could of course be used for cathode patterning, but their use is difficult for small features over a large area (e.g. passive matrix displays), and alignment to pre-existing features is difficult.

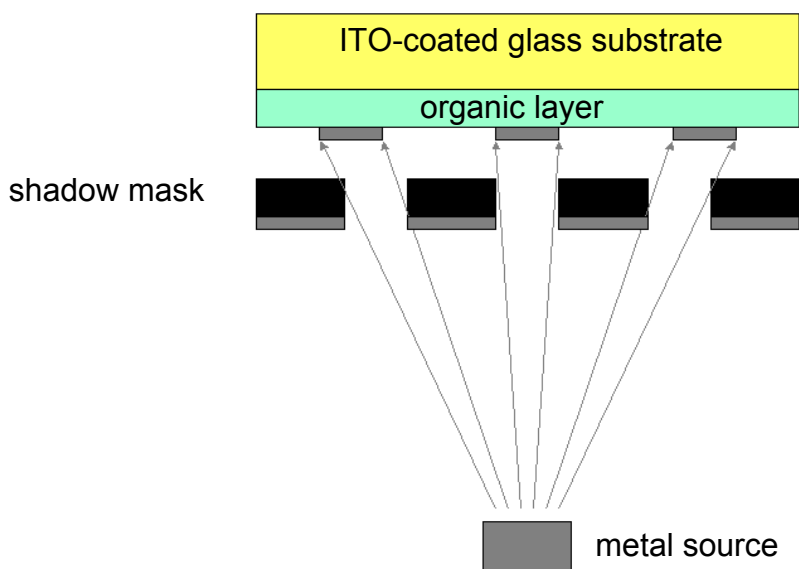


**Figure 7-3.** Cathode patterning using a shadow mask during the metal evaporation.

In some cases, photolithographic patterning of photoresist directly on top of the organic layer of OLED devices has been demonstrated where the organic material is carefully chosen to be compatible with photolithographic chemicals, but this greatly restricts the choice of organic materials [7].

In the following chapter, a two techniques are introduced whereby either conventional photolithography and dry etching are used to pattern narrow cathode features (Chapter 7.1) or transferred photoresist is employed as cathode separator (Chapter 7.2).

## 7.1 Dry Etching of the Cathode Metal Layer

To avoid any contact of photoresist, acids, developer or water with the organic material, we used dry etching to pattern the cathode metal layer. A cathode layer was deposited as a blanket metal film. Before the metal layer was etched, a layer of conventional photoresist was deposited by spin-coating on top of the cathode layer and patterned. Because the cathode metal layer is a blanket film, it can be used as a barrier to protect the organic film during the wet processing of the photolithography step as shown in Figure 7-4.

In most of the experiments described in this thesis, magnesium-silver alloys are typically used for cathodes. However, they are not easily dry-etched due to the lack of volatile

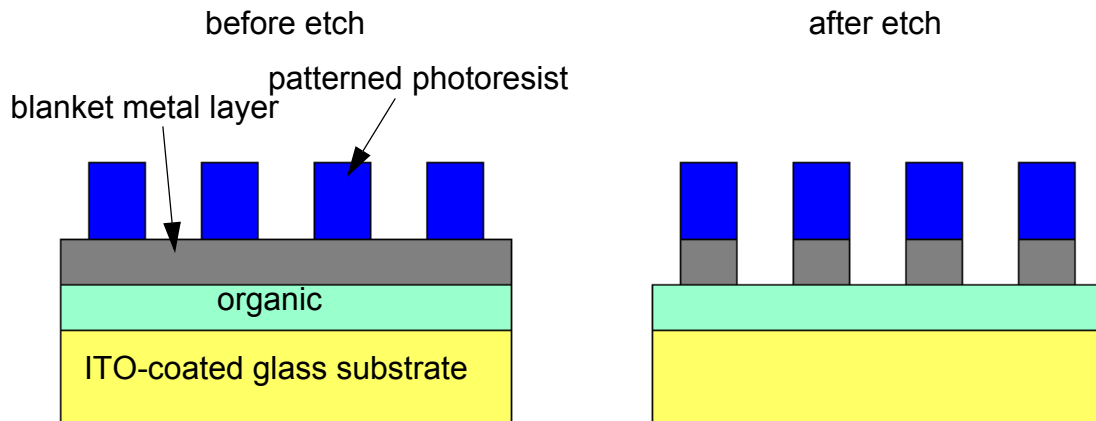


**Figure 7-4.** Patterning of metal cathodes by dry etching of a blanket metal film.

silver compounds. Aluminum by itself is not a very useful cathode for OLEDs due to its relatively high work function. At the same time, it is attractive because of its stability in air. Some efficient devices using aluminum as cathode material have been reported [8][9][10]. Further, it has been demonstrated that highly efficient OLEDs can be obtained with aluminum-lithium cathodes [11][12][13][14], where only a small amount of lithium is needed. Most significant in the context of cathode patterning, aluminum can be easily dry-etched using a chlorine plasma. Therefore, we focused on the dry etching of narrow aluminum lines. The aluminum cathode was thermally evaporated forming a blanket layer with a thickness of 1000 Å.

### 7.1.1 Device Fabrication

Before the actual etching process, the photoresist AZ 4210 was deposited at 4000 rpm onto the cathode layer and subsequently patterned. After a pre-bake for 10 min at 90 °C, the sample was exposed to UV light through a mask with the desired pattern and subsequently developed for 30 sec in AZ351 (1:5 in DI water). During the development process, the aluminum film initially blistered off the organic film. Small pinholes in the Al film and the exposed edges of the sample allowed that water came into contact with the organic film, which resulted in observed blisters. Figure 7-5 shows the damage to the OLED.

To avoid any contact of the organic with the developer, we devised the following device structure: After the aluminum film was deposited (800 Å) in the center region of the substrate (leaving the edge region uncovered), the organic at the edge of the sample was

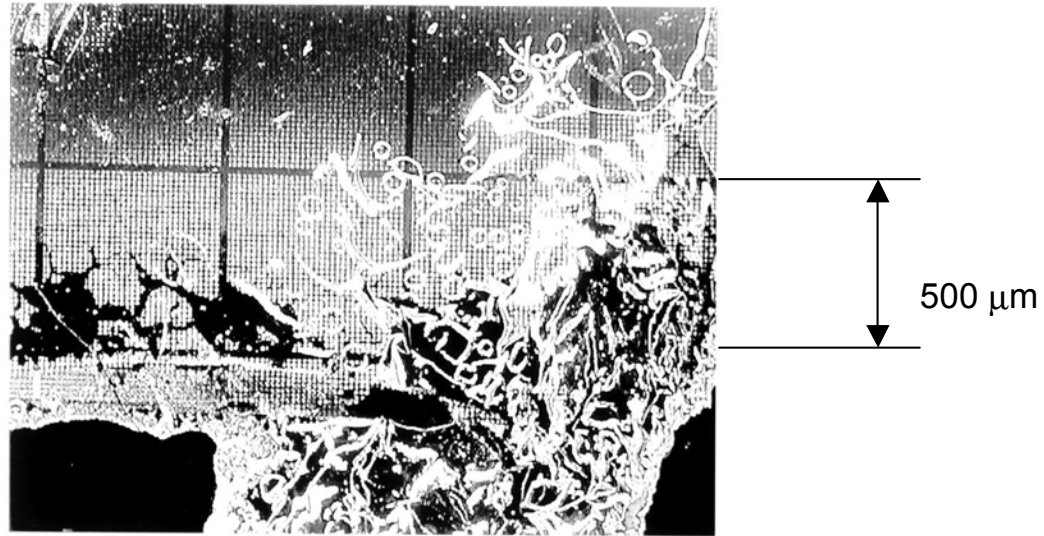


**Figure 7-5.** Damage to the aluminum film after photoresist development when only a single aluminum layer was deposited. The small features ( $<100\ \mu\text{m}$ ) are the desired photoresist patterns.

removed using a swab soaked in chloroform. A second aluminum deposition ( $1500\ \text{\AA}$ ) was carried out to completely cover the organic layer. In addition to covering the edges of the organic film, the number of pinholes in the aluminum film was drastically decreased. The resulting structure is shown in Figure 7-6. No blistering occurred during photoresist development using this device structure. The patterned device was then transferred into a parallel plate plasma etching chamber for further processing. A mixture of chlorine and boron-trichloride ( $\text{Cl}_2$  and  $\text{BCl}_3$ ) in a carrier gas is conventionally used to plasma etch Al [15].  $\text{BCl}_3$  enables the etching of aluminum oxide ( $\text{Al}_2\text{O}_3$ ) and also reduces the re-deposition of the non-volatile etching product  $\text{AlCl}_3$  [16]. However, it also slows down the etching process. Using a mixture of 1:2 ( $\text{Cl}_2:\text{BCl}_3$ ), no re-deposition occurred and the etch rate was sufficiently high (about  $75\ \text{\AA}/\text{min}$ ). Good etching results for a  $2200\ \text{\AA}$  thick Al film were obtained with argon as the carrier gas (flow rate: 200 sccm) and  $\text{Cl}_2$  and  $\text{BCl}_3$  (with flow rates 10 sccm and 20 sccm, respectively) as the etchants at a chamber pressure of 200 mtorr and a plasma power density of  $0.27\ \text{W}/\text{cm}^2$ .

The photoresist was not removed after the dry-etching of the cathode metal. Electrical connections were made by probing through the photoresist layer.

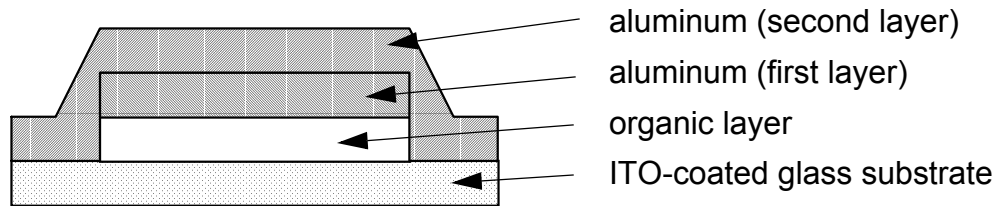


**Figure 7-6.** Device structure to avoid blistering of the aluminum film due to contact with water during the lithography process, and to reduce aluminum pinholes. [17]

### 7.1.2 Device Characterization

Figure 7-7 shows etched cathode lines with a width of  $20\ \mu\text{m}$ . Perpendicular to

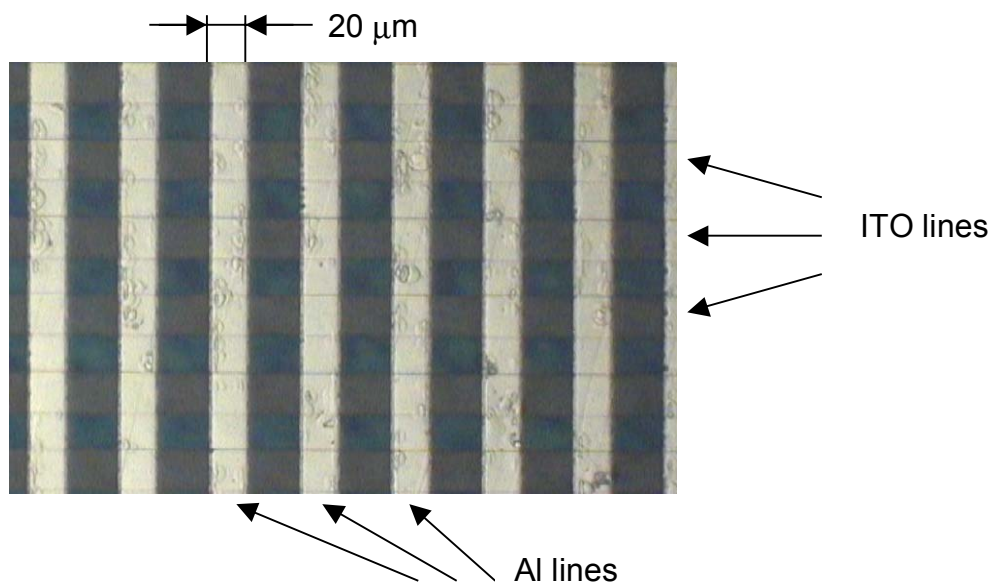


**Figure 7-7.** Micrograph of a sample with Al cathode lines fabricated with plasma etching. The width of the ITO lines and the Al lines is  $20\ \mu\text{m}$ . Note some damage to the photoresist (on top of the cathode) from metal etching can be seen. [17]

these lines run  $20\ \mu\text{m}$  ITO lines in a passive matrix pattern. Individual OLEDs are formed where the ITO lines and cathode lines intersect. However, none of these devices emitted light.

To investigate the reason for this device failure, we fabricated devices by the same procedure as above, except that the ITO and the aluminum cathode size were increased. Figure 7-8 shows electroluminescence micrographs of devices with equal ITO and aluminum line widths of  $1000\ \mu\text{m}$ ,  $500\ \mu\text{m}$ ,  $200\ \mu\text{m}$ . The emitting area of the device is smaller

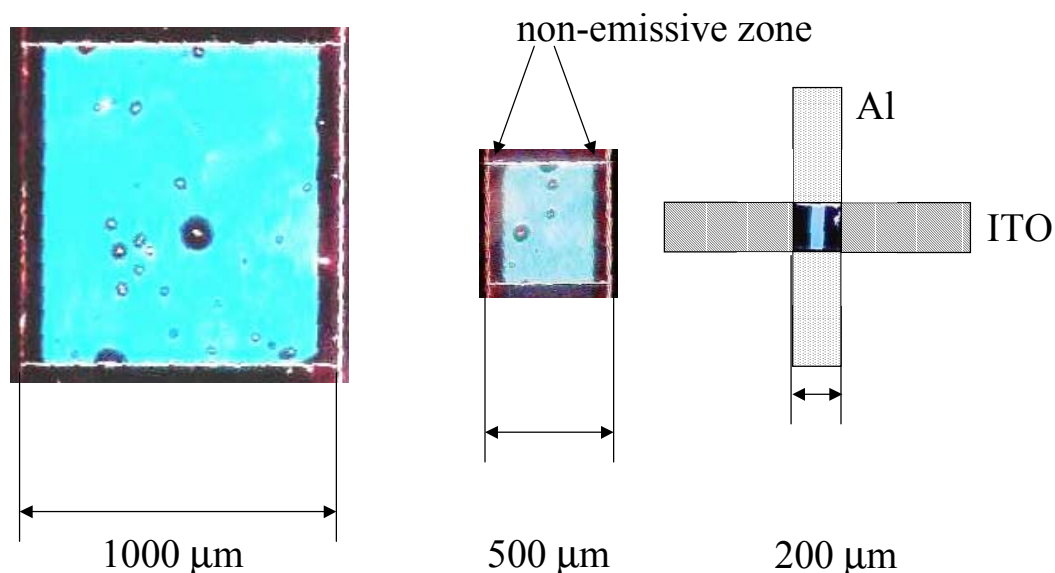


**Figure 7-8.** Electroluminescent micrograph of devices of different sizes fabricated with plasma etching of the cathodes. The ITO lines run horizontally, the aluminum lines vertically. Note the non-emissive zone in all samples along the edge of the aluminum line. The devices were exposed to air for approximately 4 hours. [17]

than the total device area due to a non-emissive region along the edge of the aluminum line. The width of this region is about  $65 \mu\text{m}$  ( $\pm 5 \mu\text{m}$ ), and is the same for all devices independent of feature size. Therefore, devices smaller than  $130 \mu\text{m}$  will not emit any light, because the device area is completely consumed by the non-emissive region. We also fabricated devices with a line width of  $100 \mu\text{m}$ , which, in accordance with this observation, did not emit any light. These devices were tested after they were exposed to air for approximately 4 hours. Figure 7-9 shows the IV curve of these devices along with the photocurrent measured in a nearby detector. The  $1000 \mu\text{m}$  device (squares) has an external quantum efficiency of about 0.14%. The external quantum efficiency of the  $500 \mu\text{m}$  device (circles) is about 0.12%, and that of the  $200 \mu\text{m}$  device (triangles) is about 0.11%. Thus the quantum efficiency does not vary much with the emitting area. Hence, little current flows in the non-emissive zone implying it has a much higher resistivity than the emissive area.

These non-emissive regions could be caused by damage to the organic layer during the etching process, especially during any "overetch" after the metal is etched away. One might imagine a reaction of chlorine radicals with the oxadiazole groups of the PVK during the etching process. Alternatively, the degradation mechanism could be similar to that of

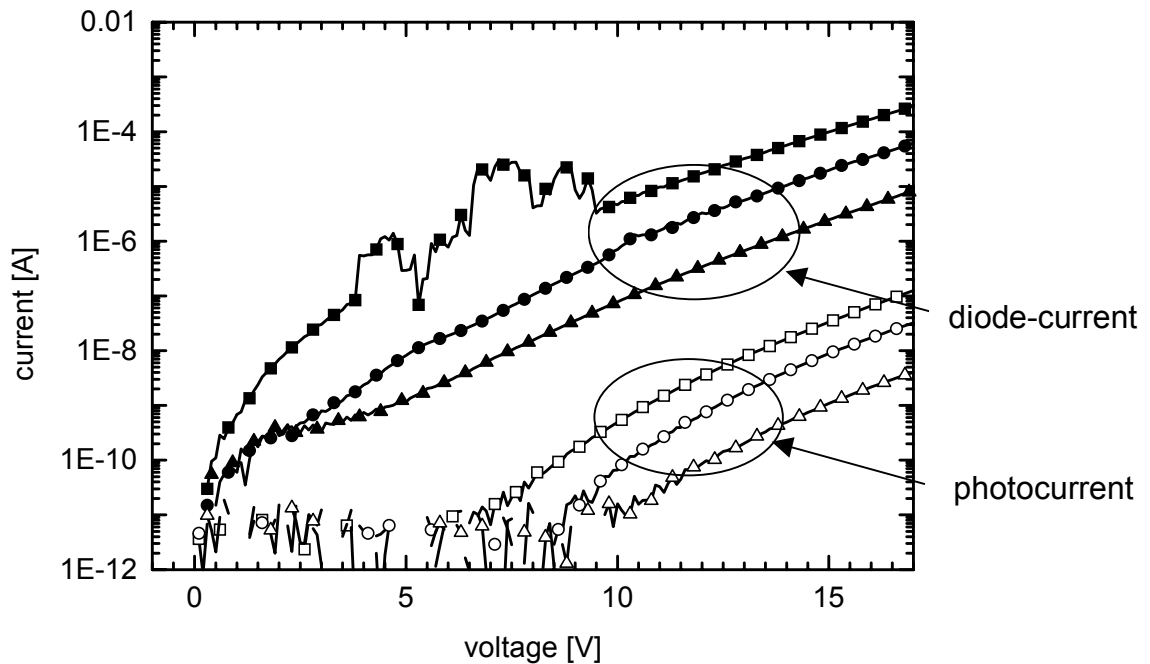


**Figure 7-9.** Current-voltage characteristics and photo current of OLEDs with plasma etched cathode: 1000  $\mu\text{m}$  device (squares), 500  $\mu\text{m}$  device (circles), and 200  $\mu\text{m}$  (triangles). The devices were exposed to air for approximately 4 hours. [17]

conventional "dark spots", i.e. degradation of the device by exposure to air/water vapor through a pinhole in the cathode. Note that the ambient can attack the OLED through the entire edge of the patterned cathode. To discern between these two mechanisms, we then compared the growth of the non-emissive zone ( $\Delta L$  in Figure 7-10) in the dry-etched device and in those with aluminum cathodes patterned by evaporation through a conventional shadow mask<sup>1</sup>. Both sets of devices had an aluminum cathode (3000 Å). The growth of dark spots in the two cases was determined by observing the devices during electroluminescence as a function of their exposure to air. No significant difference in growth rate can be inferred. Therefore, we conclude, that the damage to the organic film caused by the plasma treatment is negligible compared to the damage due to exposure to air.

To investigate the growth of the non-emissive region and its dependency on the cathode metal used and the environment, we fabricated devices with a) a 2000 Å thick aluminum cathode and b) with a Mg:Ag (10:1, 1200 Å), followed by Al (2100 Å) cathode. The cathodes were patterned by evaporation through a shadow mask. After the cathode deposi-

1. The growth rate of the non-emissive zone in different environments was analyzed by Min-Hao Lu.

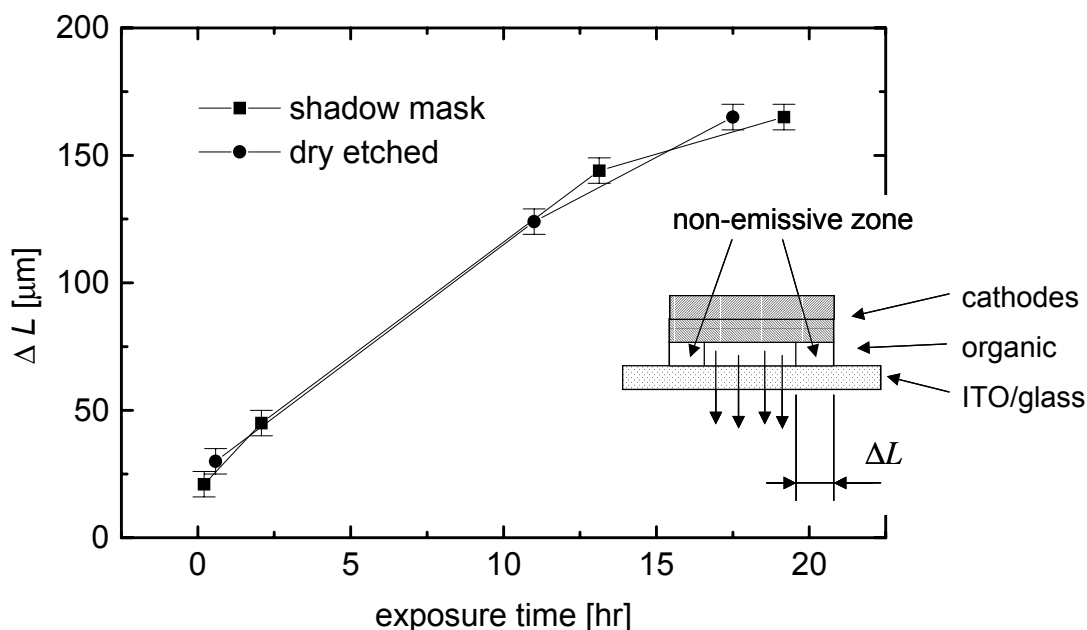


**Figure 7-10.** Growth of the non-emissive zone with time in air after (a) aluminum cathode (300 nm) patterning with plasma etching (circles), and (b) patterned cathode formation by aluminum evaporation through a shadow mask (squares).  $\Delta L$  is the width of the non-emissive zone (inset). [17]

tion, one of the samples with the pure aluminum cathode was exposed to a oxygen plasma for 4 min (oxygen flow 25 sccm, chamber pressure 100 mTorr, plasma power density  $0.22 \text{ W/cm}^2$ ) and another one to a chlorine plasma for 4 min (chlorine flow 20 sccm, argon flow 100 sccm, chamber pressure 150 mTorr, plasma power density  $0.11 \text{ W/cm}^2$ ). One sample was left untreated. As shown in Figure 7-11, no significant difference between these samples can be seen, again showing the edge effects are not related to plasma treatment. A sample with Mg:Ag/Al cathode was exposed to oxygen plasma for 4 min, whereas one sample did not undergo any plasma treatment. Similarly, these two Mg:Ag/Al samples show no significant change in the growth rate of the non-emissive region. The growth rate is substantially larger for the device with an Al cathode than for a Mg:Ag/Al cathode, even though these all devices were kept under the same storage conditions. This suggests that the formation of the non-emissive zone is related to a reaction at the organic-cathode interface, as opposed to the organic layer itself. The same conclusion was previously reported for the formation of dark spots [18][19][20].

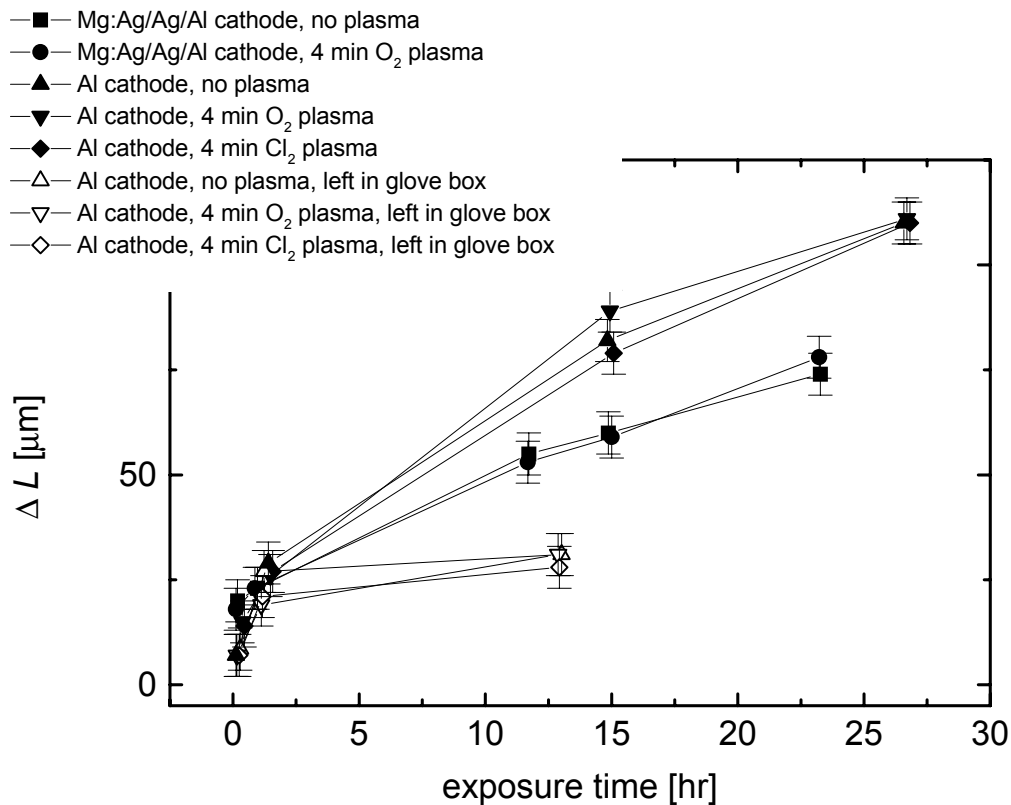


**Figure 7-11.** Growth of the non-emissive zone vs. exposure time to air for cathodes of different material and processing steps after cathode deposition. All cathodes were deposited using a shadow mask. [21]

Figure 7-12 shows electroluminescence micrographs of the same sample with a Mg:Ag/Al cathode which was exposed to oxygen plasma for 4 min.

The growth rate of the non-emissive zone in devices with aluminum cathodes can be dramatically reduced when the samples are kept in a nitrogen atmosphere (dew point - 50 °C), stressing the need for device encapsulation. These devices were exposed to air for several minutes, however, due to the time required to transfer them from the evaporator to the glove box.

For all devices, the width of the non-emissive zone shows an approximate square root dependence on time suggesting that the reaction of the organic material is limited by the diffusion of a reactant from the device edge.

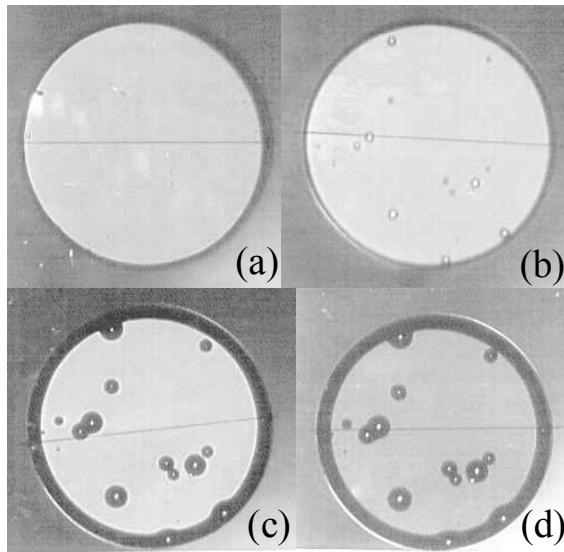


**Figure 7-12.** Electroluminescence micrographs of devices with Mg:Ag/Al cathode exposed to oxygen plasma for 4 min. The width of the non-emissive zone was 20  $\mu\text{m}$  after 11 min exposure to air, 23  $\mu\text{m}$  after one hour, 55  $\mu\text{m}$  after 12 hours, and 60  $\mu\text{m}$  after 15 hours. [21]

In summary, fine line cathode patterning is indeed possible by dry-etching with photoresist on top of the metal cathode. But it is necessary to avoid exposure to oxygen and water vapor between the processing steps until the device is encapsulated.

## 7.2 Cathode Patterning by Transferred Photoresist

### 7.2.1 Device Fabrication

Adapting the idea of cathode separators to polymeric materials, we developed a technique to pattern the cathode by depositing a layer of patterned photoresist after the spin-on of the electroactive polymer. However, conventional photolithography on top of the emissive polymer film is in most cases not possible, because the contact with solvent, water or developer will degrade the electroluminescence properties of the film [7].

#### 7.2.1.1 Lamination of Pre-Patterned Photoresist

Using the same technique of transferring a pre-patterned photoresist film as for the dye transfer (see Chapter 6.1.4.2) onto the emissive layer, we were able to pattern the cathode layer without exposing the emissive layer to water or solvents. The process is shown in Figure 7-13. After the patterning of the Riston film by conventional photolithography,

the film is then laminated at high temperature at the emissive polymer film. The process temperature during the lamination had to be very high (180 °C) because the Riston did not stick well to the hydrophobic PVK film. If the feature sizes of the Riston were large (at least 2 mm<sup>2</sup>), the Riston film could be transferred to the PVK. Separate islands of Riston photoresist did usually not transfer. Figure 7-14 shows an EL-micrograph of a device fabricated with this technology where the width of the cathode is 120 μm.

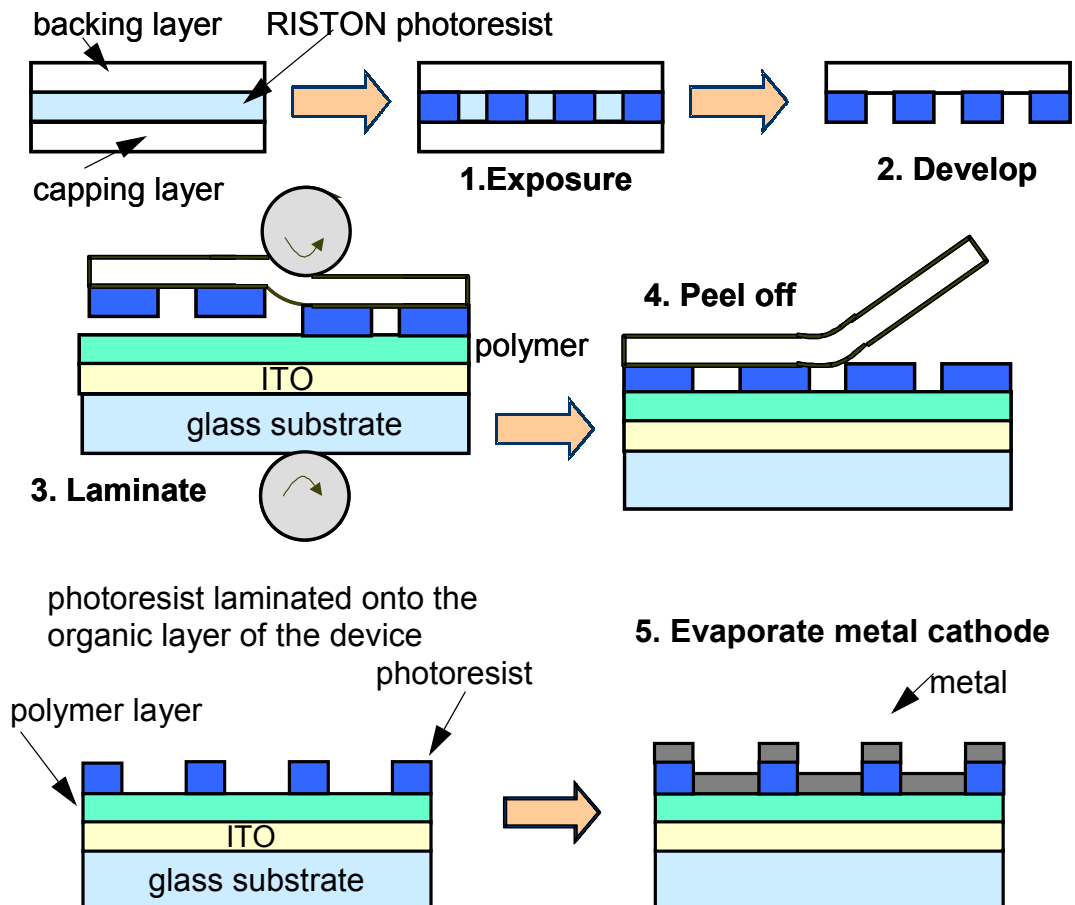


**Figure 7-13.** Schematic process to form cathode separators using transferred photoresist. [22]

### 7.2.1.2 Adhesion Promotion using conventional Adhesive

To improve the adhesion of the Riston film to the PVK layer of the device substrate, we tested different options. Exposing the Riston film to solvent vapor (acetone) prior to the lamination did indeed swell up the film and make it more sticky. But the yield of the lamination process did not improve, probably because the solvent evaporated too fast. Spraying an adhesive (“Super 77” or “Spray Mount”, both obtained from 3M) on the Riston foil

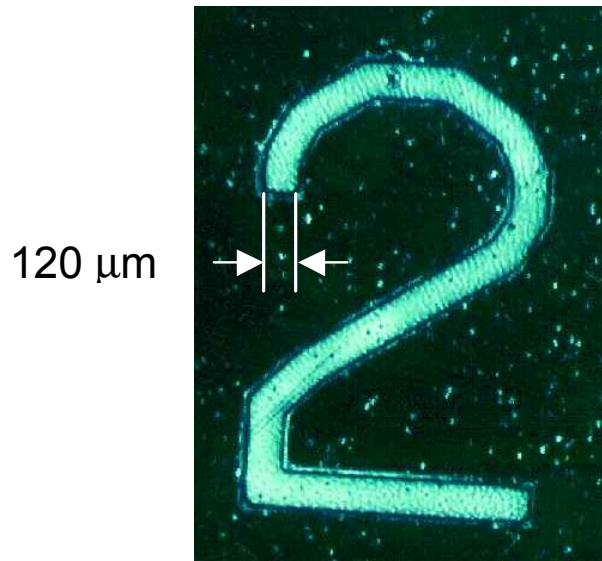


**Figure 7-14.** EL micrograph of an OLED feature fabricated using transferred photoresist. [22]

before laminating it promoted the adhesion substantially. However, the drops of the adhesive fog were too big and after lamination, some of the device area was still covered with adhesive as shown in Figure 7-15.

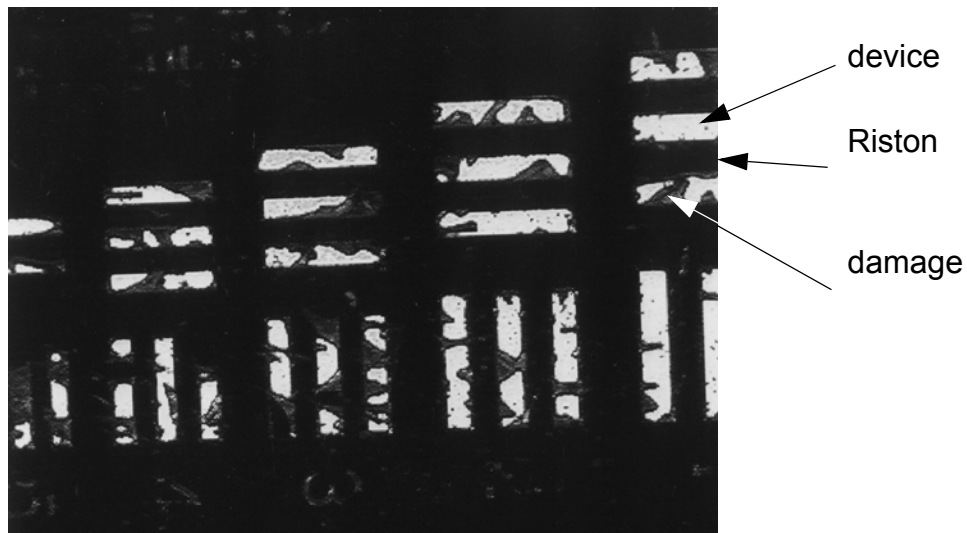


**Figure 7-15.** Device with damage due to spray-adhesive (device size 80 μm by 400 μm).

Dissolving the dried residue of the spray adhesive (“Spray Mount”) in cyclohexane yielded a opaque solution, which, when painted onto any surface, retained its adhesive properties even after the evaporation of the solvent. The painted film did not show any clus-

ters as did the film deposited by spray-coating. But we detected little islands of glue with a size of about 100  $\mu\text{m}$  after the solution was painted on the patterned Riston film with a brush and dried for 5 minutes in air. The film adhered well to the PVK layer when it was laminated at 150  $^{\circ}\text{C}$  onto the PVK film. However, it did not stick to the PVK film after it was laminated at room temperature. The resulting devices are shown in Figure 7-16. The

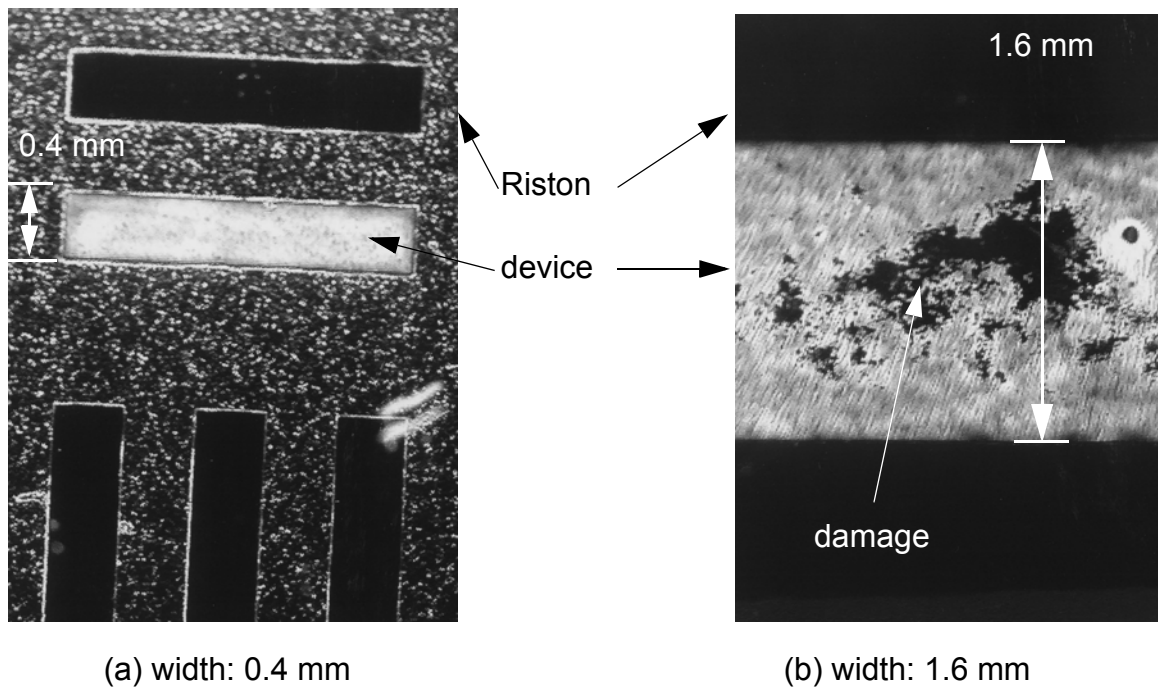


**Figure 7-16.** EL micrographs of devices with adhesion promotion layer painted onto the Riston film before the lamination process.

EL micrograph of a 400  $\mu\text{m}$  wide device does not show any damage due to adhesive contamination (Figure 7-16 a). But the device with a width of 1.6 mm showed significant damage due to contact with the adhesive (Figure 7-16 b). A schematic of the damaging process is shown in Figure 7-17. Both rubber rolls of the laminator are approximately 4 cm in diameter. Small openings in the Riston film protect the polymer film from being contaminated with the adhesive attached to the backing foil of the riston film. However, larger openings, due to the flexibility of the rubber roll and of the Riston backing foil allow the adhesive to be deposited on the device polymer film, resulting in non-emissive spots.

To avoid such undesired contact of the device polymer film with the adhesive, a glass slide placed in top of the device substrate with the Riston film sandwiched in between

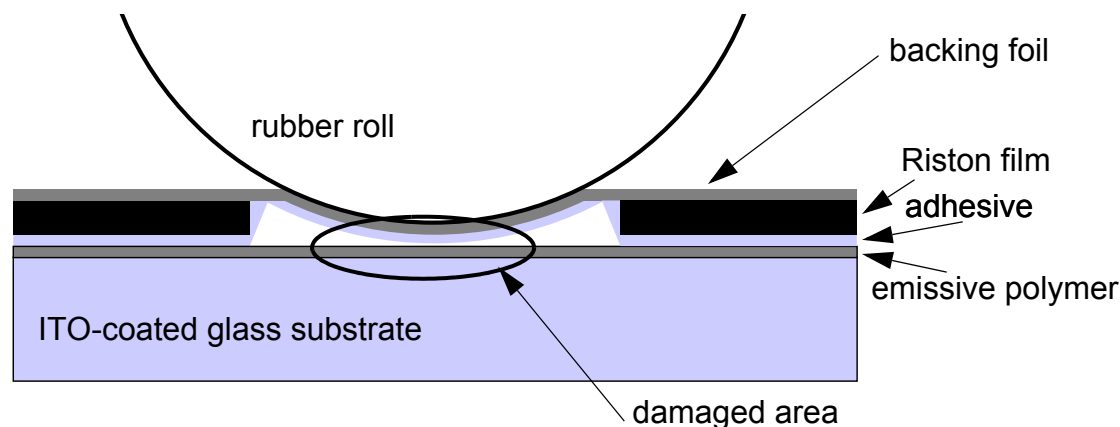


**Figure 7-17.** Contamination of the emissive polymer layer due to contact with adhesive deposited on the Riston film.

these substrate was used. Because of the stiffness of the glass slide, the Riston film did not conform to the curvature of the rubber roll and the polymer film did not show any contamination. However, the process temperature had to be significantly raised to 190 °C. Devices fabricated at this temperature demonstrated a decreased external quantum efficiency.

In addition to the spay-adhesive, we also used a copolymer containing carbazole and carboxyl groups (provided by Prof. Schwartz, Chemistry Department, Princeton University) to promote the adhesion between the PVK layer and the Riston film. Because the PVK is very hydrophobic and the Riston film hydrophilic, a interlayer made up of a polymer with both hydrophilic and hydrophobic sidegroups would be a good choice to improve the adhesion of both layers. Initial experiments, however, did not show any improvement.

### 7.2.1.3 Adhesion Promotion using a Thin Metal Layer

Riston adheres exceedingly well to metals, and evaporated metal film adhere to PVK. The good adhesion to metal was also the reason for the most successful approach of adhesion promotion of the Riston layer to the emissive polymer film. After the evaporation of a very thin layer of silver or aluminum as a blanket on the device polymer film, the Riston film was laminated onto the device at fairly low process temperatures (room temperature up to 100 °C). The adhesion to the polymer film was greatly enhanced by the thin metal film. The fabrication process is pictured in Figure 7-18. To avoid lateral conduction (which would lead to a conduction between the devices), we determined the optimal thickness of the metal film to be 40 Å. For a metal film of 10 Å, the adhesion is not much

increased compared to a device with no metal layer deposited. Lateral conduction was observed after a blanket layer of around 80 Å to 150 Å was evaporated. Because the metal probably forms islands on the polymer surface during the evaporation, the film is discontinuous for low thicknesses. When a thick layer of metal is deposited, these islands grow together and form a continuous and thus a conductive layer. The optimal process temperature for the lamination process was about 85 °C. At this temperature, the backing film could easily be removed and the device was not exposed to a harsh heat treatment. After the Riston film was laminated onto the substrate, a thick cathode metal film of Mg:Ag (1000 Å) was deposited.

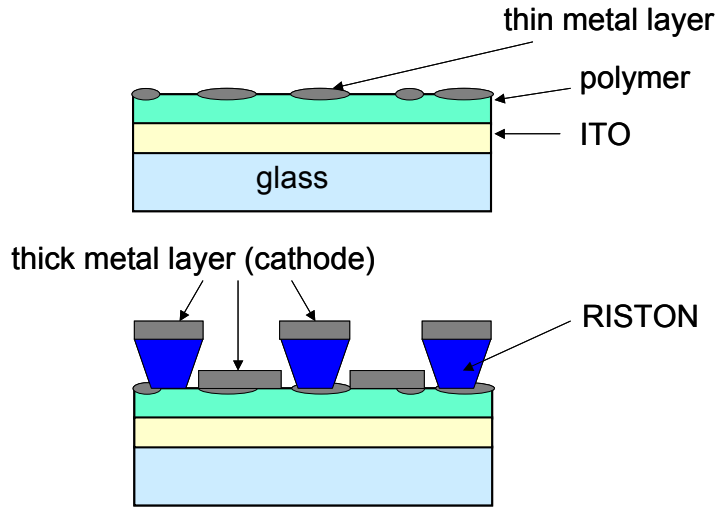


**Figure 7-18.** Adhesion promotion using a very blanket thin metal layer deposited before the lamination of the Riston photoresist. A thick cathode metal film is evaporated after the Riston layer is deposited.

Figure 7-19 show a EL micrographs of a device fabricated with this method at different magnifications. The devices are 10 mm long and 300 μm wide. The Riston stripe between the devices is 50 μm wide. A 40 Å thin silver film was deposited as a blanket film before the Riston film was laminated at 85 °C. A standard cathode was subsequently deposited (500 Å of Mg:Ag (10:1) followed by 500 Å Ag). Because the metal layer did not conduct laterally, all devices could be addressed separately and no cross-talk was observed.

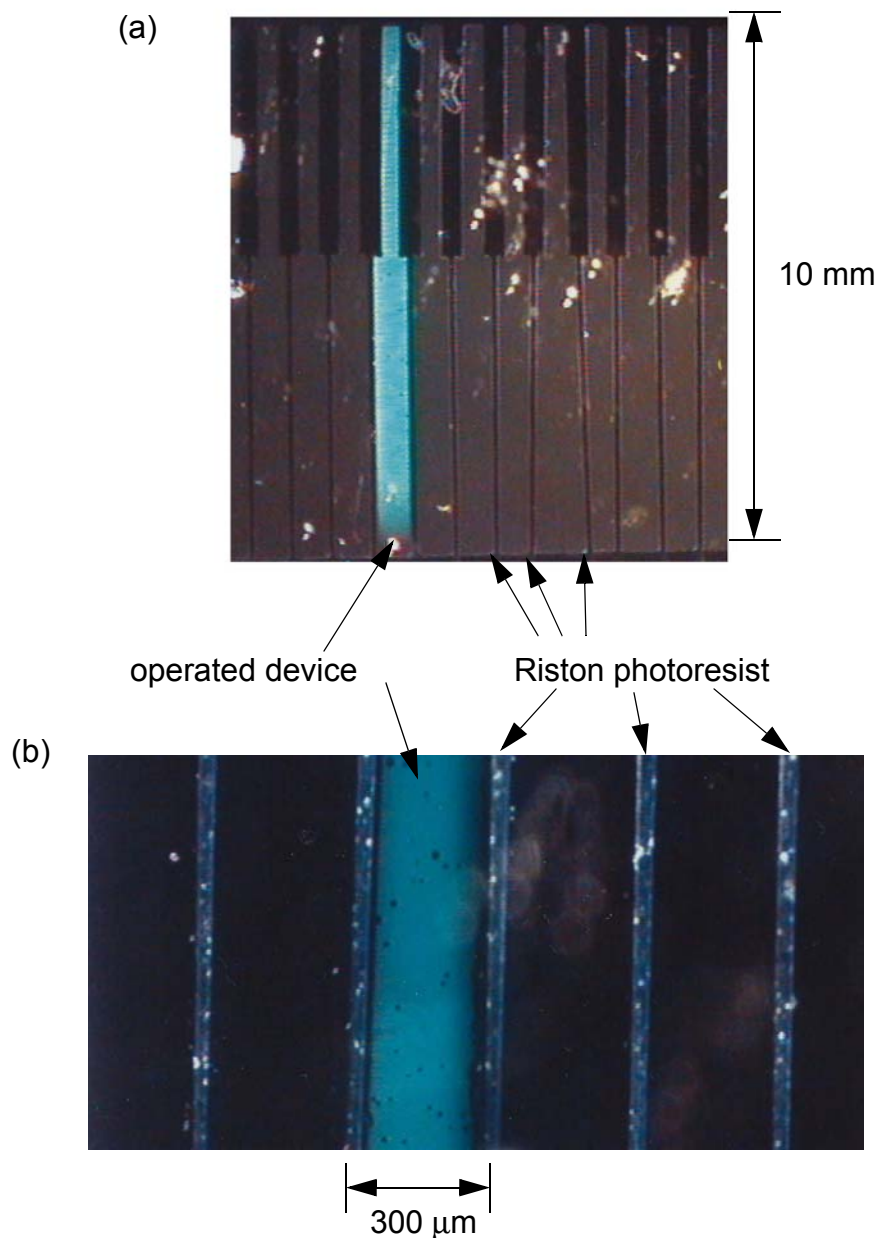


**Figure 7-19.** EL micrographs of device patterned with transferred Riston photoresist. A thin blanket silver film was deposited before the lamination process to promote the adhesion of the Riston film. Picture (b) is the fivefold magnified version of (a).

#### 7.2.1.4 Cathode Metal Lift-off

The good adhesion of the Riston film to metal was mentioned earlier (see Chapter 6.2.3). The idea of this technique was to use this property of the Riston film to lift off the cathode metal. After standard PVK/PBD/C6 devices were fabricated with a blanket 500 Å thick Mg:Ag (10:1) layer with a 500 Å thick Ag capping layer as cathode, we lami-

nated a pre-patterned Riston film on at 100 °C. In this case, the Riston film adhered very well to the cathode, and the backing layer could easily removed as pictured in Figure 7-20..

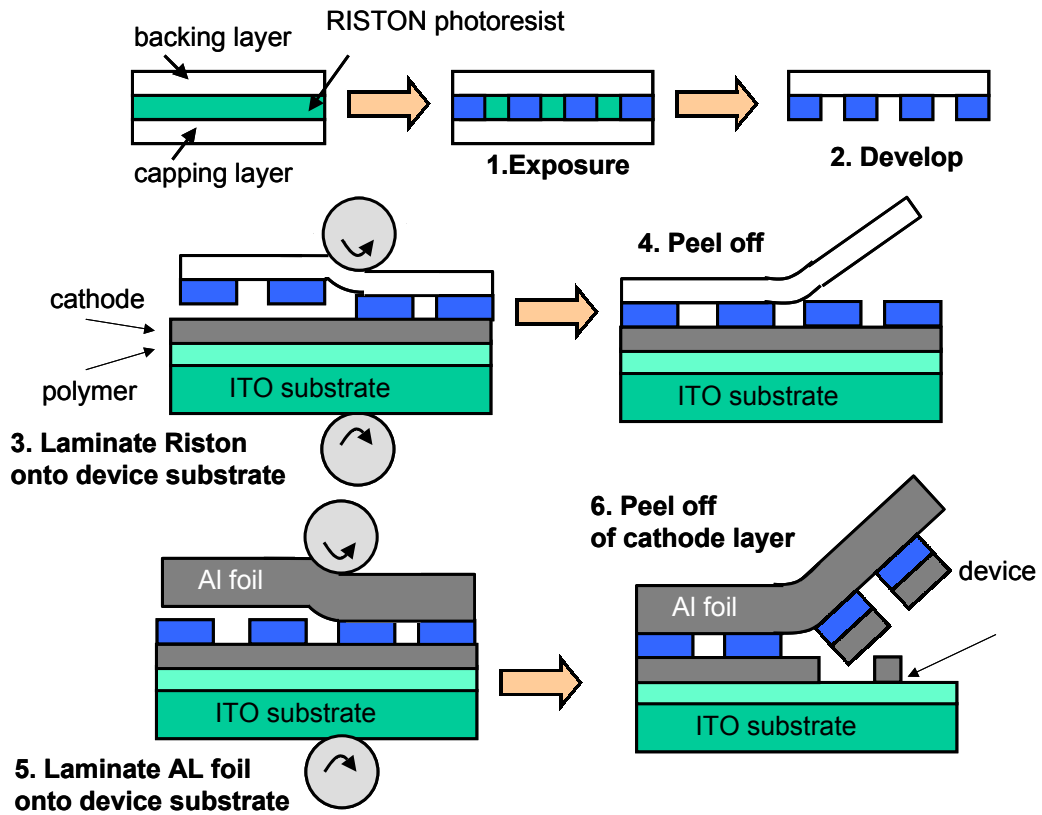


**Figure 7-20.** Cathode patterning by cathode metal lift off.

No additional adhesion promotion was necessary. A cleaned aluminum foil was then laminated on top of the Riston film at 100 °C, which adhered also very well. By removing the aluminum foil, we hoped to remove the cathode metal at places where the Riston film glued the two metal layers together and thus patterning this layer. Disappointingly, only a very small portion of the device area did come off and most of the Riston film remained on the cathode metal. In addition, even there where the cathode metal was removed, the cathode layer showed very rough edges as shown in Figure 7-21.

### 7.2.2 Lateral Conduction due to Transferred Photoresist

After the Riston photoresist was laminated onto the device substrate by any of the aforementioned methods and a metal cathode was deposited by thermal evaporation, we

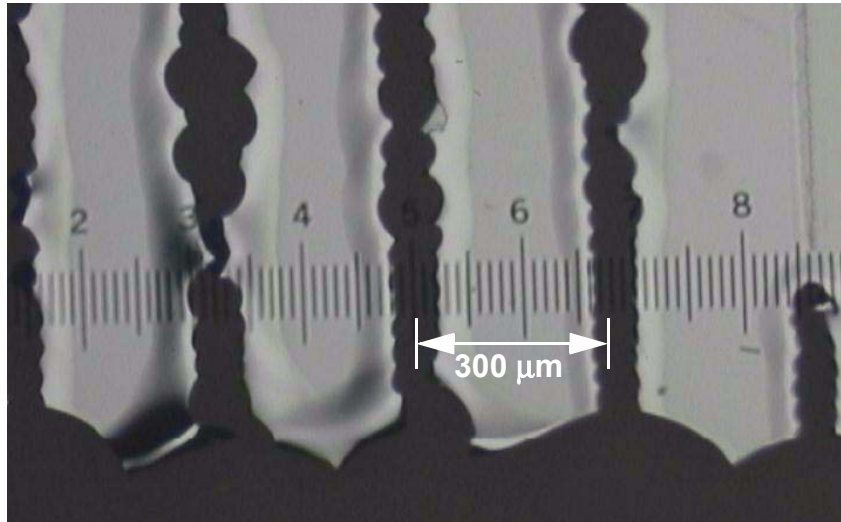


**Figure 7-21.** Micrograph of a cathode metal layer after lift-off process.

often observed conduction between random devices on the substrate, although the cathodes of these devices were supposed to be islands and thus not connected to each other.

To investigate this failure, we performed scanning electron microscopy (SEM) on a section of a laminated film on a PVK/PBD ITO/glass substrate. The micrograph of a section of 20  $\mu\text{m}$  wide lines with a 40  $\mu\text{m}$  pitch is shown in Figure 7-22(a). The wedge-like section of the Riston film is very advantageous because it ensures that no electrical conduction between separated devices is possible due to the anisotropic metal deposition as depicted Figure 7-22(b).

This observation can not clearly explain why some devices were connected, as the retrograde slope of the Riston features (schematically shown in Figure 7-22 b) should insulate the cathodes from one another. SEM analyses of a device with laminated Riston film from the top revealed that the Riston film was not cleanly removed at the edges of the openings and some thin remnants remained after the development process as shown in the micrograph in Figure 7-23. These protruding Riston pieces made contact to the cathode layer of the actual device (see schematic in Figure 7-24).

To remove these thin Riston features, we used an oxygen plasma after the patterning of the photoresist but before the transfer by lamination. The following process parameters were used: oxygen flow: 25 sccm, plasma power: 75 W, chamber pressure: 150 mTorr, process time: 4 min. The Riston film was transferred into the parallel plate reactor (10" diam-

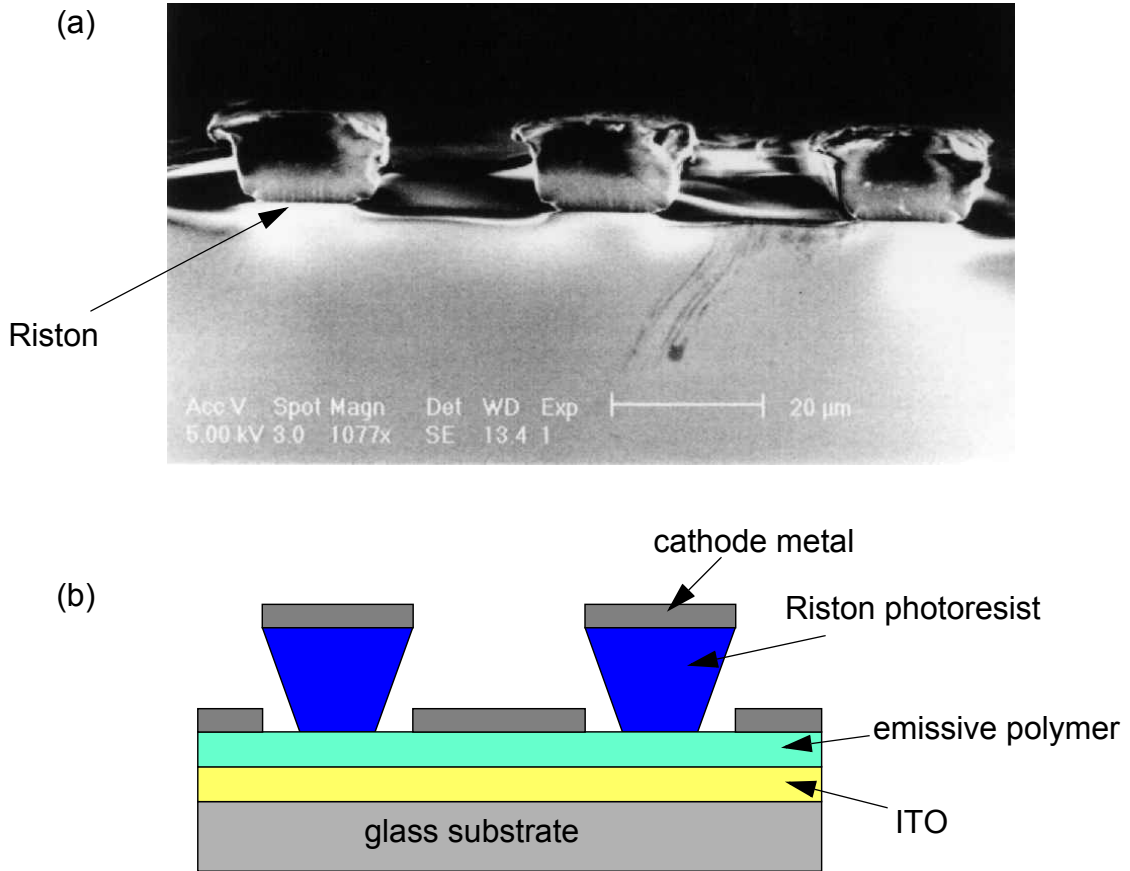
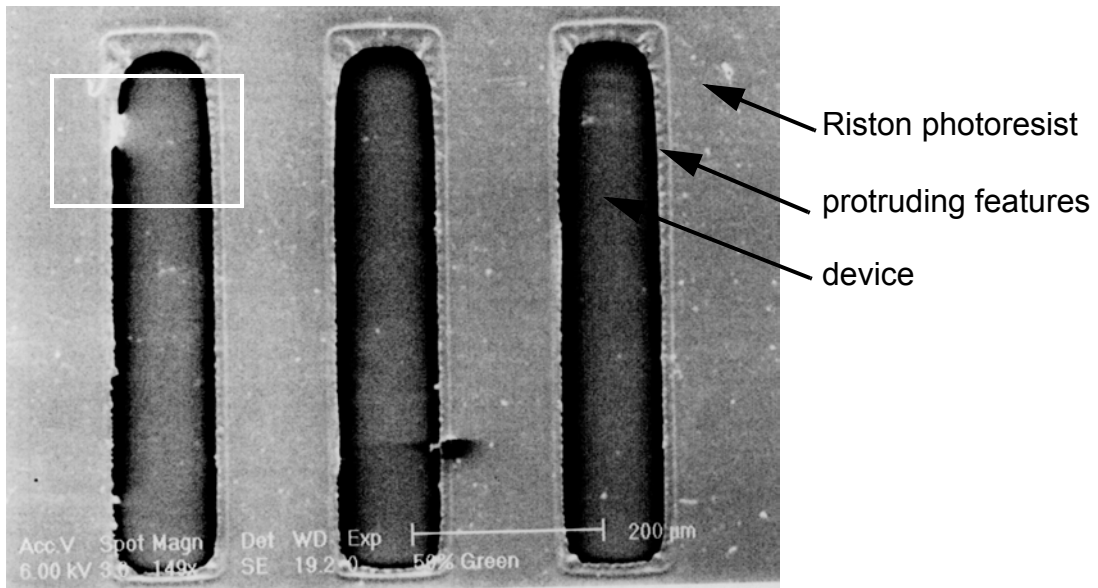


**Figure 7-22.** (a) SEM micrograph of section of a Riston photoresist laminated onto a PVK/PBD coated ITO/glass substrate; (b) insulation of separated devices due to the wedge-like structure of the photoresist.

eter) after development and drying when it was still attached to the backing foil. The film was held down on the electrode plate in the chamber with two glass slides at the edge of the Riston film. After the oxygen plasma etch, the Riston film was laminated onto the device substrate. The oxygen plasma treatment significantly reduced the number of connected devices.

### 7.3 Summary

In this chapter we showed that cathode patterning by photolithography and dry etching is a viable technology. It was demonstrated that the observed damage to the device (non-emissive zones at the edge of the cathode) are due to the exposure to air rather than due to the etching process.



magnified detail

electrical contact  
to cathode layer

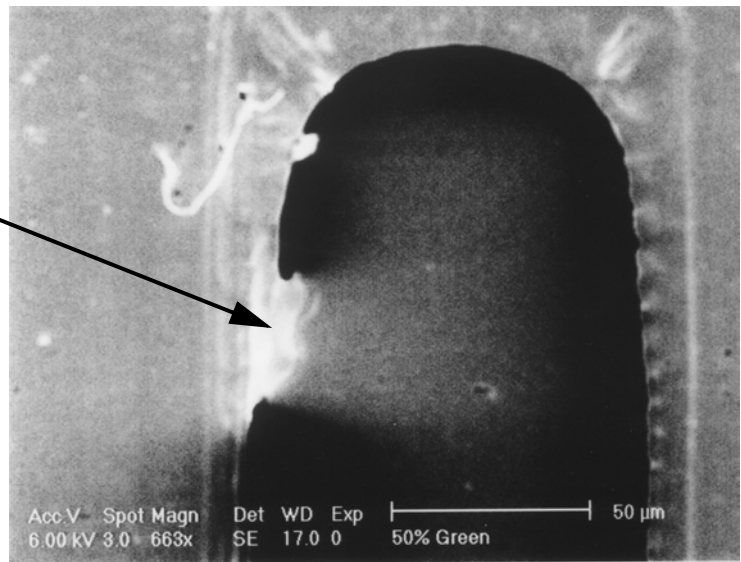


**Figure 7-23.** SEM micrograph of a device with laminated Riston film. The edges of the film show thin protruding features.

In addition, a transferred photoresist has been shown to work as a cathode separator during the deposition of the metal cathode. This method minimizes any contact of the polymer layer by patterning the photoresist previous to the transfer step.

Further work is needed to improve the reliability of these techniques.

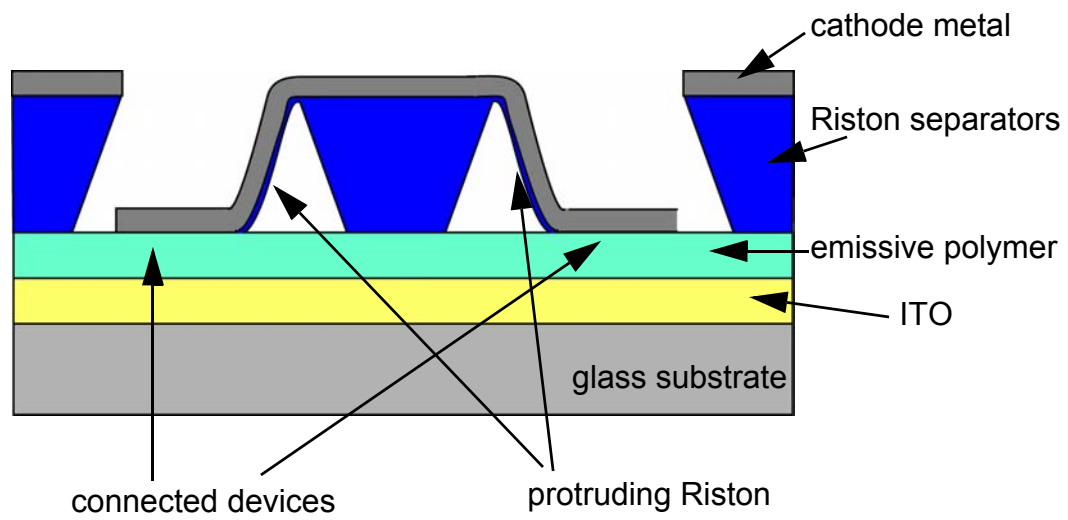


**Figure 7-24.** Schematic of connected devices due to protruding Riston film.

## 7.4 References

- [1] H. Aziz, Z. Popovic, C. P. Tripp, N.-X. Hu, A.-M. Hor, and G. Xu, “Degradation processes at the cathode/organic interface in organic light emitting devices with Ag:Mg cathodes”, *Appl. Phys. Lett.* **72** (21), 2642 (1998).
- [2] H. Aziz, Z. Popovic, S. Xie, A.-M. Hor, N.-X. Hu, C. Tripp, and G. Xu, “Humidity-induced crystallization of tris (8-hydroxyquinoline) aluminum layers in organic light-emitting devices”, *Appl. Phys. Lett.* **72** (7), 756 (1998).
- [3] P. E. Burrows, V. Bulovic, S. R. Forrest, L. S. Sapochak, D. M. McCarty, and M. E. Thompson, “Reliability and degradation of organic light emitting devices”, *Appl. Phys. Lett.* **65** (23), 2922 (1994).
- [4] V. N. Savvateev, A. V. Yakimov, D. Davidov, R. M. Pogreb, R. Neumann, and Y. Avny, “Degradation of nonencapsulated polymer-based light-emitting diodes: Noise and morphology”, *Appl. Phys. Lett.* **71** (23), 3344 (1997).
- [5] C. Py, M. D'Iorio, Y. Tao, J. Stapledon, and P. Marshall, “A passive matrix addressed organic electroluminescent display using a stack of insulators as row separators”, *Syn. Met.* **113**, 155 (2000).
- [6] P. F. Tian, P. E. Burrows, and S. R. Forrest, “Photolithographic patterning of vacuum-deposited organic light emitting devices”, *Appl. Phys. Lett.* **71** (22), 3197 (1997).
- [7] D. G. Lidzey, M. A. Pate, M. S. Weaver, T. A. Fisher, and D. D. C. Bradley, “Photo-processed and micropatterned conjugated polymer LEDs”, *Synth. Met.* **82**, 141 (1996).
- [8] Y. Cao, G. Yu, and A. J. Heeger, “Efficient, Low Operating Voltage Polymer Light-Emitting Diodes with Aluminum as the Cathode Material”, *Synth. Met.* **102**, 881 (1999).
- [9] J. Huang, Z. Xie, K. Yang, C. Li, S. Liu, Y. Li, Y. Wang, and J. Shen, “Highly efficient and bright doped organic electroluminescent diodes using an aluminum cathode”, *Optical and Quantum Electronics* **31**, 1227 (1999).
- [10] Y. He and J. Kanicki, “High-efficiency organic polymer light-emitting heterostructure devices on flexible plastic substrates”, *Appl. Phys. Lett.* **76** (6), 661 (2000).

- [11] E. I. Haskal, A. Curioni, P. F. Seidler, and W. Anderoni, "Lithium-aluminum contacts for organic light-emitting devices", *Appl. Phys. Lett.* **71** (9), 1151 (1997).
- [12] G. E. Jabbour, Y. Kawabe, S. E. Shaheen, J. F. Wang, M. M. Morrell, B. Kippelen, and N. Peyghambarian, "Highly efficient and bright organic electroluminescent devices with an aluminum cathode", *Appl. Phys. Lett.* **71** (13), 1762 (1997).
- [13] G. E. Jabbour, B. Kippelen, N. R. Armstrong, and N. Peyghambarian, "Aluminum based cathode structure for enhanced electron injection in electroluminescent organic devices", *Appl. Phys. Lett.* **73** (9), 1185 (1998).
- [14] X. Yang, Y. Mo, W. Yang, G. Yu, and Y. Cao, "Efficient polymer light emitting diodes with metal fluoride/Al cathodes", *Appl. Phys. Lett.* **79** (5), 563 (2001).
- [15] A. J. v. Roosmalen, *Dry etching for VLSI* (Plenum Press, New York, 1991).
- [16] S. Bradley, C.-H. Chen, and G. Kovall, "High density plasma etching of aluminum alloys," Eighth International IEEE VLSI Multilevel Interconnection Conference, Santa Clara, CA, USA (1991).
- [17] F. Pschenitzka, M.-H. Lu, and J. C. Sturm "Patterning of OLED Cathodes by Metal Dry Etching" Digest of Technical Papers, *Int Symp Soc Inf Disp*, 731 (2001).
- [18] J. McElvain, H. Antoniadis, M. R. Hueschen, J. N. Miller, D. M. Roitman, J. R. Sheats, and R. L. Moon, "Formation and growth of black spots in organic light-emitting diodes", *J. Appl. Phys.* **80** (10), 6002 (1996).
- [19] Y.-F. Liew, H. Aziz, N.-X. Hu, H. S.-O. Chan, G. Xu, and Z. Popovic, "Investigation of the sites of dark spots in organic light-emitting devices", *Appl. Phys. Lett.* **77** (17), 2650 (2000).
- [20] S. F. Lim, L. Ke, W. Wang, and S. J. Chua, "Correlation between dark spot growth and pinhole size in organic light-emitting diodes", *Appl. Phys. Lett.* **78** (15), 2116 (2001).
- [21] Min-Hao Lu, PhD Thesis, Princeton University (2001).
- [22] F. Pschenitzka and J. C. Sturm, "Patterned dye diffusion using transferred photoresist for polymer OLED displays", *Proceedings of SPIE - The International Society for Optical Engineering* **4105**, 59 (2001).

# 8 Summary and Future Work

In summary, this work demonstrates the fabrication process of three-color polymer devices using the dye transfer technique to obtain the different emission colors. Several aspects of the dye transfer have been investigated. The initial dye transfer from a large-area dye source using a shadow mask or a patterned dye source is a novel approach to patterning of OLEDs. To obtain efficient devices, the devices had to be annealed. A suitable method of annealing the device in a solvent vapor atmosphere has been introduced. In addition, two approaches to pattern the cathode metal layer have been demonstrated. In the first approach, we fabricated devices using dry-etching to pattern a blanket metal cathode. The second approach employed transferred photoresist to pattern the cathode film.

With all these methods on hand, we now proceed to the realization of RGB devices.

## 8.1 Realization of Integrated RGB Device using the Dye Transfer Technique

In general, for a polymer OLED display being able to emit red, green, and blue light (RGB), the three different dyes have to be transferred into the polymer film. This can be achieved by three subsequent diffusion processes. However, because only the dye with the longer wavelength will emit if two or more dyes are present (see Chapter 2.9), the blue dye can already be contained in the spin-on solution and only the red and the green dye have to be added by diffusion. The fabrication process is pictured in Figure 8-1.

An ITO-coated glass substrate was patterned by wet etch creating stripes with a width of 300  $\mu\text{m}$ . After oxygen plasma treatment of the substrate, a layer of PVK/PBD and C47 was spun on (100 mg PVK, 40 mg PBD, 0.3 mg C47 in 7 ml chlorobenzene, spun-on at 2000 rpm).

The dye substrates were glass slides with a polymer layer containing either C6 or Nile red. The polymer solution (100 mg Vylon in 10 ml chloroform) with 8% of the respec-

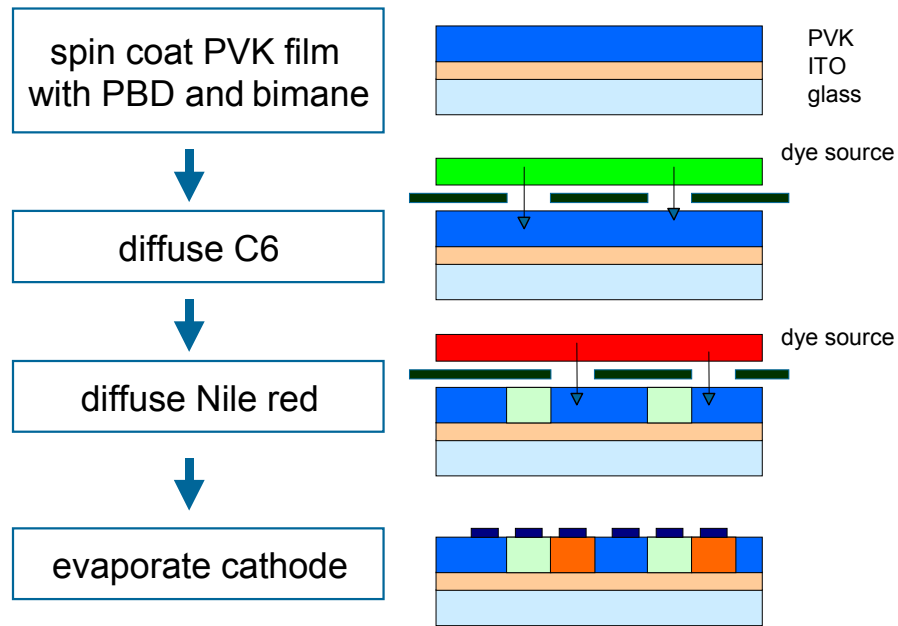


**Figure 8-1.** Dye diffusion process for an integrated RGB device [1].

tive dye was spun on at 4000 rpm. The patterned Riston layer was laminated onto the dye source and was then etched by oxygen plasma before the Riston layer was removed. The transferred dye pattern were 300  $\mu\text{m}$  wide stripes with a pitch of 900  $\mu\text{m}$ .

The dye transfer was carried out at 70  $^{\circ}\text{C}$  for 60 min in vacuum for each of the dyes. The PL images of the device are shown in Figure 8-2.

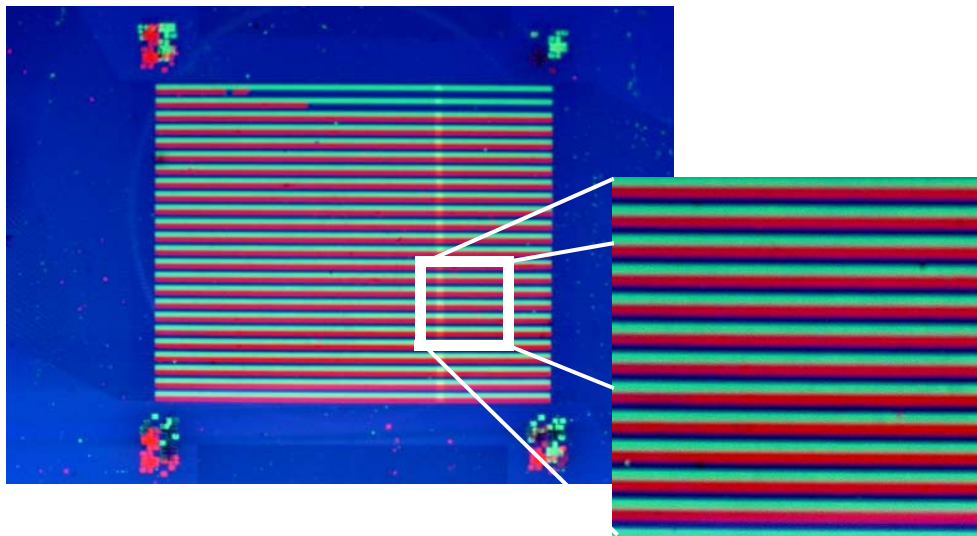


**Figure 8-2.** PL images of the device after the dye transfer (left side: entire device 78 mm x 78 mm, right side: magnified detail). [images courtesy of Ke Long]

After the two transfer steps, the sample was annealed at room temperature for 3 min in solvent vapor (130 ml gaseous acetone per liter nitrogen at 4 l/min).

Before the lamination of cathode separators, a 40 Å thin silver layer was thermally evaporated as blanket layer to enhance the adhesion of the pre-patterned Riston film on the emissive polymer layer. After the lamination a Mg:Ag (10:1) was deposited with a silver capping layer.

Figure 8-3 shows micrographs of the fabricated device.<sup>1</sup>The transferred dye is not perfectly aligned because a bit of the green and red color is “bleeding” into the blue sub-pixel. The external quantum efficiencies of this device were measured to be 0.22% for the green sub-pixel, 0.18% for the red one, and 0.08% for the blue one.

These results demonstrate the viable potential of the dye transfer technique for the fabrication of a passive matrix display.

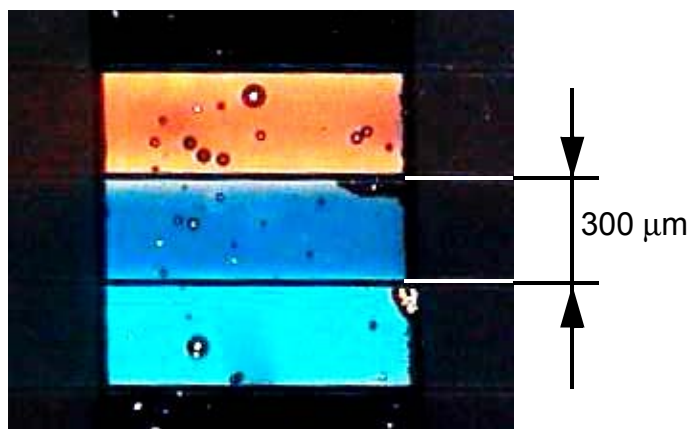


**Figure 8-3.** EL micrograph of a pixel with red, green and blue subpixel fabricated by dye transfer and cathode separators. [micrographs courtesy of Ke Long]

## 8.2 Future Work

Before the dye transfer technology can be utilized on an industrial scale, several problems have to be solved and further improvements are desirable.

The dye transfer process could be modified to transfer the two (or more) dyes simultaneously. This can be accomplished by screen printing [2][3] the polymer layer of the dye

---

1. This particular device was fabricated by Ke Long. However, three color devices employing both dye transfer and cathode patterning were previously reported by the author. [1]

source rather than etching it. Screen printing is a very mature printing technology, and printing on glass or plastic, although not as common as printing on paper, is an well understood process.

In addition to screen printing, the dye source could be completely eliminated if the dye is directly deposited onto the device polymer layer from a powder source. This process is certainly more sophisticated and needs a lot of research. However, electrostatic deposition (such as a laser printer) is capable of high resolution and enormous flexibility in terms of patterning. In this case, the pattern could be directly transferred from the computer platform to the physical device without the need to fabricate any masks or any other lithography steps.

Perhaps a more realistic approach to direct patterning is the dye sublimation technique, where the donor (the dye source) and the receptor (the device polymer layer) are in direct contact and local heating of the dye source initiates the dye transfer [4][5].

To get a better qualitative and quantitative understanding about what is happening during the solvent anneal, a detailed analysis of samples using SIMS with dye transferred after different exposure times and at different solvent concentrations is necessary.

In addition, further work is necessary to fine-tune the dye transfer process to obtain the optimal dye concentration in the device polymer film and thus increase the efficiency of the device.

Recent research results show that polyfluorenes are a promising class of emissive polymers [6][7]. Substituting PVK with this kind of polymer is desirable to fabricate more efficient and stable devices.

## 8.3 References

- [1] F. Pschenitzka and J. C. Sturm, "Patterned dye diffusion using transferred photore-sist for polymer OLED displays", *Proceedings of SPIE - The International Society for Optical Engineering* **4105**, 59 (2001).
- [2] D. A. Pardo, G. E. Jabbour, and N. Peyghambarian, "Application of Screen Printing in the Fabrication of Organic Light-Emitting Devices", *Adv. Mater.* **12** (17), 1249 (2000).
- [3] J. Birnstock, J. Blassing, A. Hunze, M. Scheffel, M. Stossel, K. Heuser, G. Wittmann, J. Worle, and A. Winnacker, "Screen-printed passive matrix displays based on light-emitting polymers", **78** (24), 3905 (2001).
- [4] R. A. Hann and N. C. Beck, "Dye diffusion thermal transfer (D2T2) color printing", *Journal of Imaging Technology* **16** (6), 238 (1990).
- [5] K. Shinozaki and H. Hirano, "Dye - polymer affinity and its effect on thermal dye-transfer printing", *Journal of Imaging Science and Technology* **38** (6), 571 (1994).
- [6] I. S. Millard, "High-efficiency polyfluorene polymers suitable for RGB applica-tions", *Synthetic Metals* **111**, 119 (2000).
- [7] M. T. Bernius, M. Inbasekaran, J. O'Brien, and W. Wu, "Progress with light-emitting polymers", *Advanced Materials* **12** (23), 1737 (2000).

# 9 Appendix

## 9.1 MATLAB code for Diffusion Depth Sensitive Photoluminescence

```
clear all
echo off all

%definitions
n=1000;           %film thickness in A
abs=500;         %absorption length of UV light
length_i=.1;    %initial dye distribution length in A
length_e=2000;  %length at end of simulation
factor=1.2;     %multiple of length interval

alpha = 2;      %linear
beta = 10;     %quadratic term of emission-ratio func
kappa = 1;     %dye enhancement

fid = fopen('output.dat','a');

%calculating number of points
length=length_i;
j=1;
while length<=length_e
    length = length*factor;
    j = j+1;
end
jmax = j;

result_length = zeros(1,j);
result_ratio_g = zeros(1,j);
result_ratio_e = zeros(1,j);

%main computation
j= 1;
length=length_i;

while j<=jmax
    result_length(j) = length;
```

```

%UV intensity from front, back
front = zeros(1,n);
back = zeros(1,n);%back means illumination through substrate

i=1:n;
front = exp(-(i-1)/abs);
back= exp (-(n-i)/abs);

%gaussian distribution of dye
y_g = zeros(1,n);
y_g = exp(-(i.*i)/(2*length^2));
ysum = sum(y_g);
y_g = y_g/ysum;

%calculation of emission intensity gauss
intensity_back = sum(back.*(alpha*y_g+kappa*beta*y_g.*y_g));
intensity_front= sum(front.*(alpha*y_g+kappa*beta*y_g.*y_g));
ratio_gauss =intensity_front/intensity_back;
result_ratio_g(j) = ratio_gauss;

%error function
y_e = zeros(1,n);
y_e = erfc (i/(2*length));
ysum = sum(y_e);
y_e = y_e/ysum;

%calculation of emission intensity error
intensity_back = sum(back.*(alpha*y_e+beta*kappa*y_e.*y_e));
intensity_front= sum(front.*(alpha*y_e+beta*kappa*y_e.*y_e));
ratio_error =intensity_front/intensity_back;
result_ratio_e(j) = ratio_error;

length = length*factor;
j = j+1;
end

%read out
length=length_i;
j=1;
while j<=jmax
    result_length(j);
    result_ratio_g(j);
    result_ratio_e(j);
    fprintf(fid,'%g %g %g \n', result_length(j), result_ratio_g(j),
result_ratio_e(j));
    length = length*factor;
    j = j+1;

```

```
end

%plot routine
hold on,
plot(result_length, result_ratio_g, 'r'),
plot(result_length, result_ratio_e, 'b'),

fclose(fid);
hold off;
clear all;
```

## 9.2 Publication and Conference Presentations

- F. Pschenitzka, J. C. Sturm, “High Resolution Photolithographic Patterning of Organic Light Emitting Diode Cathodes”, Mat. Res. Soc. Symp., San Francisco, CA, April 1998.
- J. C. Sturm, F. Pschenitzka, T. R. Hebner, M. H. Lu, C. C. Wu, W. Wilson, “Patterning Approaches and System Power Efficiency Considerations for Organic LED Displays”, in Proc. of SPIE, Vol. 3476, p. 208 (1998).
- K. A. Killeen, T. R. Hebner, F. Pschenitzka, M. H. Lu, M. E. Thompson, J. C. Sturm, “Single-Layer Polymer Blend Organic Light Emitting Diodes with Electron Transport Polymers”, Polymer Preprints, Vol. 39, p. 1099 (1998).
- J. C. Sturm, F. Pschenitzka, T. R. Hebner, M. H. Lu, C. C. Wu, S. Troian, “Printing approaches for large-area color organic LED displays”, in Proc. of SPIE, Vol. 3797, p. 208 (1999).
- F. Pschenitzka, J. C. Sturm, “Three-color organic light-emitting diodes patterned by masked dye diffusion”, Applied Physics Letters, Vol. 74, p. 1913 (1999).
- X. Jiang, R. A. Register, F. Pschenitzka, J. C. Sturm, K. A. Killeen, M. E. Thompson, “Doped Organic Light-Emitting Diodes based on Random Copolymer containing both Hole and Electron Transport Groups”, in Proc. Mat. Res. Soc. Symp., Vol. 558, p. 433 (2000).
- F. Pschenitzka, J. C. Sturm, “Three-Color Doping of Polymer OLEDs by Masked Dye Diffusion”, in Proc. Mat. Res. Soc. Symp., Vol. 558, p. 513 April 1999 (publ. 2000).
- F. Pschenitzka, J. C. Sturm, “Photographically Patterned Dye Diffusion into Organic Thin-Films for OLED Applications Using Soft Masks”, Mat. Res. Soc. Symp., San Francisco, CA, April 2000.
- F. Pschenitzka, J. C. Sturm, “Patterned Dye Diffusion using Transferred Photoresist for Polymer OLED Displays”, in Proc. of SPIE, Vol. 4105, p. 59 (2001).
- X. Jiang, R. A. Register, K. A. Killeen, M. E. Thompson, F. Pschenitzka, J. C. Sturm, “Statistical Copolymers with Side-Chain Hole and Electron Transport Groups for Single-Layer Electroluminescent Device Applications”, Chemistry of Materials, Vol. 12, p. 2542 (2000).
- F. Pschenitzka, J. C. Sturm, “Solvent-enhanced dye diffusion in polymer thin films for color tuning of organic light-emitting diodes”, Applied Physics Letters, Vol. 78, p. 2584 (2001).
- K. Long, M.-H. Lu, F. Pschenitzka and J. C. Sturm, “Novel-Three-Color Polymer Light-Emitting Devices for Passive-Matrix Flat Panel Displays”, Digest of the 59<sup>th</sup> Device Research Conference, p. 179 (2001).
- F. Pschenitzka, M.-H. Lu, and J. C. Sturm “Patterning of OLED Cathodes by Metal Dry Etching” Digest of Technical Papers, Int Symp Soc Inf Disp, p. 731 - 733 (2001).

- F. Pschenitzka, K. Long, and J. C. Sturm, "Solvent-enhanced Dye Diffusion in Polymer Thin-Films for OLED Application", *Mat. Res. Soc. Symp. Proc.* Vol. 665, C9.5 (2001).
- F. Pschenitzka, J. C. Sturm, "Excitation mechanisms in dye-doped organic light-emitting devices", *Applied Physics Letters*, Vol. 79, p. 4354 (2001).
- X. Jiang, R. A. Register, K. A. Killeen, M. E. Thompson, F. Pschenitzka, J. C. Sturm, "Effect of Exciplex Formation Between Carbazole and Oxadiazole Moieties on the Performance of Single-Layer Light-Emitting Diodes" (submitted, *Journal of Applied Physics*).
- T. Graves-Abe, F. Pschenitzka, J.C. Sturm, "Anomalous Temperature Dependence in Solvent-Enhanced Dye Diffusion in Polymer Films", *Mat. Res. Soc. Symp.*, San Francisco, CA, April 2002.

# Acknowledgement

It all begun with my parents: They were the main and unflagging source of support from early on. By instilling in me curiosity and patience, they gave me the means to achieve and, at the same time, remain sane.

Equally important was the influence of my advisor Jim Sturm. (Somehow I find the German word “Doktorvater” more suitable.) Both, from the academic and from the personal perspective, I can not imagine a better advisor. In addition to the abundant scientific input during countless discussions, his never subsiding enthusiasm and good spirit helped me to cope with the unavoidable dry spells and the times of frustration. Being the gifted teacher he is, he made my years at Princeton fruitful and the work in the lab to a certain extent even enjoyable.

To Prof. Siegurd Wagner, Prof. Rick Register and Prof. Steven Forrest I turn gratefully for making time in their busy schedule to discuss my questions.

In addition, I would like to express my gratitude to Kim Hegelbach, Debra Warren and Karen Williams, who were always very helpful. Their insider knowledge of the administration made it easy to keep the red tape to a minimum. Due to their support, the reimbursement checks arrived always before I was completely broke. I am also indebted to Mike Valenti, Joe Palmer, Jay Plett and John Bittner - they kept the reactors and computers running. In my first year in Princeton, I had to repair the metal etcher every two weeks. Albeit I learned a lot about fittings and tubing, I am glad to have left this chapter behind me. At the same time, I also learned to appreciate their work.

Beside all these important people, I also will remember fondly my fellow grad students. Especially I would like to tell my co-workers at Sturm’s lab: Keep up the great atmosphere! Among them, special thanks go out to Malcolm Carrol, Tom Hebner (who left the group way to early), Kiran Pangal, Chung-Chi Wu, Chialin Chang, Min-Hao Mike Lu, Troy Abe, Ke Long and Rebecca Peterson - they are as delightful to know as to work with.

It was my pleasure to meet many great people in the department, and they all have had a major influence on mental well-being: Among these, most importantly, are Gautam Parthasarathy, Song Lan, Amlan Majumdar, Etienne De Poortere, Robert Runser, Charalambos Anastassiou, Audrey Lee, Chongfei Shen, and Bob Min. Thanks to all of you!

It is hard to believe, but while working hard in the lab, some time was actually left which I enjoyed mostly with precious friends. Formost among these I have to mention Felicitas Wiedemann as my steadfast friend and pillar of support. As much as I like change - the warmth of our friendship should never cease.